CATALYTIC REACTIONS OF HYDROCARBONS OVER ZEOLITES

Janice E. Henderson

Doctor of Philosophy

University of Edinburgh

1986

To my Husband.

Acknowledgements

I would like to thank my supervisor Dr. H.F. Leach for his advice and encouragement throughout my period of research. I am also grateful to the other members of the catalytic research group in particular Dr. I.D Harrison, Mr N. Poole and Mr R. Brown for many useful discussions. I am grateful for the assistance given by Dr. J.L. Casci of the New Science Group, I.C.I. In addition, I would like to acknowledge the practical help given by Mr. R. Brown particularly when gas cylinders needed replacing. I thank the S.E.R.C. for the provision of a Studentship and the University of Edinburgh for laboratory facilities.

I would also like to register my thanks to my husband for his support during my period of study and his assistance in the typing of this thesis.

CONTENTS

ABSTRACT

A general review of molecular sieve zeolites preceeds a more specialised account of the properties of the zeolites H-ZSM-23, H-EU-1 and ruthenium Y.

A gravimetric study of the relatively unstudied zeolites H-ZSM-23 and H-EU-1 was carried out. The adsorption of a range of organic vapours of different molecular size indicated that both H-ZSM-23 and H-EU-1 had pore structures comprising 10-membered rings. The results suggested that two types of channel of differing size are present in H-EU-1. Catalytic characterisation utilising the isomerisation of the n-butenes and methylcyclopropane was carried out. The resulting product distributions for each zeolite were indicative of carbonium ion type mechanisms.

The isomerisation of 3,3-dimethylbut-1-ene (I) and the hydrogenolysis of alkanes were studied over a series of ruthenium Y zeolites. The isomerisation of I was found to occur readily over RuNaY20, RuNaLaY20 and RuLaY20. Carbonium ion mechanisms were responsible for the isomerisation in each case. The hydrogenolysis of n-butane, cyclopentane and 2,2-dimethylpropane occurred readily over RuNaY20 and RuNaLaY20. Comparison of apparent activation energies and initial product distributions suggests that hydrogenolysis of n-butane and 2,2-dimethylpropane occurred via a common mode of adsorption, a 1,3-diadsorbed species. A 1,2-diadsorbed species is proposed for cyclopentane hydrogenolysis.

CHAPTER 1

Zeolites

1.1. Introduction

A new group of minerals consisting of crystalline hydrated aluminosilicates of the alkali and alkaline earth metals were first recognised by Cronstedt[1] in 1756 with his discovery of stilbite. Because the mineral expelled water when heated the mineral was called a zeolite from the Greek meaning "boiling stones".

Early investigations of the properties of zeolites were carried out on specimens collected from cavities in basaltic rocks. The hydrothermal alteration of volcanic rocks led to the formation of well-developed crystals. The distribution of zeolite minerals is related to their silica content. Silica-rich zeolites such as mordenite and stilbite occur in silica-rich rocks while philipsite and chapazite which have a low silica content are characteristic of low silica-containing rocks.

In 1891, the first HMS Challenger expedition found phillipsite in the red mud of the Pacific Ocean bed[2]. This was the first report of zeolites in a sedimentary environment. It is now believed that philipsite is one of the most abundant minerals on earth.

Although all the zeolite minerals known have been found in igneous rocks only a few occur in sedimentary environments.

1.2. Synthesis

Early attempts to synthesise zeolites were based upon then current ideas concerning their mode of

formation in basaltic rocks. The reaction mixtures had the same composition as the desired product and the conditions employed were high temperature (above 473 K) and high pressure. Positive identification of the products as zeolites was not possible until the advent of X-ray diffraction.

Synthetic zeolites are formed by the crystallisation of aluminosilicate gels produced from the copolymerisation of the individual silicate and aluminate species. The crystallisation of the disordered gel phase into the ordered zeolite structure involves depolymerisation by hydroxyl ions. The ease with which the zeolites crystallise is attributed to the high reactivity of the gel, the concentration of alkali hydroxide and the high surface activity due to the small particle size of the solid phases concerned in the synthesis.

The methods currently utilised to prepare zeolites are as follows:-[3]

1. With reactive starting materials either as freshly prepared gels or as amorphous solids.
2. With a relatively high pH using an alkali metal hydroxide and/or organic base.
3. With low temperature hydrothermal conditions and with low autogeneous pressures.
4. With a high degree of supersaturation of the components in the gel phase leading to nucleation of a large number of crystals.

Zeolites have been synthesised from systems

containing organic cations from the following families:-[4]

tetra-alkylammonium (R_4N^+)

tetra-alkylphosphonium (R_4P^+)

organic complexes.

Zeolites crystallised from quaternary ammonium ions (nitrogenous zeolites) require the use of a second base, usually an alkali hydroxide. Barrer[5], using tetramethylammonium cations, first reported the synthesis of zeolites A, X and Y. More recently a number of new zeolites, many high silica containing species, have been reported from synthetic studies employing organic cations. ZSM-23[6] and EU-1[7] are typical examples.

The role of the organic cation in the synthesis process has not been entirely established but it is believed to function as a hydroxyl ion donor, a consequence of its bascity. It has also been postulated by Flanigen et al[8] that the organic cation serves as a template by organising the water molecules.

As initially prepared the zeolites synthesised as above will still contain organic species (usually rather bulky). In order to allow access to the intracrystalline system by hydrocarbon substrates, an essential requirement of catalysis, the organic cations must be removed. This is normally carried out at elevated temperatures, generally much higher than the decomposition temperature of the organic cation itself, but under conditions where the zeolite structure remains intact.

1.3. Structure and Classification

A zeolite is a crystalline aluminosilicate whose structure contains channels and/or cages filled with exchangeable cations and water molecules. The zeolite structure is based on fundamental units in which Si^{4+} or Al^{3+} is tetrahedrally coordinated to four oxygen atoms. These tetrahedral units are linked in three dimensions by oxygen bridges to form rings. According to Lowenstein[9], the alumina tetrahedra only link to silica tetrahedra so that Al-O-Al bonds are excluded and consequently the Si/Al ratio is never less than unity.

Within the zeolite framework the presence of Al atoms tetrahedrally coordinated to four oxygen atoms results in a net negative charge which must be compensated for by cations. The latter are mobile and may occupy various sites depending on their radius, charge or degree of hydration.

The structural formula for a zeolite can be expressed in terms of the structural formula for the unit cell[10] e.g.

$$M_{x/n}[(AlO_2)_x(SiO_2)_y].wH_2O$$

where M is a cation of valence n and w is the number of water molecules. The sum (x+y) is the total number of tetrahedra in the unit cell. The composition of the framework is represented by $(AlO_2)_x(SiO_2)_y$. Replacement of a silicon atom in the framework by an aluminium atom produces an excess of negative charge which is compensated for by the presence of an additional positive ion. In natural zeolites the charge compensating ions

are usually alkali or alkaline earth metals.

Classification of the many zeolite topologies into groups has been accomplished by the recognition of certain recurring subunits of structure which are specific arrays of Si (or Al) and oxygen tetrahedra. These arrangements have been called secondary building units by Meier[11]. The zeolite framework can be described by linking finite units, which may contain up to 16 tetrahedral units (T-atoms). The secondary building units are chosen such that the framework may be built from one type of unit only and are illustrated in Figure 1.1. Table 1.1 indicates the classification of the zeolite structures into groups (with examples): each group being based on a secondary building unit.

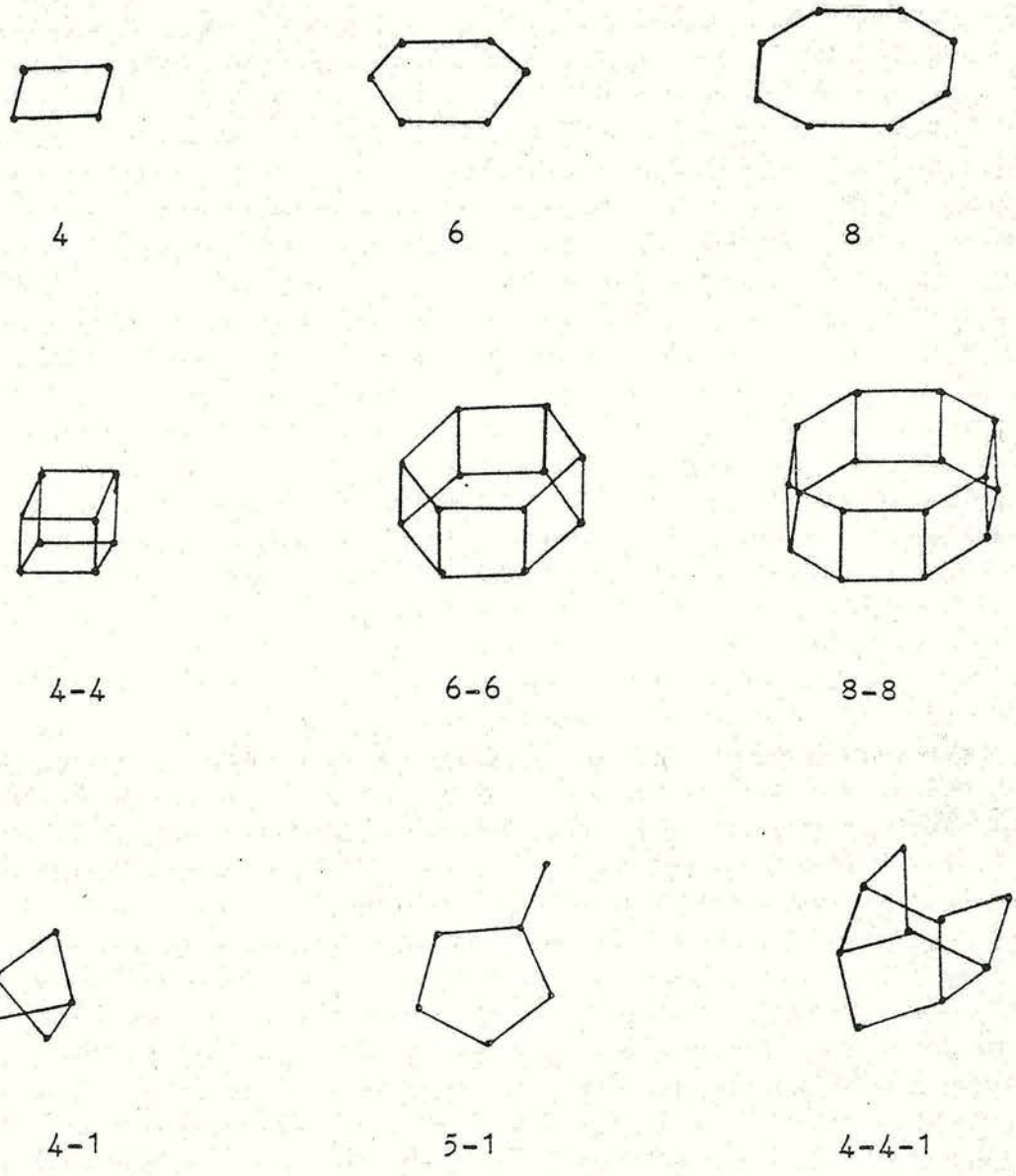

Figure 1.1. The Secondary Building Units in Zeolite Frameworks[11]

Secondary Building Unit		Examples
4,	single 4-ring	Analcine
		Phillipsite
6,	single 6-ring	Erionite
		Offretite
		Sodalite
8,	single 8-ring	Zeolite Na-P
4-4,	double 4-ring	Linde type A
6-6,	double 6-ring	Faujasite
		ZK-5
8-8,	double 8-ring	Rho
4-1,	complex 4-1 unit	Natrolite
		Thomsonite
5-1,	complex 5-1 unit	ZSM-11
		ZSM-5
		Mordenite
		Ferrrierite
4-4-1,	complex 4-4-1 unit	Stilbite

Table 1.1. Classification of Zeolite Structures based on Common Secondary Building Units[11]

The linkage of the secondary building units into chains, layers and polyhedra results in the characteristic frameworks of different zeolites. In the zeolites A, X and Y the silica and alumina tetrahedron are linked together to form a cuboctahedron[12]. The cuboctahedron is also known as the sodalite unit and is built from six- and four-membered rings (Figure 1.2). If

Figure 1.2. The structures of the Sodalite Unit and Zeolites A, X and ZSM-5.

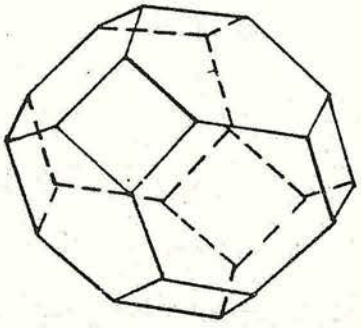

Sodalite Unit

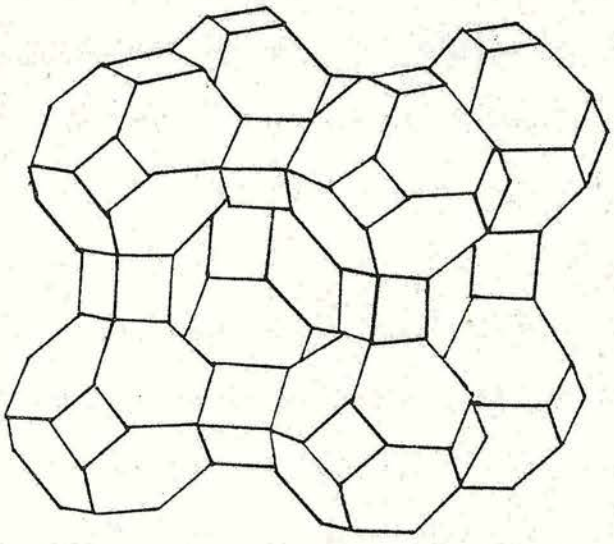

A. Zeolite A

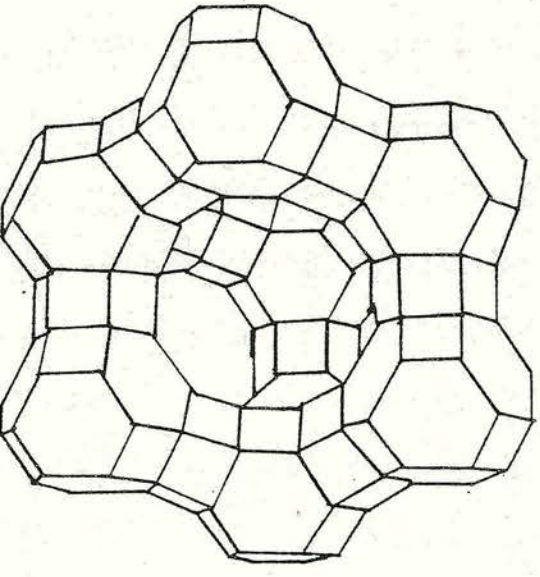

B. Zeolite X

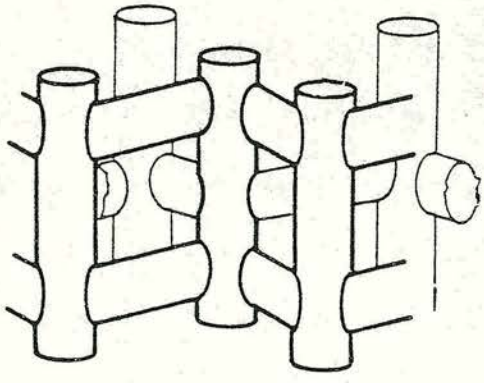

C. ZSM-5

the sodalite units are linked together by oxygen bridges between the four-membered rings, one obtains the framework shown in Figure 1.2.A which corresponds to zeolite A. An alternative arrangement linking the sodalite units by oxygen bridges between the six-membered rings results in the framework structures of zeolites X and Y (Figure 1.2B). The stacking of the sodalite units leads to larger cavities (supercages) which are connected by pores of variable sizes (four-, eight-, or twelve-membered rings). These cavities constitute the internal surface of the zeolite. Access to the supercage of zeolite A is resticted by an eight-membered ring which has a free diameter of 0.42 nm while access to the supercage of zeolites X and Y is via a twelve-membered ring with a free diameter of c.a. 0.74 nm.

ZSM-5 has a three-dimensional pore system comprising ten-tetrahedron rings intermediate in size between the pore size for zeolites A, X and Y. The pore system of ZSM-5 differs from those in zeolites A, X and Y in that supercages are not formed. However, the pore system does contain intersections where additional free space is available. The pore strucure consists of two intersecting channel systems - one straight with elliptical openings and the other sinusiodal with circular openings and perpendicular to the former (Figure 1.2.C)[13,14]. The intersections are identical in size.

The difference in pore size and type between zeolites of different framework structure has important consequences in the sorptive and catalytic properties of zeolites. Even minor structural differences give rise to very different catalytic properties.

1.4. Ion Exchange Properties

The presence of a net negative charge on the zeolite framework associated with the aluminium tetrahedra and the need for electrical neutrality to be preserved requires the presence of balancing cations within the zeolite cages and channels. These cations are mobile and exchange is possible between them and different cations in an external solution.

The high crystallinity of zeolites means that the channels and cages which characterise a particular structure are clearly defined both in their dimensions and shapes. Ion sieve effects have been observed where a particular ion is excluded from a zeolite because of its size[15] e.g. complete exchange with calcium (radius 0.198 nm.) and strontium (radius 0.226 nm.) was observed in zeolite X while exchange with barium was limited (radius 0.27nm.)[16].

The cation exchange properties of zeolites depend on a number of factors:-

1. The cation size and charge.
2. The concentration of the cation in solution.
3. The anion associated with the cation in solution.

4. The characteristics of the zeolite.

5. The Si/Al ratio of the zeolite.

Changing the Si/Al ratio in the framework alters the selectivity of the zeolite. If the Si/Al ratio is raised to a high enough value then the material becomes hydrophobic[17]. Flanigen et al[8] have reported that silicalite, which can be regarded as the all silica analogue of ZSM-5 with a Si/Al ratio of infinity, is both hydrophobic and organophilic.

Hydrogen forms of zeolites can be prepared by ion exchange of the cation by ammonium ions from an ammonium salt water solution. The subsequent thermal treatment of the ammonium-exchanged zeolite results in the liberation of ammonia and the formation of hydroxyl groups on the zeolite framework. A crystalline zeolite completely free of cations can be obtained by treating silica-rich zeolite Y in this manner but similar attempts to achieve complete hydrogen exchange of zeolites A and X results in structural collapse[18].

The most interesting cationic species from the viewpoint of catalysis are those from the transition metals. Their introduction into zeolite frameworks by ion exchange is a relatively simple technique[19] e.g. for Ni^{2+}, Co^{2+} and Cu^{2+} the procedure merely employs stirring the zeolite with aqueous solutions of the appropriate hydrated ion. Transition metals can also be introduced via the exchange of stable cationic complexes e.g. the platinum metals (Pt, Pd, Ru) are commonly exchanged as stable amine complexes. Subsequent

reduction to the zero valent state is normally achieved using hydrogen.

Zeolites have found a number of specialised applications as ion exchangers in recent years[20]. These are in detergents, in ammonia/ammonium removal from freshwater effluent, in radioisotope removal from spent pile effluent and in agriculture. The most important of these applications in terms of market turnover is in detergents where zeolites are employed as a water-softener partially replacing tripolyphosphate builders. Zeolite A is effective in the removal of Ca^{2+} but not as effective in the removal of Mg^{2+} while zeolite X exchanges Mg^{2+} rapidly[21]. Thus, a combination of the two zeolites results in the removal of both Ca^{2+} and Mg^{2+}.

1.5. Adsorption and Diffusion

Zeolites provide stable high capacity, micropore sorbents with diverse molecule sieving properties. Each framework topology provides its own unique system of channels and cavities. The behaviour is further modified by the number, location and size of the intracrystalline cations which neutralise the negative charge on the framework.

Pore structure (dimensions and network) varies greatly among zeolites. The lowest pore size is about 0.26 nm and the highest 0.74 nm[22]. Pores may lead to linear, parallel or interconnected channels. For all zeolites the pore opening is determined by the free

aperture of the oxygen ring that limits the pore. Maximum values have been calculated and are listed in Table 1.2. On the basis of pore size, zeolites can be classified into two groups: the large pore zeolites with twelve-membered rings (e.g. X and Y zeolite and mordenite) and the shape selective structures with eight- or ten-membered rings (e.g. ZSM-5, erionite and ferrierite).

n	Free Diameter (nm)
4	0.26
6	0.36
8	0.42
10	0.63
12	0.74

Table 1.2. Free Diameter of Rings of n Oxygen Atoms

The quantity of gas or vapour adsorbed by a dehydrated zeolite depends upon the equilibrium pressure, temperature and the nature of the micropores in the zeolite crystal. When exposed to a gas or vapour the intracrystalline voids and channels of the zeolite fill with the gas or vapour concerned and when the filling is complete no more adsorption occurs. This results in an adsorption isotherm of type I in the classification outlined by Brunaer[23].

The shape selective properties of zeolites are directly related to the pore size of the channels.

Further insights into the relationship existing between shape selectivity and pore dimension can be obtained by examining the relative adsorptive properties of zeolites for a range of various hydrocarbons of different critical diameter. In order to correlate the crystallographic aperture or pore size of a zeolite with the dimensional properties of various adsorbate molecules a scale of molecular dimensions must be established. In early experiments, the molecular size was based upon the equilibrium diameter of the adsorbate molecule. This approach was not very satisfactory and an improved treatment utilised the collision or kinetic diameter[24]. This was defined as the intermolecular distance of closest approach for two molecules colliding with zero energy. For long molecules, such as hydrocarbons, the critical dimension is the minimum cross-sectional diameter.

Figure 1.3 shows a correlation between pore size and the molecular kinetic diameter of some sorbate molecules and illustrates the basis for molecular sieving in that large molecules can be excluded from crystals having smaller pores[25]. The "fine tuning" or sieving which can be obtained by variation in cation type is evident for zeolite A[26]. Monovalent cations such as sodium are sited in the eight-membered windows and effectively block the pore diameter. Divalent cations (e.g. calcium) locate preferentially in the six-membered windows connecting the cages thus increasing the free diameter allowing n-alkanes to be adsorbed.

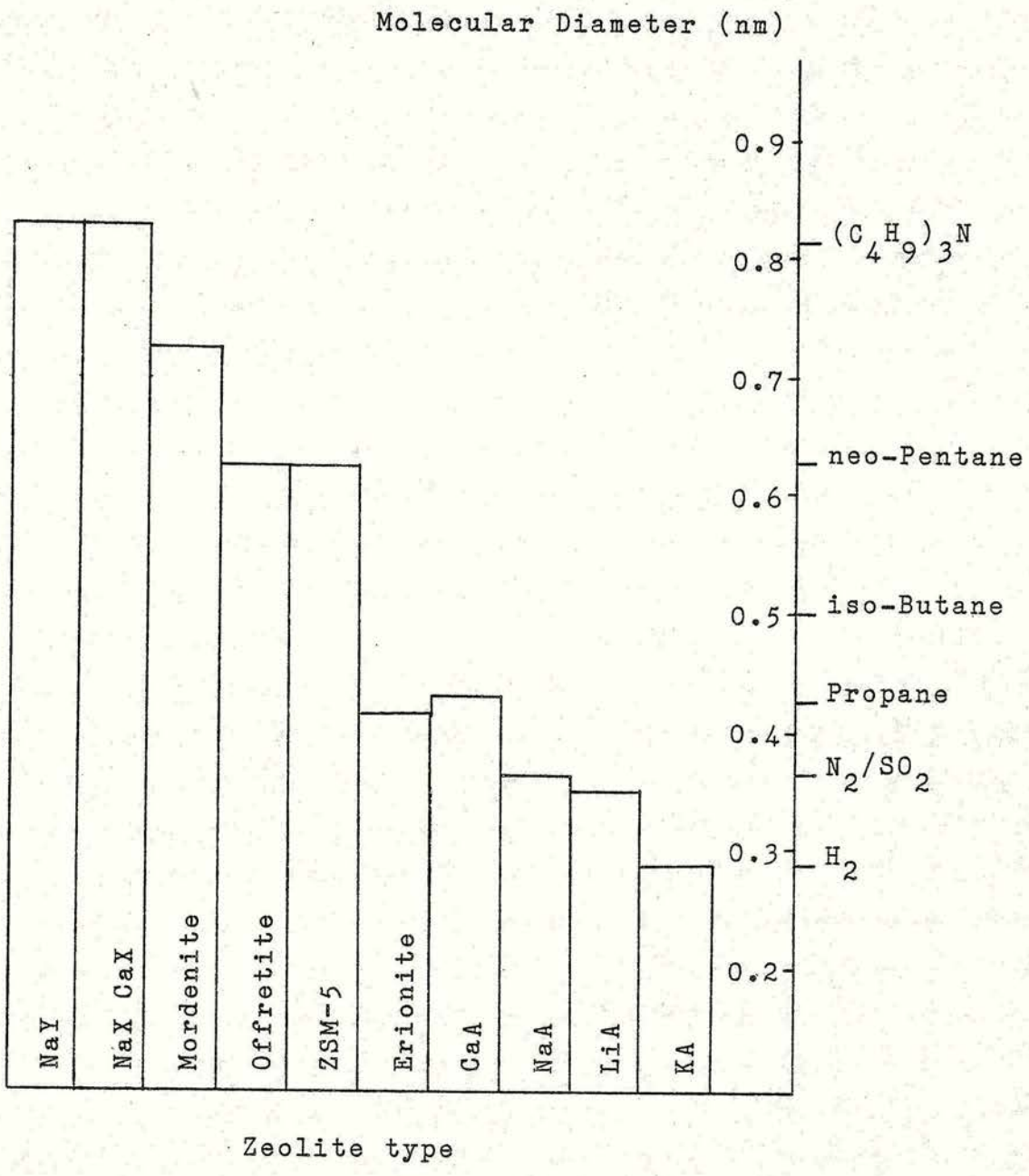

Figure 1.3. Sorption in Zeolites[25].

Adsorption processes involving physical adsorption are exothermic. At low levels of adsorption the initial adsorption heat has been related to several component interaction energies. These include dispersion and short range repulsion energies, polarisation energy and

additional components attributed to electrostatic interactions[23].

In zeolites the specificity or selectivity shown towards adsorbate molecules may be modified by methods which alter the energy of interaction. These are:-

1. By introducing small amounts of a polar adsorbate (e.g. water) which selectively locates on the most energetic sites.
2. By cation exchange.
3. By decationisation - removal of the cations from the zeolite framework alters the local electric field and field interaction.

When zeolites are used as molecular sieves and catalysts migration of the sorbates within the crystal is an important and sometimes rate controlling factor. If the rate controlling process is the activated diffusion of the adsorbate molecule through the zeolite intracrystalline channels then the process may be described by Equation 1.1.

$$Q_t - Q_0 = Bt^{0.5} + C \qquad \text{Equation 1.1.}$$

where Q_t = Amount adsorbed at time t

Q_0 = Amount adsorbed at t = 0

B and C = Constants.

Under such circumstances a plot of the amount adsorbed versus $t^{0.5}$ should yield a straight line. This activated diffusion process can be differentiated from competing processes by observing an increased rate of adsorption with an increase in temperature. The coefficient of diffusion, D, can be determined from the slope of the

$t^{0.5}$ plot if the volume of the crystals and their external surface areas are known. Diffusion coefficients and rates may depend upon molecular size or type, upon the direction of diffusion, upon crystallite size or shape, and upon the nature of the cations.

The temperature at which the adsorbate uptake occurs can play an important part in molecule sieving as diffusivities follow an Arrhenius relationship because of the energy barriers involved. For activated diffusion the variation in D with temperature is given by

$$D = D_0 e^{-E/RT} \qquad \text{Equation 1.2.}$$

where E = Activation energy for the diffusion process

T = Temperature (K)

R = Gas constant

D = Diffusivity

D_0 = Preexponential factor.

The values for the energy of activation and the diffusion coefficient are governed by the dimensions of the diffusing molecules and the free diameter of the pores. For linear molecules the cross-sectional diameter is critical in controlling passage through the pores of the zeolite. At a given temperature D may change by many orders of magnitude as a consequence of small changes in the critical dimension of the diffusing molecule.

The activation energy for diffusion of a series of molecules of increasing diameter has been observed to increase linearly in mordenite and in zeolite A[24,27]. For both zeolites the energy increases with increasing diameter. The relationship is quite good for zeolite A

but in mordenite the channel system results in anomolous diffusion behaviour for nitrogen and oxygen.

A study of the diffusion of n-alkanes in the potassium form of zeolite T (an intergrowth of erionite and offretite) found that the diffusion coefficient diminished at first with increasing chain length reaching a minimum at C_8 before rising to a maximum at C_{12} and then declining[28]. It was considered that all molecules larger than C_8 were too long to align themselves fully stretched along the cavity of zeolite T. Molecules with 10 or more carbon atoms in the chain would simultaneously extend through two eight-membered windows.

In catalytic processes on zeolites the reactants must diffuse inwards and the products outwards. The counter-diffusion of the latter species may seriously affect the apparent activity and selectivity for a given reaction. Counter-diffusion occurs readily in the three dimensional pore system of zeolite Y[29]. In a one dimensional system such as mordenite, however, molecules with dimensions close to that of the pores cannot freely counter-diffuse because they cannot pass the other molecules in the pores[30].

1.6. Catalytic Properties

Since zeolites were first used in petroleum processing in the 1960's, zeolite catalysis has undergone dramatic advances and has been the subject of several reviews[31,32,33].

The major industrial processes that employ zeolite

catalysts are listed in Table 1.3 together with their respective zeolite usages[34].

Process	Weight %	Catalyst Examples
catalytic cracking	90	RE-Y, H-Y
hydrocracking	9	Co, W, Ni, Pt or Pd on H-Y, mordenite, erionite
organic chemicals	<1	RE-Y, ZSM-5
inorganic chemicals	<1	H-mordenite

Table 1.3. Zeolite Usage in the Chemical and Fuel Industries[34].

The largest application of zeolite catalysts is in catalytic cracking where a rare earth, magnesium or hydrogen form of Y is normally used. Dual functional catalysts incorporating cobalt, tungsten, nickel, platinum or palladium supported on H-Y, mordenite or erionite are used in hydrocracking. At the present time organic and inorganic chemical technologies have relatively little use for zeolite catalysts although this could change.

Heterogenous catalysis requires that the reactant species be transported to and transformed at reactive surface sites. As the ratio of external surface to internal surface for zeolite crystals (of about 1 μm in size) is about 0.5 percent, a requirement for zeolite

catalysis is that the reactants can enter the crystal and the products can exit. Access to the interior of the zeolite is controlled by the pore size. For practical zeolite catalysis the pores must contain eight-, ten- or twelve-membered rings. Another property of zeolites that makes them interesting heterogenous catalysts is that they have exchangeable cations allowing the introduction of cations with various catalytic properties. If these cationic sites are exchanged for H^+, then the resultant zeolites can have a very high number of strong acid sites.

On entering the pore system the sorbate molecule is subject to strong forces of interaction with the zeolite. The charged nature of the framework and the presence of the cations generates electrostatic fields. These fields are large when the counter ions are polyvalent (e.g. Mg^{2+}, Ce^{3+}) and require several AlO_4^- units for neutralisation. A similar situation pertains when the zeolite contains a large concentration of aluminium.

1.6.1. Active Sites in Zeolites

The major application of zeolite catalysts involves hydrocarbon transformations in which the acidity of the zeolite plays a vital role. Proton acidity is introduced by one of the following methods:-

1. Ammonium ion exchange followed by thermal decomposition of the ammonium ions.

$$NaZ + NH_4^+(aq.) \rightleftharpoons NH_4Z + Na^+(aq.)$$

$$NH_4Z \rightleftharpoons NH_3(g) + H^+$$

2. Ion exchange with polyvalent cations.

$$M(H_2O)^{n+} \rightleftharpoons MOH^{(n-1)} + H^+$$

3. Reduction of appropriate counter ions to a lower valency state e.g.

$$Ni^{2+} + H_2 \longrightarrow Ni^0 + 2H^+$$

Both Bronsted and Lewis acid sites are found in zeolites. The former are protons attached to lattice oxygen atoms while the latter can be charge compensating cations or trigonal aluminium atoms at oxygen deficient sites or at cation positions[35]. On heating to temperatures above 823 K the Bronsted sites are converted to Lewis sites by loss of water.

Although it has been recognised for some time that acidity is correlated with catalytic properties[35,36], such correlations have as yet not been completely rationalised[37]. This is probably a consequence of the complex nature of the reactions, which involve structural, electronic and collective properties of the zeolite and the interacting molecules.

Infra-red spectroscopy has proved a useful tool for the study of hydroxyl groups and it has been extensively applied to acidic zeolites[36]. Changes in the spectra of the zeolite itself and of molecules adsorbed on the surface can yield direct information about the surface, how molecules adsorb, where they adsorb and how they interact. Most zeolite studies have been made using basic molecules such as ammonia, pyridine and piperidine as surface probes. These molecules interact with Bronsted acid sites, Lewis acid sites and cations.

Pyridine adsorbed on Y zeolites has been utilised to give a quantitative assessment of Bronsted and Lewis acidity[38,39]. Steric hinderance introduced onto the pyridine by methyl or ethyl substitution at appropriate positions gives further information on hydroxyl accessibility in the zeolite structure. 2,6-Dimethylpyridine has been shown to have a high selectivity towards Bronsted sites[40].

The catalytic properties of acid zeolites depend on the number of active sites as well as their strength. As the catalytic sites for acid catalysis are associated with aluminium atoms Haag et al[41] investigated a range of ZSM-5 samples with varying aluminium content. The activity of the samples towards n-hexane cracking was found to be linearly related to the aluminium content and extrapolated to zero activity at zero aluminium content. High resolution magic-angle spinning nuclear magnetic resonance identified the catalytic site for acid catalysis to be a protonated tetrahedral aluminium ion in the framework.

1.6.2. Shape Selective Catalysis

Molecular shape selective catalysis was first reported by Weisz and Frilette in 1960[42]. Critical discussions and reviews of molecular shape selective effects in catalysis have reported by Csicery[43], Weisz[44] and Derouane[22].

In heterogenous catalysis the reaction proceeds through several steps: diffusion and adsorption of the

reactant, formation of the activated intermediate, reaction and desorption and diffusion of the product. The shape selectivity principle is based on these different steps and results in different types of shape selectivity.

1. Reactant selectivity occurs when only a fraction of the reaction molecules are able to penetrate the intracrystalline pores of the zeolite. These molecules react at the active sites located inside the zeolite. The remaining molecules, too large to diffuse into the zeolite pores remain essentially unchanged.

An example of reactant selectivity is hydrogenation over calcium A-type molecular sieve containing platinum[42]. The linear but-1-ene was readily hydrogenated whereas the branched chain isobutene was found to be non-reactive.

In addition to size exclusion, the orientation of the reactant molecule at the pore mouth may prevent entry to the zeolite. Electrostatic interactions may take place between the net dipolar moment of the reactant molecule and the electrostatic field at the pore mouth, orientating the diffusing molecule in a favourable or unfavourable configuration with respect to the pore mouth. The role of electrostatic effects has been demonstrated for the isomerisation of but-1-ene to cis and trans but-2-ene by zeolite A[45]. Both but-1-ene and trans but-2-ene pass easily through the pore mouth since they are properly orientated whereas cis but-2-ene cannot.

2. Product selectivity occurs when some of the products formed within the pores are too bulky to diffuse out as observed products. They are either converted to less bulky molecules or cause deactivation of the catalyst by blocking the pores.

The effect of pore size on the selectivity of dimethylether conversion to alkenes has been identified by Comerais et al[46], who compared the activities and selectivities of H-erionite, H-ZSM-5 and zeolite H-Y. They reported that over the zeolites with a smaller pore opening there was preferential formation of C_2 alkenes compared to C_3 alkenes and that the formation of isobutane increased with increasing pore size.

Product molecular shape selectivity is found in a variety of reactions which use ZSM-5 catalysts and aim at the selective preparation of para-aromatic compounds. Such processes are the disproportionation and alkylation (by methanol) of toluene[47,48,49] and xylene isomerisation[47]. Factors which increase the diffusion path length such as increasing the crystal size or decreasing the effective pore size of the ZSM-5 catalyst favour the formation of p-xylene[49]. Modification with phosphorus or magnesium reduces the size of the pore openings and channel dimensions permitting p-xylene and smaller molecules to diffuse out[48].

3. Restricted transition state selectivity occurs when certain reactions are prevented because the corresponding transition state would require more space than is available in the pores. Neither reactant nor potential

product are prevented form diffusing through the pores. Reactions requiring smaller transition states may proceed unhindered.

Transition state selectivity has been observed for isobutane transformation over H-ZSM-5[50]. Over a variety of zeolites including H-mordenite the reaction has a bimolecular mechanism and is accompanied by the formation of propane and pentanes. In H-ZSM-5 there is not enough space at the channel intersection for two isobutane molecules to be accomodated simultaneously and consequently the pentanes are not formed.

Reactant and product type selectivities and transition state selectivities can be distinguished by particle size effects. Reactant and product selectivities are mass transfer limited and therefore affected by crystallite size whereas restricted transition state selectivity is not. Such distinctions were used by Haag et al[51] to determine the causes of shape selectivity in the cracking of C_6 and C_9 alkanes and alkenes over H-ZSM-5. It was found that branching had a major effect, while the total length of the chain had a minor effect, and the presence or absence of an alkenic bond had no strong influence on diffusivity. The selective cracking of n-alkanes compared to mono-methyl alkanes was due to a higher intrinsic rate constant of the n-alkane with diffusional mass transport playing no role. In contrast dimethyl alkane cracking was strongly diffusion inhibited.

During hydrocarbon reactions over zeolites,

carbonaceous residues and eventually "coke" can be formed. The coking reaction has been shown by Rollman and Walsh[52] to be a shape selective reaction which is related to the pore size and geometry. Coking is less severe in ZSM-5 than in larger pore zeolites because the pores in the former lack sufficient space for the polymerisation of "coke" precursors.

4. Molecular traffic control can occur in zeolites with more than one type of pore system. Reactant molecules may preferentially enter the zeolite through one of the pore systems while products diffuse out through the other.

ZSM-5 has two types of channels both of which have ten-membered ring openings[11]. Linear aliphatics can diffuse in both channel systems but aromatics and isoalkanes prefer the linear elliptical channels[53]. Reactant molecules may enter through the circular sinusoidal pores while the bulkier product molecules diffuse out through the linear elliptical pores.

Mirodatos and Barthomeuf[54] have proposed the concept of an energetic selectivity. In a study of the cracking of alkanes over a variety of zeolites including erionite, ZSM-5 and mordenite the occurence of secondary reactions was found to depend on an energetic selectivity which characterised the cages and channels. The smaller and more tortuous the space where the molecules react, the higher the field gradient and the more secondary reactions are favoured.

1.7. Metal Zeolite Catalysts

When synthetic zeolites became available in large quantities, their usefulness as a carrier for dispersed metals was rapidly recognised[42]. Metal loaded zeolites act as bifunctional catalysts and make efficient use of the expensive platinum metals by maintaining them in a highly dispersed state. They also add to the system selectivity due to the size and shape of their pores.

Metals can be introduced into zeolites by various methods. The most common technique is ion exchange and subsequent reduction but other techniques include adsorption from the gas phase of metal containing compounds (e.g. carbonyls) and metal vapours or the introduction of metals during synthesis. Precise treatment conditions of ion exchanged zeolites are needed to obtain reproducible and well defined states of the metal phase.

Ruthenium loaded zeolites have been the subject of several investigations[55,56]. The state of dispersion of ruthenium in zeolites has been found to be influenced not only by the pretreatment conditions but also by the method of introduction[57]. Chen *et al*[58] found that the activity and selectivity of ruthenium zeolites in Fischer-Tropsch synthesis was influenced by (a) the method of preparation and (b) the metal loading. Catalysts prepared by an incipient wetness technique produced mainly methane while catalysts prepared by vapour impregnation exhibited much higher selectivies for C_2-C_4 alkenes and higher hydrocarbons. The catalytic

performance of ruthenium loaded zeolites in Fischer-Tropsch synthesis also depends on the sequences of oxidations and reductions to which they are subjected during the pretreatment procedure[59]. Finely dispersed ruthenium in zeolite Y results mainly in the formation of C_1-C_3 hydrocarbons but following oxidation and reduction longer chain hydrocarbons are produced with a maximun yield at C_{11}.

The reductive decomposition of platinum amine complexes in faujasites has been well documented. Thermal decomposition of the $Pt(NH_3)_4^+$ complex results in the formation of a hydride species (PtH^+)[35]. The platinum can be further reduced in hydrogen to metallic platinum. The reduced platinum migrates preferentially to and interacts with paramagnetic centres in the zeolite. These sites are most probably Fe^{3+} substituted for Al^{3+} in the lattice or Fe^{3+} in cationic positions. Oxidation of the amine complexes prior to reduction has been found to influence the dispersion of the platinum[60]. Heating above 873 K induces the migration of Pt^{2+} ions into the sodalite cages and upon reduction the platinum atoms trapped inside these cages do not chemisorb hydrogen or oxygen. Hydrogen with a kinetic diameter of 0.289 nm does not enter the sodalite cages which have a free diameter of 0.22 nm.

The position of metal aggregates in zeolites can be determined by transmission electron microscopy (t.e.m.)[61,62] and X-ray photoelectron spectroscopy[63]. Metal particles of about 1 nm in diameter which fit into

the supercages can result from the agglomeration of transition metals in faujasites. However, metal particles exceeding supercage dimensions have been found for palladium, platinum, nickel and ruthenium in a faujasite matrix using t.e.m.[64]. Electron diffraction indicated that such aggregates were single crystals.

The dispersion of metals is usually determined by hydrogen chemisorption, however, the stoichiometry of the adsorption may depart from the usually assumed H/M = 1 ratio. A change in H/Pt = 1 to H/Pt = 1.35 has been reported for hydrogen chemisorption at 300 and 900 K respectively on platinum loaded Y zeolite[65]. The additional hydrogen uptake can only be desorbed above 750 K and has been attributed to hydrogen in bridged positions between metal and support atoms. If zeolites are treated under conditions such that a bimodal particle size distribution exists the adsorption experiments indicate an average size.

Fraissard et al[66,67] have developed a nuclear magnetic resonance method of measuring metal dispersion in zeolites. The method is based on the n.m.r. chemical shift of ^{129}Xe and depends upon the number of collisions of xenon atoms with the cage wall or with metal aggregates. In an n.m.r. study of xenon adsorbed on PtNaY[67] between four and eight platinum atoms were found per aggregate depending on the method of preparation. Electron microscopy had previously sugggested that the particle size was 1 nm corresponding to approximately 50 atoms.

Temperature programmed reduction (TPR) has been used to study the redox behaviour of copper ions in zeolites X and Y[68]. Two separate processes for the reduction of Cu^{2+} to Cu^{+} were identified in both CuY and CuX. These two processes have been attributed to the reduction of Cu^{2+} ions occupying sodalite and supercage sites. The method of TPR followed by temperature programmed oxidation has been used by Verdonck et al[55] to determine the metal particle size distribution of ruthenium in zeolite Y. Larger particles are oxidised at increasing temperatures. Ruthenium in the supercages (1.4 nm) was oxidised at room temperature while the oxidation of 2.0-4.0 nm clusters in crystal holes required temperatures in the range 423-623 K.

The activity of metal loaded zeolite catalysts depends to a large extent on pretreatment conditions and the optimum calcination temperature is related to the nature of the compensating cation. The platinum metal surface area in Y zeolites has been found to depend on the degassing procedure prior to reduction[35]. Initial treatment in air or oxygen results in an increased dispersion and determines the platinum surface area, A linear relationship exists between the surface area and the platinum catalytic activity. Coughlan et al[69] have observed a similar relationship for a series of ruthenium loaded zeolite catalysts. The turnover numbers for benzene hydrogenation were found to increase with increasing metal surface area and dispersion.

CHAPTER 2

Catalytic Reactions

In this thesis the isomerisation of n-butenes and methylcyclopropane over H-ZSM-23 and H-EU-1 and the isomerisation of 3,3-dimethylbut-1-ene and hydrogenolysis of alkanes over a series of ruthenium Y zeolites have been investigated to gain information on the nature of the reaction mechanisms. A general introduction to these reactions is presented in this chapter.

2.1. Isomerisation Reactions

2.1.1. n-Butene Isomerisation

The isomerisation of n-butenes has been the subject of many investigations. This reaction has a highly selective nature and does not require extreme conditions. Most of the reported results of n-butene isomerisation are concerned with the product distribution from the isomerisation of but-1-ene. This distribution is thought to be a potential guide to the reaction mechanism.

Bond and Wells[70] observed cis but-2-ene/trans but-2-ene product ratios of less than unity for but-1-ene isomerisation over metal catalysts and interpretated their results in terms of a radical mechanism in which the stability of the various adsorbed butyl radicals controlled the product ratio. It was calculated that cis/trans ratios should lie between 0.5 and 0.8 at temperatures below 423 K.

Haag and Pines[71] have demonstrated that but-1-ene isomerisation over sodium dispersed on alumina can be represented by a reversible first order reaction as follows:

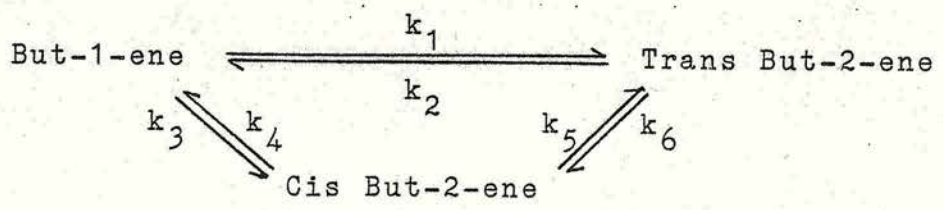

Cis/trans product ratios of greater than unity have been observed over basic oxides such as BaO[72], MgO[73], ZnO[74] and La_2O_3[75]. The prefential formation of cis but-2-ene from but-1-ene has been explained in terms of a carbanion mechanism in which initial abstraction of an allylic hydrogen from an adsorbed alkene species generates a π-allyl carbanion. Two species are possible: the syn and anti π-allyl which may convert via the σ-allyl. The anti configuration is more stable than the syn configuration and since either may be formed from but-1-ene while only the former may commute with cis but-2-ene and only the latter with trans but-2-ene high cis/trans ratios result (Figure 2.1). Studies by Chang et al[74] have observed π-allylic species over ZnO.

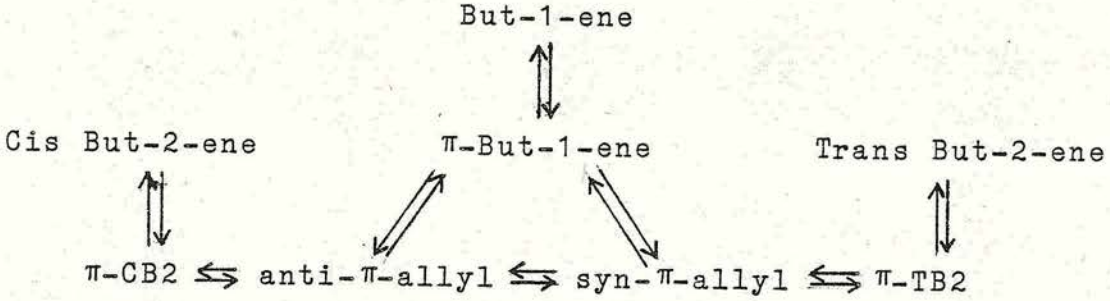

Figure 2.1. Carbanion Mechanism for But-1-ene Isomerisation

Over acid catalysts Turkevich and Smith[76] proposed a "hydrogen switch" mechanism for the n-butene isomerisation reaction in which the catalyst can act as both a donor and acceptor of protons. This mechanism, however, does not allow for direct cis-trans interconversion.

Haag and Pines[77] studied the isomerisation of n-butene over alumina and proposed a carbonium ion mechanism with a common intermediate, the secondary butyl carbonium ion, for double bond shift and cis-trans isomerisation. To account for the observed rate data it was suggested that the elimination of a proton from the carbonium ion proceeds through slow rearrangement to a pi-complex with subsequent rapid proton loss (Figure 2.2). The relative energies of the pi-complexes were of the following increasing order: cis but-2-ene > trans but-2-ene = but-1-ene.

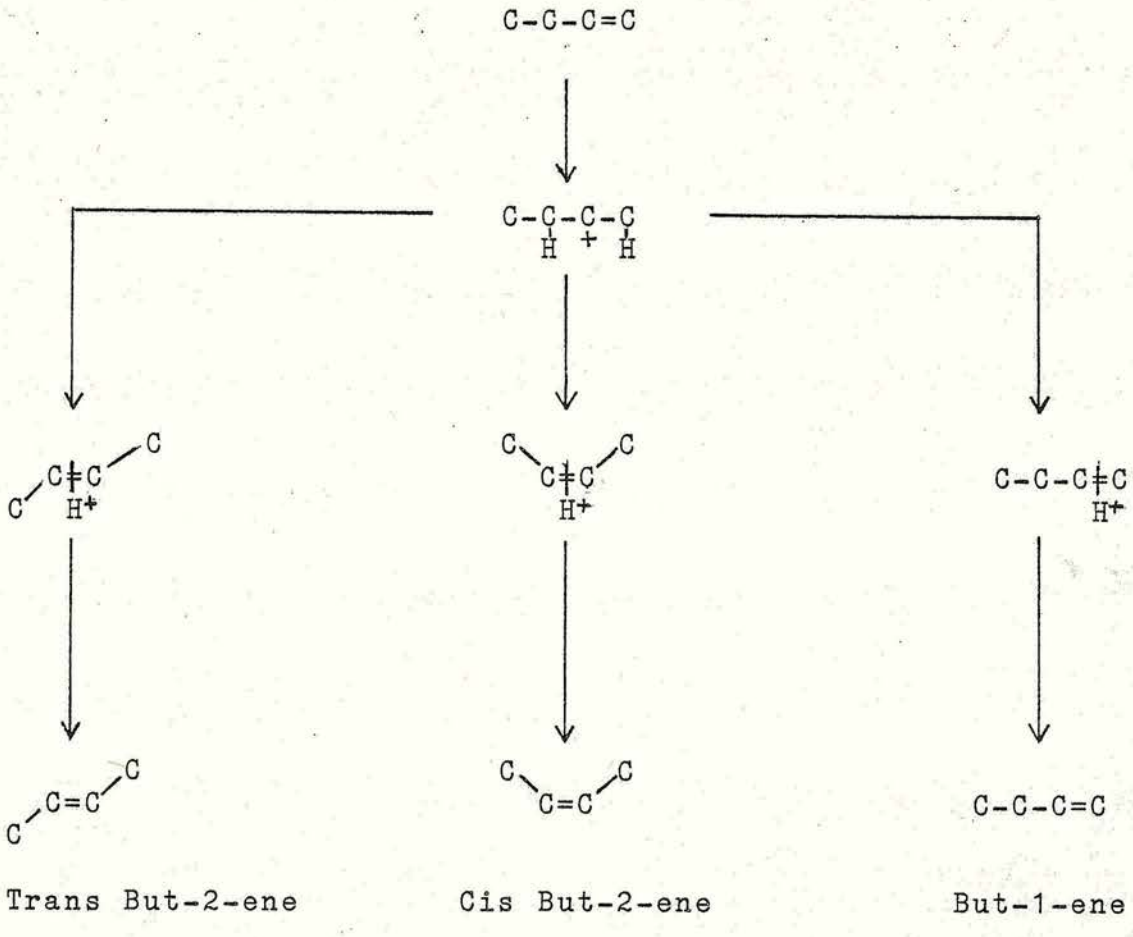

Figure 2.2. Loss of Proton from Secondary Butyl Carbonium Atom via a pi-Complex

Foster and Cvetanovic[78] attempted to correlate selectivity with catalyst type. Over basic catalysts they noted the initial exclusive formation of cis but-2-ene from but-1-ene and of but-1-ene from either cis or trans but-2-ene. In contrast over acid catalysts there was a less pronounced selective formation of cis but-2-ene from but-1-ene and initially exclusive cis-trans isomerisation rather than double bond shift. The authors proposed that a carbanion mechanism occurred

over basic catalysts and a carbonium mechanism over acid catalysts. The differences in the reaction course with cis and trans but-2-ene on acid and basic catalysts was attributed to a lack of rotation in the carbanion intermediate over basic catalysts.

In an investigation of the kinetics of n-butene isomerisation over silica-alumina, Hightower and Hall[79] found the reaction to be insensitive to temperature and silica-alumina ratio. The data were consistent with a mechanism which involved a common carbonium ion intermediate, the secondary butyl carbonium ion. Figure 2.3 illustrates the structure of the secondary butyl carbonium ion.

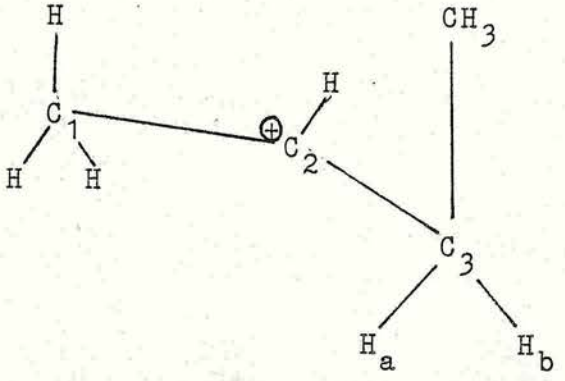

Figure 2.3. Secondary Butyl Carbonium Ion Intermediate Postulated by Hightower and Hall[79]

The C_1, C_2-H and C_3 atoms lie in a plane parallel to the surface. Due to steric interaction, the methyl group extends away from the catalyst and free rotation is inhibited about the C_2-C_3 bond whereas rotation about C_1-C_2 may occur more readily. The carbonium ion may be

formed from but-1-ene by proton addition at C_1 and subsequent proton removal leads to but-2-ene formation. The two hydrogen atoms (labelled a and b) are geometrically different and elimination of H_a or H_b gives cis but-2-ene or trans but-2-ene respectively. Since the two C_3-H bonds are energetically similar H_a and H_b have an equal chance of removal and temperature independent cis/trans ratios close to unity are predicted. The mechanism for but-1-ene isomerisation is illustrated in Figure 2.4.

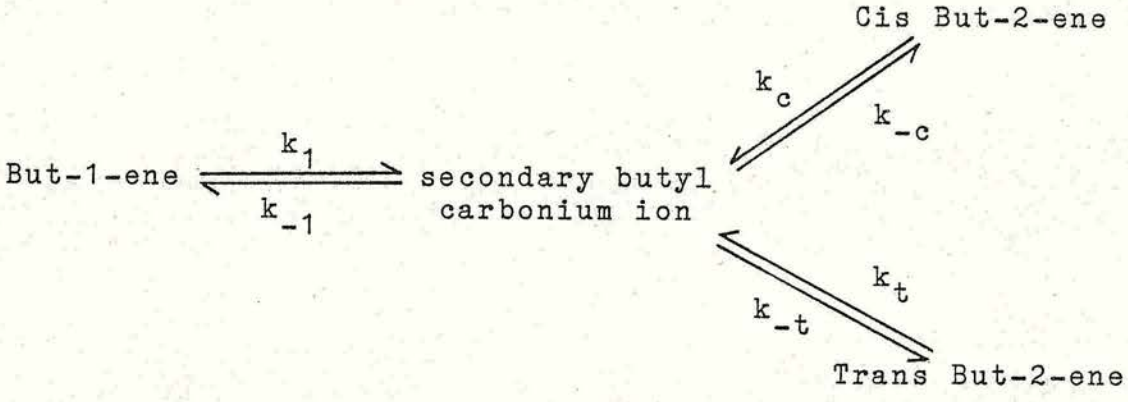

Figure 2.4. Carbonium Ion Mechanism for Butene Isomerisation involving the Secondary Butyl Carbonium Ion

Misono et al[80] have examined the correlation between the selectivity of butene isomerisation and the acid strength of the catalyst for a series of metal sulphates. The selectivity of cis-trans isomerisation and double bond migration from but-2-ene was found to change linearly with acid strength while the cis/trans

ratios from but-1-ene isomerisation were relatively insensitive to catalyst composition with values between 1.1 and 1.25. The cis but-2-ene/but-1-ene ratio was 1.8 for $MgSO_4$-SiO_2 but 10.1 for H_2SO_4-SiO_2. In a further study Misono and Yoneda[81] reported that differences in the energy barriers determined the selectivity and activity. With increasing acid strength an increase in the but-2-ene/but-1-ene ratio was found. This was attributed to a decrease in the height of the energy barrier of but-2-ene formation relative to that of but-1-ene formation. The results were interpreted on the basis of a carbonium mechanism with a common intermediate which become more stable and long lived as the acid strength of the catalyst increased.

Evidence for the formation of a strongly adsorbed polymeric residue on the surface of silica-alumina during contact with butene has been presented by Hightower and Hall[82]. Microcatalytic techniques indicated that only a small fraction of the protons on the surface were involved in the isomerisation. The data were explained on the basis of a common secondary butyl carbonium intermediate formed on induced proton sites in the residue. On alumina very little residue was formed and it could be displaced by subsequent slugs of butene. The rate determining step in both double bond shift and cis-trans isomerisation was found to involve C-H bond cleavage.

Ballivet et al[83] have reported the deactivation of silica-alumina on the introduction of cis but-2-ene and

have derived two independent rate laws to describe the deactivation process: a rapid irreversible adsorption on the Lewis sites and a much slower adsorption on the Bronsted acid sites. The action of poisoning reagents allowed the attribution of a known rate to a particular site.

The published literature on n-butene isomerisation over zeolites has shown that the data are consistent with the triangular reaction scheme suggested by Haag and Pines[71]. First order rate constants together with initial cis/trans ratios close to unity have been observed.

The activity of ammonium ion exchanged clinoptilolite has been found to increase with pretreatment temperature up to 723 K[84]. For each ammonium ion that decomposes an acidic hydroxyl group is formed in the lattice and at temperatures greater than 673 K dehydroxylation occurs resulting in the formation of Lewis acid sites. At pretreatment temperatures above 873 K lattice destruction begins and the selectivity of the catalyst changes with a rapid increase in the cis/trans product ratio. Poisoning experiments with ammonia and pyridine led the authors to conclude that the active sites for butene isomerisation were hydroxyl groups on the external surface. It was observed that potassium exchanged clinoptilolite had practically no activity for the interconversion of the n-butenes.

Lombardo et al[85] reported the variation in activity and selectivity for NaY modified by calcium exchange. As

the Ca^{2+} content (acidity) was increased cis-trans isomerisation of the but-2-ene was enhanced relative to double bond migration. The addition of a small amount of water was found to further increase the activity. Modification of the catalyst by exchange of potassium or lithium for sodium did not produce a significant change in the activity of the catalyst.

Using infra-red analysis and mass spectroscopic studies Weeks et al[86] have studied the isomerisation of but-1-ene over calcined ammonium Y zeolite. The rapid isomerisation of but-1-ene preceeded the formation of a saturated surface species whose formation was independent of zeolite hydroxyl concentration. In a further study on ammonium Y zeolites Jacobs et al[87] found a rapid initial decrease in conversion with reaction time followed by a much slower decrease until steady state conversion was reached. The results were processed according to the method of Ballivet[83]. The authors demonstrated that a preferential adsorption of but-2-ene caused deactivation of the zeolite. Changes in the initial activity for but-1-ene disappearance were found to parallel changes in the concentration of supercage hydroxyl groups. During the self-poisoning period most of the active hydroxyl groups were irrreversibly consumed. The concentration of residual hydroxyl groups was responsible for the continued activity.

Datka[88] found that the infra-red spectrum of but-1-ene adsorbed on NaY zeolite was similar to that observed for liquid but-1-ene while but-1-ene adsorbed on

NaHY with more than 40% of the sodium exchanged was hydrogen bonded to hydroxyl groups. Butenes adsorbed on NaHY were found to undergo oligomerisation, the rate being influenced by the concentration and acid strength of the hydroxyl groups. The rate of oligomerisation is fast until butene trimers are formed in the zeolite supercages. The product of butene oligomerisation was found not to be stable at temperatures higher than 373 K.

Results obtained by Cross et al[89] suggest that the preferential formation of trans but-2-ene from but-1-ene over nickel exchanged X zeolite was indicative of a mechanism involving radical intermediates. Experiments carried out in the presence of D_2, where the rate was enhanced and extensive exchange occurred, and D_2O, where the rate was reduced and little exchange occurred, were consistent with a radical rather than a carbonium ion mechanism.

In a review of the isomerisation data obtained on a range of X zeolites exchanged with transition metal ions Cross et al[90] found that on cerium X and the majority of samples cis/trans ratios close to unity consistent with a carbonium ion type mechanism were observed. The nickel and manganese exchanged zeolites had distinctly lower cis/trans ratios which were indicative of a radical mechanism. The reaction over zinc exchanged X was found to depend on the amount of exchanged Zn^{2+} and the cis/trans product ratios decreased with an increase in Zn^{2+} exchanged.

Hoser and Krzyzanowski[91] reported studies on cobalt

exchanged X zeolites. The authors found that the activity increased rapidly after exchange of sodium for cobalt had exceeded 28%. The cis/trans ratios obtained were typical of reactions proceeding in the presence of acid catalysts. However, the product ratios found in the isomerisation of cis but-2-ene showed a preferential double bond shift with respect to geometrical isomerisation. The authors suggested that this may be associated with the obstructed rotation of the carbonium ion in the pores of the zeolite lattice.

Microwave spectroscopy has been used by Dirringer and Fajula[92] to study the reaction of the n-butenes over deuterated mordenite and faujasite. Isomer ratios and deuterium content indicated a carbonium ion mechanism in which the secondary butyl carbonium ion rearranged via intermolecular shifts and the formation of protonated methylcyclopropanes on the zeolite surface before forming new molecules.

The isomerisation of n-butene was used by Tsuchiya et al[93] to compare the activities of H-Y and H-ZSM-5. The rates and activation energies of double bond migration over ZSM-5 catalyst did not differ greatly from those over H-Y catalyst. However, the rate constants and activation energies in cis/trans isomerisation over H-ZSM-5 were much smaller and higher than those over H-Y respectively. The difference in activity was considered to be due to supression of cis/trans isomerisation in the channels of H-ZSM-5 i.e. transition state selectivity.

2.1.2. 3,3-Dimethylbut-1-ene Isomerisation

The isomerisation of 3,3-dimethylbut-1-ene (I) has been studied over alumina by Haag and Pines [77,94] who postulated a carbonium ion mechanism. The isomerisation of I involves the formation of a secondary carbonium ion which rearranges to the more stable tertiary carbonium ion. The subsequent loss of H^+ from this species results in the formation of 2,3-dimethylbut-1-ene (II) and 2,3-dimethylbut-2-ene (III). The reaction scheme is illustrated in Figure 2.5.

A correlation between the extent of isomerisation and the acidity of the catalyst was reported by Pines and Haag[94]. On strongly acidic catalysts 2,3-dimethylbutene was found to be further isomerised to methylpentenes.

Whitmore's carbonium ion theory can also explain Figure 2.5[95]. An alkyl shift in a carbonium ion is thermodynamically favoured when the new ion is more stable (i.e. more substituted) and the shift from (a) to (b) should be easy. As an alkyl shift occurs at higher temperatures than proton addition or abstraction equlibrium ratios of II and III will be found.

The isomerisation of I over γ-alumina has been studied by Irvine et al[96]. The activity for isomerisation was found to increase with increasing catalyst activation temperature, pretreatment with hydrogen sulphide and the addition of fluoride. It was concluded that the skeletal isomerisation of I occurred via a carbonium ion intermediate on Bronsted acid centres. Initial product ratios were found to be greater

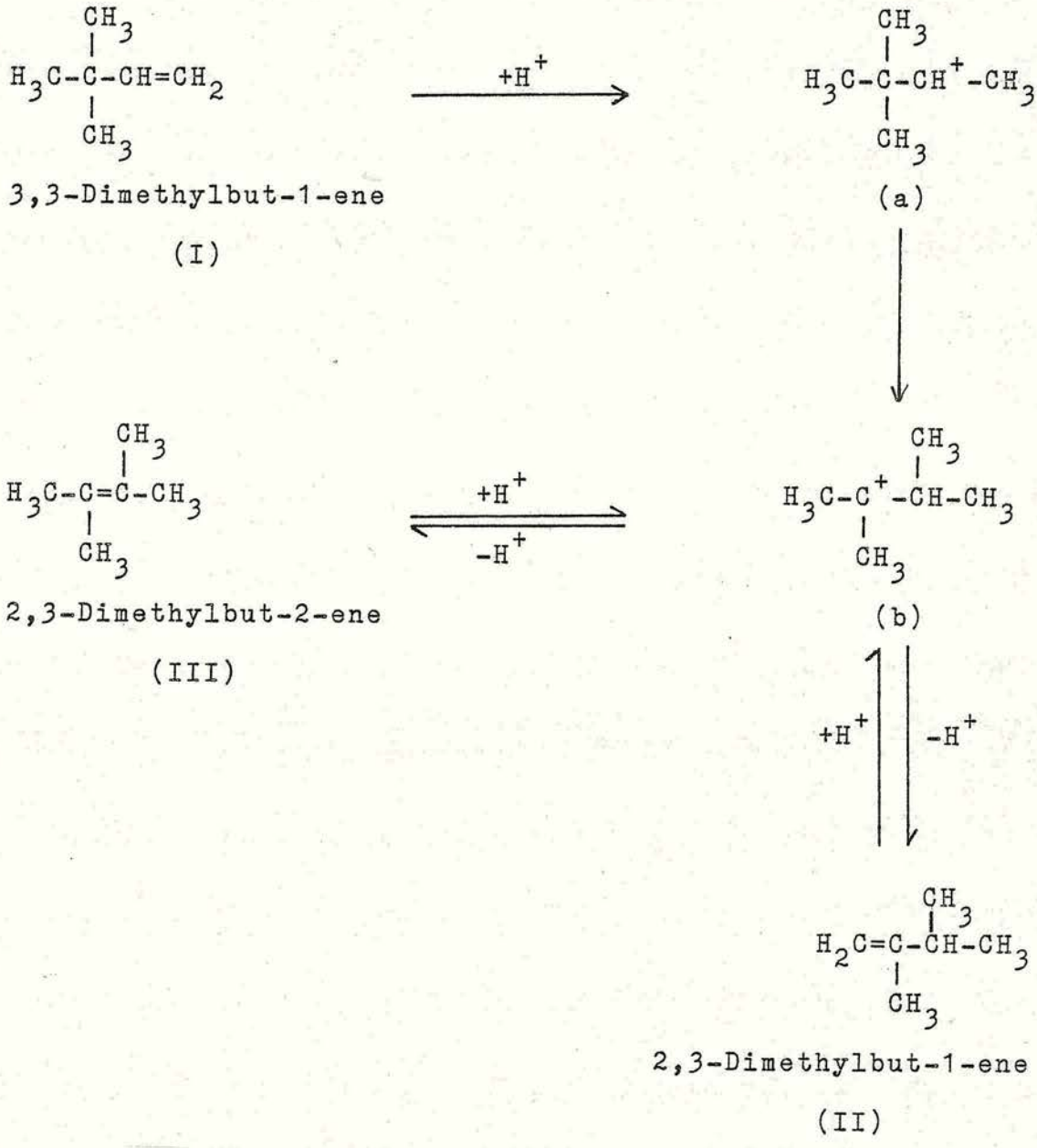

Figure 2.5. Isomerisation of 3,3-Dimethylbut-1-ene

than the expected equilibrium values and it was concluded that this was further evidence against a Lewis site mechanism.

The nature of the reactive intermediate formed on the catalyst surface has been studied by exchange reactions with deuterium or deuterium oxide[97,98]. On catalysts such as magnesium oxide which do not readily form carbonium ions, no isomerisation of I occurs and the main reaction is the exchange of the three vinyl hydrogen atoms of I rather than the exchange of the nine hydrogen atoms in the methyl groups[97]. MgO was found to facilitate a rapid interconversion of II and III at room temperature. However, II and III can be interconverted by mechanisms involving carbanions or radicals. MgO has been shown by Baird and Lunsford[73] to be an effective catalyst for the isomerisation of the n-butenes and the evidence suggested a carbanion mechanism. Thus the rapid interconversion of II and III on MgO was thought by Kemball et al[97] to occur by an allyl carbanion formed by loss of H^+ from either alkene.

Published literature on 3,3-dimethylbut-1-ene isomerisation over zeolites is confined to zeolites X[91,97-99] and Y[100]. The reaction scheme of Haag and Pines[77,94] (Figure 2.5) is thought to be operative in all cases.

Exchange reactions of I with deuterium oxide have been studied by Kemball et al[97] over Na^+, Ce^{3+}, Ni^{2+} and Ca^{2+} exchanged X zeolite. Extensive exchange of I occurred accompanied by isomerisation. For catalysts

giving rise to carbonium ions from I any or all of the twelve hydrogen atoms may be replaced simultaneously with isomerisation to form II and III if an adequate supply of deuterium is available as D^+. The activity of the zeolites showed a variation with the charge on the cations. The zeolites with divalent ions, CaX and NiX had similar activities but NaX was much less active.

Virtually no exchange of I with deuterium was observed over CaX, NaX and CeX[97]. In the case of NiX stepwise exchange of I with deuterium occurred as rapidly as the multiple exchange with deuterium oxide.

A study of the isomerisation of I over a series of copper exchanged X zeolites found the reaction to proceed via a carbonium ion intermediate[98]. Water was found to inhibit the isomerisation process and this was explained in terms of the formation of a copper aquo complex. The temperature ranges necessary to observe the exchange reaction of I and II with deuterium oxide over CuX were found to be similar to those required for isomerisation. The exchange reaction of I was multiple in character whereas stepwise exchange of II occurred. The isomerisation of I is promoted by deuterium oxide which provides a source of D^+. The secondary carbonium ion formed by the addition of D^+ to I rearranges to the more stable tertiary ion from which II and III are produced. Several interconversions take place between the alkenes II and III and the tertiary ion before desorption of the products in a multiply exchanged state with identical isotopic compositions[99].

The isomerisation reaction of I over copper exchanged Y zeolite produced II and III but also proceeded via disproportionation and self-hydrogenation to yield 2,3-dimethylbutane[100]. The authors proposed a model whereby two processes occured on exposure of Cu^{2+} zeolite to the alkene: (i) reduction of a copper ion to generate a Bronsted catalytic site and (ii) alkene isomerisation on these sites. The active site for alkene isomerisation was thought to be the proton produced when Cu^{2+} was reduced.

Hoser and Krzyzanowski[91] investigated the isomerisation of I over cobalt exchanged X zeolites pretreated at various temperatures. The catalytic activity was found to be affected by the degree of exchange and by the pretreatment temperature. The isomerisation of I was carried out at 348 K because with a higher degree of cobalt exchange, in addition to II and III, methylpentenes were also produced indicating strongly acidic sites. Catalysts pretreated at 473 K were more active than those having identical cobalt ion contents and pretreated at 673 K. It was postulated by the authors that the centres responsible for catalytic activity were hydroxyl groups formed by the cleavage of residual water molecules by tetrahedral-coordinated Co^{2+} ions e.g.

$$Co(OH_2)^{2+} \rightleftharpoons CoOH^{+} + H^{+}$$

New hydroxyl groups are formed by the addition of protons to lattice oxygen atoms.

2.1.3. Methylcyclopropane Isomerisation

Cyclopropane and its methyl-substituted derivatives are stable molecules which can thermally and catalytically isomerise with the opening of the cyclopropane ring to give a range of products. The ring opening of cyclopropane yields a single product, propane.

Larson et al[101] used deuterium in microcatalytic experiments to demonstrate that one hydrogen atom was exchanged intermolecularly during cyclopropane isomerisation over silica-alumina. The data were explained by either (a) a carbonium ion mechanism requiring a $C_3H_7^+$ (Bronsted site) intermediate surface complex or (b) a bimolecular hydride transfer mechanism involving a $C_3H_5^+$ (Lewis type) surface intermediate. The isomerisation of cyclopropane over deuterated sodium Y zeolite was investigated by Bartley et al[102] who concluded that both exchange and isomerisation proceeded via a non-classical protonated cyclic carbonium ion intermediate, in which the proton exists in the ring plane in a bridging position between two carbon atoms formed by the reaction between the Bronsted site on the catalyst and an adsorbed cyclopropane.

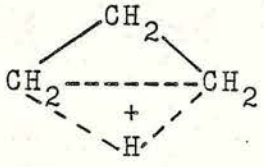

Infra-red and mass spectral evidence has indicated that when cyclopropane is passed over hydrogen Y zeolite at room temperature isobutane is formed as a major

product[103]. A mechanism for this transformation involving the formation of a non-classical carbonium ion which rearranges forming a methyl ion and ethene has been proposed e.g.

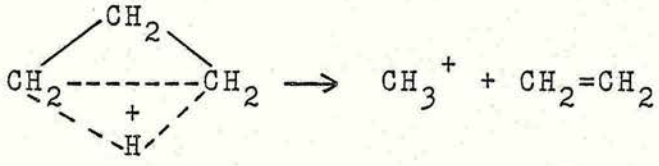

The methyl ion subsequently attacks another cyclopropane molecule forming a methylcyclopropane ion which rearranges to form isobutane.

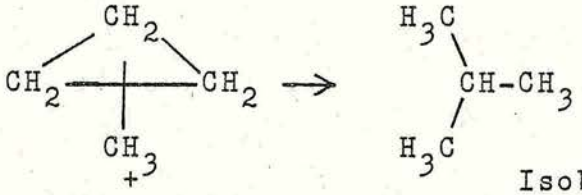

Isobutane

The isomerisation of methylcyclopropane (MCP) may occur with the formation of a carbonium, carbanion or radical intermediate. Loss or gain of a proton at various positions in the ring would result in an ionic intermediate the stability of which determines the product distribution. The order of stability for carbonium ions is tertiary > secondary > primary whereas for carbanions this order is reversed. The possible products resulting from a carbonium ion mechanism assuming that primary carbonium ions will not be formed are listed in Table 2.1.

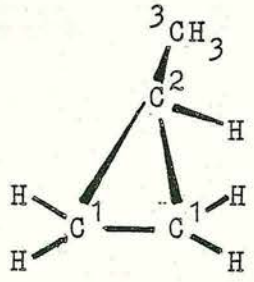

Type of Mechanism	Centre of Interaction with MCP	Products
H^- loss	1 2 3	n-butenes isobutene cyclobutane and/or but-1-ene
H^+ gain	1	n-butenes

Table 2.1. Possible Products Arising from a Carbonium Ion Mechanism in MCP Isomerisation

The only products observed from MCP isomerisation over silica-alumina were the n-butenes in the ratio:[104,105]

but-1-ene : cis but-2-ene : trans but-2-ene = 1 : 1 : 2.

The authors concluded that a proton addition mechanism was operative with a non-classical cyclopropyl carbonium ion intermediate.

MCP isomerisation has been studied over zeolite omega[106]. The absence of isobutane and cyclobutane in the products was indicative of a proton addition mechanism. A mechanism of this type involving the secondary butyl carbonium ion intermediate had been previously postulated for the interconversion of the n-butenes over zeolite omega. In the case of MCP isomerisation the product distribution was different (trans but-2-ene > but-1-ene > cis but-2-ene) from that

observed in n-butene isomerisation (trans but-2-ene > cis but-2-ene > but-1-ene) and was compatible with the non-classical cyclopropyl carbonium ion as intermediate.

2.2. Hydrogenolysis

Hydrogenolysis reactions of alkanes involve the cleavage of carbon-carbon bonds and the formation of carbon-hydrogen bonds. The reactions are exothermic and are catalysed by various transition metals. The simplest hydrocarbon hydrogenolysis reaction is that with ethane which yields methane as the sole reaction product. With larger molecules a range of reaction products is possible since the adsorbed reactant may fragment at more than one carbon-carbon bond. The distribution of primary hydrogenolysis products depends on the catalyst used. Two extremes of behaviour exist: total fragmentation of an adsorbed molecule to give methane as the only product or the rupture of only a single carbon-carbon bond in a reacting molecule.

A comparison of catalytic activities[107] of a range of metals for the hydrogenolysis of ethane under a standard set of reaction conditions gave the following activity sequence:-

Os > Ru > Ni > Rh > Ir > Re > Co > Fe > Cu > Pt ~ Pd

From the results of ethane hydrogenolysis it was concluded that the platinum and non-platinum metals showed different patterns of catalytic behaviour and that the activity sequence was related to electronic and

geometric factors. The increase in hydrogenolysis activity could be correlated with the percentage d character of the metal bond[108]. This concept was introduced in Paulings valence bond theory of metals to represent the extent of participation of d orbitals in the bonding between atoms in a metal lattice. The 4d metals (ruthenium, rhodium and palladium) and the 5d metals (osmium, iridium and platinum) gave a satisfactory correlation when the catalytic activity was related to the percentage d character. The activities for the non-platinum metals (iron, cobalt and nickel) were found not to vary with the percentage d character and were interpretated by introducing a geometric factor.

Kikuchi et al[109] studied the hydrogenolysis of n-pentane over a series of supported Group VIII transition metals and obtained the following sequence of activity:-

$$Ru > Rh > Pt > Ni > Co > Ir > Pd \sim Fe$$

The position of platinum in the activity series for n-pentane hydrogenolysis is somewhat higher than for ethane hydrogenoysis. A distinction between the platinum and non-platinum metals was also found to be evident in the cleavage modes of carbon-carbon bonds in n-pentane hydrogenolysis e.g. on the Group VIII platinum metals all the carbon-carbon bonds ruptured (on a statistical basis) while on nickel hydrogenolysis proceeded via successive demethylation at the terminal carbon-carbon bond of the adsorbed n-pentane.

Supported ruthenium has been used to study the

hydrogenolysis of the alkanes ethane[110], propane[110], butane[111,112], n-pentane[109], 2,2-dimethylpropane[113] and cyclopentane[114].

The hydrogenolysis of ethane and propane over supported ruthenium catalysts has been studied by Galvagno et al[110]. In propane hydrogenolysis, the ratio methane/ethane in the reaction products was found to be always greater than unity and was explained by considering the reaction scheme:-

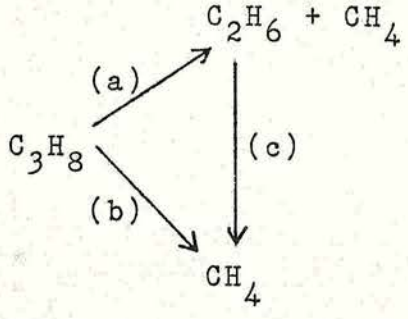

As the rate of hydrogenolysis of ethane was much lower than that of propane it was concluded that reaction (c) played no significant role in the reaction, and that propane hydrogenolysis takes place through two parallel reactions namely (a) and (b). The authors also found that no direct correlation between the catalytic activity and the extent of dispersion of ruthenium seemed to exist.

Methane formation has been found to predominate on ruthenium black and ruthenium supported on silica for n-butane hydrogenolysis[111]. In a further study Sarkany et al[112] concluded that in the hydrogenolysis of n-butane on ruthenium black the initial multiple rupture was a consequence of slow product desorption, the rate limiting step.

Kikuchi et al[109] found that for n-pentane hydrogenolysis multiple bond breaking (extensive degradation) occurred at low partial pressure of hydrogen while at high partial pressure of hydrogen the amounts of methane and ethane were equal respectively to those of butane and propane. At high partial pressure of hydrogen each carbon-carbon bond has about the same probability of being cracked i.e. hydrogenolysis is unselective with respect to bond type.

In a study of 2,2-dimethylpropane hydrogenolysis on supported metal catalysts containing Ru, Rh, Pd, Os, Ir, Pt and Au Boudart and Ptak[113] found ruthenium to be the most active metal and gold the least active. The order of activity was correlated with Paulings percentage d-bond character. Ir, Pt and Au were found to isomerise 2,2-dimethylpropane to 2-methylbutane.

In the hydrogenolysis of cyclopentane on silica supported ruthenium[114] the only observed products were methane and ethane. A mechanism for the hydrogenolysis was proposed:-

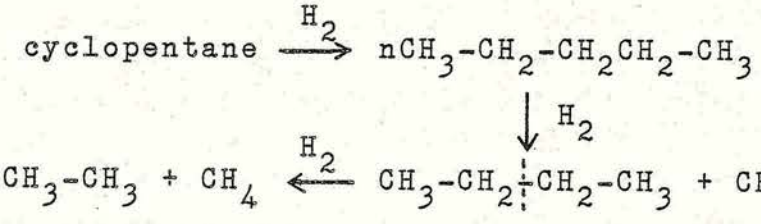

Few reports of alkane hydrogenolysis over zeolites exist in the literature. Sauvion et al[115] have studied the catalytic activity of metallic nickel particles dispersed in zeolite X for n-butane hydrogenolysis. Multiple bond rupture was found to occur giving

considerable yields of methane from both the hydrogenolysis of propane and of ethane. Metallic nickel particles with a diameter size of 1 nm located inside the supercages were found to be inactive or scarcely active while 2-3 nm diameter particles dispersed inside the lattice were active with an activity similar to that obtained using 2.5 nm diameter particles supported on silica.

CHAPTER 3

Experimental

3.1. Catalysts

3.1.1. H-ZSM-23

The H-ZSM-23 sample was initially synthesised as K-ZSM-23 zeolite by Dr. A. Araya, Edinburgh University.

When synthesised in the alkali metal form ZSM-23 is easily converted to the hydrogen form generally by intermediate formation of the ammonium form as a result of ammonium ion exchange and calcination of the ammonium ion to yield hydrogen.

The sample of K-ZSM-23 was calcined at 873 K for 16 hours in air and then at 1073 K for a further 4 hours to remove the organic cation. The sample was ion exchanged by overnight stirring in 50 ml of 1M NH_4Cl/g of sample. After exchange the sample was washed several times with distilled water and dried at 373 K for 2 hours. The sample was ground to a fine powder and calcined at 873 K overnight to give the hydrogen form.

Prior to use the sample was pelleted and the pellets crushed and sieved. The 250-500 μm fraction was used.

3.1.2. H-EU-1

Two samples of H-EU-1 were obtained from the New Science Group, Petrochemicals and Plastics Division, Imperial Chemical Industries PLC, Wilton. The samples were synthesised according to European Patent Application 0042226[7]. Prior to ion exchange the samples were calcined in static air at 723 K for 24 hours and then at

823 K for a further 24 hours. The hydrogen form of the EU-1 samples was prepared by ion exchange with Molar hydrochloric acid. Two 4 hour ion exchanges were carried out at 333 K using 50 ml of acid per gram of zeolite. The samples were supplied as fine white powders and prior to use the samples were pelleted, crushed and sieved. The 250-500 μm fraction was used.

3.1.3. Ruthenium Y

The three ruthenium Y samples used in this study were obtained from Dr. P.A. Jacobs, Centrum voor Oppervlakteschеikunde en Colloidale Scheikunde, K.U. Leuven, De Croylaan 42, B3030 Leuven (Heverlee), Belgium.

Sample (1) RuNaY20 was a NaY zeolite (4.2 meg.g exchange capacity) with 30% of the Na^+ ion exchanged with $[Ru(NH_3)_6]Cl_3$.[116]

Sample (2) RuNaLaY20 was NaY first exchanged with La(III) up to 70% followed by Ru exchange.[116]

Sample (3) RuLaY20 was first exchanged with La and then 20% exchanged with Ru.[116]

3.2. Chemicals

The nitrogen, air and hydrogen used in the gas chromatograph operation were obtained from the British Oxygen Company and required no further treatment.

But-1-ene, trans but-2-ene, cis but-2-ene, 2,2-dimethylpropane and n-butane were obtained from the Matheson Company as C.P. grade (99% pure) or research grade (99.9% pure). These gases were thoroughly degassed

prior to use by repeated cycles of freezing, pumping and thawing.

3,3-Dimethylbut-1-ene, 2,3-dimethylbut-1-ene and 2,3-dimethylbut-2-ene were supplied by Fluka A.G Chemicals with stated purities of greater than 99%. After purification, carried out as above, these liquids were stored in cold fingers fitted with Rotaflo teflon taps.

Cyclopentane, n-pentane, cyclohexane and n-hexane were obtained from B.D.H. Chemicals Ltd.

Methylcyclopropane was supplied by I.C.N. Pharmaceuticals Inc.

2,3-Dimethylbutane (99% pure) was obtained from Cambrian Chemicals Ltd.

o-Xylene and p-xylene (99% pure) were supplied by Imperial Chemical Industries P.L.C.

Methanol (AR grade) was obtained from Fisons Ltd.

The following compounds were used as potential poisons for the isomerisation of 3,3-dimethylbut-1-ene over the RuY catalysts employed in this study:-

(a) Water : demineralised water was degassed prior to use by repeated cycles of freezing, pumping and thawing.

(b) Acetone : acetone (AR) was obtained from Fisons Ltd.

(c) Ammonia : ammonia was supplied by the British Oxygen Company. Prior to use it was dried by repeated distillation from sodium metal.

The hydrogen used for the reduction of the RuY zeolites was purified by passage through a JMM hydrogen

diffusion unit and a liquid nitrogen trap. The purified hydrogen was stored in a glass bulb attached to the vacuum line.

3.3. Catalytic Experiments

3.3.1. Gas Handling and Reaction System

(a) Recirculating System with G.C. Analysis

The apparatus was constructed from Pyrex glassware and is represented schematically in Figure 3.1. A "U" shaped reaction vessel incorporating a ground glass sinter (porosity 1) was connected to the apparatus via Quickfit swivel joints. The swivel joints were lubricated with Apiezon "T" grease and were air cooled.

Two mercury diffusion pumps backed by rotary vacuum pumps were capable of evacuating the apparatus to approximately 133×10^{-6} Nm^{-2} (10^{-6} torr). Liquid nitrogen traps were used to prevent contamination of the system from the mercury diffusion pumps. The ground glass joints were all sealed with Apiezon "N" grease to maintain a high vacuum. The attainment of this high vacuum was confirmed prior to each experiment by means of a McLeod Gauge. A mercury manometer enabled pressures in excess of 133 Nm^{-2} (1 torr) to be measured.

A Metal Bellows Company pump was used to achieve recirculation of the gases through the catalyst bed. The flow rate could be altered by changing the voltage using a Variac and the resulting flow rate read on a flow meter incorporated in the line.

Figure 3.1. Recirculating Gas Handling System

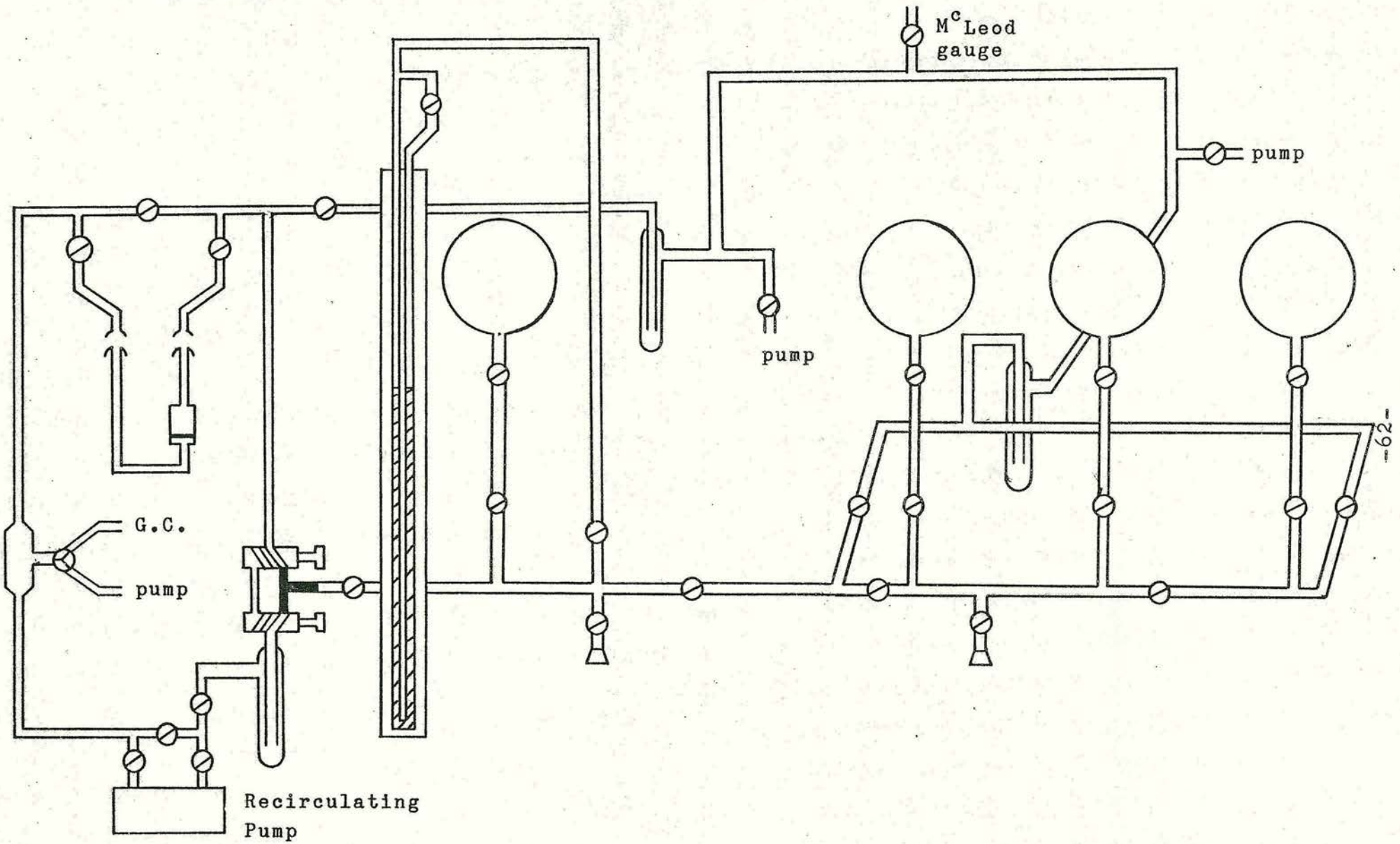

Close fitting silica furnaces were used to heat the catalyst samples. The temperature of the furnace was controlled by a thermocouple attached to a Eurotherm Temperature Controller. The precise temperature of the sample was measured by a second thermocouple placed down a pocket projecting into the catalyst bed. The sample temperature was measured by a Comark Digital Thermometer.

Once the gaseous reactant molecules had been introduced to the catalyst sample, samples of the gas phase were withdrawn at appropriate time intervals by manipulation of a three-way tap attached to a Carle Sampling Valve incorporating an evacuable sample loop. Analysis by gas chromatography followed. Each sample withdrew c.a. 2% of the gas phase present in the recirculating system at the time of sampling.

(b) Static System with G.C. Analysis.

The apparatus used in this study is shown in Figure 3.2. The reaction vessels used were constucted in Pyrex glass and attached to the vacuum line via a watercooled jacket. A vacuum of better than 133×10^{-6} Nm^{-2} was achieved by two rotary oil pumps supplying roughing vacuum to two glass three stage mercury diffusion pumps. Cold traps held at 77 K by liquid nitrogen were used to trap any volatile species and to prevent any back-diffusion of mercury vapour into the system.

Conventional high vacuum Springham taps lubricated with Apiezon "N" grease were used throughout the line. Prior to each catalytic experiment a M^{c}Leod Gauge was

Figure 3.2. Static Gas Handling System

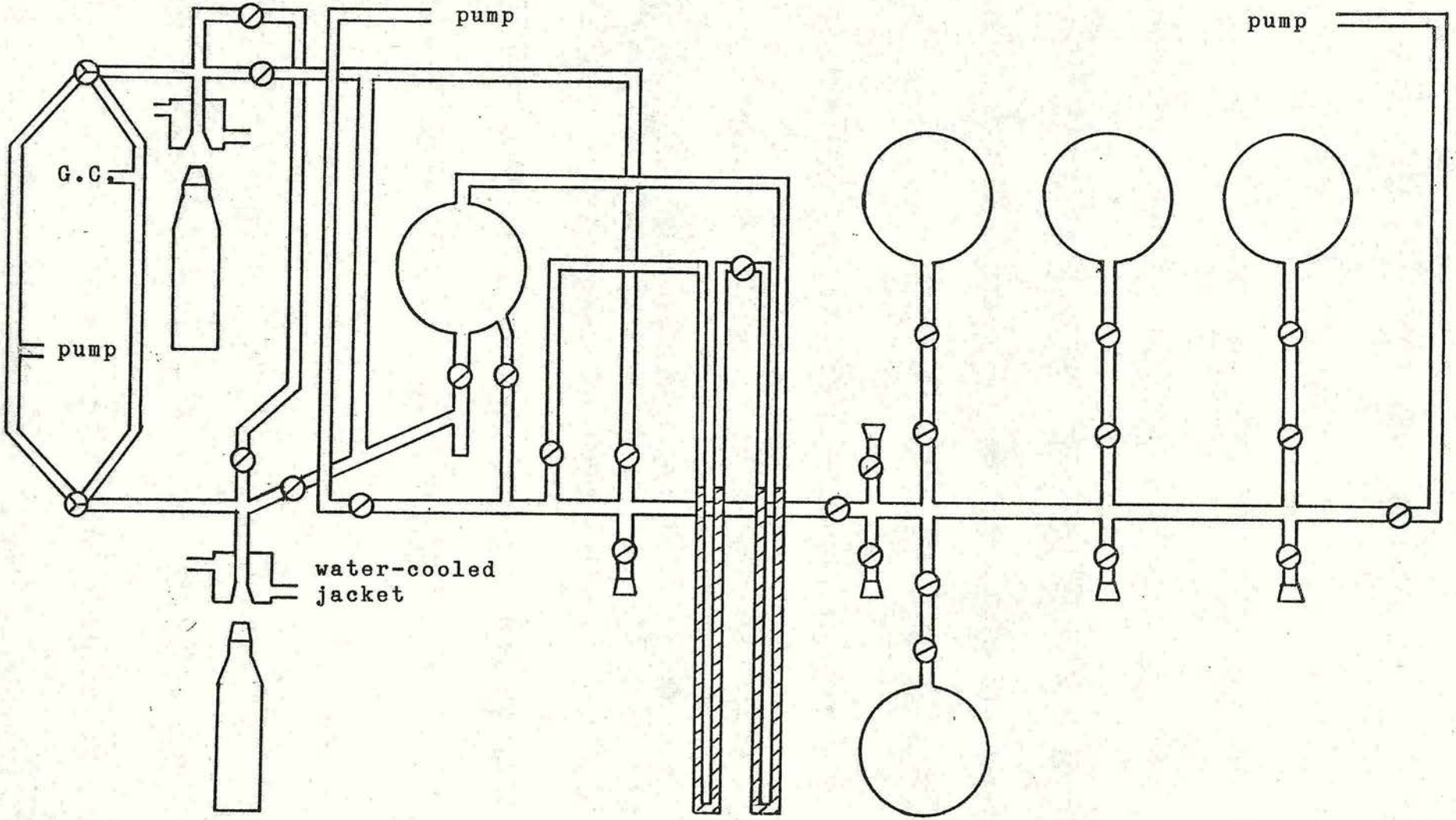

used to check that a satisfactory vacuum (less than 133×10^{-5} Nm^{-2}) had been established. All other gas measurements were made with a mercury manometer.

The apparatus, as illustrated in Figure 3.2 allowed two separate reaction vessels to be outgassed simultaneously (high temperature evacuation over a period of time) thus enabling two separate experiments to be conducted at any one time.

The catalyst samples were outgassed by means of a close fitting furnace controlled by a Eurotherm Temperature Controller. An accurate measure of the catalyst temperature was made by a thermocouple placed in close proximity to the catalyst sample via an inlet in each reaction vessel.

The reaction temperatures employed were achieved by furnace, "slush baths" or by water bath. The "slush baths" were formed by the semi-freezing of an appropriate organic solvent with liquid nitrogen. The constituents and resulting temperatures of these "slush baths" are given in Table 3.1.

Constituent of "Slush-Bath"	Temperature/K
p-Xylene	286
Cyclohexane	280
Aniline	266
o-Xylene	248
Arklone	237
Trichloromethane	209
Acetone/CO_2(solid)	195

Table 3.1. The Constituents of the Constant Temperature "Slush Baths" Employed in this Study.

Samples of the gas phase (c.a. 1%) were removed from the reaction vessel as required by manipulation of a three-way tap attached to a Carle sampling valve incorporating a 0.2 cm^3 evacuable sample loop, and analysed by gas chromatography.

3.3.2. Gas Chromatographic Apparatus

Samples of the gas removed from the reaction vessel were admitted to the chromatographic column by adjusting the sample valve. The single loop sampling valve configuration required two valve rotations (each at 60° to the normal) to complete the sampling cycle. The columns used to resolve reactant and products in the reactions studied are listed in Table 3.2. Optimum operating conditions are also tabulated. The resolved components were eluted to a hydrogen/air flame ionisation detector. The resulting signals were amplified by a

Reactant	Column(s)	Inlet Pressure/kNm^{-2}			Temp./K
		Air	H_2	N_2	
n-Butenes	4 m of 0.32 cm o.d. stainless steel loaded with bis-methoxy ethyl adipate (13.5%) and di-2-ethyl hexyl sebacate on 80/100 mesh chromosorb P	172	117	103	Ambient
MCP	50 m stainless steel capillary column coated with OV101 silicone oil	172	117	20	258
DMB's	4 m of 0.32 cm o.d. stainless steel loaded with 15% OV101 silicone oil on chromosorb W (80/100 mesh)	172	117	172	313
Alkanes	3 m of 0.32 cm o.d. stainless steel loaded with n-octane on porasil C	172	117	345	Ambient

Table 3.2. Chromatographic Columns and Conditions Used.

MCP = methylcyclopropane

DMB'S = dimethylbutenes

Perkin Elmer amplifier and parallel amplified signals supplied to a Servoscribe potentiometric chart recorder and a Hewlett Packard 3373B Integrator which converted the gas chromatographic signal into a digital form. The integrator measured the peak areas generated by the chromatographic detector and automatically printed the area in micro-volt seconds on pressure sensitive paper. The integrated peak areas were assigned to the various components of the gaseous mixture. Sensitivity factors were determined by preparation and analysis of standard mixtures of hydrocarbons. Correction of the observed peak areas by these factors enabled quantitative analysis to be accomplished.

3.3.3. Experimental Procedure

(a) Isomerisation of n-Butenes and Methylcyclopropane

Isomerisation reactions of the n-butenes and methylcyclopropane (MCP) were carried out on H-ZSM-23 and H-EU-1 using the recirculating system described previously in Section 3.3.1.

Typically, c.a. 0.04g of catalyst (particle size 250-500 μm) was placed in a clean, dry reaction vessel. The reaction vessel was attached to the gas handling system and slowly evacuated. The catalyst temperature was raised to the required activation temperature (of typically 723 K) and outgassed at this temperature under vacuum for 16 hours.

After outgassing the catalyst was cooled to the required reaction temperature. A known quantity of

reactant ($\sim 10^{21}$ molecules) was admitted to the recirculating section with the reaction vessel closed off. The recirculating pump was then switched on. The taps to the reaction vessel were opened and the flow rate adjusted to the required value.

The reaction was monitored by removing samples from the gas phase at regular intervals and analysing by gas chromatography. After use the reaction vessels were cleaned with liquid detergent, rinsed with distilled water and dried in an oven ($\sim$373 K).

(b) Isomerisation of 3,3-Dimethylbut-1-ene

Isomerisation reactions of 3,3-dimethylbut-1-ene were carried out on the three ruthenium Y zeolite samples. The reactions were carried out on the static line previously described in Section 3.3.1.

Typically c.a. 0.05g of catalyst was placed in the reaction vessel. The reaction vessel was attached to the gas handling system and slowly evacuated. The catalyst temperature was raised to the activation temperature of 573 K over a period of 90 minutes and the catalyst outgassed for a period of 16 hours under vacuum.

After outgassing the catalyst was cooled to room temperature. 180 torr ($\pm$5 torr) of hydrogen was admitted to the reaction vessel and the catalyst temperature raised to 573 K over a period of 90 minutes. On reaching 573 K, 30 minutes were allowed to elapse before evacuation of the reaction vessel for 100 minutes. On achievement of a good vacuum (better than 133×10^{-5} Nm^{-2}) the catalyst was cooled to the required

reaction temperature by means of the appropriate "slush bath".

A known quantity of reactant ($\sim 10^{19}$ molecules) was admitted to the reaction vessel and the reaction monitored by gas chromatography. The admission of the reactant into the reaction vessel marked the initial starting time of the analysed catalytic reaction.

(c) Hydrogenolysis Reactions of Alkanes

Alkane hydrogenolysis reactions were carried out on the three ruthenium Y samples using the static line described previously. The initial pre-treatment of outgassing and reduction were carried out as described in (b) above.

The reaction mixture consisted of a 10 : 1 ratio of hydrogen to alkane with a pressure of 580 Nm^{-2} of alkane in the reaction vessel corresponding to a charge of 2.44×10^{19} molecules. The gases were premixed for a minimum of 45 minutes before reaction. The reaction was monitored by gas chromatography.

3.3.4. Treatment of Data

Knowledge of peak areas for each component of the sample gas phase and the sensitivity factors of the analytical apparatus for each component allowed the percentage of the individual components of each sample to be calculated. By plotting a graph of percentage composition against time a reaction profile could be obtained.

(a) Isomerisation of n-Butenes and Methylcyclopropane

The rate of disappearance of but-1-ene was calculated assuming first order kinetics, the triangular scheme of

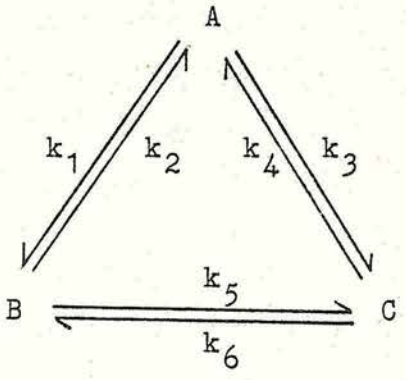

where A = But-1-ene

B = Trans but-2-ene

C = Cis but-2-ene.

was considered as

$$\text{But-1-ene} \xrightarrow{k} \text{Products}$$

The data are plotted according to the reversible first order rate equation.

$$\ln(x-x_e) = -kt + \ln(a-x_e) \qquad \text{Equation 3.1.}$$

where a = Initial concentration of reactant

x = Percentage of reactant at time t

x_e = Percentage of reactant at equilibrium.

The isomerisation of methylcyclopropane involves an irreversible ring-opening step and the data are plotted according to the first order rate equation,

$$\ln x = -kt + \ln a \qquad \text{Equation 3.2.}$$

where a = Initial concentration of methylcyclopropane

x = Concentration of methylcyclopropane at time t.

(b) Isomerisation of 3,3-Dimethylbut-1-ene

From the reversible first order equation (Equation 3.1) the rate of disappearance of 3,3-dimethylbut-1-ene could be found.

Kilpatrick et al[117] have calculated the equilibrium data for C_6 alkenes. The value of x_e for 3,3-dimethylbut-1-ene was very small compared to x and it was found that it could be neglected without significantly affecting the accuracy of the results.

(c) Hydrogenolysis Reactions of Alkanes

It was found to be more informative to express the hydrogenolysis product distributions in terms of the total carbon in the sample associated with each product. The integral for each peak was multiplied by its respective sensitivity to express the value in terms of moles. This value was then corrected for the number of carbons present to give a value expressed in terms of reactant equivalents and this could then be expressed in terms of percentage of total carbon in the sample. In addition, mole per mole values were required for the calculation of initial product distributions. Mole per mole values are defined as the number of moles of product produced per mole of alkane reacted.

Initial rates were calculated by taking the tangent to the curve from a plot of percent versus time. The rate constants obtained were adjusted to allow for any slight variation in the weight of catalyst and quantity of alkane introduced into the reaction vessel and the resulting k expressed in units of molecules^{-1} s^{-1} g^{-1}.

Initial product distributions were calculated by plotting the mole per mole values against mole per mole alkane reacted (i.e. 100 - mole per mole alkane) and taking the gradients as the initial product distribution.

(d) Calculation of the Apparent Activation Energy

The value of the first order rate constant at different reaction temperatures can be related to the apparent activation energy by the Arrhenius equation.

$$\ln k = \ln A - E_a/RT \qquad \text{Equation 3.3.}$$

where k = Rate constant

A = Frequency factor

E_a = Activation energy

R = Universal gas constant

T = Temperature/K

Thus a plot of lnk against 1/T has a gradient of $-E_a/R$. The apparent activation energy can thus be established.

3.4. Adsorption Experiments

The adsorption of gases by the use of a microbalance has been described by several authors[118,119]. Its facility for measuring rapid changes of sample weight directly is of great advantage in adsorption studies.

3.4.1. Apparatus

(a) The Balance

A Cahn RG Automatic Electrobalance with a maximum

sensitivity of 1 x 10^{-4}g was used in this study. The balance operates on the null-balance principle and is illustrated in Figure 3.3. When the sample weight changes, the beam tends to deflect momentarily; the attached flag moves correspondingly altering the amount of light to the phototube and hence the phototube current. A two-stage servo amplifier amplifies this current which is then applied to a coil attached to the beam. The coil is in a magnetic field, and acts like a d.c. motor exerting a force to restore the beam to its original balance position.

The restoring current and the voltage which it develops across the coil are directly proportional to the change in sample weight. A known, accurately calibrated voltage across the coil must be subtracted using a potentiometer to allow accurate display on a recorder. A dial (the mass dial) on the potentiometer is calibrated directly in milligrams corresponding to the amount of voltage being subtracted. The excess coil voltage is then applied to a Servoscribe Potentiometric chart recorder. Various weight ranges can be displayed on the recorder by attenuating the voltage.

The zeolite sample was placed in a specially constructed Pyrex glass bucket with a nichrome wire handle. The sample bucket was suspended from loop A by a nichrome hang-down wire. The maximum sample load which could be suspended was 1g. A counter weight consisting of small pieces of metal placed in a similar Pyrex glass bucket was suspended from loop C by a hang-down wire.

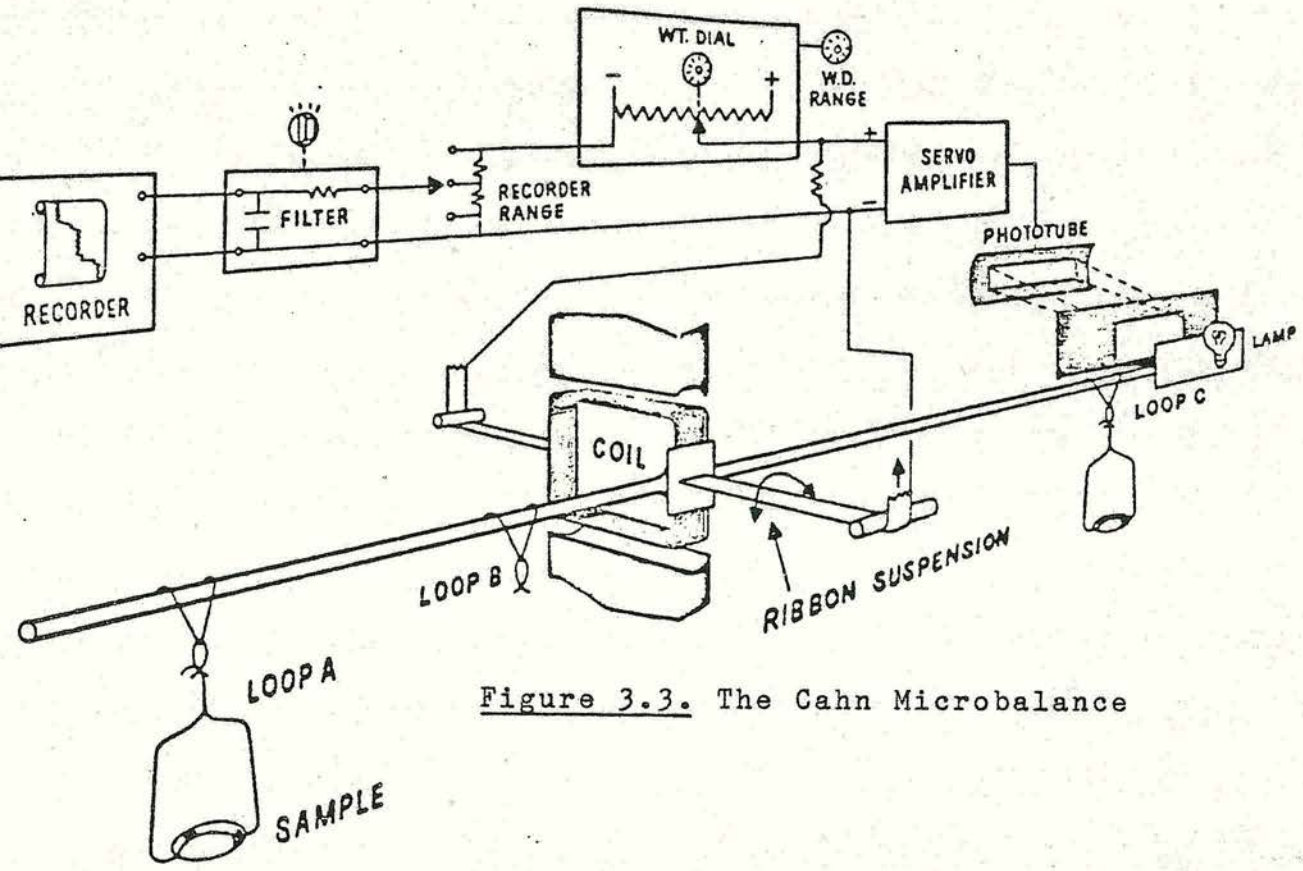

Figure 3.3. The Cahn Microbalance

Figure 3.4. The Vacuum bottle in which the balance is placed

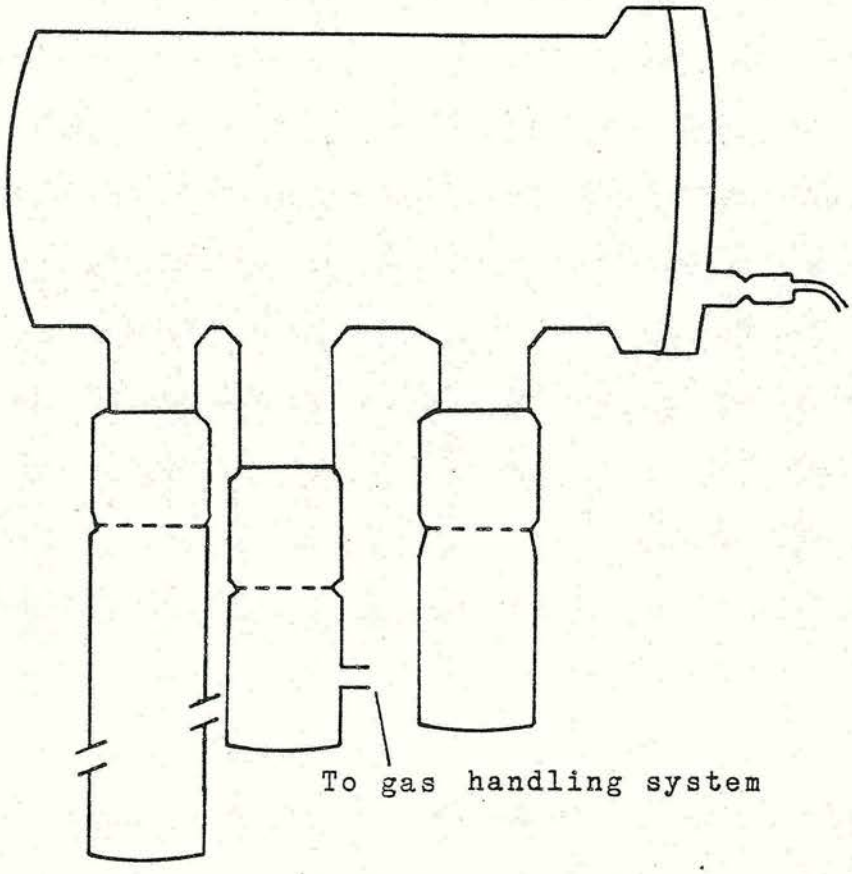

A large vacuum bottle (Figure 3.4) was used to house the electrobalance. The electrical connecting cable was accomodated on a metal cap which was clamped in position with springs. A Viton O-ring and high vacuum silicone grease provided a vacuum seal. The hang-down wires of the sample and counter weight passed through ground glass joints into attached cylindrical adsorption vessels. The balance chamber was connected to the vacuum line via a third joint.

(b) The Vacuum Line

The apparatus used comprised of a gas handling section and an adsorption section. The gas handling apparatus, illustrated schematically in Figure 3.5 was constructed of Pyrex glass. High vacuum Springham greaseless taps were used throughout the line. The vacuum was measured using a M^{c}Leod gauge. All other gas measurements were made with a mercury manometer. The hydrocarbons to be studied were stored in ampoules with attached glass bulbs and were admitted to the main apparatus by the manipulation of the taps. The gas handling apparatus was connected to the adsorption chamber via Pyrex tubing.

The adsorption section consisted of the vacuum bottle housing the balance and the hang-down tubes attached to it. To facilitate easy removal the hang-down tube containing the sample bucket and its suspension wire was in two sections. The lower section which was subjected to high temperatures during sample outgassing was constructed of silica. The upper Pyrex section had a

Figure 3.5. Gas Handling Apparatus for Adsorption Studies

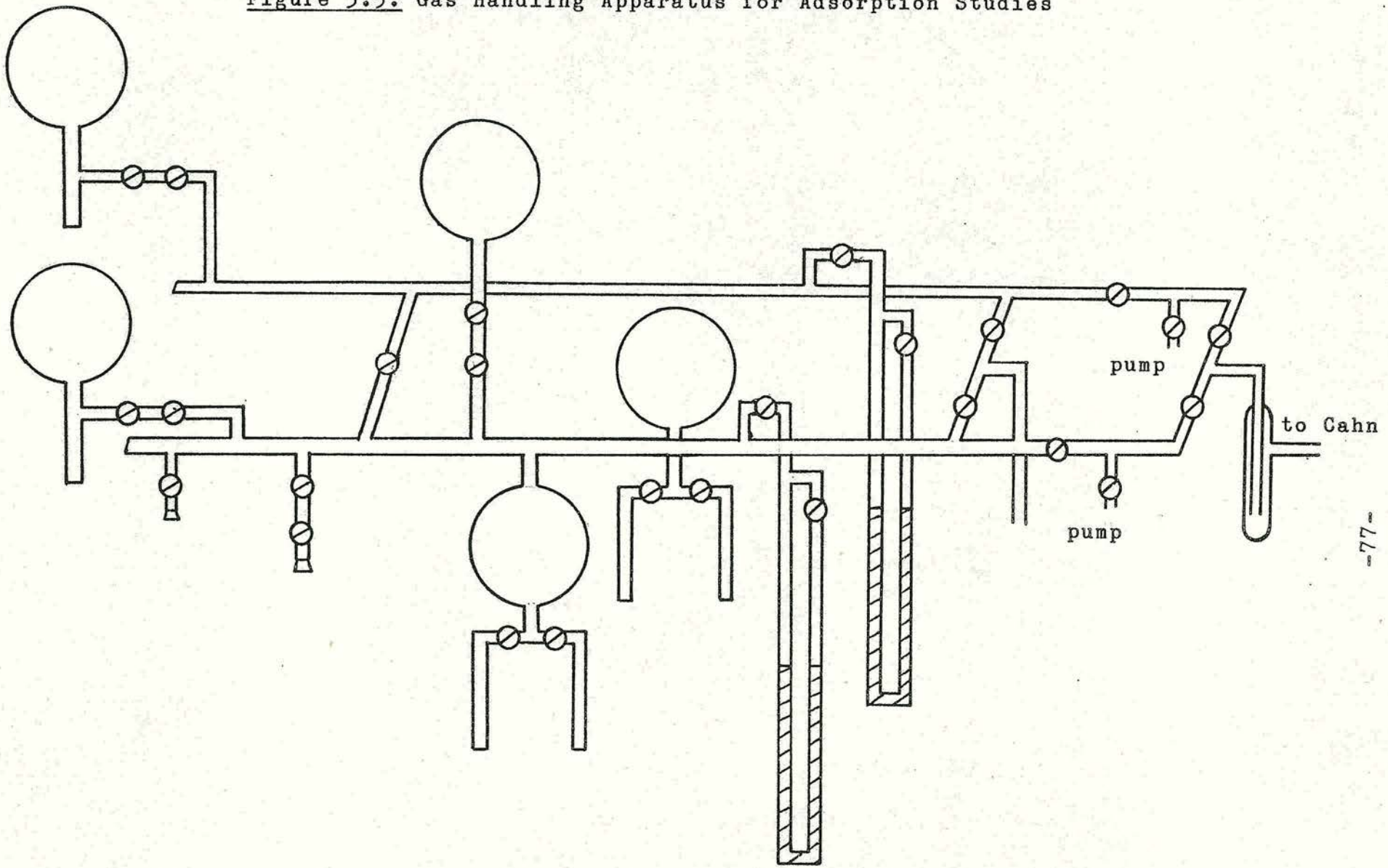

graded seal at its lower end and was joined to the lower section by a ground silica joint lubricated with Apiezon "T" grease.

Vacuum of 133×10^{-6} Nm^{-2} was achieved in the gas handling and adsorption apparatus by the use of two rotary oil pumps supplying roughing vacuum to two glass three-stage mercury diffusion pumps.

The sample was outgassed by the use of a close fitting furnace. The temperature of the furnace was controlled by a thermocouple linked to a Stanton Redcroft Linear Temperature Programmer incorporating a Eurotherm unit. Accurate determination of the sample temperature was achieved by placing another thermocouple, connected to a digital thermometer, down a silica pocket in the adsorption vessel to a position level with the sample.

The temperature range for meaningful adsorption data is limited to that where neither condensation nor reaction occurs. In the butene absorption systems studied the possible occurence of reactions at low temperature necessitated the use of "slush baths" whose preparation is described in Section 3.3.1. The temperature of the sample was taken to be the same as that of the bath after the adsorption vessel had been immersed for periods in excess of one hour

3.4.2. Procedure

Before use, the balance was calibrated according to the manufacturer's instructions using accurately standardised weights. A sample weight of 0.04g was used,

counterbalanced by a suitable substitution weight. The precise weight of the sample could be determined by summation of the mass dial value, the recorder deflection and the substitution weight.

The adsorption section of the apparatus was evacuated. To avoid "spurting" of the sample and to mimimise disturbance of the balance system, it was necessary to remove and admit gases slowly.

Preliminary experiments found that on removal of the furnace and cooling there was a weight gain of c.a. 0.5 mg. This "gettering" was found to be neither linear with time nor reproducible. However, it was found that reproducable adsorption results could be obtained if the initial sample weight was that taken after cooling to the required adsorption temperature.

The gravimetric arrangement used allowed a continuous recording of sample weight with time and enabled rates of adsorption to be measured for different adsorbates. In addition, adsorption isotherms could be carried out by admitting successive doses of adsorbate to the adsorption section and recording the equilibrium weight and the equilibrium pressure.

The basic pattern of the adsorption experiments involved regeneration of the sample after the adsorption run by outgassing at elevated temperatures (H-ZSM-23 ; 873 K, H-EU-1 ; 823 K) and treatment with oxygen for a minimum of 60 minutes. The original weight of the sample was restored and good reproducibility ($\pm 3\%$) was observed.

3.4.3. Treatment of Results

During adsorption or desorption, the recorder trace shows the variation of sample weight with time and thus gives a measure of the rate of adsorption. It is possible to distinguish between adsorption on the external surface only, rapid sorption into the pores and diffusion controlled sorption. When the rate controlling process in the adsorption of a gas is diffusion then the process may be described according to Equation 1.1. Based on this equation a plot of the amount adsorbed versus $t^{0.5}$ should yield a straight line although a foot resulting from very rapid adsorption occuring on the external surface of the zeolite may occur near the start of adsorption.

The application of the Langmuir equation as expressed in Equation 3.4 enabled the volume of a monolayer of gas required to cover the surface (V_m) to be established.

$$\frac{P}{V} = \frac{P}{V_m} + \frac{1}{V_m b} \qquad \text{Equation 3.4.}$$

where V = Quantity adsorbed at pressure P

V_m = Volume of a monolayer

b = Langmuir constant.

A plot of P/V versus P yields a straight line with slope of $1/V_m$.

3.5. Other Techniques

3.5.1. Surface Area Measurements

The surface areas of the zeolite samples studied were determined by nitrogen adsorption at 77 K in a constant volume apparatus. A measured volume of gas was admitted to the sample and after equilibrium had been established the residual pressure was measured and the amount of gas remaining in the gas phase calculated. The difference in these two quantities corresponds to the volume of adsorbate adsorbed. The results are plotted according to the B.E.T. equation (Equation 3.5).

$$\frac{P}{V(P_0-P)} = \frac{1}{V_m C(T)} + \frac{(C(T)-1)P}{V_m C(T) P_0} \qquad \text{Equation 3.5.}$$

where P = Equilibrium adsorbate gas pressure at the isotherm temperature

V = Volume of gas adsorbed at pressure P

P_0 = Saturated vapour pressure of the adsorbate at the isotherm temperature

V_m = Volume of gas corresponding to monolayer coverage of the surface

$C(T) \propto \exp(\Delta H_{ads} - \Delta H_{liq})/RT$

A plot of $P/V(P-P_0)$ versus the relative pressure P/P_0 should give a straight line of slope $S = C(T)-1/V_m C(T)$ and intercept $I = 1/V_m C(T)$ such that $V_m = 1/S+I$.

The required surface area of the catalyst can be easily calculated from V_m provided that the cross-sectional area of the adsorbate molecule is known.

The area of the catalyst sample A (m^2) is given by

$$A = \frac{V_m \times N_A \times A_m}{22.4 \times 10^{-3}} \qquad \text{Equation 3.6.}$$

where N_A = Avogadro's constant

V_m = Volume of gas corresponding to monolayer coverage

A_m = Molecular cross-sectional area of the adsorbate.

so that the area of 1g of sample (specific surface area) is given by A/X ($m^2 g^{-1}$) if the weight of sample used is Xg.

3.5.2. X-Ray Diffraction

X-Ray diffraction traces were obtained using a Phillips PW 1050/80 powder diffractometer (fitted with an automatic sample changer) utilising CuKα radiation.

3.5.3. Scanning Electron Microsopy

Scanning electron micrographs of ZSM-23 were obtained by the use of a Cambridge Stereoscan 604 fitted with a Practica L2 camera.

The details of scanning electron micrographs of EU-1 were kindly supplied by I.C.I.

3.5.4. Temperature Programmed Reduction

The technique of temperature programmed reduction (TPR) in which the uptake of hydrogen is monitored as the

temperature of a catalyst sample is raised has been shown[120] to be capable of yielding information about the extent of catalyst reduction, the mutual interaction of metals in a multimetallic catalyst and the nature of any metal-support interaction.

A weighed amount of sample (typically 50 mg) was placed in the TPR reactor and connected to the apparatus. Before the actual TPR measurement it was possible to subject the sample to a variety of pretreatments using a gas handling system and furnace. The reducing gas consisted of 5% vol. hydrogen in argon. Prior to use the gas was purified by passage through a deoxygenation catalyst and a bed of molecular sieve to remove water. The gas stream was passed through one arm of a Perkin Elmer type F33 thermal conductivity detector, through the reactor and finally via a solid CO_2/ethanol bath through the second arm of the thermal conductivity detector where any change in the hydrogen concentration was monitored. The flow rate of the reducing gas was 10 ml min^{-1}. The change in hydrogen concentration with time and temperature was displayed on a Kipp and Zonen BD9 two channel chart recorder. Since the gas flow is constant, the change in hydrogen concentration is proportional to the rate of reduction. Distinct reduction processes in the sample show up as peaks in the TPR spectrum. The total consumption of hydrogen was determined as the area under the TPR spectrum.

The temperature of the catalyst was recorded by means of a thermocouple inserted into a pocket in the

catalyst bed used in conjunction with a Comark digital thermometer. A second thermocouple linked to a Stanton Redcroft temperature programmer controlled the temperature of the furnace. A heating rate of 10 K min^{-1} was used.

Prior to use the reduction of bulk Ni_2O was used to quantify the hydrogen uptake.

3.5.5. X-Ray Fluorescence Spectroscopy

The composition of the zeolite samples used in this study were obtained by X-ray fluoresence spectroscopy. The analysis for ZSM-23 was kindly carried out by Dr. A. Araya and for H-EU-1 by I.C.I.

CHAPTER 4

Results and Discussion:- Part I

Characterisation of the Zeolites

4.1. Nature of the Catalysts H-ZSM-23 and H-EU-1

4.1.1. Chemical Analysis

(a) H-ZSM-23

ZSM-23 is a high silica zeolite which has been found to have smaller pore openings than ZSM-5, ZSM-11 or ZSM-12 and larger than those of erionite or zeolite ZK-5[146]. ZSM-23 has a composition expressed in terms of mole ratios of oxides, and in the anhydrous state of

$(0.7\text{-}2.8)R_2O : (0.08\text{-}0.25)M_2O : Al_2O_3 : (50\text{-}220)SiO_2$

where R is a nitrogen containing cation and M is an alkali metal especially sodium[6].

The results of the chemical analysis by X-ray fluorescence spectroscopy of the as "synthesised" ZSM-23 are given in Table 4.1.

Composition	W/W
Na_2O	0.015
Al_2O_3	1.30
SiO_2	37.8
K_2O	0.21

Table 4.1. Chemical Analysis of ZSM-23 by X-ray Fluorescence Spectroscopy

From the data in Table 4.1. the sample of as synthesised ZSM-23 has a composition in the anhydrous state of

$$56SiO_2 . Al_2O_3 . 0.11K_2O . 0.01Na_2O.$$

(b) H-EU-1

EU-1 is a novel high silica zeolite which is crystallised from reaction mixtures containing the bis-quaternary ammonium ion, hexamethonium (hexane-1,6-bis(trimethylammonium))[121].

Zeolite EU-1 is formed in the system,

$$SiO_2\text{-}Al_2O_3\text{-}Na_2O\text{-HEX } X_2\text{-}H_2O$$

where HEX = $[(CH_3)_3N\text{-}(CH_2)_6\text{-}N(CH_3)_3]^{2+}$ and X represents a halide ion. The samples used in this study were synthesised using hexamethonium bromide.

EU-1 can only be formed from reaction mixtures with SiO_2/Al_2O_3 ratios of 30-60 unless other reaction parameters are also changed[122]. On increasing the SiO_2/Al_2O_3 ratio to 120 another zeolite, EU-2, is formed along with EU-1. Further reductions in the aluminium content of the mixture result in the formation of pure EU-2 at an SiO_2/Al_2O_3 ratio of 300/1. The range of SiO_2/Al_2O_3 ratios from which EU-1 may be crystallised may be extended by the addition of crystalline material to the reaction mixture so that it constitutes about 5% (w/w) of the solid silica[121].

Table 4.2 lists the chemical analysis of the two samples of EU-1 in the hydrogen form, used in this study. In the table and in subsequent chapters the two samples of H-EU-1 are referred to as H-EU-1(A) and H-EU-1(B).

Catalyst Sample	SiO_2/Al_2O_3	Na_2O	Residual Carbon %[a]
H-EU-1(A)	34	0.001	c.a. 1.25
H-EU-I(B)	49.6	0.002	c.a. 1.5

[a] Determined by thermal gravimetric analysis (ICI)

Table 4.2 Composition of H-EU-1 Samples

The experimental Si/Al ratios of the zeolites studied together with listed literature values of these and other commonly used zeolites are shown in Table 4.3.

Zeolite	Si/Al (experimental)	Si/Al (literature)
ZSM23	56	25-110[4]
H-EU-1(A)	34	30-60[122]
H-EU-1(B)	49.6	30-60[122]
ZSM-5		20-8000[123]
ZSM-11		10-45[123]
Zeolite X		1-1.5[12]
Zeolite Y		1.5-3.0[12]

Table 4.3. Si/Al Ratios of some Zeolites

It is evident from the data in Table 4.3 that the zeolites EU-1 and ZSM-23 studied in this thesis have

similar Si/Al ratios; all of which are significantly higher than those of the commonly used zeolites X and Y. As the Si/Al ratio is increased the thermal stability, hydrothermal stability and acid stability increases. The composition of the zeolite framework (Si/Al) has a significant effect on the sorptive properties of the zeolite. With an increase in the Si/Al ratio the cation density and electrostatic field strengths decrease and the affinity of the zeolite surface for non-polar sorbates increases (against polar sorbates). While aluminium-rich zeolites sorb water in preference to hydrocarbons the converse is true for silica-rich zeolites.

4.1.2. X-Ray Diffraction

The technique of X-ray diffraction is based on Bragg's Law which takes the form of the equation

$$n\lambda = 2d\sin\theta$$

which relates the wavelength of the radiation (λ) to the angle of incidence (θ) and the distance (d) between the Bragg planes. Thus when X-rays impinge upon a crystalline material they give rise to a series of reflections - the diffraction pattern.

Since most synthetic zeolites have crystals smaller than that required for single crystal X-ray studies (minimum 75 μm), X-ray powder diffraction patterns are obtained. While each zeolite has a particular pattern it can be altered slightly by the framework compostion, the degree of hydration and by ion exchange.

X-ray powder diffraction traces of H-ZSM-23, H-EU-1(A) and H-EU-1(B) are shown in Figure 4.1-3. Diffraction analyses of the zeolites before and after pretreatment enabled their crystallinity to be assessed in a qualitative manner.

(a) H-ZSM-23

The relative intensities of the peaks and the observed d-spacings (calculated from the diffraction traces using the Bragg equation) were in good agreement with the literature values[6]. The broadening of the peaks is due to the small crystal size. Samples pretreated at elevated temperatures displayed traces in which little structural collapse was evident. This is illustrated in Figure 4.1 which compares the diffraction traces obtained from H-ZSM-23 and a sample outgassed at 723 K for 16 hours. The relative intensities for the outgassed sample were found to be altered slightly. The angles, however, were not altered. Since the angles at which the peaks are observed depend only on the size and shape of the unit cell whereas their relative intensities depend on unit cell contents, the slight alteration in the latter may be a consequence of the packing of a small sample for analysis. All the peaks detected in the trace of the non-outgassed sample were present in the trace of the outgassed sample indicating that little, if any, structural collapse had occurred.

Figure 4.1. X-Ray Diffraction Traces of H-ZSM-23

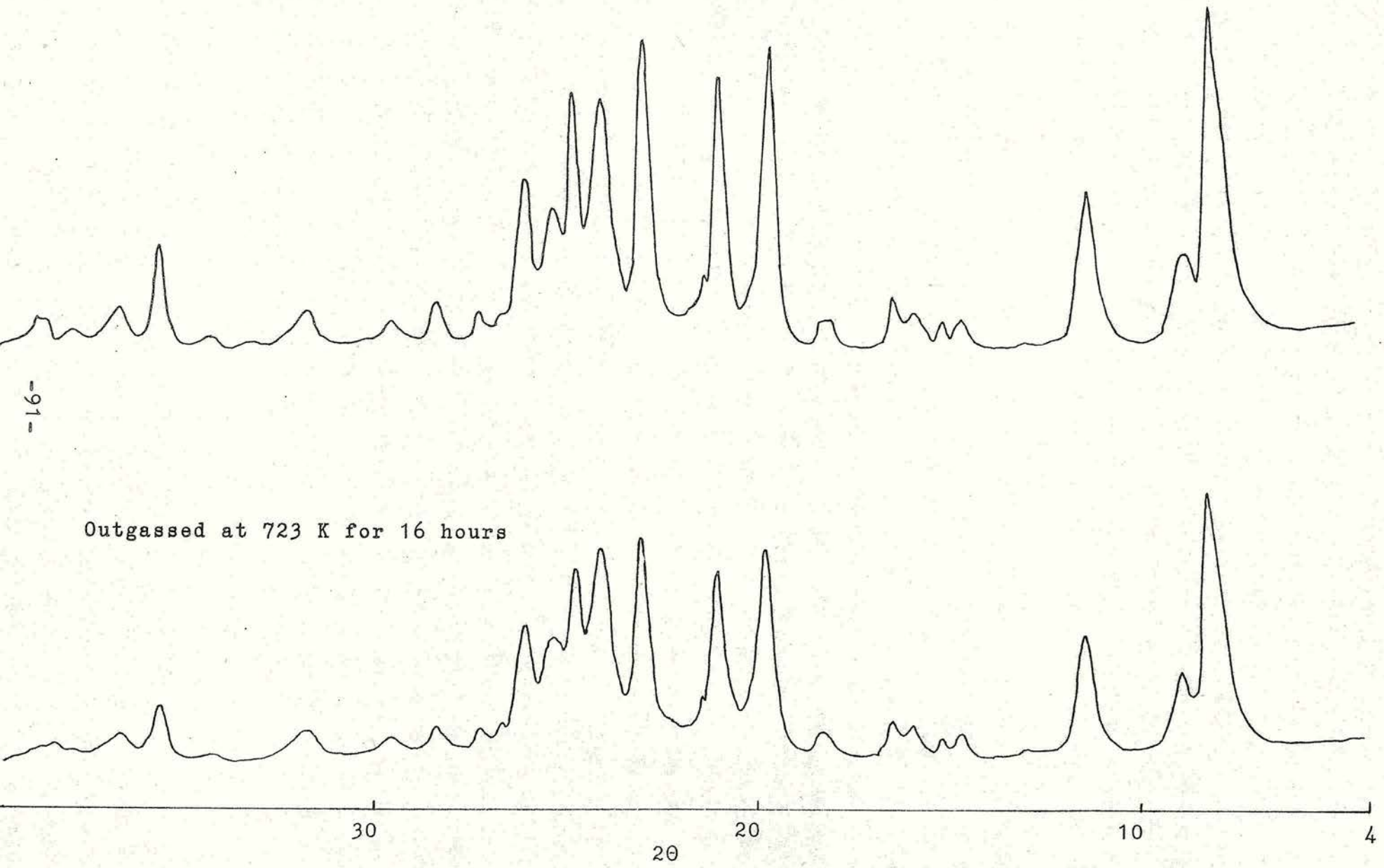

Figure 4.2. X-Ray Diffraction Traces of H-EU-1(A)

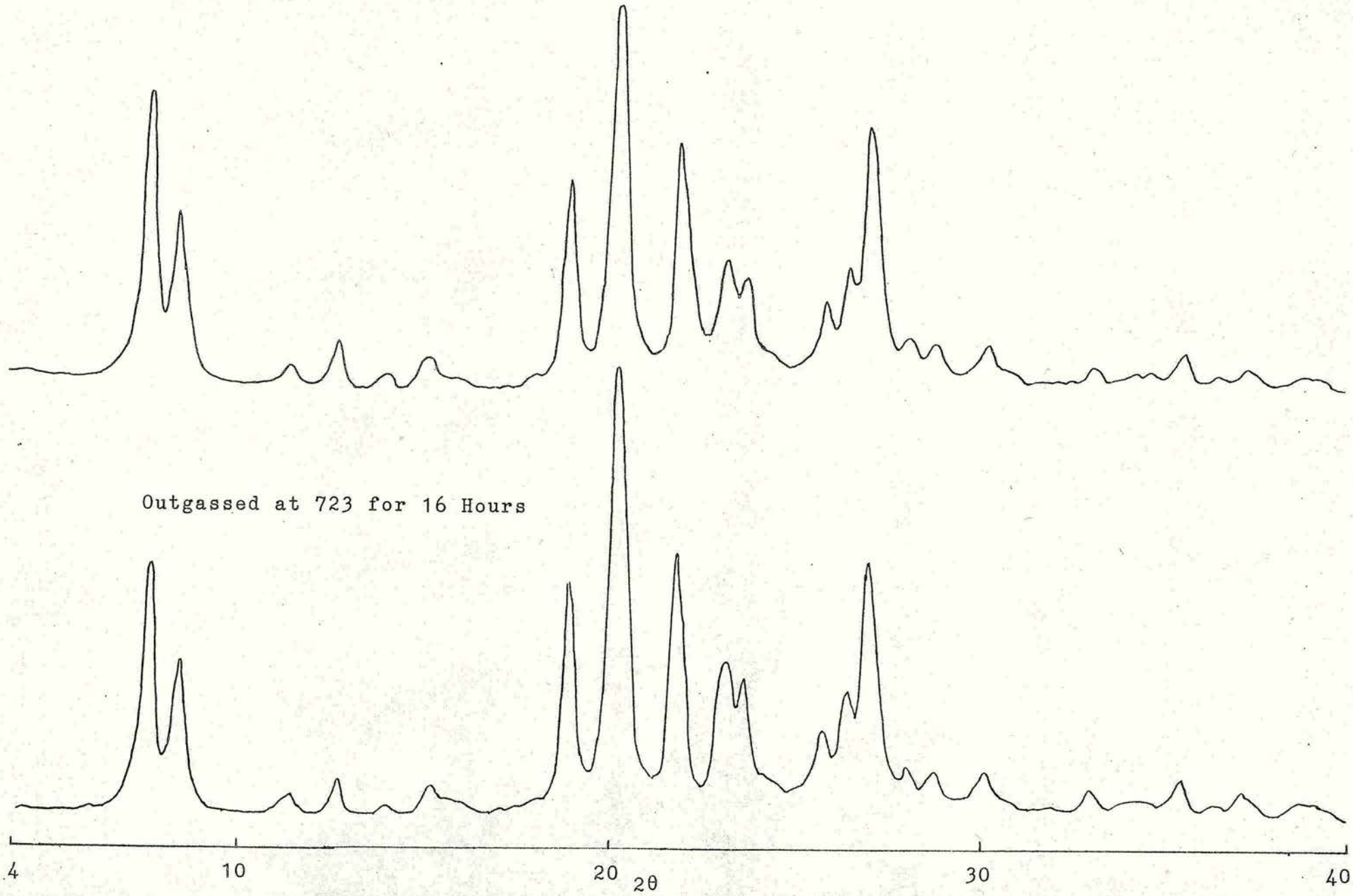

Figure 4.3. X-Ray Diffraction Traces of H-EU-1(B)

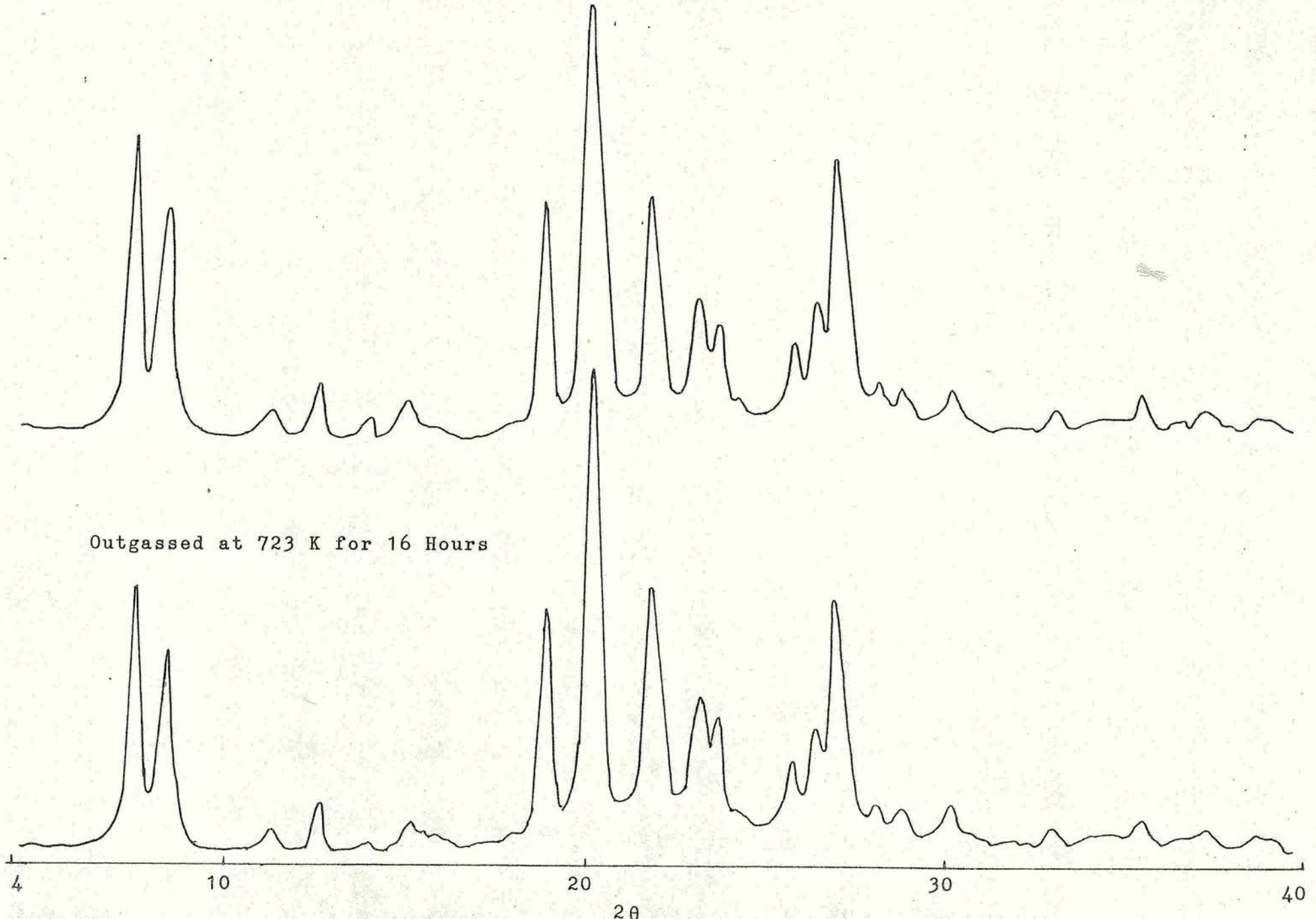

(b) H-EU-1

The diffraction traces of H-EU-1(A) and H-EU-1(B) are illustrated in Figures 4.2 and 4.3 respectively. Peaks were observed at approximately the same angles for the two different samples and the calculated d-spacings were in good agreement with the literature[7]. Comparison of the H-EU-1(B) trace with that of H-EU-1(A) illustrates that both samples contain the same peaks. The trace for H-EU-1(A) however, shows a slight broadening of the peaks which is indicative of a small crystal size. The relative intensities of the peaks was found to differ slightly between the two samples.

Traces for samples outgassed at 723 K for 16 hours are also illustrated in Figures 4.2 and 4.3 No peaks were lost on outgassing and the angles were not altered indicating little, if any, structural collapse had occurred.

Although the diffraction pattern of EU-1 is unique it has several features in common with those of other high silica zeolites. The diagnostic lines for EU-1 closely resemble those for ZSM-23 as illustrated in Table 4.4. It was originally thought[7] that an analogy could be drawn between the relationship of EU-1 and ZSM-23 and the ZSM-5/ZSM-11 family of zeolites which from the literature appear to have similar X-ray diffraction data but in fact have related but significantly different three-dimensional frameworks[124]. However recent work[121] has shown that this is not the case and that the similarity between the diffraction patterns of EU-1 and

ZSM-23[a]		EU-1[b]	
d/A	I/I_o	d/A	I/I_o
11.2	m	11.03	vs
10.1	w	10.10	s
-		9.72	w
7.87	w	-	
-		6.84	w
-		5.86	vw
5.59	w	-	
5.44	w	-	
4.90	w	-	
4.53	s	4.66	vs
-		4.31	vs
-		4.00	vs
3.90	vs	-	
-		3.82	s
3.72	vs	3.71	s
3.62	vs	-	
3.54	m	-	
3.44	s	3.44	m
3.36	w	3.36	m
-		3.26	s
3.16	w	3.16	vw
3.05	w	3.11	vw
2.99	w	2.96	vw
2.85	w	-	
-		2.71	vw
2.54	m	2.55	w
2.47	w	2.48	vw
2.40	w	2.42	vw
2.34	w	2.33	vw
-		2.30	vw
-		2.13	vw

Table 4.4. Comparison of Diffraction Lines for ZSM-23 and EU-1

[a] The diffraction lines for ZSM-23 were taken from Table 1 US Patent 4,100,217 (1978)[6].

[b] The diffraction lines for EU-1 were taken from Table 1 European Patent Application 0042226 (1981)[7].

ZSM-23 is only superficial.

4.1.3. Surface Areas

The surface areas of the zeolites H-ZSM-23 and H-EU-1 were determined by nitrogen adsorption, the data being plotted according to the BET equation (Equation 3.5). A typical plot is illustrated in Figure 4.4.

In addition, surface area measurements were carried out using n-butane as the adsorbate due to the close proximity of the critical diameter of this molecule (0.51 nm) with that of but-1-ene (0.495 nm). The zeolite samples were pretreated in vacuo in the temperature range 669-752 K for 16 hours prior to adsorption. The samples were then cooled to a temperature of 273 K and exposed to a pressure of but-1-ene in a known volume for five minutes. At the end of this period, the residual but-1-ene pressure was noted and the sample evacuated for thirty minutes at 273 K to remove the gaseous but-1-ene molecules and probably any physically adsorbed but-1-ene molecules. This process enabled the maximum number of but-1-ene molecules adsorbed by the sample to be established. The n-butane surface areas of the zeolite plus adsorbed butene systems were then established at 273 K. The cross-sectional area of the n-butane molecule was taken as 44.4×10^{-20} m^2 [125].

(a) H-ZSM-23

The surface areas of samples of H-ZSM-23 outgassed

Figure 4.4. BET plot of H-ZSM-23 outgassed at 628 K for 16 hours

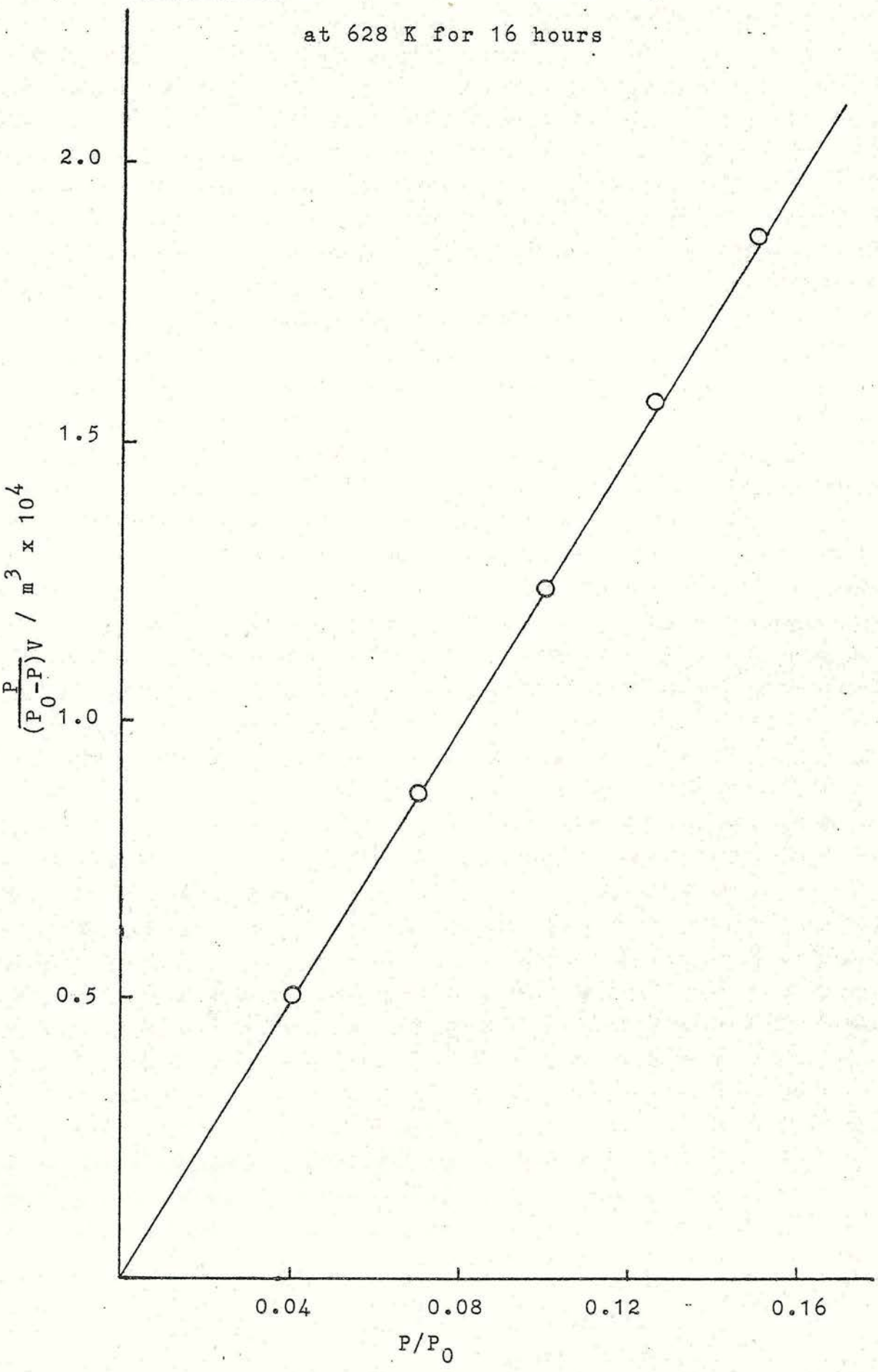

for 16 hours in the temperature range 579-935 K vary slightly with temperature as illustrated in Table 4.5.

Outgassing Temperature/K	Outgassing Time/hrs.	Surface Area $/m^2g^{-1}$
579	16	157
628	16	178
723	16	205
935	16	176

Table 4.5. Effect of Pretreatment Temperature on the Surface Area of H-ZSM-23

The value of 205 m^2g^{-1} for an outgassing temperature of 723 K is in good agreement with the literature[6,126].

The n-butane surface areas before and after the adsorption of but-1-ene (5.3×10^{20} molecules per gram of catalyst) on H-ZSM-23 at 273 K were 154 and 93 m^2g^{-1} respectively. The results indicate that the surface area of the the zeolite was substantially reduced (by 55% of the original surface area) after adsorption of but-1-ene and subsequent evacuation. Figure 4.5 illustrates how the prior adsorption of but-1-ene reduced the volume of n-butane adsorbed.

(b) H-EU-1

A similar survey of the effect of pretreatment temperature on the surface areas of the two H-EU-1 (outgassed for 16 hours) samples was carried out. The

Figure 4.5. Effect of Adsorbed Butene on the Adsorption of n-Butane by H-ZSM-23 at 273 K

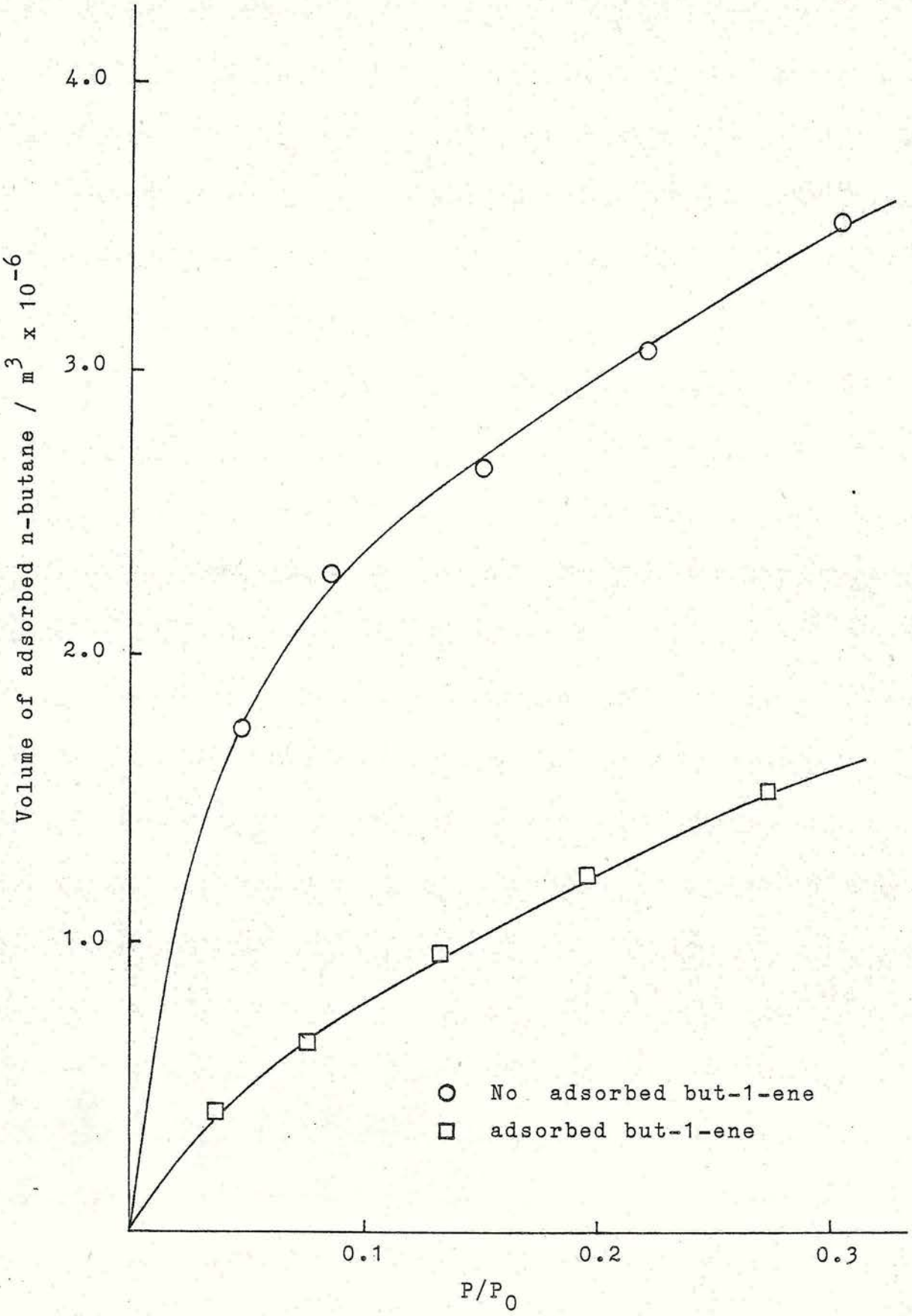

results, which are listed in Table 4.6, indicate that the surface area of H-EU-1(A) and H-EU-1(B) did not change significantly as the catalyst pretreatment temperature was increased. The data suggest that pretreatment at elevated temperatures did not result in any structural collapse.

Catalyst	Outgassing Temperature/K	Surface Area /m^2g^{-1}
H-EU-1(A)	528	345
	622	352
	679	361
	728	364
	858	358
H-EU-1(B)	541	302
	632	332
	752	331

Table 4.6. Effect of Pretreatment Temperature on the Surface Area of H-EU-1

The n-butane surface areas before and after the adsorption of but-1-ene on the H-EU-1 samples, are given in Table 4.7. The prior adsorption of but-1-ene was found to reduce the volume of n-butane adsorbed by both H-EU-1(A) and H-EU-1(B) resulting in plots similar to those obtained for H-ZSM-23 (Figure 4.5). The results indicate that the surface area of H-EU-1 was substantially reduced (by 29% and 14% of the original

n-butane surface areas for H-EU-1(A) and H-EU-1(B) respectively) by adsorption and subsequent evacuation of but-1-ene. Comparison of the n-butane results prior to adsorption indicates that H-EU-1(B) has a larger surface area than H-EU-1(A) which is in marked contrast to the nitrogen adsorption results.

Catalyst	Maximum Number of But-1-ene Molecules per g. of catalyst	n-Butane Surface Area[125] $/m^2g^{-1}$
H-EU-1(A)	-	231
H-EU-1(A)	8.1×10^{20}	65
H-EU-1(B)	-	261
H-EU-1(B)	7.0×10^{20}	37

Table 4.7. The n-Butane Surface Areas of the Zeolite plus Adsorbed But-1-ene System at 273 K for H-EU-1

4.1.4. Scanning Electron Microscopy

Electron microscopy is used extensively to study the habit and surface topology of synthetic zeolites.

(a) H-ZSM-23

Scanning electron micrographs of H-ZSM-23 indicated that the crystals were so small that they were below the resolution of the instrument. This is in agreement with the observed broadening of the X-ray diffraction trace as described previously in Section 4.1.2.

(b) H-EU-1

A bimodal distribution of crystallite sizes has been indicated by scanning electron microscopy of H-EU-1(A)[127] while a study of the crystalline morphology of H-EU-1(B) has indicated that the sample is largely composed of ellipsoidal "crystals" 1-5 μm in length[127].

4.2. Adsorption Studies

An investigation of the sorptive properties of H-ZSM-23 and H-EU-1 was performed gravimetrically using the Cahn microbalance described in Chapter 3.

4.2.1. H-ZSM-23

(a) Adsorption of Alkanes, Aromatics and Methanol

The adsorption of a range of organic vapours of different molecular size (kinetic diameter 0.38-0.60 nm[24]) on H-ZSM-23 (powder) was investigated after outgassing at 873 K. Typical sorbate-uptake curves are shown in Figure 4.6. The sorbate uptake curves reveal that molecules of kinetic diameter less than the dimensions of the zeolite pore openings, such as n-hexane are rapidly adsorbed and approach their sorption capacity within 15 minutes. In contrast, molecules such as p-xylene and cyclohexane, whose diameters are close to or greater than the channel dimensions are only slowly adsorbed. In such cases, values of the sorbate uptake recorded after 15 minutes, (Table 4.8), are not true sorption capacities but represent relative rates of

Figure 4.6. Sorbate Uptake Curves for H-ZSM-23 at 296 K

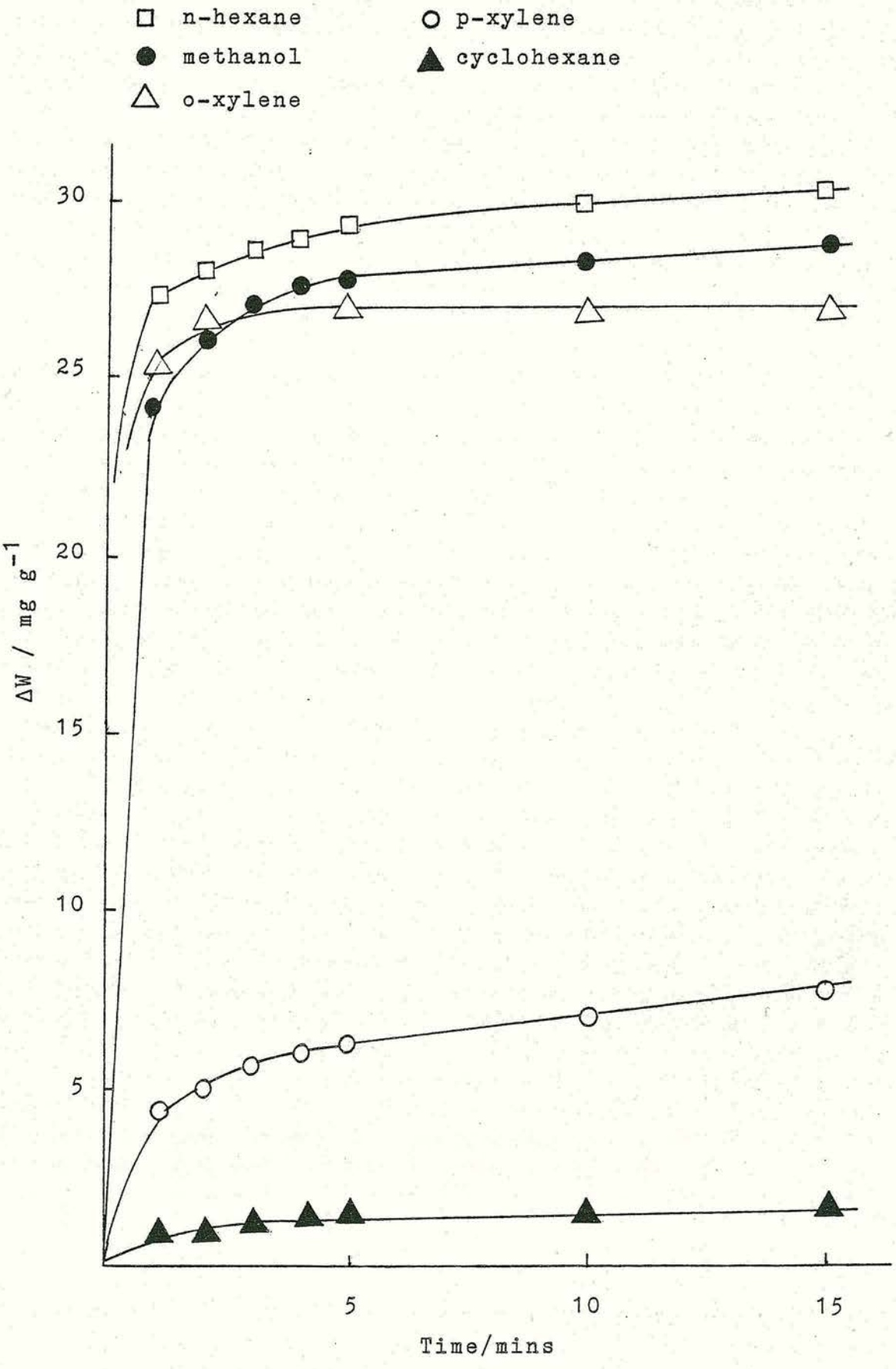

adsorption by the zeolite.

Sorbate	Critical Diameter/nm[24]	Sorbate Uptake V/ccg^{-1}
methanol	o.385	0.037
n-hexane	0.430	0.046
n-pentane	0.430	0.042
p-xylene	0.585	0.009
cyclohexane	0.600	0.002

Table 4.8. Sorbate Uptake on H-ZSM-23 at 15 Minutes

These data yield valuable information about the pore structure of H-ZSM-23. A plot of sorbate-uptake (after 15 minutes) vs. kinetic diameter of the sorbate molecule as illustrated in Figure 4.7 reveals a cut-off in sorbate-uptake at a molecular diameter of about 0.6 nm and is consistent with the presence of ten-membered ring channels[23].

The fast uptake of n-hexane and the slow sorption of p-xylene also provides evidence that H-ZSM-23 has ring channels of a size that would be provided by ten-membered rings. Hydrocarbon sorption by eight-membered rings of silicon and aluminium is limited to n-hexane and molecules of a larger cross-section are excluded[128]. The zeolite ferrierite has been shown to comprise of both eight- and ten-ring channels[129] which are of the dimensions 0.43 x 0.55 nm (ten-ring) and 0.34 x 0.48 nm (eight-ring)[11]. Sorption measurements over hydrogen

Figure 4.7. Sorbate Uptake (after 15 mins.) as Function of Sorbate Kinetic Diameter

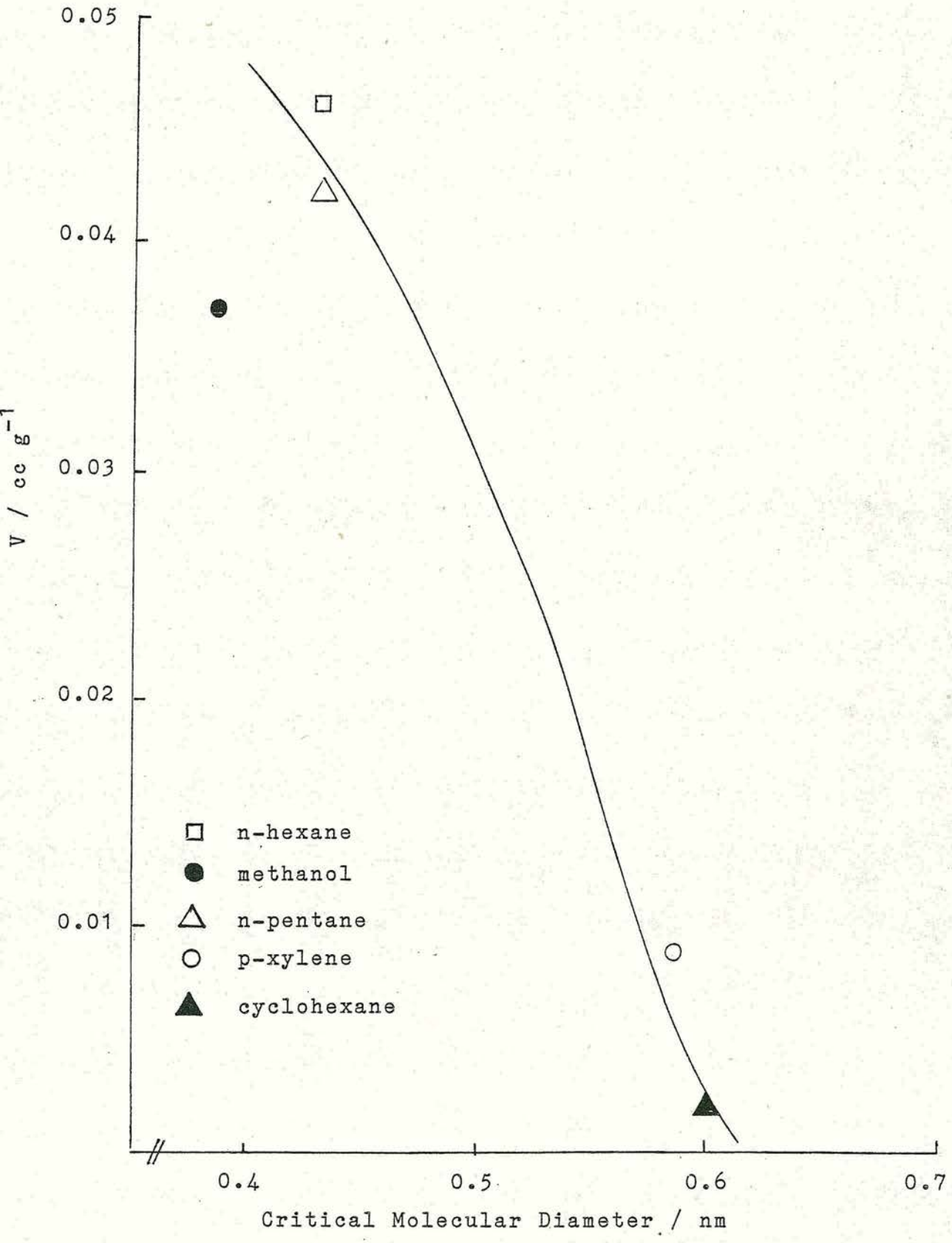

ferrierite indicate a high sorption capacity for n-alkanes and a low sorption capacity for iso-alkanes and aromatics[129].

The steric effects of H-ZSM-23 can be illustrated by the product distribution in methanol conversion. In this process[130] the reaction proceeds from methanol to alkenes to aromatics (primarily polymethylbenzenes). When catalysed by H-ZSM-23 the major hydrocarbon products are in the range C_{1-5}[131]. The C_5 cutoff for H-ZSM-23 results from steric restrictions which limit the formation of hydrocarbon products larger than C_5.

Adsorption isotherms for the sorbates were determined by measurement of the quantity of gas adsorbed at different equilibrium pressures and are illustrated in Figure 4.8. Isotherms of non-polar guest molecules are as a rule of Type I in Brunauer's classification[23] where the limiting value of adsorption reflects the filling of the micropores.

The Langmuir equation originally applied to the adsorption of molecules in a monolayer on an open surface; the classical interpretation of the Type I isotherm is based upon this model. Since zeolites exhibit the Type I isotherm the Langmuir equation can be applied. The Langmuir model assumes that the adsorption potential is uniform i.e. no surface heterogeneity exists. However, this is not true in most cases of zeolite adsorption[24]. The data in Figure 4.8 have been plotted according to the Langmuir equation (Equation 3.4) where the monolayer capacity, or in the case of

Figure 4.8. Sorbate Adsorption Isotherms on H-ZSM-23 at 296 K

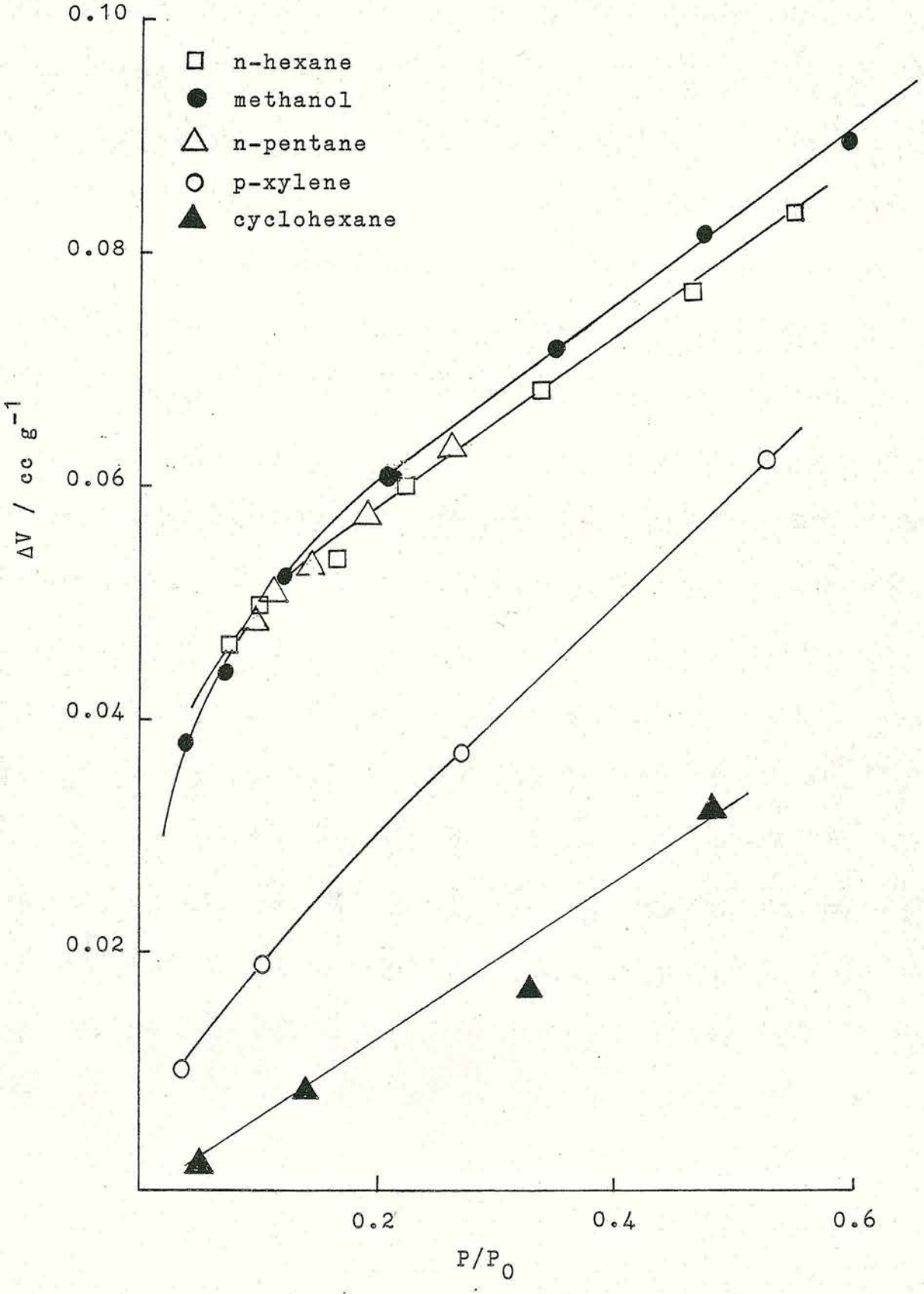

zeolites, the point corresponding to pore filling, is given by V_m. Linear plots were obtained for all sorbates with the exception of cyclohexane which had shown only surface adsorption and little uptake. Table 4.9 lists the weights of sorbates corresponding to pore filling (from the gradient of the Langmuir plot) together with the area occupied per molecule[125] and the calculated monolayer coverage (or surface area).

Sorbate	Pore Volume /ccg^{-1}	Area per Molecule nm^{-2} [125]	Area of Monolayer /m^{2}g^{-1}
methanol	0.076	0.219	246
n-hexane	0.072	0.562	190
n-pentane	0.074	0.492	196
p-xylene	0.030	0.538	87

Table 4.9. Volumes of Sorbates Corresponding to Void Filling of H-ZSM-23

A comparison of the pore volumes given in Table 4.9 indicates that the values obtained for methanol, n-hexane and n-pentane are in good agreement. The value for p-xylene was found to be significantly lower indicating that part of the internal surface was not accessible to p-xylene. Comparison of the surface areas given in Table 4.9 with the surface area measured by nitrogen adsorption (205 m^{2}g^{-1}) shows the value for p-xylene to be lower which again is consistent with the

fact that part of the internal surface accessible to nitrogen molecules is inaccessible to p-xylene. The apparent high surface area obtained from methanol may be a consequence of the value taken for the area occupied per molecule. It has been found that the apparent cross-sectional area of the adsorbed molecule is not constant but varies with the adsorbent, temperature of adsorption and choice of reference substance[125].

The kinetics of adsorption of methanol, n-hexane, n-pentane and p-xylene in H-ZSM-23 are illustrated in Figure 4.9(a) and (b) in which weight increase is plotted against $t^{0.5}$. The diffusion plots indicate that there is rapid adsorption of n-hexane, n-pentane and methanol which is consistant with the presence of ten-ring channels. If eight-ring channels were present then a rapid adsorption of methanol and a slower diffusion controlled adsorption of n-hexane and n-pentane would be expected. Only the adsorption of p-xylene shows a linear portion of the curve which is indicative of a diffusion controlled sorption, the diffusion law (Equation 1.1) being obeyed. The straight line portion tails off to a curve at higher values of $t^{0.5}$, this is due to the approximations involved in Equation 1.1. The calculation of diffusivities from experimental rate curves requires a detailed knowledge of the shape and size distribution of the zeolite crystals, parameters which were not available in the present study.

Figure 4.9. Sorbate Diffusion Plots

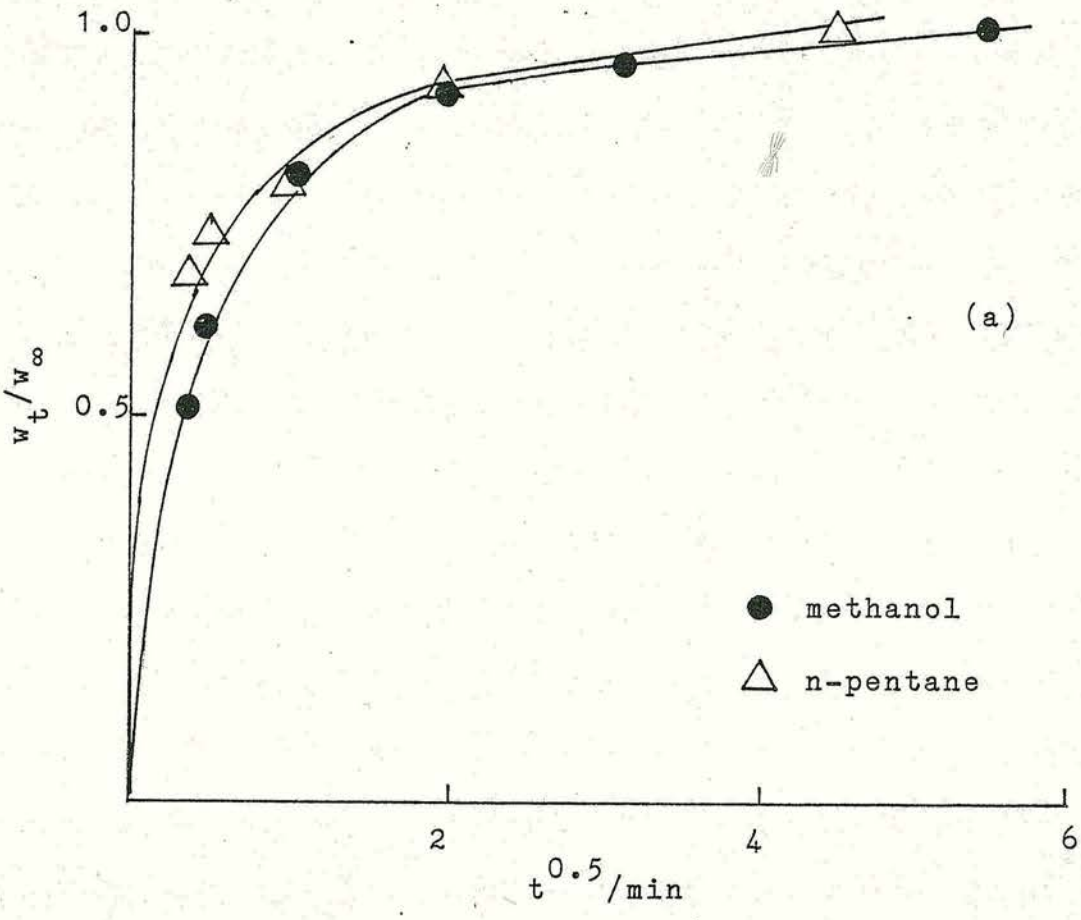

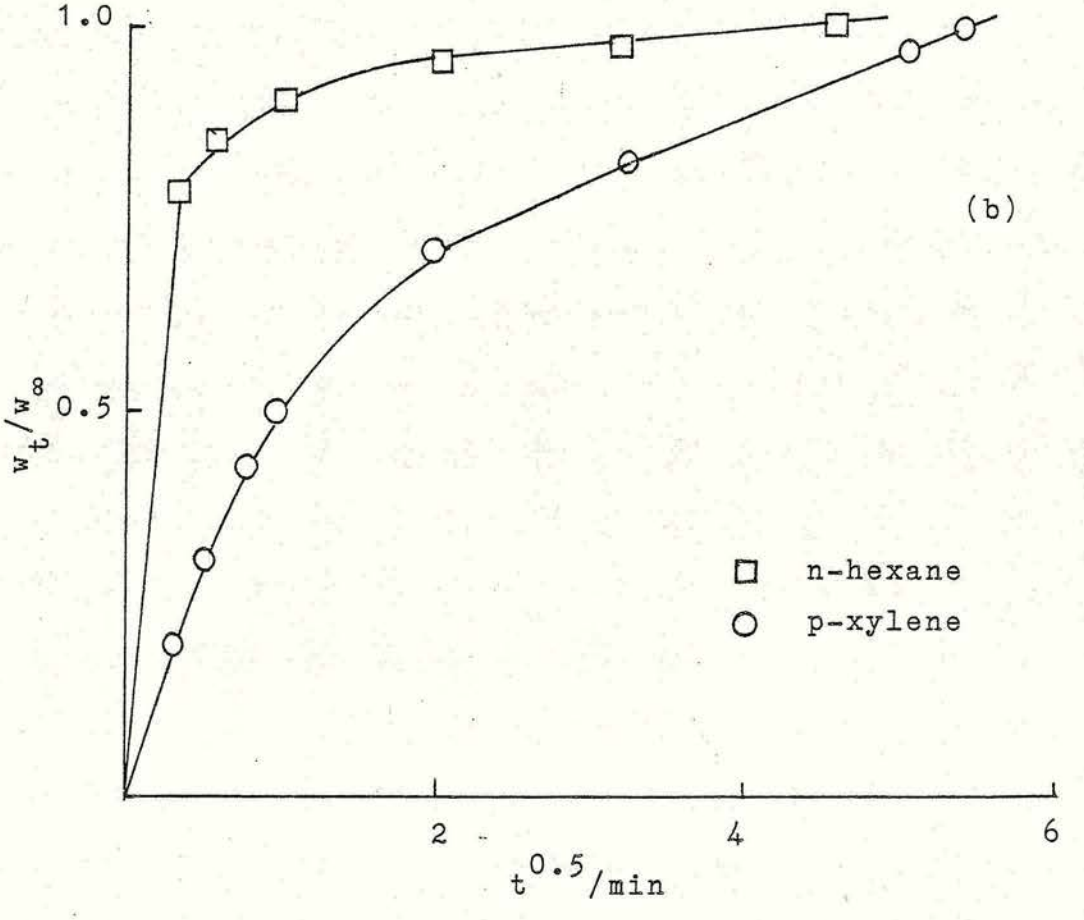

(b) Adsorption of Butenes

The adsorptions of but-1-ene, cis and trans but-2-ene on zeolite H-ZSM-23 were investigated after outgassing at 873 K. An adsorption temperature of 202 K was chosen in order to minimise the isomerisation reaction of the butene adsorbate. Rapid adsorption was observed for all butenes, which is consistent with the presence of ten-membered ring channels. The zeolite erionite has been shown to have eight-membered ring channels of dimensions 0.36 x 0.52 nm[11] in which there was a diffusion controlled sorption of but-1-ene and little sorption of cis but-2-ene[106]. Increase in weight of the zeolite as a result of adsorption as a function of time is illustrated in Figure 4.10. Similar profiles were observed for all the n-butenes. Table 4.10 lists the amount of n-butene adsorbed (after 15 minutes). The results are expressed as mg/g of hydrated zeolite.

Sorbate	Critical Diameter nm[132]	Weight Adsorbed mg/g
but-1-ene	0.495	36.92
trans but-2-ene	0.495	40.12
cis but-2-ene	0.558	38.09

Table 4.10 Weights of n-Butenes Adsorbed by H-ZSM-23

Adsorption isotherms for the n-butenes were obtained at 202 K and indicated that the amounts adsorbed

Figure 4.10. Rates of Adsorption of the n-Butenes at 202 K on H-ZSM-23

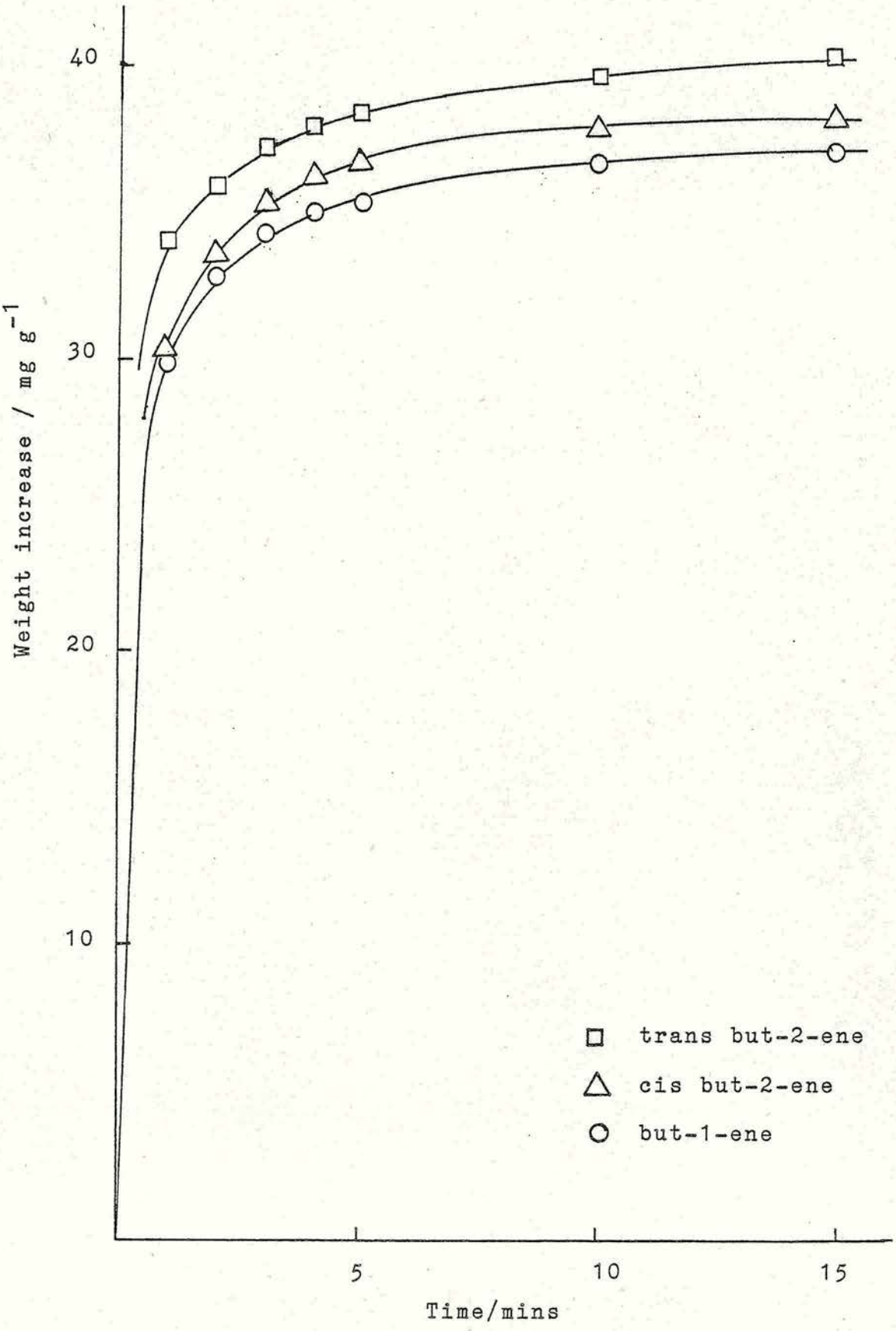

at a value of $P/P_0 \leq 0.5$ were essentially identical. The adsorption isotherms of cis and trans but-2-ene indicate an apparent condensation at pressures below the saturated vapour pressure at 202 K; at P/P_0 of 0.58 for cis but-2-ene and 0.50 for trans but-2-ene.

The isotherm data have been plotted according to the Langmuir equation (Equation 3.4). Linear plots were obtained for all three butenes (Figure 4.11). Weights of the n-butenes corresponding to pore filling together with the area occupied per molecule[125] and the calculated surface area are listed in Table 4.11.

Sorbate	Pore Volume /ccg^{-1}	Area of Molecule nm^2 [125]	Area of Monolayer /m^{2}g^{-1}
but-1-ene	0.097	0.378	235
trans but-2-ene	0.090	0.334	195
cis but-2-ene	0.095	0.385	244

Table 4.11. Volumes of Butenes Corresponding to Void Filling of H-ZSM-23

The area covered by a monolayer of n-butene molecules compares favourably with that obtained by nitrogen adsorption (205 m^2g^{-1}) suggesting that the internal surface accessible to nitrogen is also accessible to the n-butenes.

Consideration of the kinetics of adsorption of the n-butenes as given by the diffusion law (Equation 1.1)

Figure 4.11. Langmuir Plots for the Adsorption of the n-Butenes on H-ZSM-23

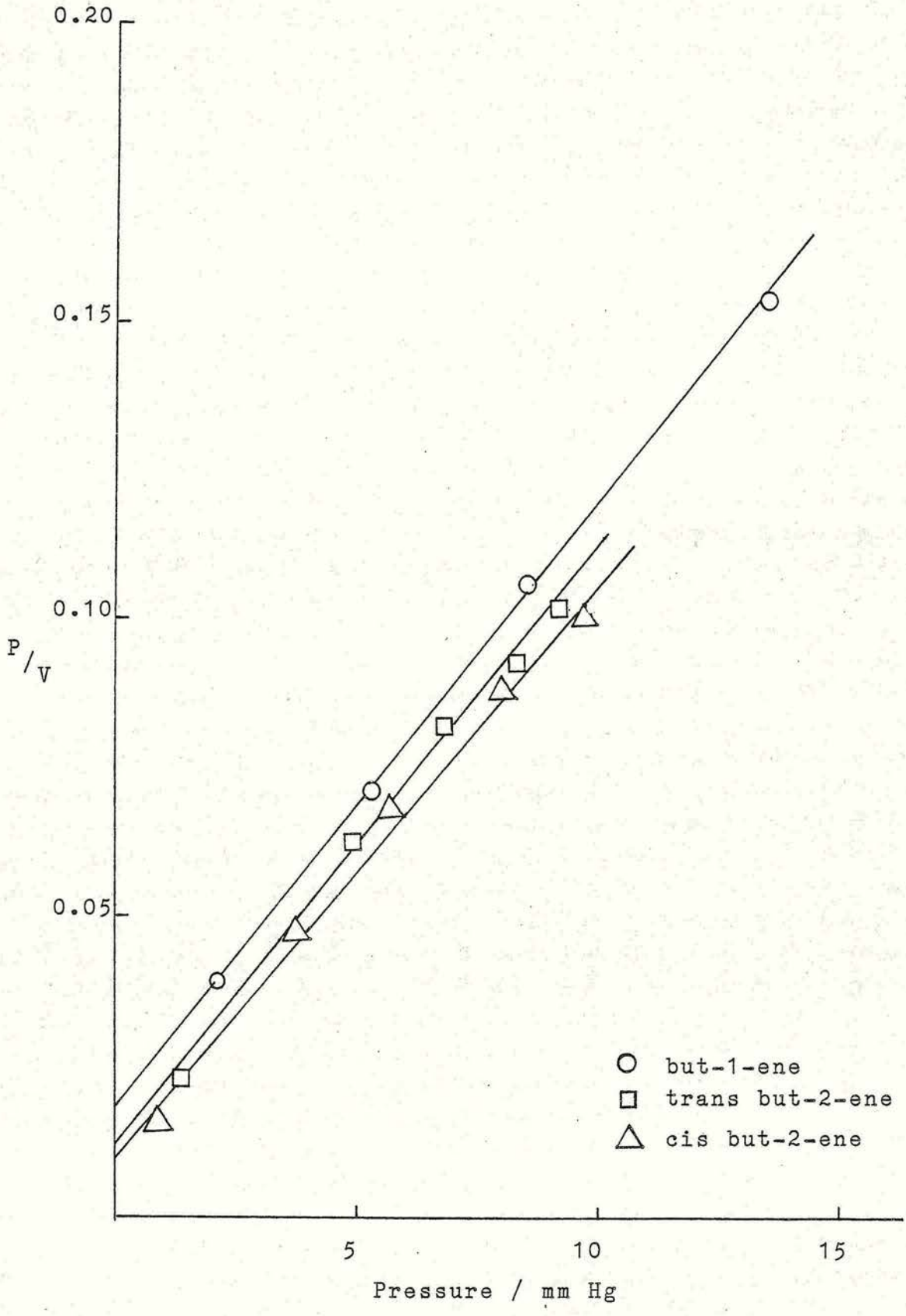

provides evidence that there is a rapid uptake with little diffusion control as illustrated in Figure 4.12. The diffusion plots suggest that the rates of diffusion vary in the order:-

but-1-ene $\geqslant$ trans but-2-ene > cis but-2-ene.

Trans but-2-ene exhibits a zero dipole moment whereas both but-1-ene and cis but-2-ene have dipole moments thus the order of the rates of diffusion cannot be a function of this parameter alone. Trans but-2-ene has the same critical diameter as but-1-ene (0.495 nm) whereas cis but-2-ene has a larger critical diameter (0.558 nm) thus the sorption rate must be a function of this parameter. Comparison of Figure 4.12 with Figure 4.9(a) and (b) gives an order of diffusivities of:-

alkanes > methanol > alkenes > p-xylene.

Summary of Adsorption Results in H-ZSM-23

The sorption data recorded for H-ZSM-23 are indicative of a pore diameter of c.a. 0.6 nm. This is consistent with a pore structure comprising ten-membered rings similar to the type found in ZSM-5[13]. However, the reduced BET surface area and n-hexane capacity - both of which are less than that reported for ZSM-5[133] suggest that the pore structures of the two zeolites although containing similarities are far from identical. Further evidence is provided for this by the differences in the hydrocarbon product distribution observed in methanol conversion viz a cutoff at C_5 in H-ZSM-23 compared to C_9 over ZSM-5. These results suggest that cavities of the

Figure 4.12. Diffusion Plots for the n-Butenes

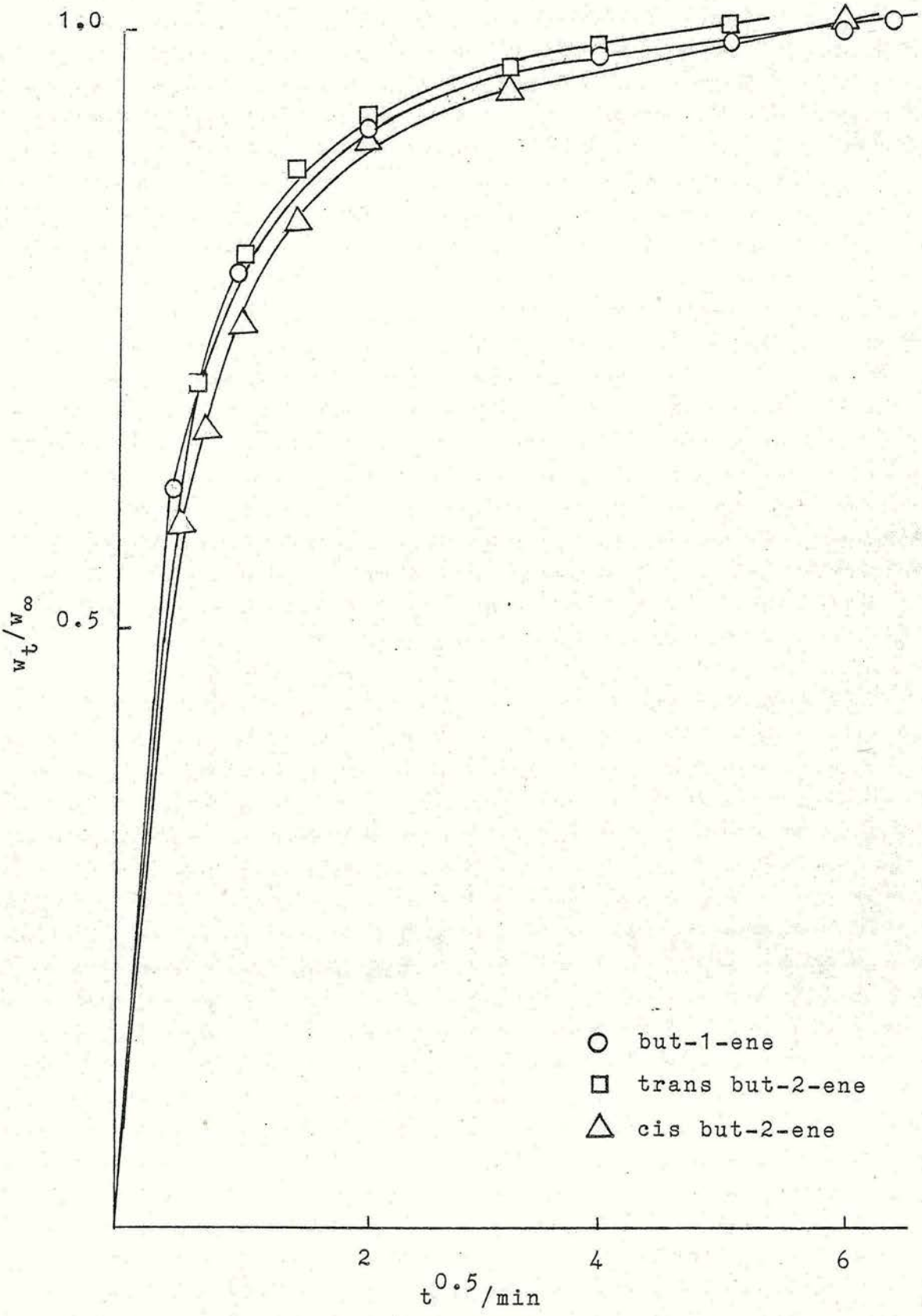

type formed in ZSM-5 by the intersection of the two channel systems are absent from the intracrystalline pore structure of H-ZSM-23 since it is these to which the formation of aromatic hydrocarbons is primarily attributed[22].

4.2.2. H-EU-1

(a) Adsorption of Alkanes, Aromatics and Methanol

An investigation of the sorptive properties of the hydrogen form of zeolites EU-1(A) and EU-1(B) was performed after outgassing at 823 K. A range of organic vapours of different molecular size (kinetic diameters 0.38-0.68 nm[24] were used in the study. Typical sorbate-uptake curves for H-EU-1(A) and H-EU-1(B) are illustrated in Figure 4.13 and Figure 4.14 respectively. The sorbate-uptake curves reveal that molecules such as methanol and n-hexane are rapidly adsorbed and approach their sorption capacity within 15 minutes. In contrast, molecules such as o-xylene, 2,3-dimethylbutane and cyclohexane whose diameters are similar to or greater than the channel dimensions are rapidly adsorbed and approach a lower constant uptake after 15-20 minutes. The low capacity observed for o-xylene, 2,3-dimethylbutane and cyclohexane might reflect exclusion from certain parts of the intracrystalline pore structure and indicate the presence of two types of channel. The slow sorption of p-xylene may be an indication of a special packing arrangement or a strong molecule-molecule interaction or diffusion control.

Figure 4.13. Sorbate Uptake Curves for H-EU-1(A) at 296 K

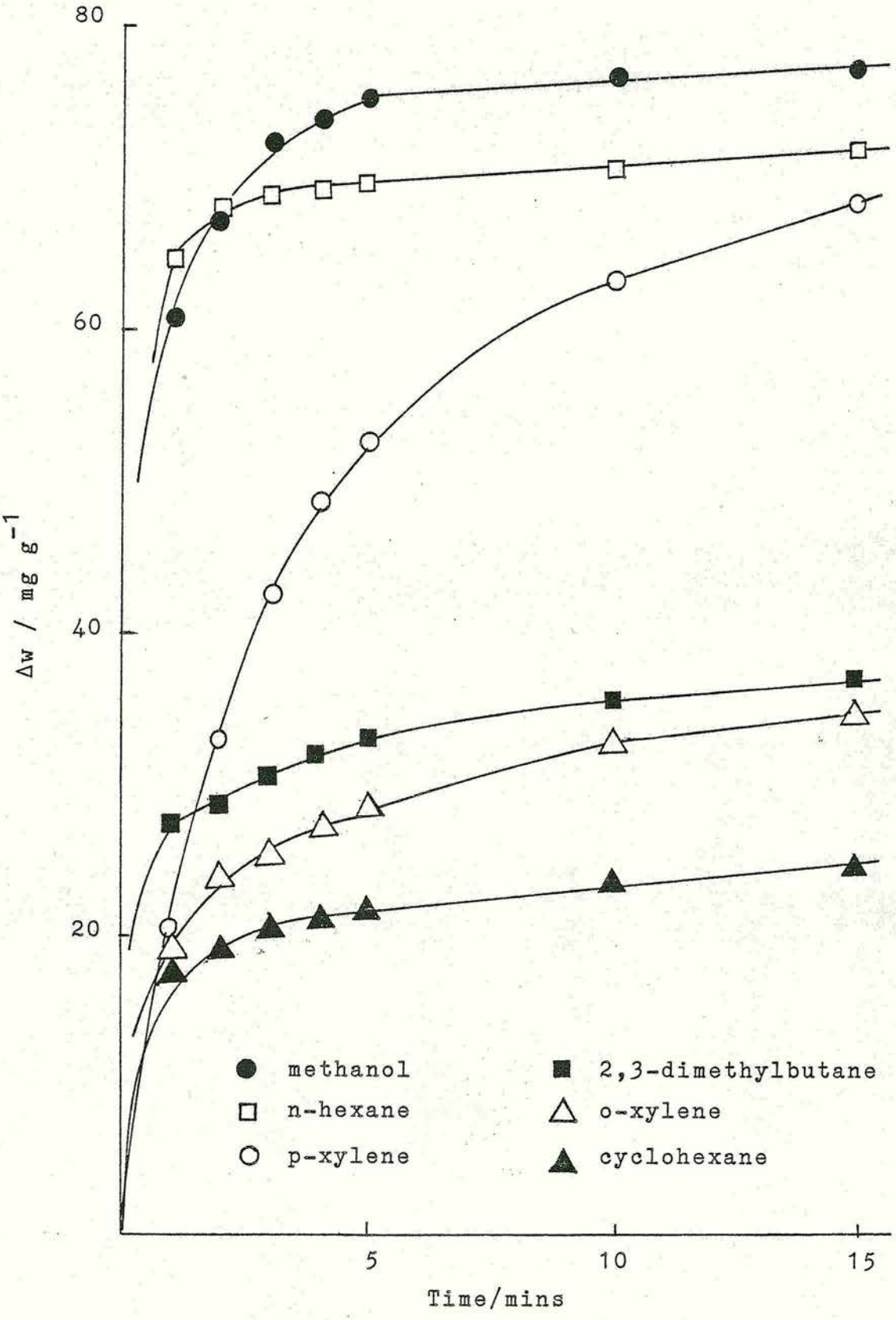

Figure 4.14. Sorbate Uptake Curves for H-EU-1(B) at 296 K

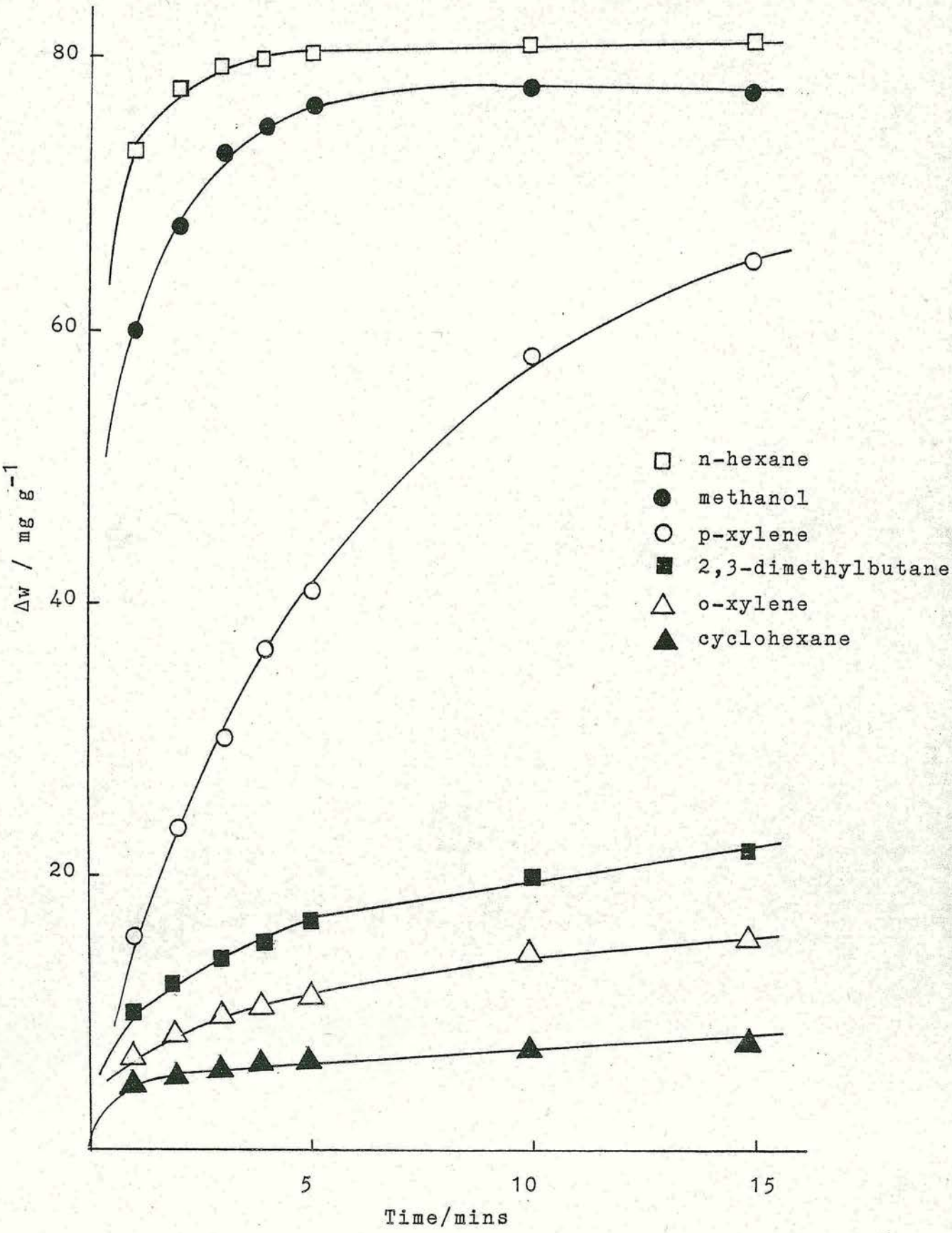

Olsen et al[14] found for p-xylene adsorption in ZSM-5, that at a certain intracrystalline concentration, the p-xylene molecules pack in a new configuration which is more economical of space.

Values of sorbate-uptake at 15 minutes for H-EU-1(A) and H-EU-1(B) are given in Table 4.12.

Sorbate	Critical Diameter nm[24]	Sorbate Uptake V/ccg^{-1}	
		H-EU-1(A)	H-EU-1(B)
methanol	0.385	0.097	0.098
n-hexane	0.430	0.107	0.123
p-xylene	0.585	0.080	0.076
cyclohexane	0.600	0.032	0.010
2,3-dimethylbutane	0.610	0.056	0.033
o-xylene	0.680	0.039	0.018

Table 4.12. Sorbate Uptake at 15 Minutes for H-EU-1(A) and H-EU-1(B)

These data provide valuable information on the pore structure of H-EU-1. For example plots of sorbate-uptake vs. kinetic diameter of the sorbate molecule as illustrated in Figure 4.15(a) and (b) reveal a cutoff in sorbate-uptake at a molecular diameter of c.a. 0.6 nm. This indicates that the channel structure of H-EU-1 comprises ten-membered rings which is in excellent agreement with the reported pore dimensions[7,121]. The differences in sorbate-uptake for 2,3-dimethylbutane,

Figure 4.15. Sorbate Uptake (after 15 mins.) as a Function of Sorbate Kinetic Diameter

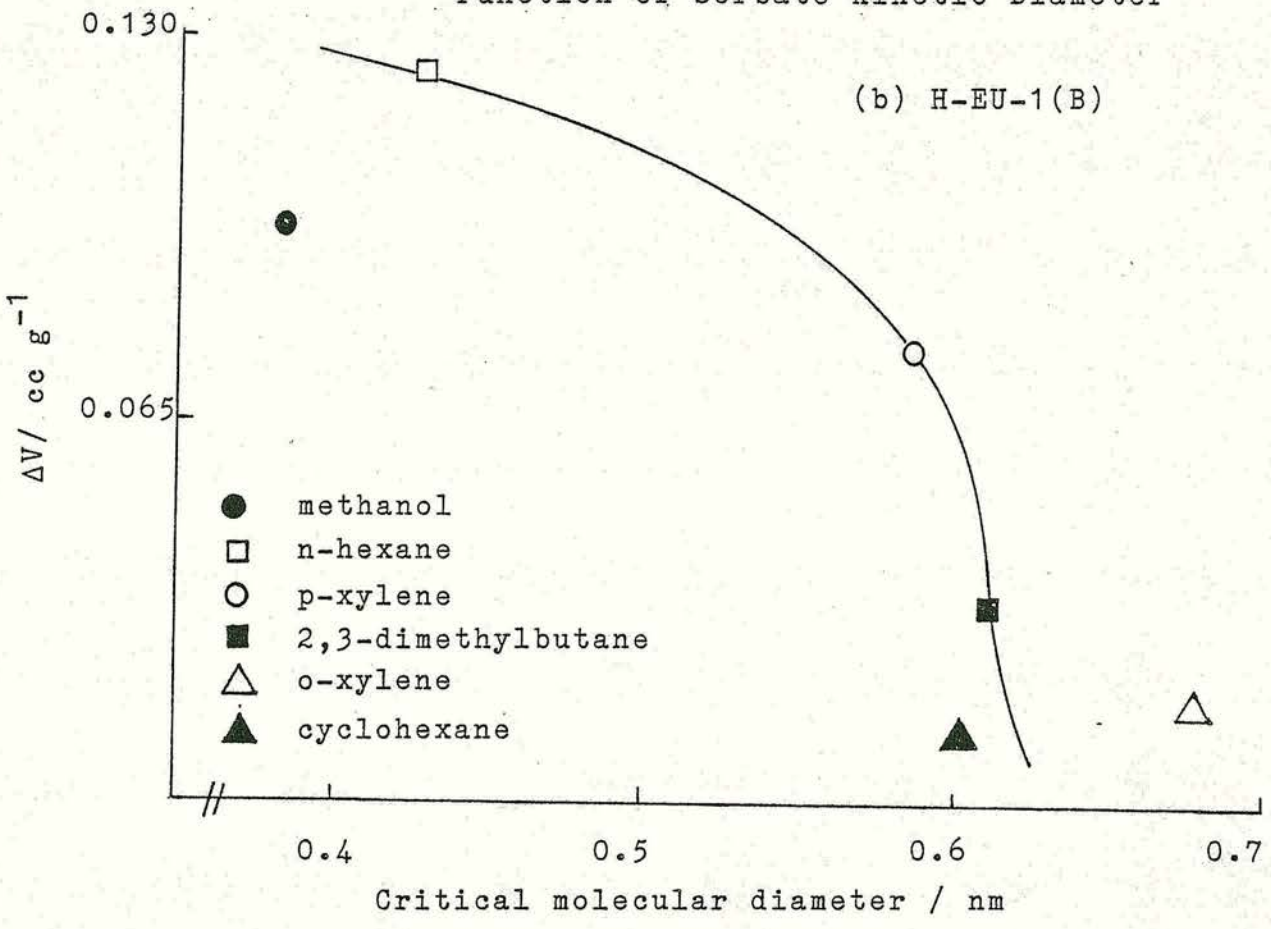

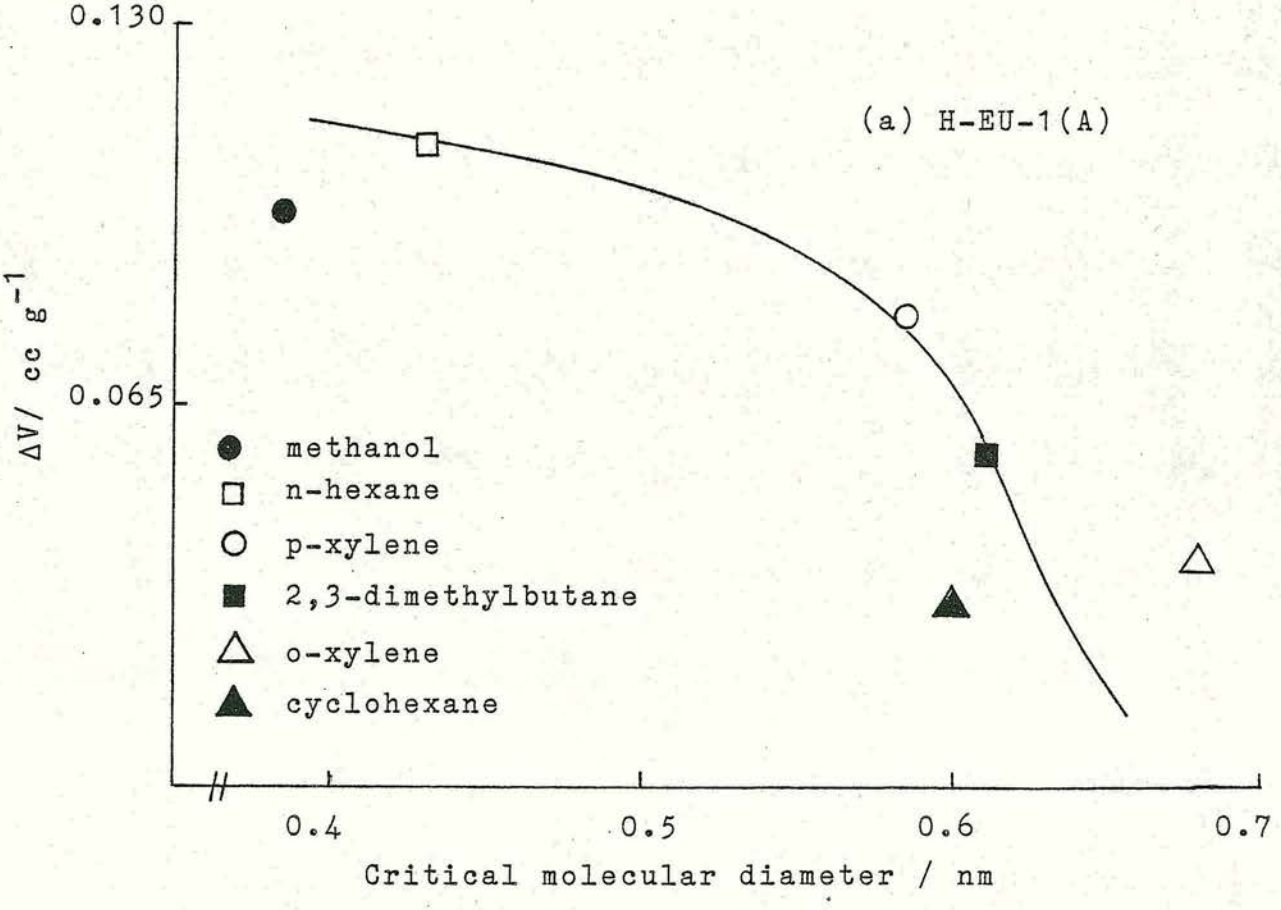

o-xylene and cyclohexane between the two samples of H-EU-1 can be explained by consideration of the different crystallite sizes. H-EU-1(B) comprises of crystals which are 1-5 μm in length while the crystal size of H-EU-1(A) is smaller. Smaller crystals will have an increased number of pore openings available and consequently the sorbate-uptake for molecules such as 2,3-dimethylbutane will be higher.

Adsorption isotherms were determined for the above sorbates on both samples of H-EU-1 and are illustrated in Figure 4.16 and Figure 4.17. H-EU-1 exhibits Type I isotherms in Brunauer's classification and therefore the Langmuir equation (Equation 3.4) can be applied. For isotherms of Type I plots of P/V versus P (P = pressure; V = amount sorbed) tend to be straight lines of slope $1/V_m$ as the limiting sorption V_m is approached. This method was employed for all the data in Figure 4.16 and Figure 4.17 to obtain values of V_m. Linear plots were obtained for all sorbates on both samples. The weights of sorbates corresponding to pore filling, together with the area occupied per molecule[125] and hence the calculated surface area are listed in Tables 4.13 and 4.14 for H-EU-1(A) and H-EU-1(B) respectively.

The pore volumes obtained for methanol, n-hexane and p-xylene for both samples of H-EU-1 are very similar. However, the pore volumes obtained for cyclohexane, 2,3-dimethylbutane and o-xylene are lower than that obtained for methanol although still substantial. This would seem to suggest that sorption on the external

Figure 4.16. Sorbate Adsorption Isotherms for H-EU-1(A)

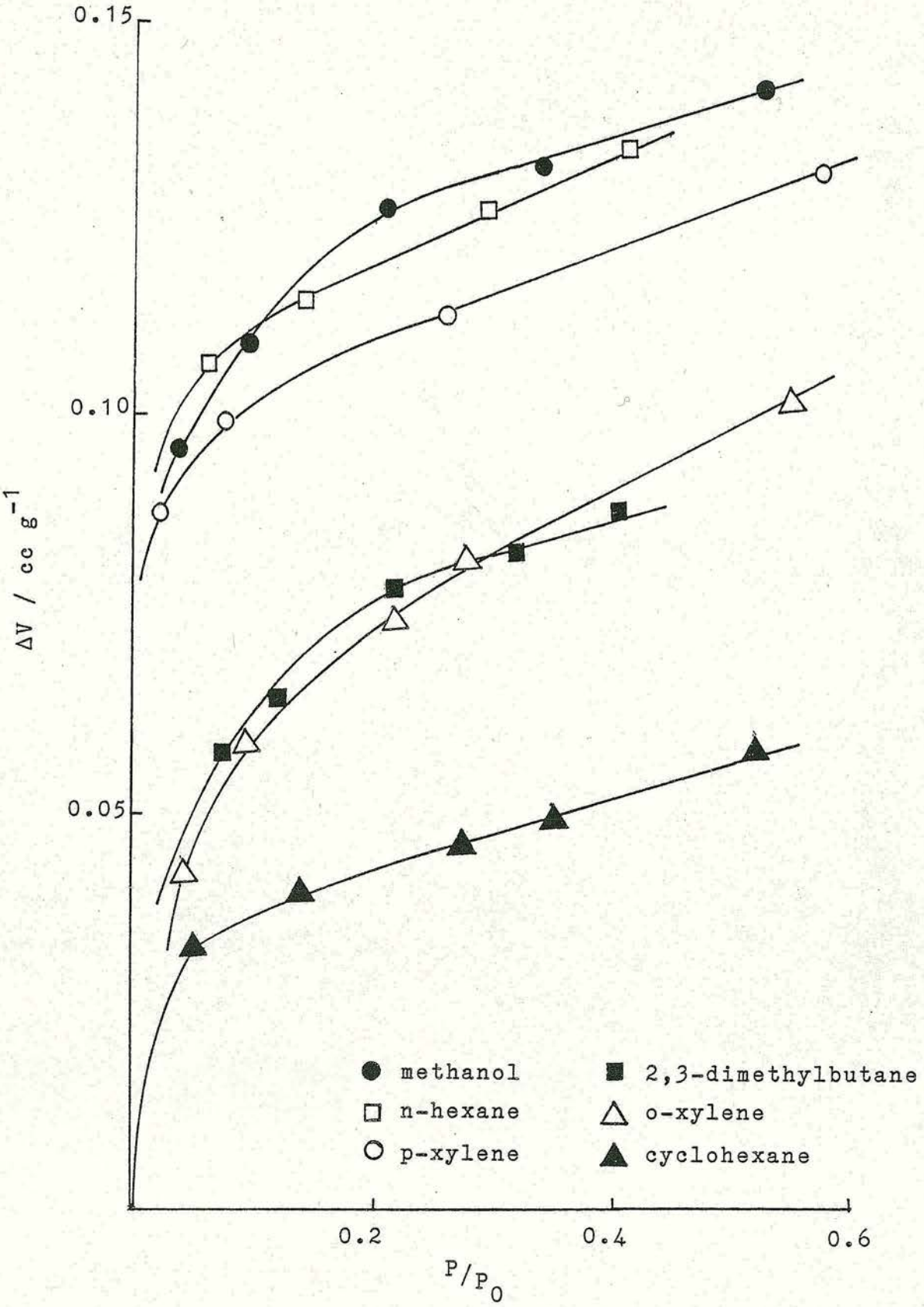

Figure 4.17. Sorbate Adsorption Isotherms for H-EU-1(B)

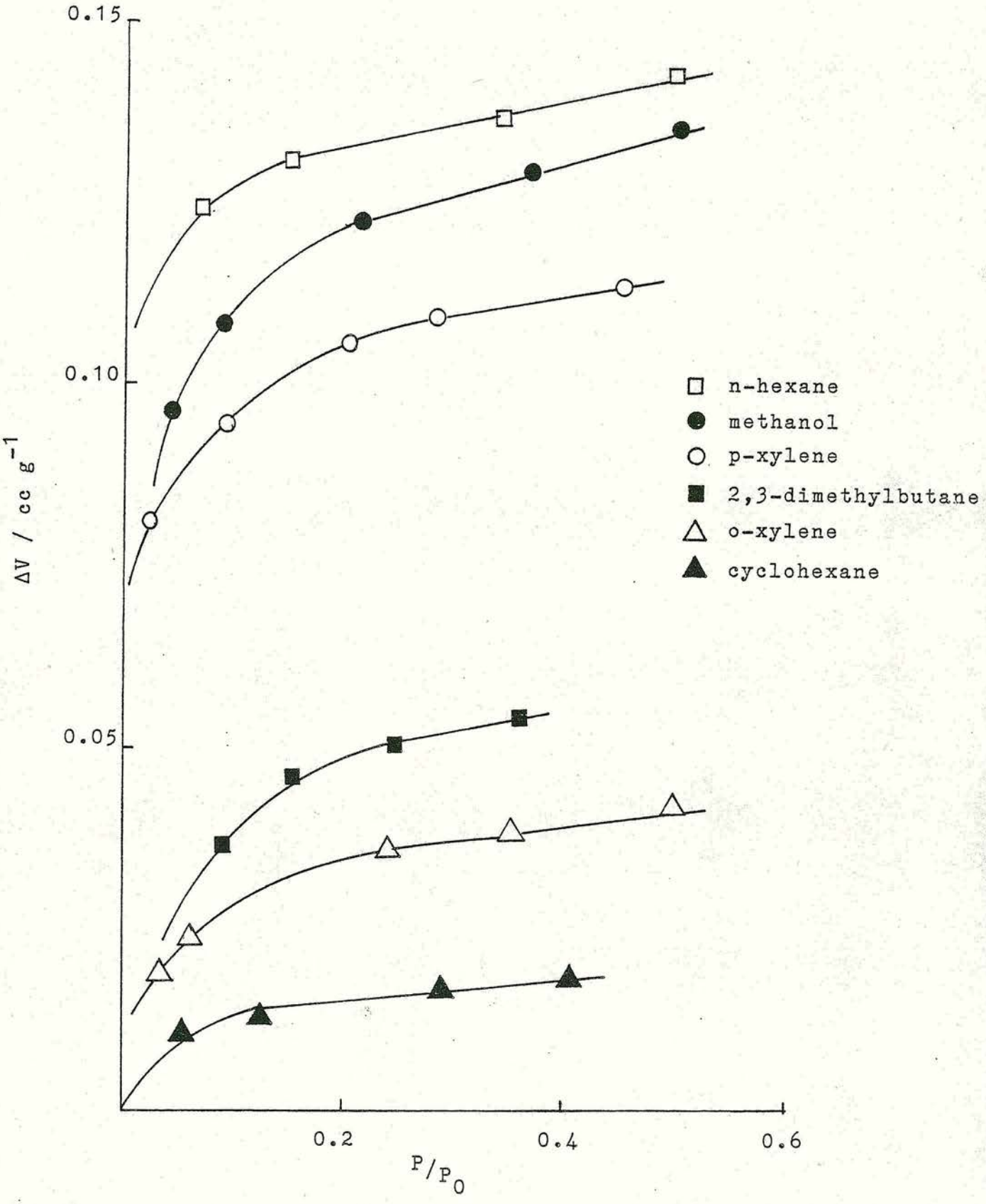

Sorbate	Pore Volume /ccg^{-1}	Area per Molecule nm^2 125	Area of Monolayer /m^{2}g^{-1}
methanol	0.147	0.219	479
n-hexane	0.141	0.562	374
p-xylene	0.139	0.538	365
cyclohexane	0.088	0.417	205
2,3-dimethylbutane	0.102	-	-
o-xylene	0.095	-	-

Table 4.13. Volumes of Sorbates Corresponding to Void Filling of H-EU-1(A)

Sorbate	Pore Volume /ccg^{-1}	Area per Molecule nm^2 125	Area of Monolayer /m^{2}g^{-1}
methanol	0.145	0.219	473
n-hexane	0.147	0.562	390
p-xylene	0.125	0.538	329
cyclohexane	0.022	0.417	51
2,3-dimethylbutane	0.060	-	-
o-xylene	0.052	-	-

Table 4.14. Volumes of Sorbates Corresponding to Void Filling of H-EU-1(B)

surface of the crystallites is not occurring but that part of the intracrystalline pore structure is accessible to these molecules i.e. two types of channel exist. p-Xylene has access to both channel systems. Differences in the pore volumes between the two samples can be attributed to the difference in crystallite size.

Comparison of the surface areas for different sorbates with the surface area determined by nitrogen adsorption for H-EU-1(A) (364 m^2g^{-1}) shows the values for n-hexane and p-xylene to be in good agreement. However, in the case of H-EU-1(B), comparison with the surface area determined by nitrogen adsorption (331 m^2g^{-1}) only the value for p-xylene is in good agreement. The surface area determined for methanol adsorption was found to be much larger than that determined by nitrogen adsorption in both cases. This could possibly be a result of the value taken for the area occupied per molecule for methanol. For both samples the surface area determined by cyclohexane adsorption was much less than that obtained from nitrogen adsorption indicating that cyclohexane has difficulty in filling all the pores. It was not possible to determine the surface areas from 2,3-dimethylbutane and o-xylene adsorption as no values for the area occupied per molecule for these species could be found in the literature.

Consideration of the kinetics of adsorption for the different sorbates as illustrated by the diffusion law (Equation 1.1) indicates that diffusion plays a role in adsorption over both zeolites samples. Straight line

portions indicative of diffusion controlled sorption were observed in plots of weight increase against $t^{0.5}$ for p-xylene and o-xylene on both samples of H-EU-1. In the case of p-xylene and o-xylene adsorption over H-EU-1(A) and p-xylene over H-EU-1(B), a small foot was observed near the start of the curve as illustrated in Figure 4.18 for H-EU-1(A). This foot can be attributed to surface adsorption on the external surface of the crystals. It has been shown[24] that the surface areas of crystalline powders may be measured by extrapolation of the diffusion plot to $t^{0.5} = 0$. Comparison of the slopes of the $t^{0.5}$ plots for o-xylene and p-xylene indicates that o-xylene appears to diffuse faster than p-xylene. In the previous discussion it has been suggested that there are two types of channel present in H-EU-1 of which p-xylene has access to both. The slower rate of diffusion for p-xylene can be explained by consideration of the size of the channels: p-xylene is able to diffuse rapidly into the channels that sorb o-xylene but diffuses slowly into the other tighter channels which exclude o-xylene.

Calculation of the diffusion coefficient from the slope of the $t^{0.5}$ plots requires a more detailed knowledge of the crystal shape and size distribution. It should be noted that different diffusivities can be obtained from different samples of the same zeolite. The Si/Al ratios vary between the two samples of H-EU-1 and thus the cation concentrations and locations in the intracrystalline channels and cavities will vary between the two samples. These factors can result in different

Figure 4.18. Sorbate Diffusion Plots

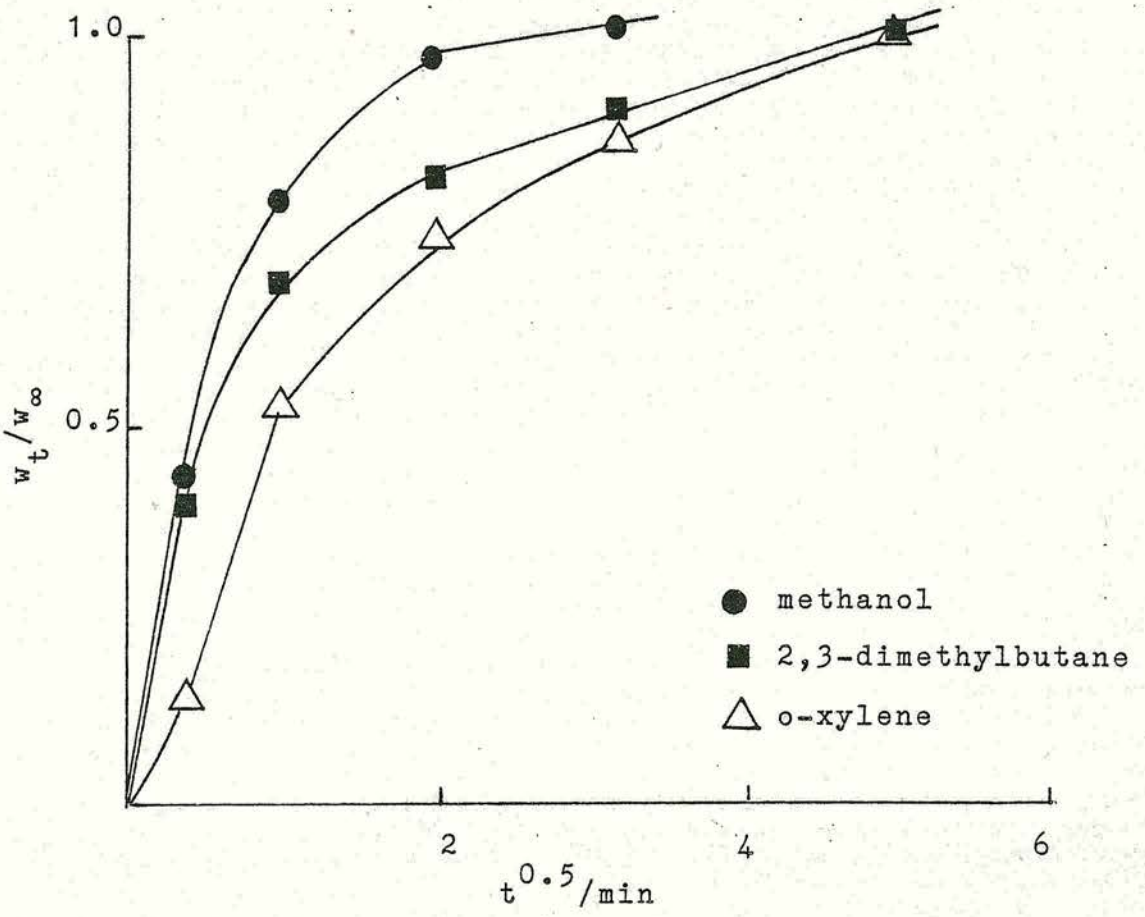

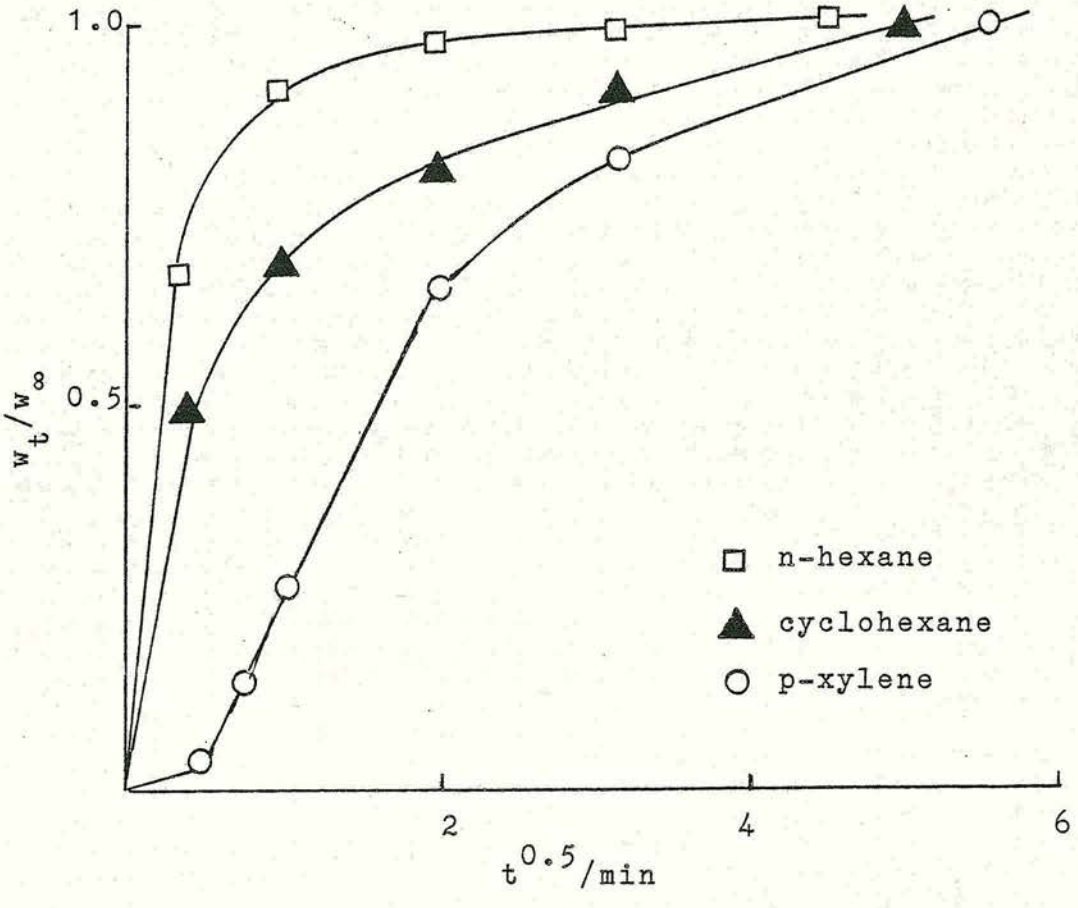

values of diffusivities. In addition, crystal size can have an effect on diffusivities as larger crystals have correspondingly longer diffusion paths.

(b) Adsorption of Butenes

The adsorptions of but-1-ene and cis and trans but-2-ene on H-EU-1(A) and H-EU-1(B) were investigated gravimetrically after outgassing at 823 K. In order to minimise reaction and avoid condensation of the butenes an adsorption temperature of 202 K was chosen. Rapid adsorption of all the n-butenes was observed on both samples of H-EU-1. H-EU-1(A) appeared to show a slight preference for but-1-ene. The weight increases (mg/g of zeolite) observed as a function of time for the adsorption of the n-butenes are illustrated in Figure 4.19 and 4.20 for H-EU-1(A) and H-EU-1(B) respectively. Similar profiles were observed for all adsorbates. The increases in weight observed after 15 minutes are listed in Table 4.15.

Sorbate	Critical Diameter nm[132]	Weight Adsorbed mg/g	
		H-EU-1(A)	H-EU-1(B)
but-1-ene	0.495	78.74	78.49
trans but-2-ene	0.495	73.57	76.53
cis but-2-ene	0.558	72.93	77.90

Table 4.15. Weights of n-Butenes Adsorbed by H-EU-1

Figure 4.19. Rates of Adsorption of the n-Butenes on H-EU-1(A)

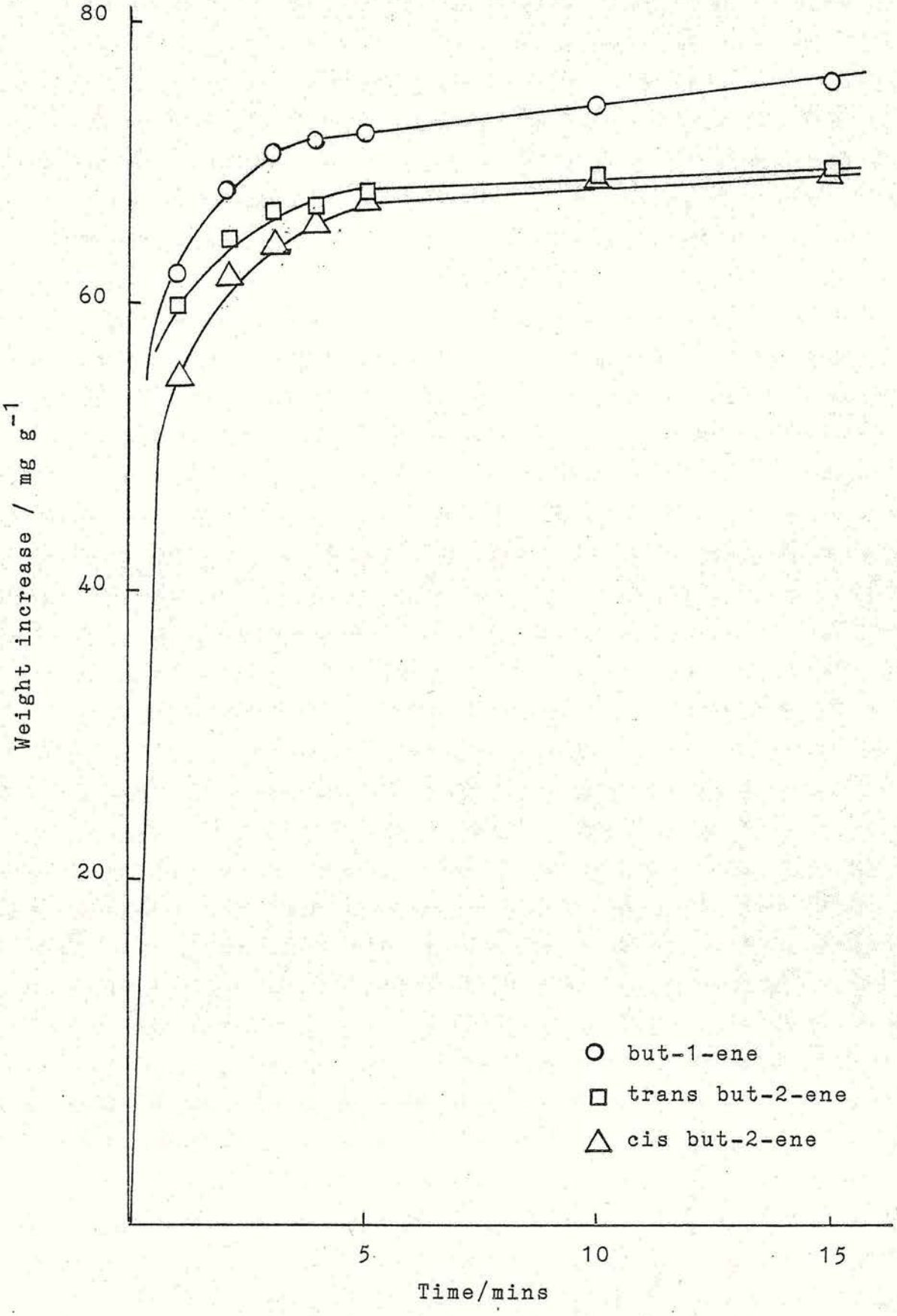

Figure 4.20. Rates of Adsorption of the n-Butenes on H-EU-1(B)

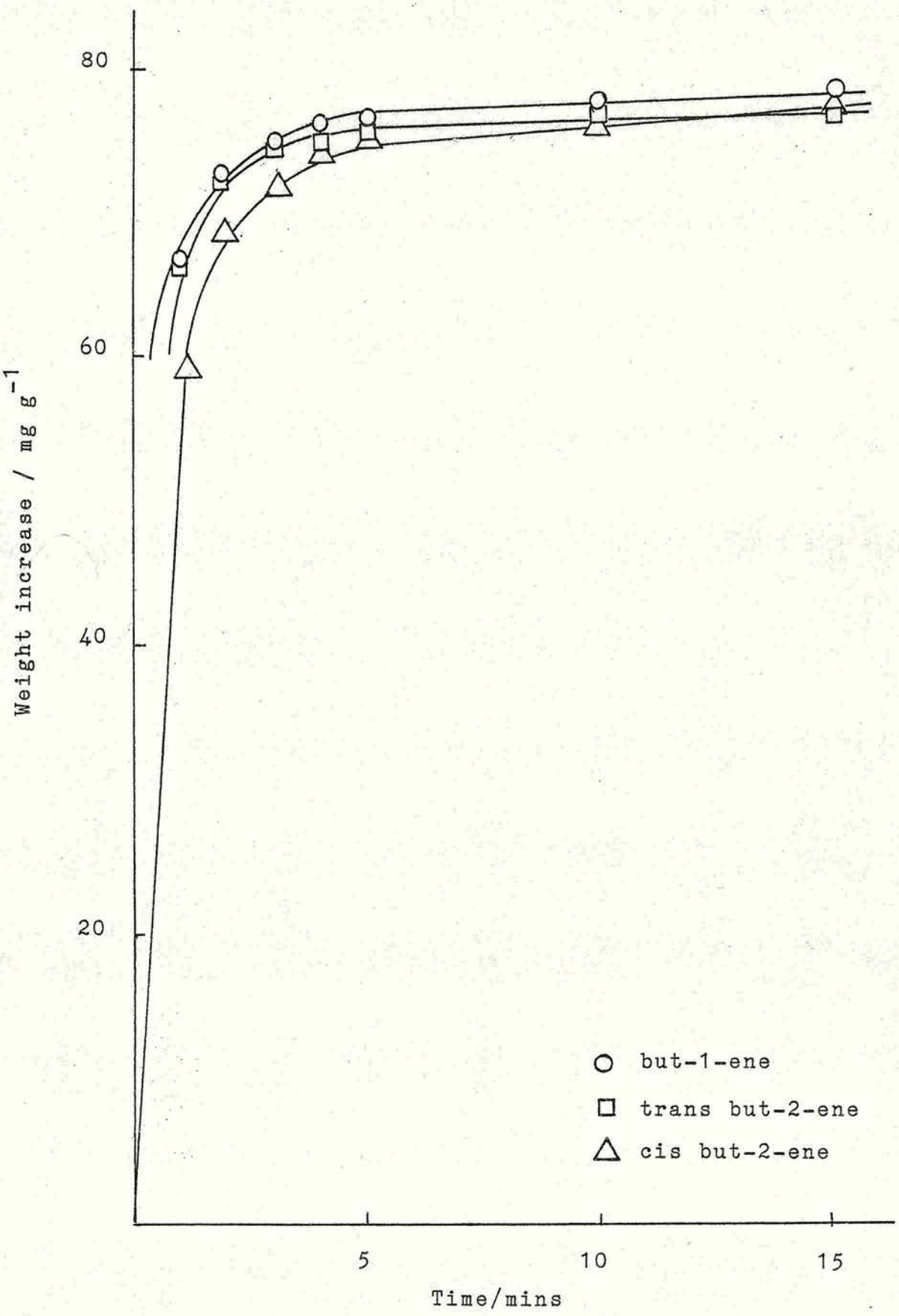

Adsorption isotherms for the n-butenes were recorded at 202 K for both samples of H-EU-1 and are illustrated in Figure 4.21 and 4.22. H-EU-1(A) demonstrates a higher affinity for but-1-ene (as illustrated by Figure 4.21) than cis or trans but-2-ene. This affinity for but-1-ene is also apparent over H-EU-1(B) but not to such an extent. Trans but-2-ene has the same minimum cross-sectional area as but-1-ene and would thus be expected to show the same sorption volume as but-1-ene.

Langmuir plots were obtained for all sorbates according to Equation 3.4. Linear plots were obtained in all cases. Weights of sorbates corresponding to pore filling together with the area occupied per molecule and the calculated monolayer coverage (surface area) are given in Tables 4.16 and 4.17.

Sorbate	Pore Volume /ccg^{-1}	Area per Molecule nm^2 125	Area of Monolayer /m^{2}g^{-1}
but-1-ene	0.161	0.378	388
trans but-2-ene	0.147	0.334	318
cis but-2-ene	0.149	0.385	383

Table 4.16. Volumes of n-Butenes Corresponding to Void Filling of H-EU-1(A)

Figure 4.21. Adsorption Isotherms for the n-Butenes on H-EU-1(A)

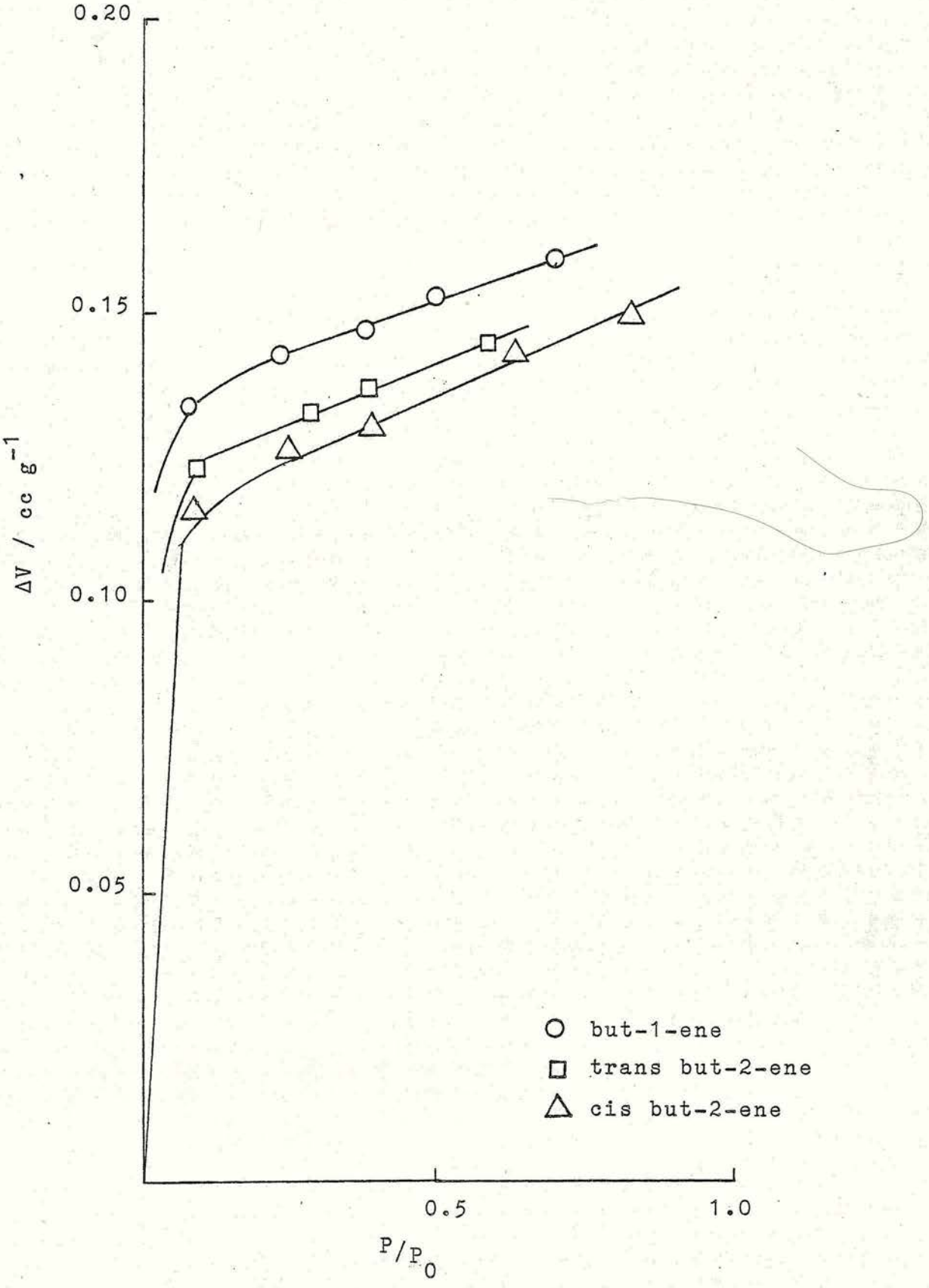

Figure 4.22. Adsorption Isotherms for the n-Butenes on H-EU-1(B)

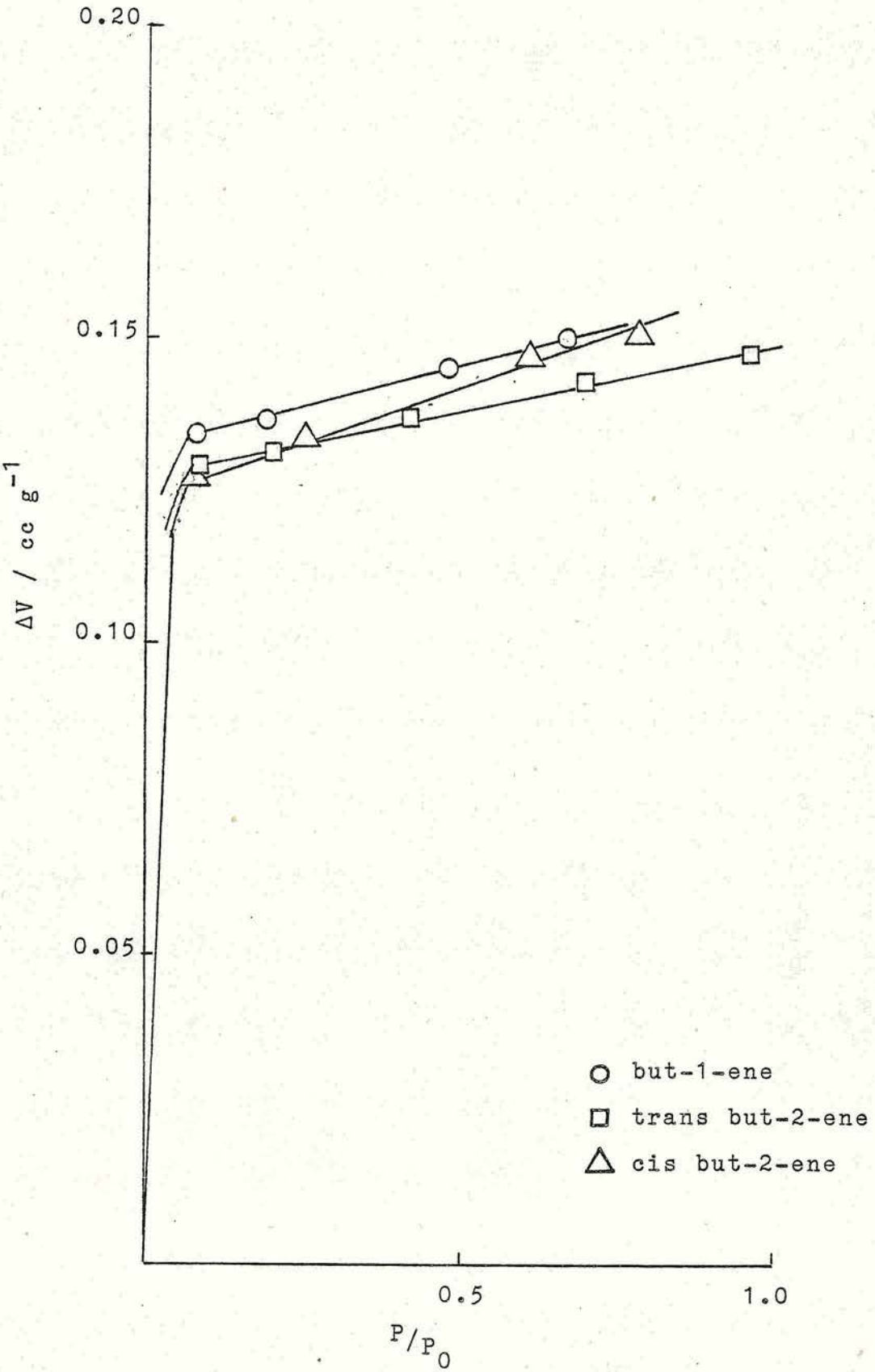

Sorbate	Pore Volume /ccg^{-1}	Area per Molecule nm^2 125	Area of Monolayer /m^{2}g^{-1}
but-1-ene	0.147	0.378	355
trans but-2-ene	0.139	0.334	301
cis but-2-ene	0.149	0.385	383

Table 4.17. Volumes of n-Butenes Corresponding to Void Filling of H-EU-1(B)

The data in Tables 4.16 and 4.17 when compared to the surface areas obtained by nitrogen adsorption (364 m^2g^{-1} for H-EU-1(A) and 331 m^2g^{-1} for H-EU-1(B)) indicate that the internal surface which is available to nitrogen is also available to the butene molecules i.e. the butene molecules have access to both types of channel.

The kinetics of adsorption of the butenes in H-EU-1, in which weight increase is plotted against $t^{0.5}$ (Equation 1.1) indicated that there was rapid adsorption with little diffusion control. The diffusion plots suggest that the rates of diffusion vary in the order

but-1-ene = trans but-2-ene > cis but-2-ene

and that diffusion of the butenes is faster in H-EU-1(A) than in H-EU-1(B). The order of diffusion is that expected on consideration of the size of the sorbate molecules. Trans but-2-ene has the same critical diameter as but-1-ene (0.495 nm) while cis but-2-ene has a larger critical diameter (0.558 nm). H-EU-1(B) has

been shown previously in Section 4.1.4 to have a larger crystal size than H-EU-1(A) and thus has a correspondingly longer diffusion path and thus slower rates of diffusion.

Summary of Adsorption Results in EU-1

The sorption data recorded for the different samples of H-EU-1; the sorption of p-xylene and the low capacity for cyclohexane indicate that H-EU-1 has a pore diameter of c.a. 0.6 nm. This is consistent with a pore structure comprising 10-membered rings similar to the type found in ZSM-5[13]. In addition the results suggest that two types of channel of differing size are present: one which is able to sorb cyclohexane and one which cannot. Both channel types were shown to be accessible to p-xylene although the adsorption was diffusion controlled. Differences in sorbate uptake between the two samples of H-EU-1 can be attributed to the differences in crystal size.

4.3. Nature of the Ruthenium Y Catalysts

4.3.1. Chemical Composition

The three ruthenium Y samples were prepared by ion exchange with $[Ru(NH_3)_6]Cl_3$ and were pretreated as described previously in Chapter 3. Chemical analysis of the RuY samples was carried out by neutron activation analysis*. The results are listed in Table 4.18.

Zeolite	Chemical Analysis (wt. percent)		
	Na	Ru	La
RuNaY20	2.70	5.11	-
RuNaLaY20	2.18	1.77	7.31
RuLaY20	2.07	1.55	8.21

Table 4.18. Chemical Analysis of RuY Zeolites by Neutron Activation Analysis*

* Neutron Activation Analysis kindly carried out by I.C.I.

$[Ru(NH_3)_6]^{3+}$ is the most common starting material for the formation of Ru^0 particles[57]. The final state of the ruthenium depends very much upon the atmosphere under which the complex is decomposed; that is, under hydrogen, oxygen, a vacuum or an inert atmosphere. In a Y-type zeolite the smallest metal particles may be obtained by heating $[Ru^{3+}(NH_3)_6]Y$ sample under vacuum followed by reduction[55]. It has been demonstrated by several authors[55,134], that decomposition of the supported $[Ru(NH_3)_6]^{3+}$ complex is accompanied by autoreduction of the ruthenium. Above 523 K, molecular nitrogen has been observed in the desorbed gases. Some disagreement, however, exists concerning the extent of this reduction. Elliot and Lunsford[61] report an autoreduction to an average oxidation state of Ru^{II}; whereas Verdonck et al[55] observed that up to 80% of the

ruthenium was reduced to Ru^0. The differences in the amount of autoreduction can possibly be explained in terms of the weight percent ruthenium contained by the samples and the fact that Ru^0 is an effective catalyst for ammonia synthesis and decomposition. The temperature used for the reduction of the ruthenium has been shown to have an influence on the activity as a catalyst[58]. The activity was found to reach a maximum at a reduction temperature of 573 K. The decrease in activity with increasing reduction temperature above 573 K has been attributed by Jacobs et al[134] to the sintering of metal particles. The lower activity at 523 K is probably due to incomplete reduction. A reduction temperature of 573 K was used in this study.

At 298 K $[Ru(NH_3)_6]^{3+}$ undergoes a reaction both in air and under vacuum as indicated by a change in the colour of the sample from nearly white to pink[57], the colour of the samples used in this study. Spectroscopic results[135] indicate that the complex is hydrolysed into a pentammine hydroxy complex, $[Ru^{III}(NH_3)_5OH]^{2+}$. At higher temperatures, the residual hydration water causes further hydrolysis and ruthenium-red, $[Ru^{III}(NH_3)_5\text{-}O\text{-}Ru^{IV}(NH_3)_4\text{-}O\text{-}Ru^{III}(NH_3)_5]^{6+}$, becomes a dominating species[135,136]. The ruthenium-red complex is destroyed by heating the sample under vacuum or in oxygen at 398 K.

X-Ray diffraction techniques have been used[56] to identify atomically dispersed Ru^0 inside the sodalite cavity at site II' in a RuY zeolite. This atomically

dispersed Ru^0 was removed by the addition of oxygen and was not regenerated by subsequent reduction in hydrogen. The Na^+ ions within the zeolite always occupy sites I' and II and are generally unaffected by the redox chemistry involving the ruthenium. Pederson and Lunsford[63] found that at elevated temperatures before or after reduction the presence of oxygen resulted in the formation of RuO_2 on the external surface of the zeolite. An infra-red study of CO adsorption on RuY has identified three types of sites on the reduced catalyst[137]. It was suggested that these three types of site are associated with highly dispersed (probably atomically) ruthenium, ruthenium clusters and ruthenium particles greater than 1.0 nm.

4.3.2. Surface Areas

The surface areas of the three RuY zeolites were determined by nitrogen adsorption according to the BET equation (Equation 3.5). The surface areas were determined after outgassing at 573 K for 16 hours followed by reduction and subsequent evacuation as detailed in Section 3.3.3. The results are listed in Table 4.19.

Sample	Surface Area/m^2g^{-1}	
	Before Reduction	After Reduction
RuNaY20	554	545
RuNaLaY20	524	517
RuLaY20	484	476

Table 4.19. Surface Area Measurements for the RuY Samples

The above results suggest that there was a slight but not significant loss in surface area after reduction of the sample.

4.3.3. Temperature Programmed Reduction

Temperature programmed reduction (TPR) studies were carried out on all three RuY samples using the apparatus described previously in Section 3.5.4.

It has been shown by Uytterhoeven[19] that reduction of a metal ion in a zeolite is generally achieved using hydrogen; the overall stoichiometry being

$$M^{n+} + {}^{n}/_{2}H_2 \rightarrow M^0 + nH^+ \qquad \text{Equation 4.1.}$$

The protons react with the zeolite lattice to produce hydroxyl groups whose presence has been established by infra-red spectroscopy.

$$nZO^- + nH^+ \rightarrow ZOH \qquad \text{Equation 4.2.}$$

A correlation has been observed between the reducibility of a metal ion in a zeolite and the standard electrode potential[19]. The standard electrode potential of

Ru^{3+}/Ru^{0} is -0.67 V[138] while the electrode potential of La^{3+}/La^{0} is -2.37 V[139]. Thus it can be concluded that ruthenium will be reduced before lanthanum.

The design of the TPR apparatus enabled samples to be outgassed at varying temperatures and also allowed oxidation to be carried out. The RuY samples were outgassed overnight at room temperature due to problems in removing all traces of oxygen from the system. At higher temperatures the ruthenium was found to react with any oxygen present. Two temperatures were used for oxidation: room temperature and 573 K. In both cases the oxidation was carried out using 5% vol. oxygen in helium and a contact time of 150 minutes.

The three RuY samples were outgassed overnight at room temperature under flowing argon and the subsequent TPR traces illustrated in Figure 4.23. The TPR traces of the RuY samples reveal the existence of three maxima in the rate of hydrogen uptake. The temperature of the maxima for reduction and the hydrogen consumption (from the area under the spectrum) are listed in Table 4.20.

Catalyst	T_{max}/K			Hydrogen Consumption moles/g
	1	2	3	
RuNaY20	413	482	573	1.23×10^{-4}
RuNaLaY20	433	493	606	2.34×10^{-4}
RuLaY20	410	478	580	2.80×10^{-4}

Table 4.20. Values for T_{max} and Hydrogen Consumption for RuY

Figure 4.23. TPR Profiles of RuY Zeolites

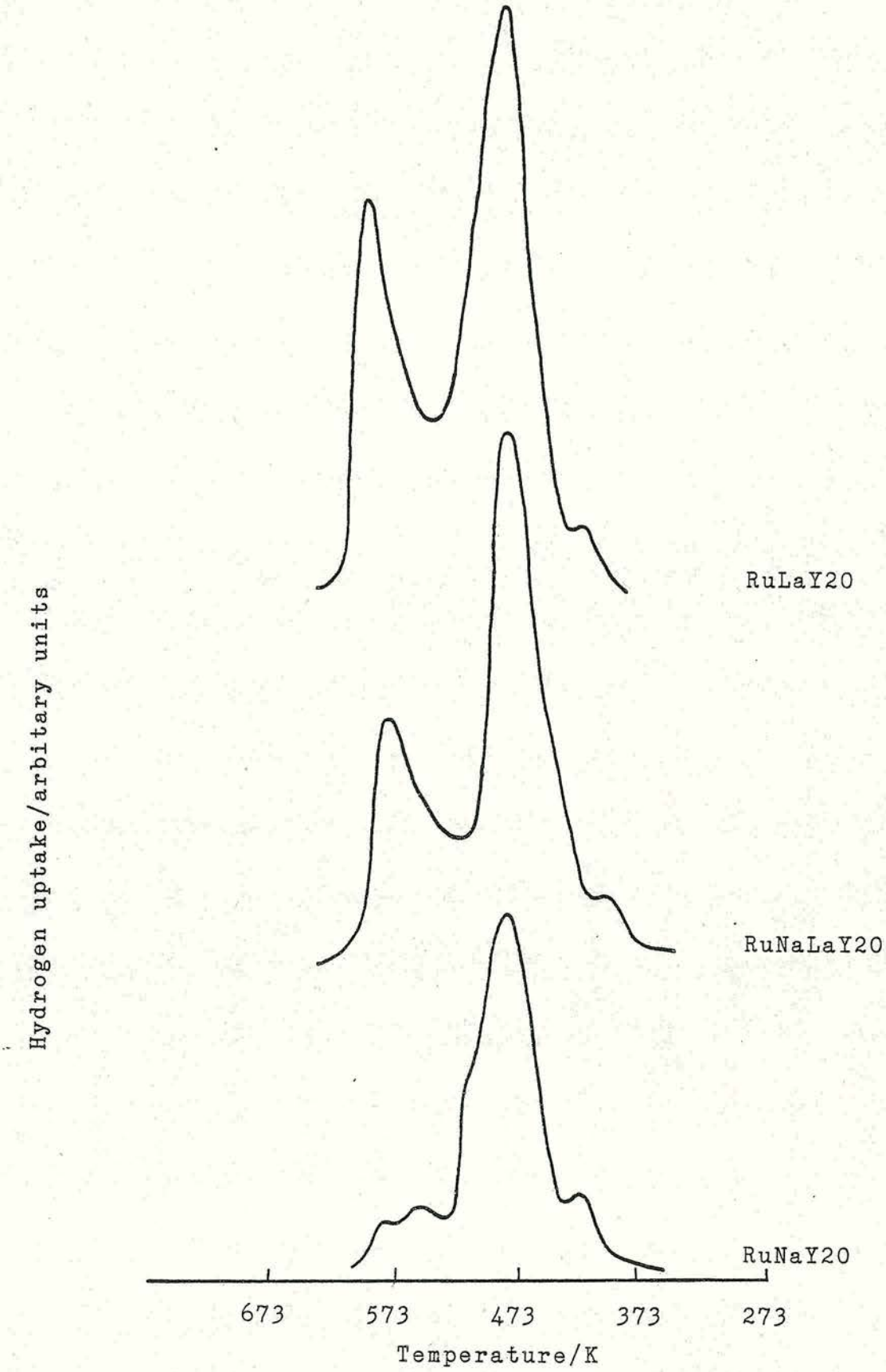

The average valency of the ruthenium after each maxima is shown in Equation 4.3.

$$Ru^{III} \xrightarrow{410\text{-}433} Ru^{II} \xrightarrow{478\text{-}493} Ru^{I} \xrightarrow{573\text{-}606\ K} Ru^{0}$$

Equation 4.3.

and is in good agreement with the results obtained by Verdonck et al[140] who obtained temperatures for the maxima of 423, 493 and 563 K respectively. The amount of hydrogen consumed increases with decreasing amount of ruthenium present in the sample (Tables 4.18 and 4.20). Ru^0 is an effective catalyst for ammonia synthesis and decomposition thus the formation of any Ru^0 would aid the decomposition of the complex. During the course of the TPR, hydrogen was evolved due to decomposition of the NH_3 ligands to N_2 and H_2. One peak was obtained for hydrogen evolution from RuNaY20 and RuLaNaY20 (T_{max} 699 K and 713 K respectively) while two peaks were obtained from RuLaY20 (T_{max} 673 and 707 K). Consideration of the number of moles of hydrogen consumed and evolved suggested that some of the ruthenium was already present as Ru^0 before the TPR was carried out out and that some autoreducton had occurred during the outgassing at room temperature overnight.

Oxidation at room temperature and 573 K produced similar profiles with different T_{max} values. The trace consisted of a single maxima for the samples oxidised at room temperature while the samples oxidised at 573 K exhibited a single maxima with a slight shoulder to the

lower temperature side. There is disagreement in the literature concerning the number of oxygen atoms chemisorbed on surface ruthenium atoms. Goodwin[141] found that values varied between 2.14 and 3.5, and, even on the same catalyst successive measurements yielded quite different ratios. A value for the O_2/Ru ratio of greater than two could be due to oxygen spillover, to the bulk oxidation of large particles or to the formation of stabilized RuO_3 or RuO_4. Verdonck et al[55] found that ruthenium was oxidised as follows -

$$Ru^0 + O_2 \rightarrow RuO_2 \qquad \text{Equation 4.4.}$$

The degree of oxidation of the RuY samples as determined from the TPR of the oxidised samples has been calculated using the previous equation and the values are listed in Table 4.21 together with the T_{max} values.

Catalyst	T_{max} Oxidation at Room Temp./K	T_{max} Oxidation at 573 K /K	Percent Oxidation at Room Temp.	Percent Oxidation at 573 K
RuNaY20	355	429	33	76
RuNaLaY20	368	452	24	99
RuLaY20	363	445	48	99

Table 4.21. Values for T_{max} and Percent Oxidation at Room Temperature and 573 K for RuY

Further experiments showed that the sample could not be regenerated and that the oxidation at 573 K was not

reversible.

Using a temperature programmed oxidation technique, Verdonck et al[55] obtained results suggesting that finely dispersed particles located in the zeolite cages are oxidised at ambient temperatures while ruthenium clusters, possibly located in holes in the zeolite crystal, are oxidised at around 550 K. RuO_2 is highly mobile and at elevated temperatures will rapidly migrate to the surface of the zeolite.

Measurement of hydrogen desorption and uptake by means of the TPR apparatus has been shown[142] to give rapid and useful information about the ruthenium metal dispersion. After the TPR treatments the sample was cooled to ambient temperature in 5% vol. hydrogen in argon (during which hydrogen adsorption occurred) and subsequently heated at a rate of 20 $Kmin^{-1}$ while the hydrogen desorption was recorded.

Hydrogen chemisorption on RuY has been studied in some detail by several authors[141-144] to determine the number of hydrogen atoms chemisorbed per ruthenium surface atom. It has been suggested[141] that the ratio of adsorbed hydrogen to surface ruthenium atoms was one given the assumptions made for calculations and the errors inherent in experimental measurement.

Temperature programmed desorption (TPD) measurements were recorded for all samples before and after oxidation. In all cases, before oxidation the traces showed a broad maximum around 433 K. Minor amounts of hydrogen were recovered at higher

temperatures. The amount of hydrogen recovered during a TPD was less than that adsorbed during cooling to ambient temperature. It has been shown[143] that on ruthenium two distinct types of hydrogen chemisorption occur at room temperature i.e. a rather strong activated chemisorption and a weak non-activated chemisorption (reversible). The reversibly bound hydrogen includes hydrogen in the physisorbed state and hydrogen species in the weakly chemisorbed state, either a transition state at total surface coverage or an adsorbed state on low energy sites. Desorption occurs when the adsorbate-adsorbent bond acquires the required activation energy for desorption in the form of vibrational energy. The first peak in the TPD spectrum is thus the weakly held hydrogen while the peaks at higher temperatures are due to the more strongly held hydrogen. The TPD traces recorded after oxidation at 573 K revealed a small peak due to desorption, followed by a small peak due to adsorption followed by several peaks due to desorption.

The metal dispersion, defined as the ratio of hydrogen atoms adsorbed to the total amount of ruthenium atoms, obtained from the desorption peaks is given in Table 4.22.

	Dispersion		
	RuNaY20	RuNaLaY20	RuLaY20
(1) After initial TPR	0.37	0.37	0.49
(2) After oxidation at room temp.	0.34	0.38	0.41
(3) After oxidation at 573 K	0.07	0.05	0.07

Table 4.22. Value for Dispersion (Ratio of Hydrogen Atoms to Ruthenium Atoms) on RuY

The results indicate that there is a slight loss in dispersion after oxidation at room temperature. However, oxidation at 573 K causes a much greater loss in dispersion. The oxidation of the ruthenium at ambient temperature does not result in migration of the ruthenium while oxidation at elevated temperatures results in migration to the external surface[63]. The oxidation at 573 K results in an increase in the ruthenium cluster size. It should also be noted that there is an increase in dispersion with decreasing ruthenium metal content i.e. smaller clusters of ruthenium are formed when the ruthenium metal content is low.

The metal surface area per gram of metal was calculated using 9.03×10^{-20} m^2 [69] as the area of a ruthenium atom and by assuming that one hydrogen was

adsorbed by each ruthenium metal atom. The average crystallite size was calculated from the surface area data assuming the metal particles to be cubes of side L with all faces accessible to hydrogen. The area (A) per gram of exposed metal is given by $6L^2n$, where n is the number of crystallites per gram. If $p(= 12.2 \times 10^6\ kgm^{-3})$[69] is the density of metallic ruthenium then $n = 1/pL^3$ and

$L\ (in\ m) = 6/pA = (4.918 \times 10^{-7})/A$ Equation 4.5.

The metal surface areas and crystallite sizes are listed in Table 4.23.

	RuNaY20		RuNaLaY20		RuLaY20	
	S.A.	C.S.	S.A.	C.S.	S.A.	C.S.
(1) After initial TPR	197	2.50	204	2.41	263	1.87
(2) After oxidation at room temp.	184	2.67	204	2.41	221	2.22
(3) After oxidation at 573 K	38	12.94	28	17.86	36	13.66

S.A. :- surface areas given in m^2g^{-1} of metal.

C.S. :- crystallite size given in nm.

Table 4.23. Surface Areas and Crystallite Sizes for RuY

The results confirm that with oxidation at room temperature there is a slight loss in the metal surface

area and an increase in the crystallite size. The ruthenium metal surface area does not appear to increase with increasing percent ruthenium content suggesting that the particles present in RuNaY20 are larger than those found in RuLaNaY20 and RuLaY20. This was indeed found to be the case.

The initial crystallite size appears to be larger than that expected to allow ruthenium to be present in the supercages (diameter 1.3 nm). Metal particles exceeding supercage dimensions have been found embedded in a Faujasite matrix with aggregate sizes ranging from 3 nm for palladium, 4 nm for ruthenium to 8 nm for platinum and nickel[64]. The results in this study can be rationalised in two ways. The first explanation proposed by Verdonck et al[55] involves the localised destruction of the zeolite lattice by water to form cracks and holes. Filling of these voids by ruthenium metal could result in average particle sizes greater than the free diameter of the zeolite supercages. The second explanation suggested by Gustafson and Lunsford[145] is that in the presence of hydrogen the mobility of the ruthenium is increased resulting in an agglomeration of the metal in several adjacent supercages such that the particles are connected through the 12-membered rings. However, the presence of even a few relatively large crystallites will be able to significantly increase the average crystallite size calculated.

Summary

When $[Ru(NH_3)_6]^{3+}$ was ion exchanged into a Y-type zeolite the complex was found to undergo a reaction in air to form a pentammine hydroxy complex. TPR studies indicated that after reduction the average size of the ruthenium crystallites was such that they exceeded the supercage dimensions. However, the ruthenium could be located in voids in the zeolite lattice or in agglomerates in several adjacent supercages where the particles may actually be connected through the 12-membered rings. Finely dispersed (probably atomically) ruthenium particles are oxidised at room temperature while oxidation at 573 K results in almost total oxidation of the ruthenium to RuO_2 accompanied by the formation of large crystallites outside the zeolite framework.

CHAPTER 5

Results and Discussion:- Part II

Isomerisation Reactions over H-ZSM-23 and H-EU-1

The aim of this chapter is to compare the activity of H-ZSM-23 and H-EU-1 as catalysts and consider the nature of the active sites for n-butene isomerisation and methylcyclopropane isomerisation. The catalysts were pretreated at 723 K for 16 hours and the reactions carried out using a flow rate of 1.20×10^{-2} dm^3 s^{-1} unless otherwise stated.

5.1. Reactions over H-ZSM-23

5.1.1. But-1-ene Isomerisation

The variation in surface area with temperature of zeolite H-ZSM-23 has been discussed previously in Section 4.1.3. Samples pretreated at 723 K for 16 hours exhibited the maximum surface area of 205 $m^2 g^{-1}$.

A typical reaction plot for but-1-ene isomerisation over H-ZSM-23 is illustrated in Figure 5.1. The only products observed were cis but-2-ene and trans but-2-ene. Extrapolation of the conversion curves to zero contact time shows always about 2% conversion of but-1-ene although the starting material was pure isomer. The derived first order plot is shown in Figure 5.2. All samples studied regardless of reaction temperature exhibited first order plots in which an initial fast rate (lasting for c.a. 25 minutes) and a slower steadier rate were apparent. The results are given in Table 5.1, the first order rate constants quoted being those of the slower steady rate. There appeared to be a "tailing off" of the first order plot after 150 minutes in all cases.

Figure 5.1. Reaction Profile for But-1-ene Isomerisation over H-ZSM-23 at 340 K

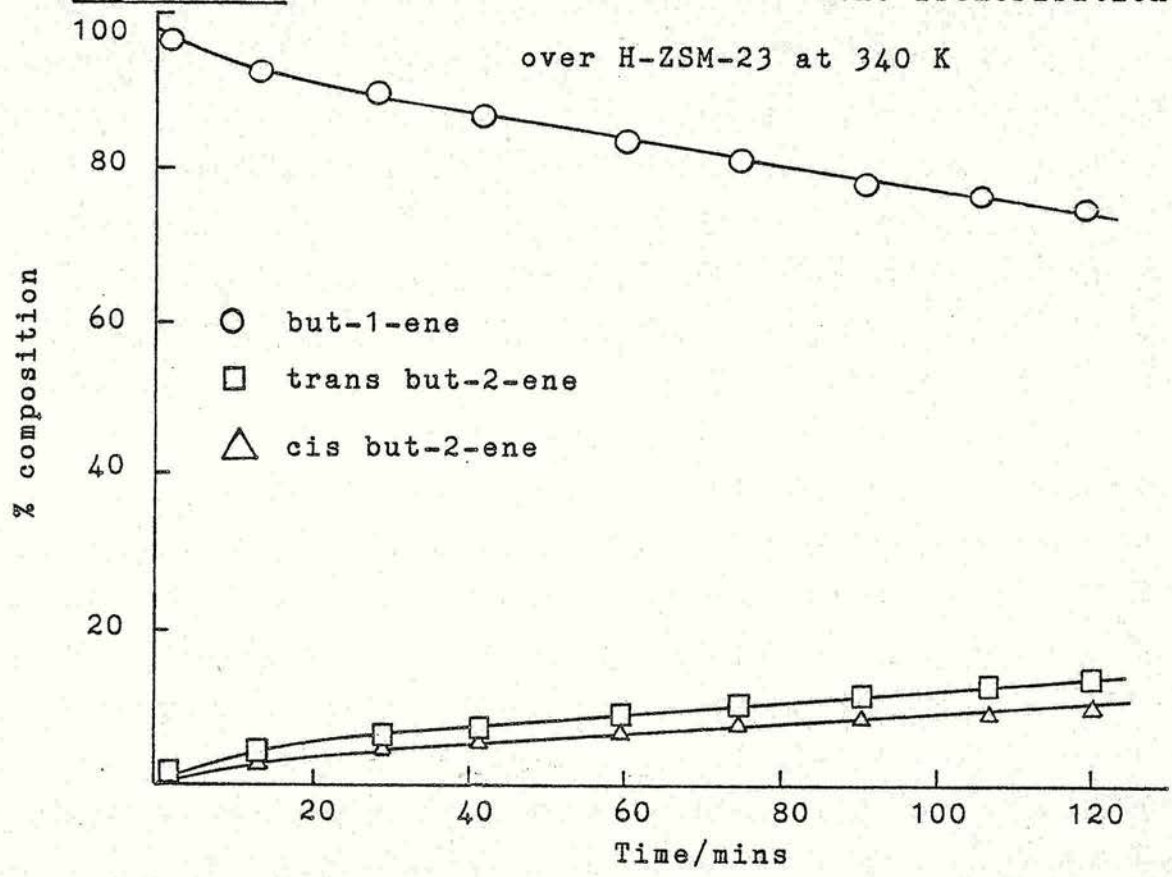

Figure 5.2. Derived First Order Plot

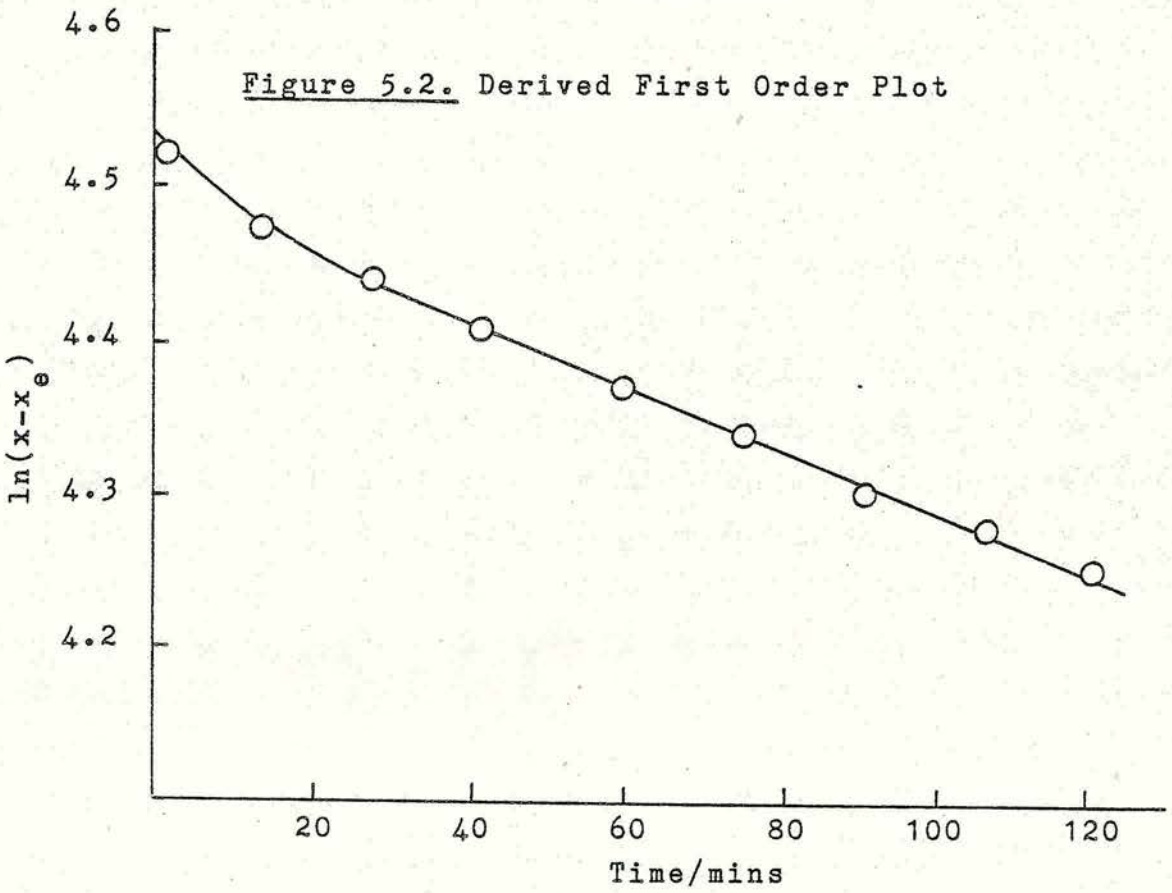

The "tailing off" appeared to be related to the time of contact rather than extent of conversion.

Reaction Temperature/K	Rate Constant/10^{18} molecules $s^{-1}g^{-1}$	Cis/Trans Product Ratio	
		Initial	Equilibrium
330	1.11	0.61	0.34
340	1.86	0.61	0.35
340	1.68	0.62	0.35
345	2.06	0.62	0.36
353	2.51	0.61	0.38
386	12.06	0.52	0.43
387	10.54	0.60	0.43
393	22.50	0.56	0.44

Table 5.1. First Order Rate Constants for But-1-ene Isomerisation over H-ZSM-23

The data from Table 5.1 can be used to construct an Arrhenius plot as shown in Figure 5.3. The apparent activation energy was calculated to be 48 kJ mol^{-1}.

At the end of the first isomerisation run (k_1) (typically 150-180 minutes duration) the catalyst sample was evacuated: either for 30 minutes at reaction temperature or for 16 hours at 723 K. These pretreatments were anticipated to be sufficient to remove (a) all gaseous molecules from the reaction vessel and (b) probably any physically adsorbed molecules from the samples. After the period of evacuation but-1-ene was re-admitted to the catalyst sample at the original

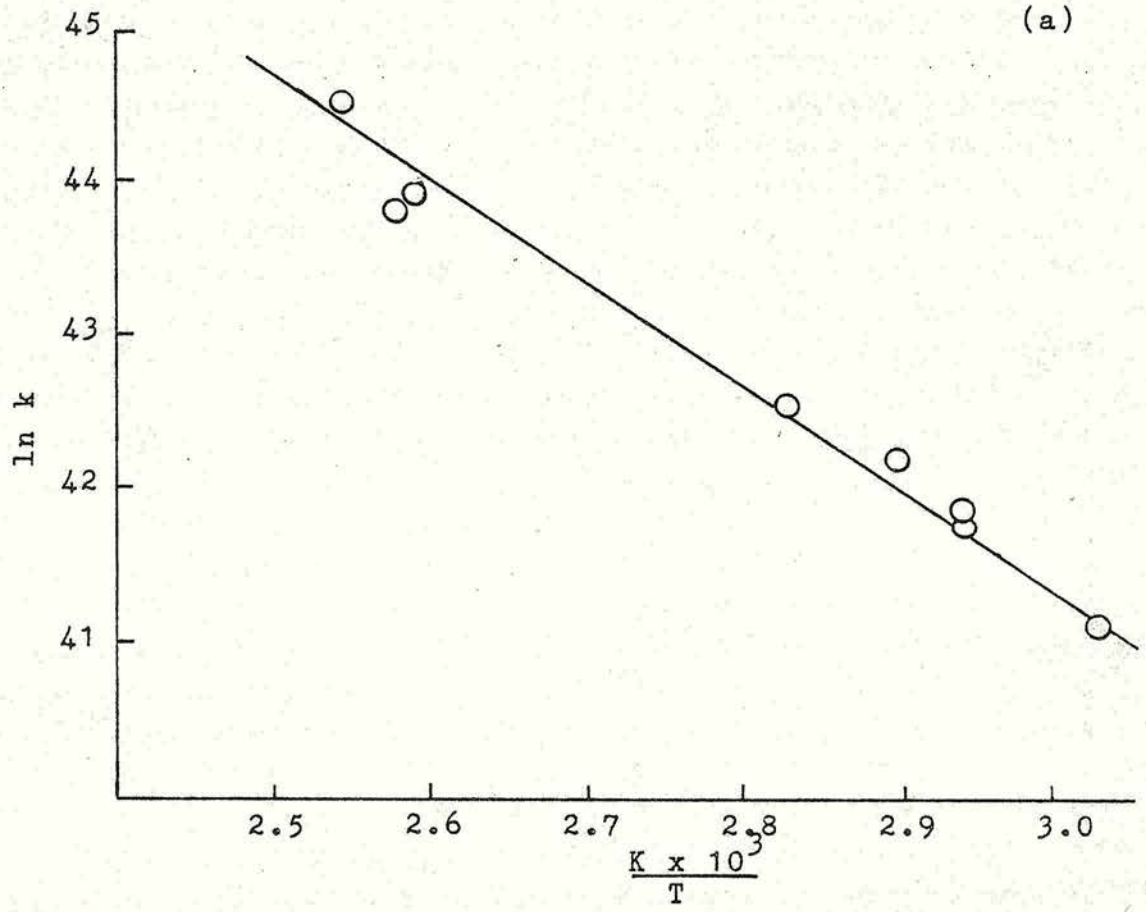

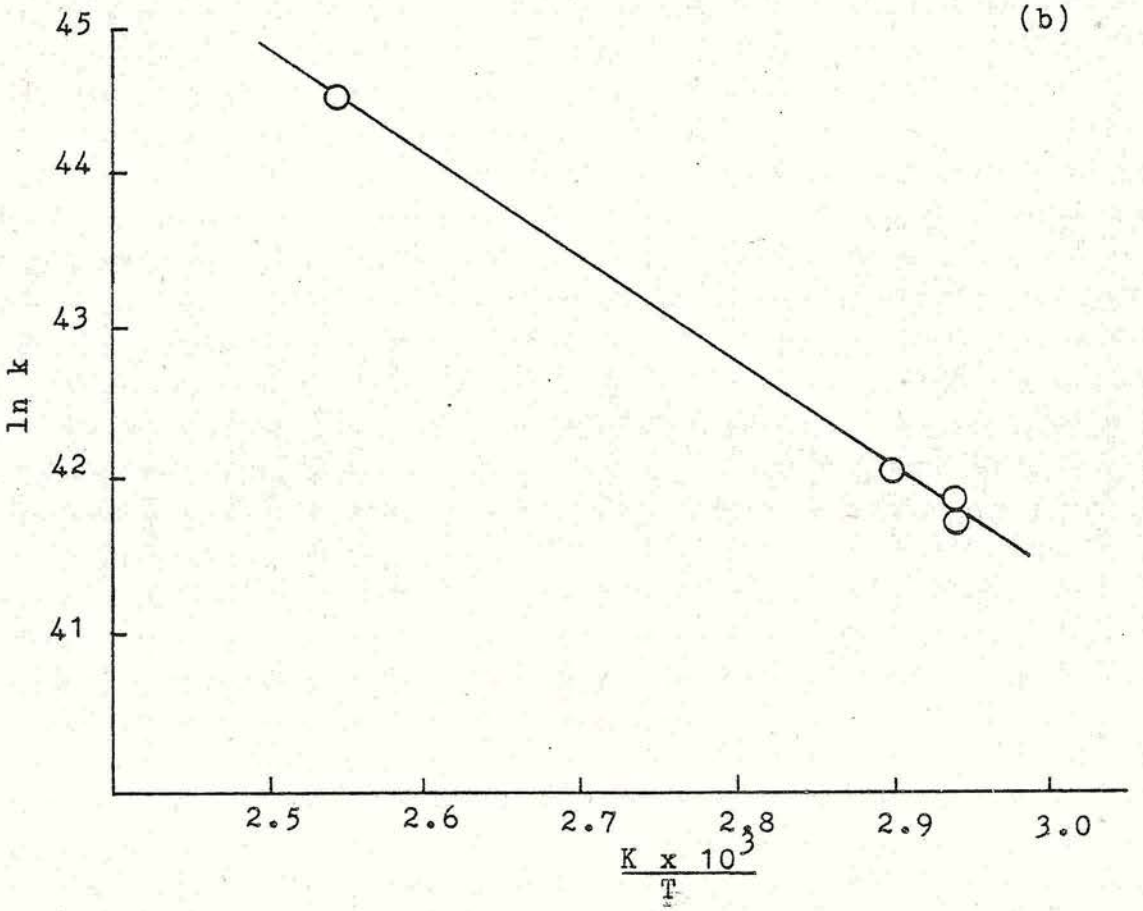

Figure 5.3. Arrhenius Plots for the Isomerisation of But-1-ene over H-ZSM-23

(a) Run 1 (b) Run 2

reaction temperature. The data recorded for this second run i.e. k_2, were treated in a similar manner to those of Run 1. Table 5.2 demonstates that after evacuation for 30 minutes the first order rate constant for Run 2 was reduced with respect to Run 1 whereas evacuation at 723 K for 16 hours restored the activity to its original value. The ratio of the first order rate constants (k_2/k_1) is also shown in Table 5.2 for each reaction temperature studied.

Reaction Temp./K	Evacuation Temp./K	Evacuation Time/hours	Rate Constant/10^{18} molecules $s^{-1}g^{-1}$	k_2/k_1
386	386	0.5	6.87	0.57
340	723	16	1.99	1.07
340	723	16	1.69	1.00
345	723	16	1.88	0.91
393	723	16	21.12	0.94

Table 5.2. First Order Rate Constants (k_2) for Run 2 But-1-ene Isomerisation over H-ZSM-23

Table 5.2 demonstrates that H-ZSM-23, after 30 minutes evacuation was significantly deactivated by the presence of but-1-ene molecules. Extrapolation of the reaction plot to zero time showed that at zero time there was 100% but-1-ene present. The Run 2 isomerisation followed first order kinetics. However, the induction period was found to be reduced to c.a. 15 minutes while the "tailing off" appeared to occur after a longer

contact time. Cross et al[89] reported that the induction period observed during but-1-ene isomerisation over NiX could be reduced but not eliminated by undertaking second runs in a similar manner to that described here.

Evacuation at 723 K for 16 hours was found to restore the activity of the catalyst. The apparent activation energy value for Run 2 (52 kJ mol^{-1} from Figure 5.3) does not differ markedly from the value for Run 1 (48 kJ mol^{-1}).

A third reaction was carried out at 345 K. The sample was evacuated for a further 16 hours after Run 2 and but-1-ene admitted at the original reaction temperature. The results are listed in Table 5.3.

Run	Rate Constant/10^{18} molecules $s^{-1}g^{-1}$	k_2/k_1	k_3/k_1	Initial Cis/Trans Product Ratio
1	2.06			0.62
2	1.88	0.91		0.67
3	1.57		0.76	0.66

Table 5.3. Repeat Runs on H-ZSM-23 at 345 K

The above results indicate that evacuation at 723 K for 16 hours will restore the activity for Run 2 while the activity of the sample for Run 3 is reduced.

Experiments were carried out in which the flow rate was altered. The first order rate constants and the initial cis/trans but-2-ene product ratios obtained are given in Table 5.4.

Flow Rate/10^{-2} dm^3 s^{-1}	Rate Constant/10^{18} molecules $s^{-1}g^{-1}$	Initial Cis/Trans Product Ratio
0.88	1.69	0.60
1.20	1.86	0.61
1.20	1.68	0.62
1.80	1.61	0.59

Table 5.4. Effect of Flow Rate on the Rate Constant and Cis/Trans Product Ratio at 340 K

The above results suggest that varying the flow rate had no significant effect on the first order rate constant obtained. The induction period was also observed to be independent of the flow rate.

Product Selectivity

Cis and trans but-2-ene were the only products of the reaction, no isobutene being observed. In the temperature range studied the cis/trans but-2-ene product ratio was always less than unity. Figure 5.4 demonstates the change in the cis/trans but-2-ene product ratio with percent conversion and temperature. The dotted lines represent the extrapolation of the product ratio to zero percent conversion in order to determine the reactant product selectivity at zero but-1-ene conversion i.e. $(cis/trans)_0$. A change in the product ratio with extent of reaction is apparent: an increase in the product ratio with increasing conversion of but-1-ene. At the higher reaction temperatures of 386 K and 393 K the

Figure 5.4. Alteration of Cis/Trans But-2-ene Product Ratio with Extent of Reaction over H-ZSM-23

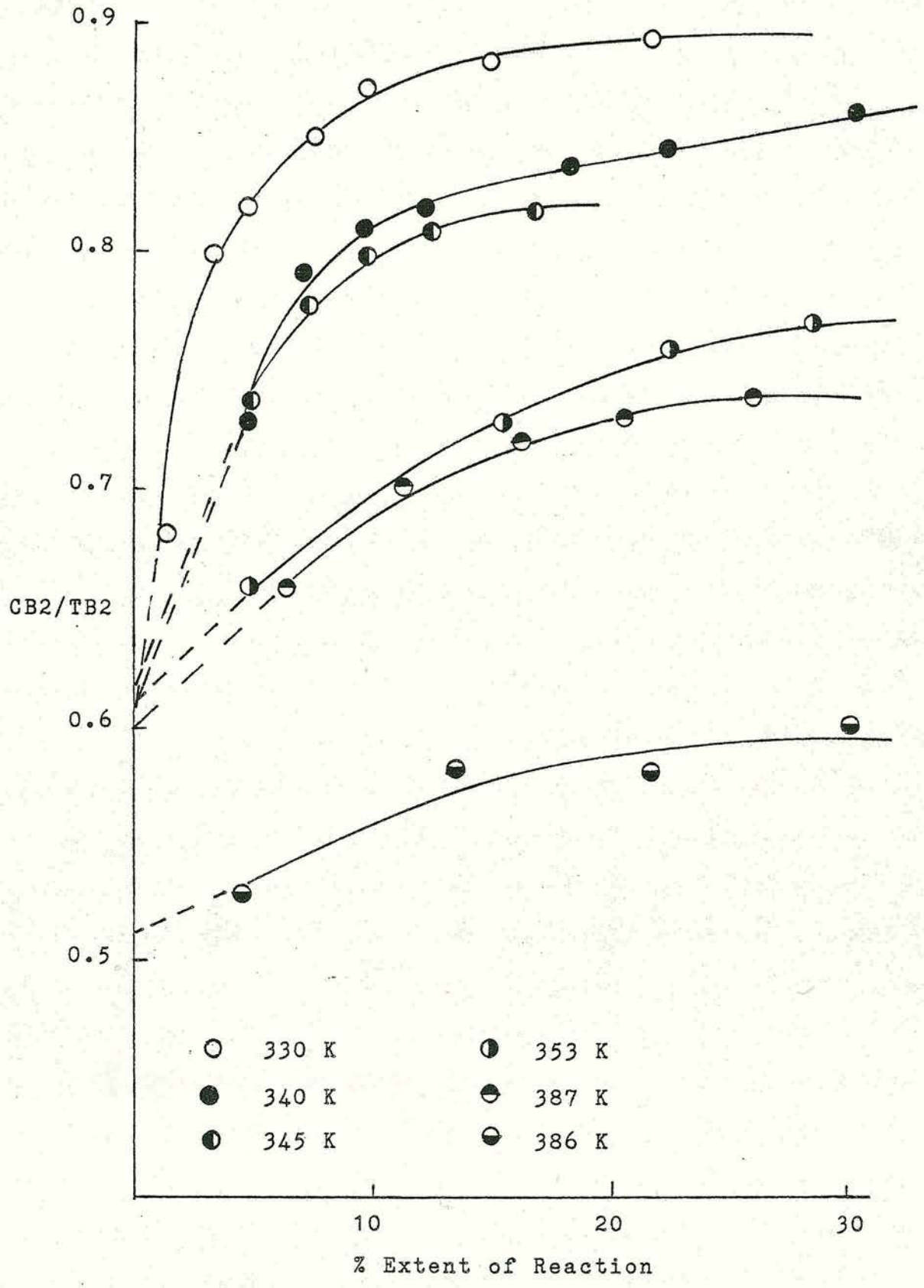

product ratio appears to reach a constant value. An alteration in the product ratio with temperature was also observed with higher reaction temperatures giving lower final cis/trans but-2-ene ratios.

Comparison of the $(cis/trans)_0$ ratios with the thermodynamic equilibrium values at the relevant (Table 5.1) temperature indicates the selective nature of the isomerisation. The experimental values are higher than the equilibrium values indicating that the isomerisation of but-1-ene over H-ZSM-23 was subject to kinetic control, with more cis but-2-ene initially formed than indicated by the equilibrium value. No variation in the initial product ratio with temperature was observed. Varying the flow rate appeared to have no effect on the $(cis/trans)_0$ values obtained (Table 5.4).

The Run 2 $(cis/trans)_0$ product ratios were found to be similar to the $(cis/trans)_0$ values obtained for Run 1. A similar trend was observed in the variation of the product ratio with percent conversion and temperature.

5.1.2. But-2-ene Isomerisation

Experiments using cis but-2-ene and trans but-2-ene as reactants were undertaken to provide more data on product selectivity. The catalyst samples were pretreated in a similar manner to those used in but-1-ene isomerisation. A typical reaction profile for trans but-2-ene is illustrated in Figure 5.5. The derived first order plot is shown in Figure 5.6. Extrapolation of the product composition graphs to zero reaction time

Figure 5.5. Reaction Profile for Trans But-2-ene Isomerisation over H-ZSM-23 at 375 K

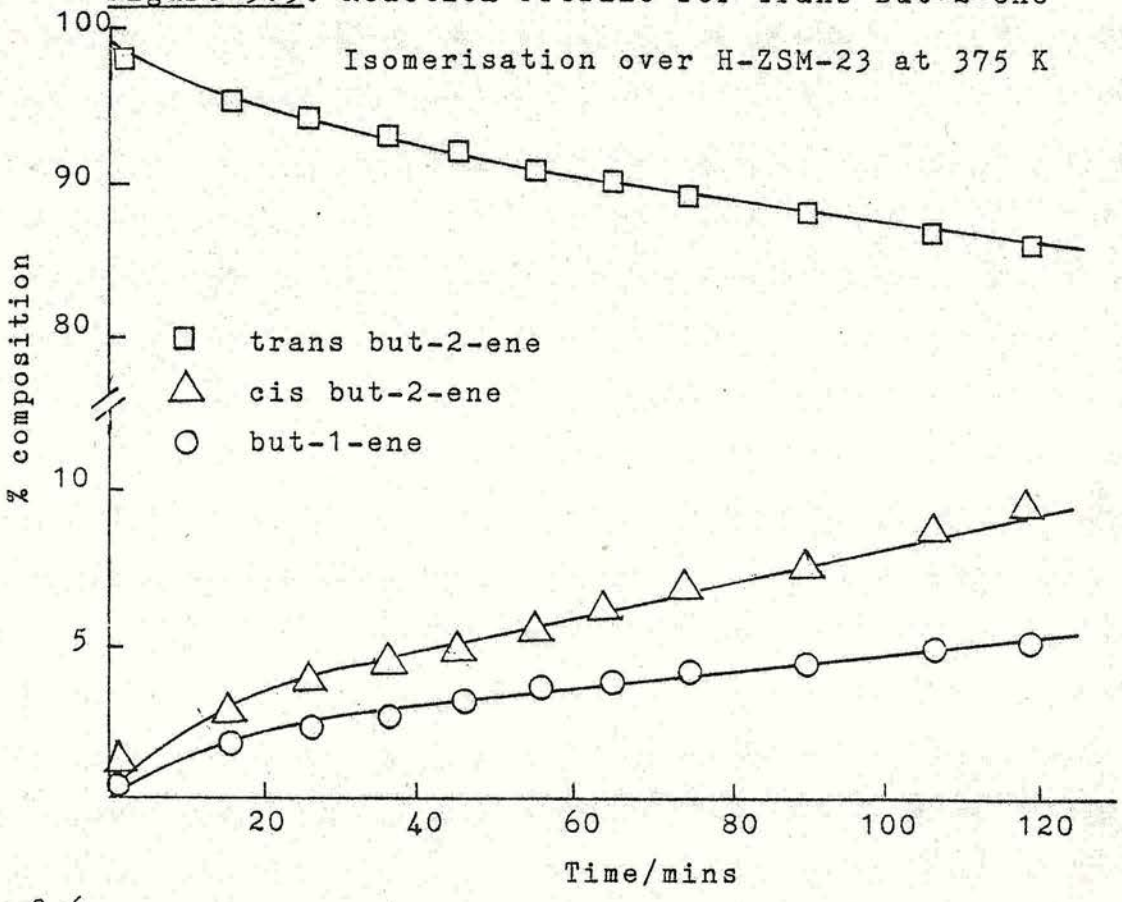

Figure 5.6. Derived First Order Plot

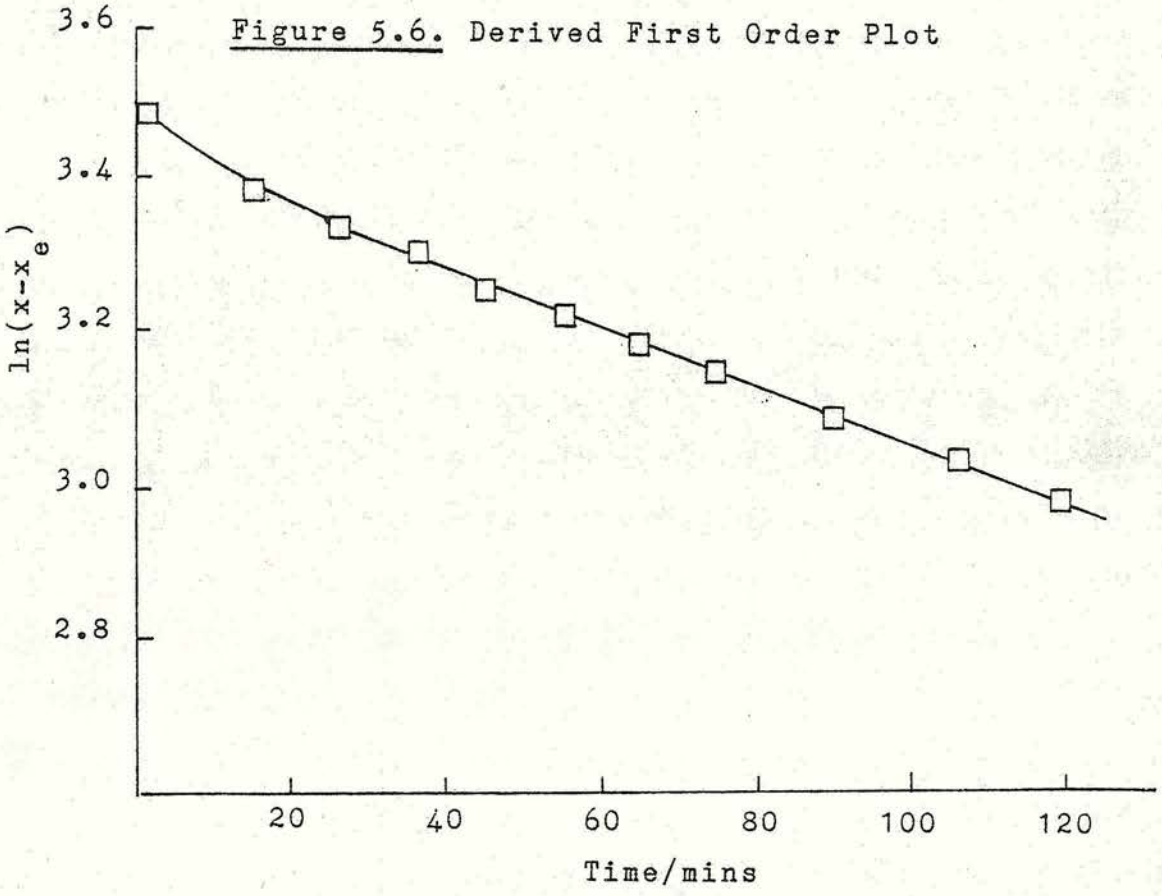

indicated that c.a. 1.5% conversion of cis but-2-ene and c.a. 1% conversion of trans but-2-ene had occured.

The first order plots for cis but-2-ene and trans but-2-ene isomerisation were similar to those obtained for but-1-ene isomerisation in that they displayed an initial fast rate followed by a slower steady rate. Unlike those obtained for but-1-ene the first order plots for cis and trans but-2-ene did not show a "tailing off" after c.a. 150 minutes. The induction period observed for cis and trans but-2-ene isomerisation was found to last for c.a. 15 minutes compared with 25 minutes for but-1-ene isomerisation. For the reactions of but-1-ene and cis but-2-ene the initial and steady first order rates were in the ratio of c.a. 2.1:1 while for trans but-2-ene the ratio was c.a. 2.6:1.

The first order rate constants for the isomerisation of cis and trans but-2-ene are listed in Tables 5.5 and 5.6. The respective Arrhenius plots are illustrated in Figure 5.7 and 5.8. The apparent activation energies were calculated to be 59 kJ mol^{-1} and 39 kJ mol^{-1} for cis and trans but-2-ene respectively.

Figure 5.7. Arrhenius Plot for the Isomerisation of Cis But-2-ene over H-ZSM-23

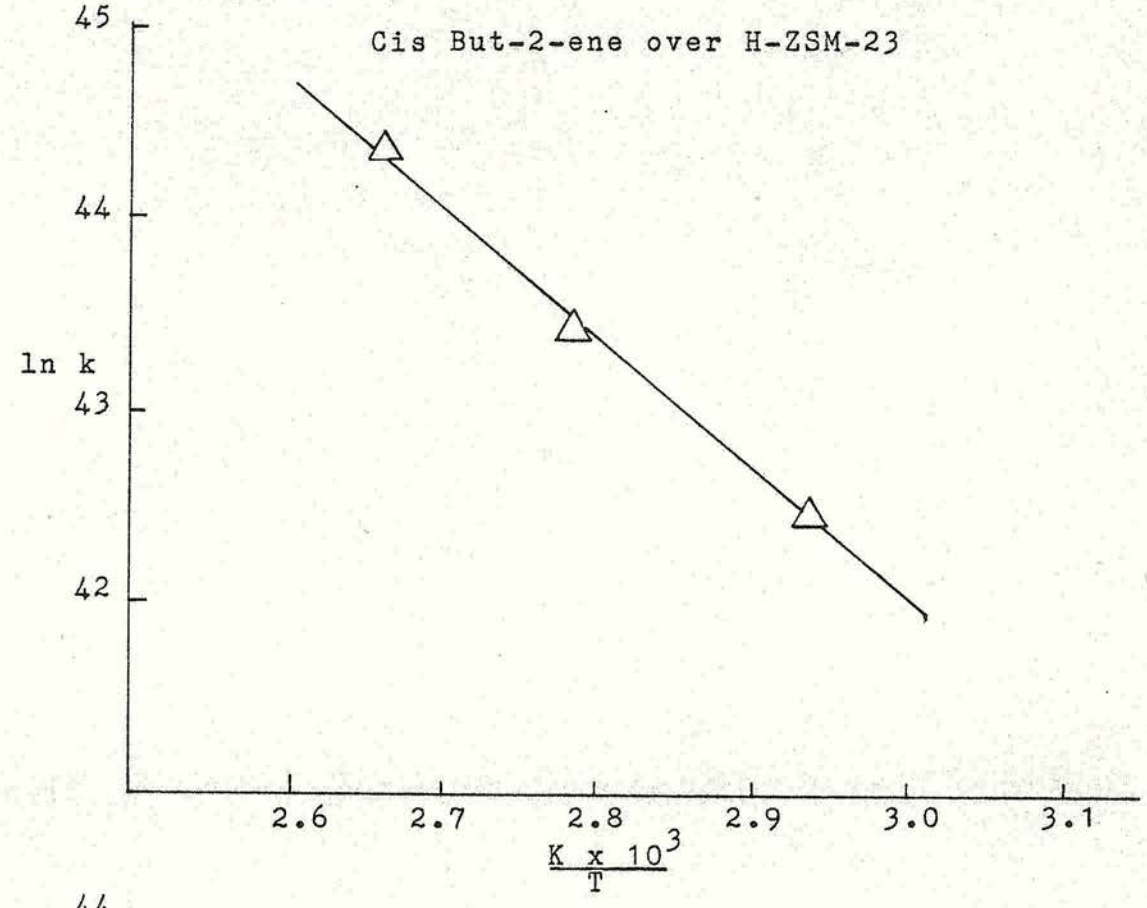

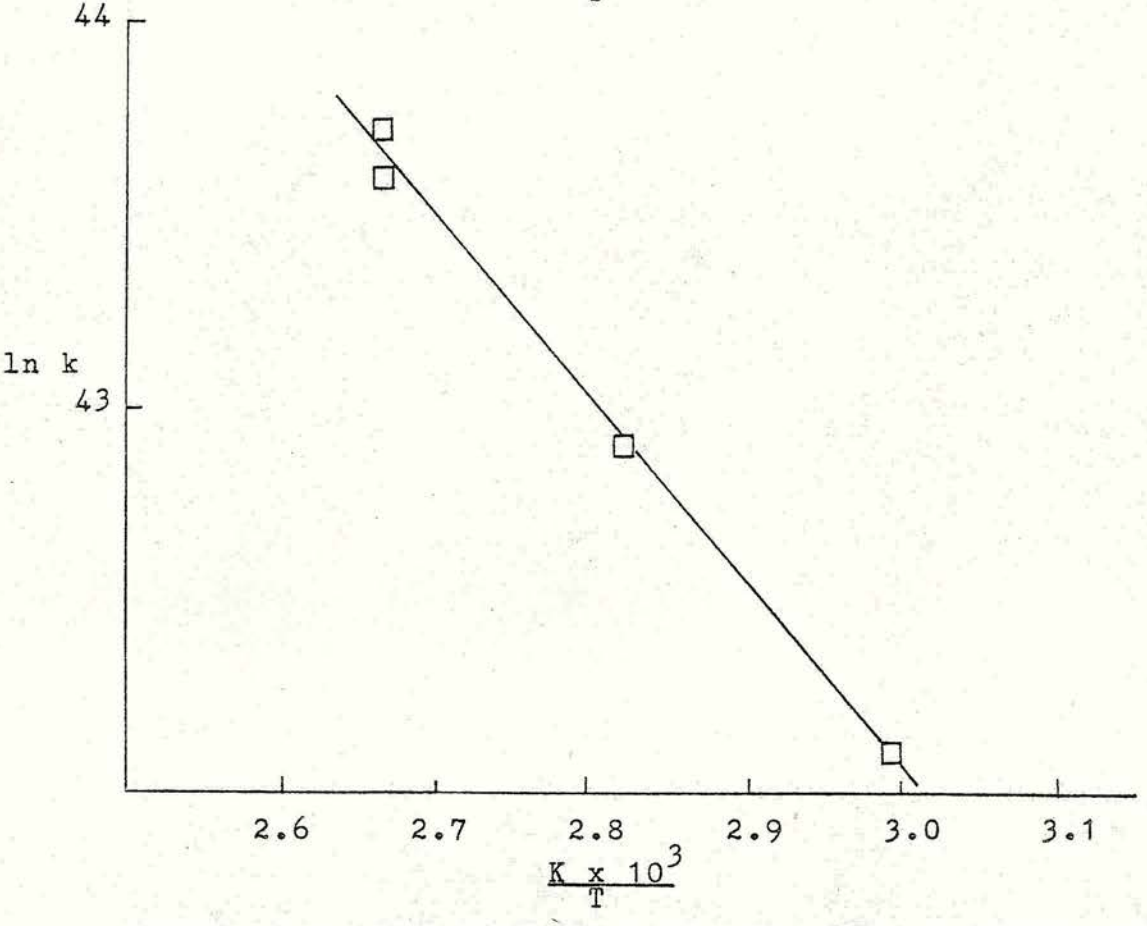

Figure 5.8. Arrhenius Plot for the Isomerisation of Trans But-2-ene over H-ZSM-23

Reaction Temperature/K	Rate Constant/10^{18} molecules $s^{-1}g^{-1}$	TB2/B1 Product Ratio	
		Initial	Equilibrium
341	2.70	1.42	14.09
359	7.25	2.60	11.55
375	18.10	1.98	9.33

Table 5.5. Rate Constants for the Isomerisation of Cis But-2-ene over H-ZSM-23

Reaction Temperature/K	Rate Constant/10^{18} molecules $s^{-1}g^{-1}$	CB2/B1 Product Ratio	
		Initial	Equilibrium
334	1.92	4.80	5.32
355	4.25	4.50	4.63
365	5.77	5.08	4.34
375	9.66	5.41	4.09
375	8.50	4.81	4.09

Table 5.6. Rate Constants for the Isomerisation of Trans But-2-ene Isomerisation over H-ZSM-23

Several experiments were carried out in which the sample was evacuated at 723 K for 16 hours after an initial isomerisation run and a second dose of but-2-ene admitted. This treatment had been found to be sufficient to restore the activity of H-ZSM-23 after but-1-ene isomerisation. The Run 2 data were treated in a similar manner to those of Run 1 and are listed in Tables 5.7 and 5.8 for cis but-2-ene and trans but-2-ene respectively.

Reaction Temperature/K	Rate Constant/10^{18} molecules $s^{-1}g^{-1}$	Initial TB2/B1 Product Ratio	k_2/k_1
359	5.22	1.89	0.72
375	14.79	2.62	0.82

Table 5.7. First Order Rate Constants (k_2) for Run 2 Cis But-2-ene Isomerisation over H-ZSM-23

Reaction Temperature/K	Rate Constant/10^{18} molecules $s^{-1}g^{-1}$	Initial CB2/B1 Product Ratio	k_2/k_1
334	1.62	3.30	0.84
355	3.81	3.78	0.90
365	5.41	3.06	0.94
375	9.76	3.02	1.01
375	10.03	3.60	1.18

Table 5.8. First Order Rate Constants (k_2) for Run 2 Trans But-2-ene Isomerisation over H-ZSM-23

The Run 2 isomerisations of cis but-2-ene exhibited first order rate constants which were lower than those obtained during Run 1: indicative of some deactivation of the catalyst. The length of the induction period was not affected. The Run 2 isomerisations of trans but-2-ene have similar first order rate constants to those obtained during Run 1 as shown by the k_2/k_1 ratio in Table 5.8 indicating that the activity of the sample was restored. The apparent activation energy for the Run 2 isomerisation of trans but-2-ene was found to

46 kJ mol^{-1}.

Several experiments were carried out in which the flow rate was altered. The results are listed in Table 5.9 where it is apparent that an alteration in the flow rate does have an effect on the rate constant. With increasing flow rate the rate constant was found to decrease at 341 K for cis but-2-ene and 375 K for trans but-2-ene. No such effect was observed in the isomerisation of but-1-ene over H-ZSM-23.

Reactant	Flow Rate /10^{-2} dm^3 s^{-1}	Rate Constant/10^{18} molecules $s^{-1}g^{-1}$
cis but-2-ene	0.75	1.06
	1.20	0.74
	1.58	0.68
trans but-2-ene	0.75	15.23
	1.20	9.66
	1.20	8.50
	1.67	9.85

Table 5.9. Effect of Flow Rate on Rate Constants for the Isomerisation of Cis But-2-ene at 341 K and Trans But-2-ene at 375 K

A more detailed study of the effect of flow rate on the isomerisation of trans but-2-ene over H-ZSM-23 revealed that the apparent activation energy obtained for a flow rate of 1.83 x 10^{-2} dm^3 s^{-1} (38 kJ mol^{-1}) was similar to that obtained with a flow rate of

1.20×10^{-2} dm^3 s^{-1} (39 kJ mol^{-1}) while the apparent activation energy for a flow rate of 0.75×10^{-2} dm^3 s^{-1} (72 kJ mol^{-1}) differed considerably. The rate constants are tabulated in Table 5.10.

Flow Rate /10^{-2} dm^3 s^{-1}	Reaction Temperature/K	Rate Constant/10^{18} molecules $s^{-1}g^{-1}$
0.75	335	1.02
	344	1.53
	355	3.63
	375	15.23
1.83	335	1.91
	355	4.56
	375	9.81
	390	12.63

Table 5.10. Effect of Flow Rate On Rate Constants for Trans But-2-ene Isomerisation over H-ZSM-23

The first order plots for the reactions listed above all exhibited an initial fast rate and a slower steady rate. Induction periods of 25 minutes were observed in all cases with the exception of the reactions with a flow rate of 0.75×10^{-2} dm^3 s^{-1} at temperatures greater than 344 K.

Product Selectivity

The reaction of either but-2-ene isomer resulted in the formation of but-1-ene and the other but-2-ene isomer as the only products. For each catalyst sample analysed the ratio of the two resulting isomers was calculated and plotted against percent conversion of the starting isomer. The ratio was found to vary with the extent of reaction as illustrated in Figure 5.9 until equilibrium was approached. The alteration in the product ratio during the first 5-10% of reaction (Figure 5.10) made accurate determination of the initial product ratio very difficult particularly at higher temperatures.

The trans but-2-ene/but-1-ene ratio shows a slight decrease initially and then increases steadily while the cis but-2-ene/but-1-ene ratio with trans but-2-ene as reactant displays an initial sharp decrease followed by a slower increase. The initial product ratios have been estimated and are listed in Tables 5.5 and 5.6 together with the equilibrium values for cis but-2-ene and trans but-2-ene respectively. No variation in the product ratios with temperature was apparent. The initial values resulting from the isomerisation of trans but-2-ene suggest that cis but-2-ene and but-1-ene are formed in equilibrium proportions. Conversly, the initial product ratios for the isomerisation of cis but-2-ene differ considerably from the thermodynamic equilibrium ratios and are indicative of a favoured double bond migration with respect to cis-trans isomerisation. Similar product ratios have been obtained by several authors for cis

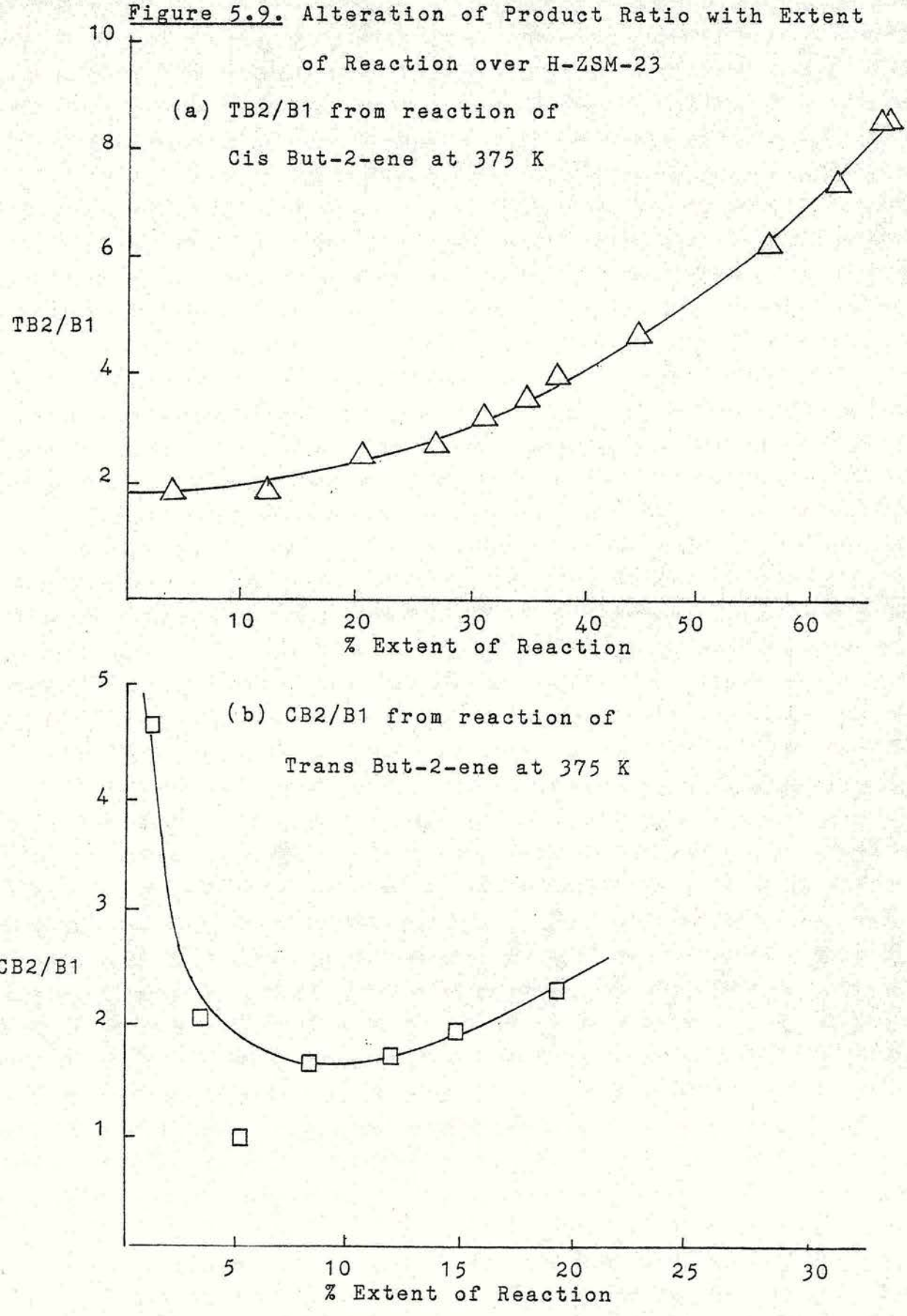
Figure 5.9. Alteration of Product Ratio with Extent of Reaction over H-ZSM-23
(a) TB2/B1 from reaction of Cis But-2-ene at 375 K
TB2/B1
% Extent of Reaction
(b) CB2/B1 from reaction of Trans But-2-ene at 375 K
CB2/B1
% Extent of Reaction

Figure 5.10. Alteration of Product Ratio in the Initial Stages of But-2-ene Isomerisation

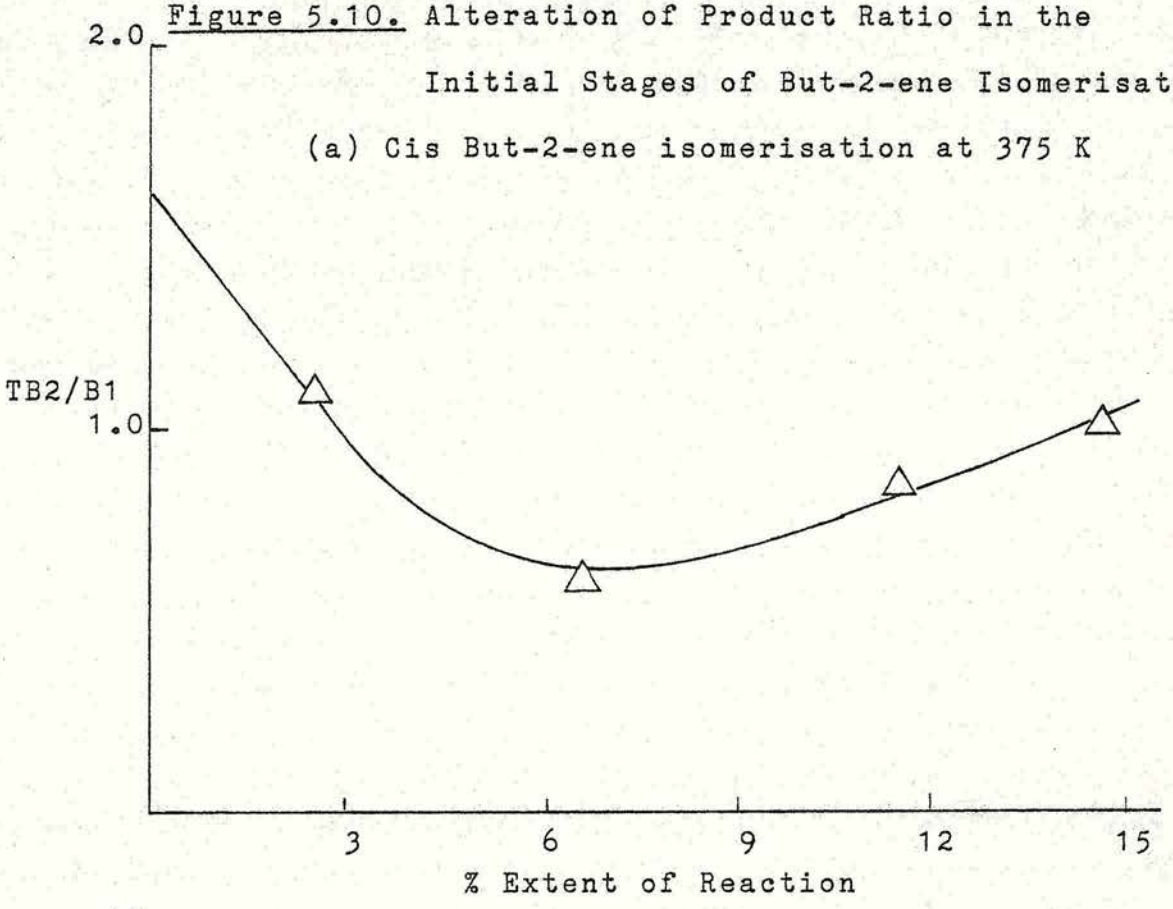

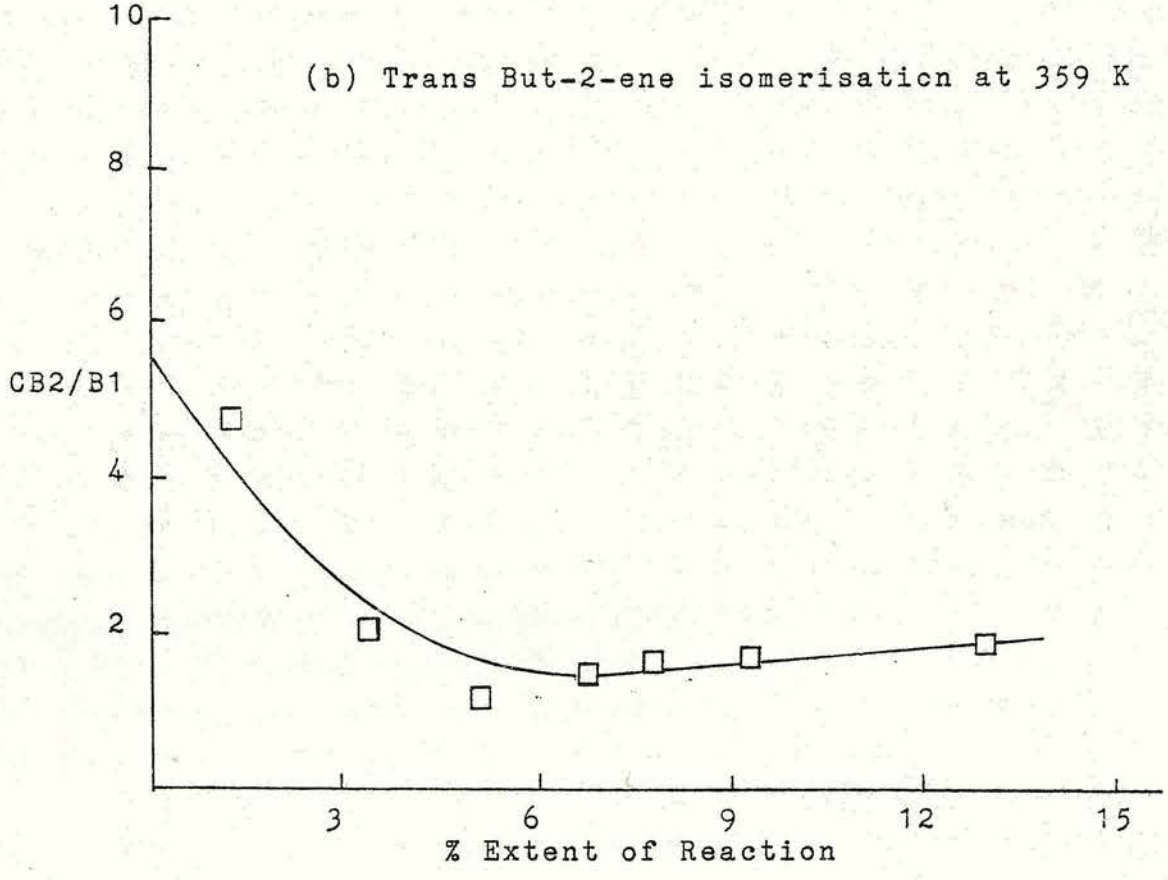

but-2-ene isomerisation[85,91,154].

The Run 2 isomerisation of cis but-2-ene exhibited similar initial product ratios (Table 5.7) to those obtained during Run 1. The initial cis but-2-ene/but-1-ene product ratio observed during the Run 2 isomerisation of trans but-2-ene (Table 5.8) appeared to be lower than that observed during Run 1 suggesting that more but-1-ene is formed. Varying the flow rate appeared to have no effect on the initial product ratios.

Discussion

The results described previously are compatible with the triangular reaction scheme proposed by Haag and Pines[71] in which all six possible reactions occur.

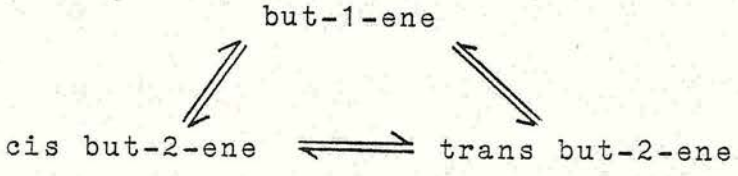

Studies on product ratios in the catalysed isomerisation of the n-butenes have been undertaken by numerous investigators[78,81] who have demonstrated that the product ratios are closely dependent upon the nature of the active centre at the catalyst surface. The initial product distribution resulting from but-1-ene isomerisation is indicative of the reaction mechanism. Cis/trans but-2-ene product ratios of less than unity have been observed over metal catalysts[70] and such results have been interpretated in terms of a radical

mechanism in which the stability of the various adsorbed butyl radicals controls the product ratio.

In the presence of acid catalysts unobstructed rotation in the carbonium ion makes cis-trans isomerisation the favoured reaction relative to the displacement of the double bond, and the formation of cis but-2-ene from but-1-ene is less favoured. Cis/trans but-2-ene product ratios which are near unity and temperature independent are considered to be indicative of a carbonium ion mechanism[35,85].

The initial cis/trans but-2-ene product ratios resulting from but-1-ene isomerisation over H-ZSM-23 were higher than the thermodynamic equilibrium values suggesting that the reaction is kinetically controlled. The initial product ratios are in the range 0.52-0.62 and appear to be temperature independent. The observed product ratio would be distorted if there was preferential adsorption of one of the but-2-ene isomers, however, mass balance calculations during the course of the reaction suggest that there was no such adsorption. Cis/trans but-2-ene product ratios of less than unity have been found by several authors[84,155] who considered them to be indicative of a mechanism involving the secondary carbonium ion intermediate.

With catalysts in a pellet form any limitation associated with transport to or from the active centres can lead to a lower concentration of reactants or a higher concentration of products inside the pellet than in the gas stream. An increase in temperature will

increase the likelihood of diffusional limitation[156]. The but-1-ene isomerisation results for H-ZSM-23 indicate that the cis/trans but-2-ene product ratio increases with extent of reaction - to near unity. The effect of reaction temperature on the product ratio with extent of reaction as illustrated in Figure 5.4 indicates that at higher reaction temperatures lower cis/trans but-2-ene product ratios are observed. Consequently, it is quite possible that the observed products ratios are to some extent modified by diffusional considerations.

The results of the adsorption studies (Chapter 4) indicate that all the n-butenes have access to the internal surface of H-ZSM-23 thus H-ZSM-23 does not exhibit reactant selectivity. Reactant selectivity occurs only when access to the active sites is restricted for one or more of the observed reactant molecules. Consideration of the observed kinetics of sorption suggests the rates of diffusion vary in the order but-1-ene $\geqslant$ trans but-2-ene $>$ cis but-2-ene. However, the adsorption results were obtained using H-ZSM-23 powder while pellets in the size range 250-500 μm were used in the catalytic study. A study of the rate of adsorption of ethane on zeolite 4A[24] has revealed that the effective diffusivity was lower for pellets than for the pure crystal. Thus, the differences in the diffusion rates in H-ZSM-23 may be reflected in the product distribution i.e. product selectivity. Product molecules which are delayed in the zeolite crystals may undergo further reaction. Cis but-2-ene may react

further to form trans but-2-ene and but-1-ene causing a lowering of the cis/trans but-2-ene product ratio from unity.

Activation energies for diffusion in zeolite 5A derived from the temperature dependence of the limiting diffusivity at zero sorbate concentration show a correlation with the critical diameter of the sorbate molecule. But-1-ene and trans but-2-ene which have the same critical diameter were reported[157] to have similar diffusional activation energies of 14.5 kJ mol^{-1} while the larger cis but-2-ene molecule had a substantially larger diffusional activation energy of 38.6 kJ mol^{-1}.

Consideration of the but-1-ene isomerisation results lead to the conclusion that the operative reaction mechanism involves the secondary butyl carbonium ion as intermediate. The reduction of the temperature independent cis/trans but-2-ene product ratio from unity is due to diffusion effects.

The initial product ratios resulting from the isomerisation of trans but-2-ene suggest that the reaction products (but-1-ene and cis but-2-ene) are formed in equilibrium proportions. However, the initial product ratio for the isomerisation of cis but-2-ene was found to differ considerably from the thermodynamic equilibrium value and is similar to data reported by several authors[85,91,154,155]. Lombardo et al[85] have suggested that the selectivities for product formation depend on the differences in the energy barrier between the carbonium ion and the individual products over NaY

zeolites. Alternatively, it has been proposed by Hoser and Krzyzanowski[91] that the favoured migration of the double bond with respect to cis-trans but-2-ene isomerisation was associated with the obstructed rotation of the carbonium ion in the pores of the zeolite.

The variation in the rate constant obtained for cis and trans but-2-ene isomerisation when the flow rate was varied is further evidence for diffusion control.

Extrapolation of the product composition curves to zero contact time always shows a conversion of 1-2% although the starting material was pure isomer. Similar results were obtained by Detrekoy et al[84] using H-clinoptilolite. They suggested that after the formation of a carbonium ion some oligomerisation can occur and that the oligomer cannot leave the zeolite channels at the reaction temperature. Further evidence for the formation of butene polymer is presented in Section 4.1.3. The surface area results suggest that there is a loss in the n-butane surface area upon exposure to but-1-ene. The loss in activity of acidic catalysts upon exposure to but-1-ene has been previously reported in the literature[87,155]. Evidence for the formation of butene polymer has been presented by several authors[88,155,158,159].

It is possible that the presence of polymeric butene limited the diffusion of the larger cis but-2-ene molecules accounting for the product ratios observed during but-1-ene isomerisation. The rise in the cis/trans but-2-ene product ratio as but-1-ene

isomerisation proceeds might just suggest a change in the seat of activity i.e. from within the zeolite channels to the non-shape selective surface.

The Run 2 results obtained for but-1-ene isomerisation show that the activity of H-ZSM-23 can be restored by evacuation at 723 K but not by evacuation at reaction temperature. This is in agreement with the results presented by Detrekoy et al[84]. Weeks and Bolton[160] have observed that butene adsorbed on hydrogen Y zeolite could not be physically desorbed at room temperature. Evacuation at room temperature followed by but-1-ene isomerisation resulted in a product composition graph which revealed 0% conversion at zero contact time indicating that the butene polymer had not been removed. Evacuation at 723 K was sufficient to restore the activity of H-ZSM-23 for but-1-ene and trans but-2-ene isomerisation but not for cis but-2-ene isomerisation. It is possible that access to the zeolite channels is restricted for the larger cis but-2-ene molecule by the presence of some residual butene polymer resulting in a loss in activity.

During hydrocarbon reactions involving aromatic compounds or alkenes over zeolites carbonaceous residues ("coke") are formed[22]. The "coking" reaction is a shape selective reaction controlled by the zeolite pore structure[52]. If "coking" occurs within the pores of the zeolite a loss in catalytic activity must result[159]. In addition the selectivity may be modified. The "tailing off" observed during but-1-ene isomerisation over

H-ZSM-23 may well be due to a loss of activity as a result of "coking".

It has been postulated by Wright et al[161] that ZSM-23 may have a one dimensional tunnel structure. Mordenite has a one dimensional pore structure in which molecules with dimensions close to those of the pore cannot freely counter-diffuse[30]. If H-ZSM-23 has a one dimensional pore structure then the diffusion of the reactant in the presence of products may well be precluded and could account for the "tailing off" observed during but-1-ene isomerisation. However, a similar effect would be expected in cis and trans but-2-ene isomerisation.

5.1.3. Methlycyclopropane Isomerisation

The isomerisation of methylcyclopropane (MCP) over H-ZSM-23 was carried out in the temperature range 368-408 K. A typical reaction profile is illustrated in Figure 5.11. Unlike the n-butenes, MCP isomerisation over H-ZSM-23 followed first order kinetics from the beginning of the reaction as illustrated by the typical first order plot in Figure 5.12. Comparison of the rate constants for MCP isomerisation with those for but-1-ene isomerisation showed MCP isomerisation to be slower than but-1-ene isomerisation within the observed temperature range. Good first order kinetics were observed for conversions of up to c.a. 95%. The first order rate constants are given in Table 5.11. From the Arrhenius plot illustrated in Figure 5.13 the apparent activation

Figure 5.11. Reaction Profile for MCP Isomerisation over H-ZSM-23 at 394 K

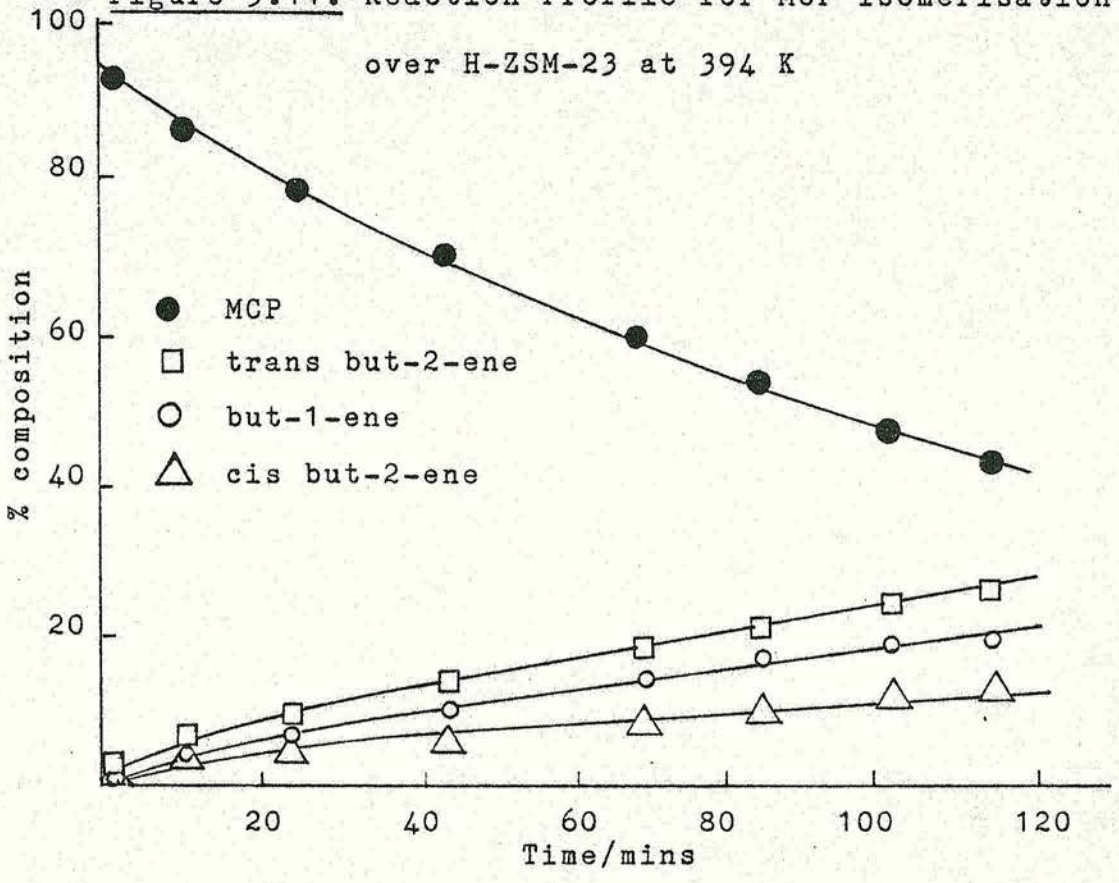

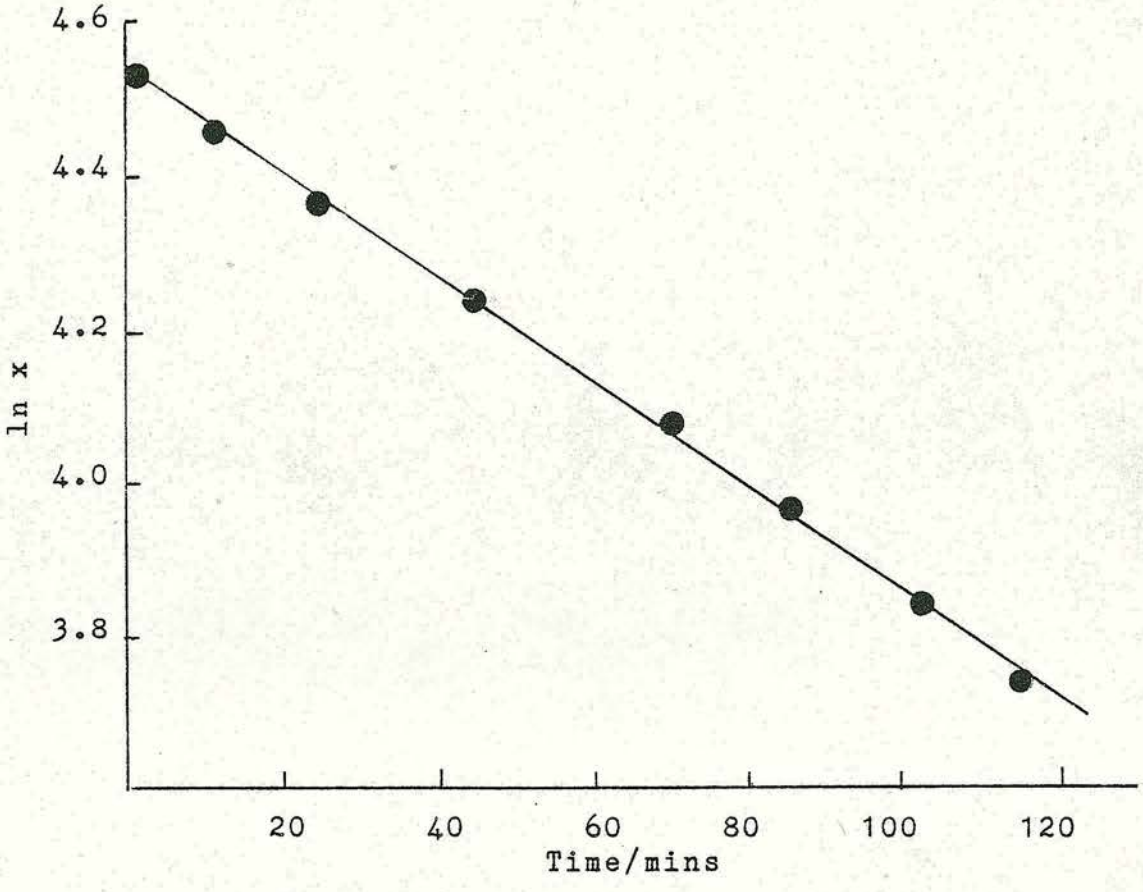

Figure 5.12. Derived First Order Plot

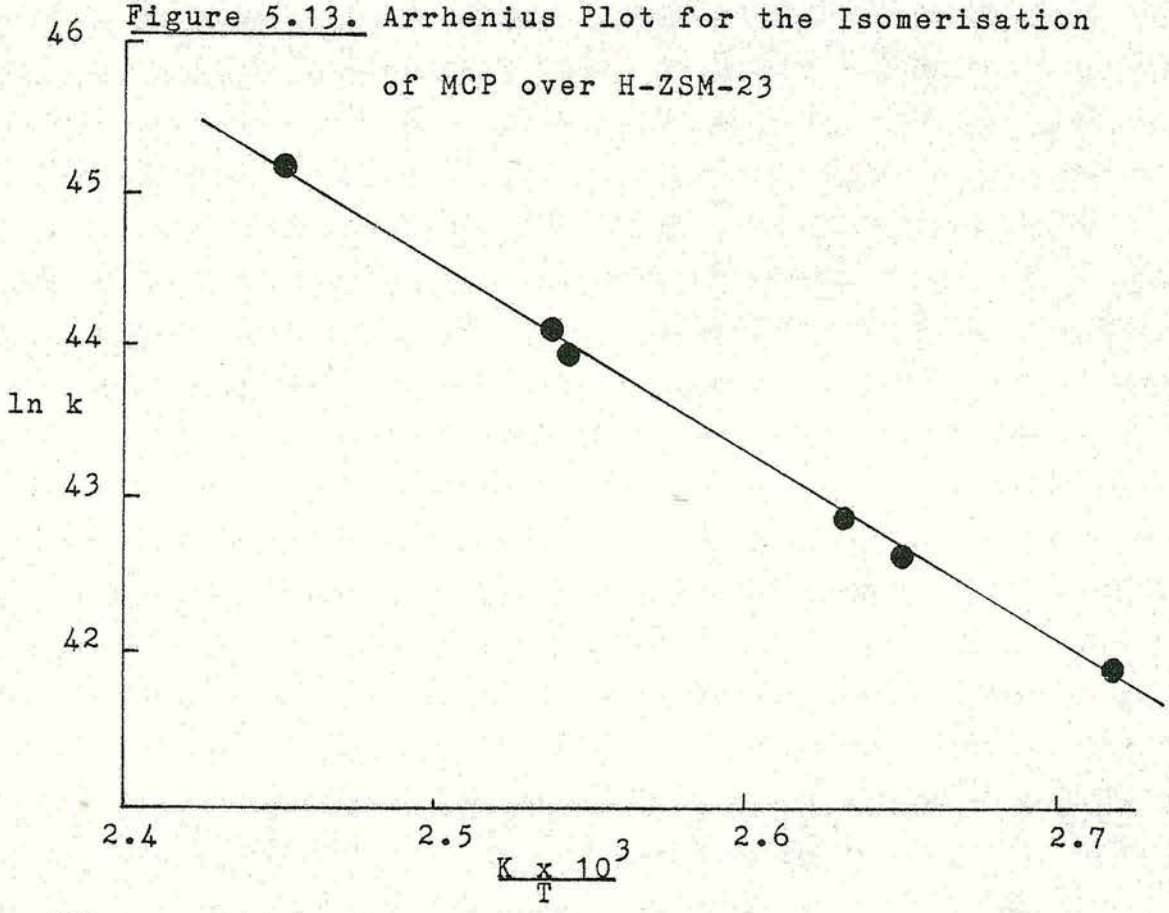

Figure 5.13. Arrhenius Plot for the Isomerisation of MCP over H-ZSM-23

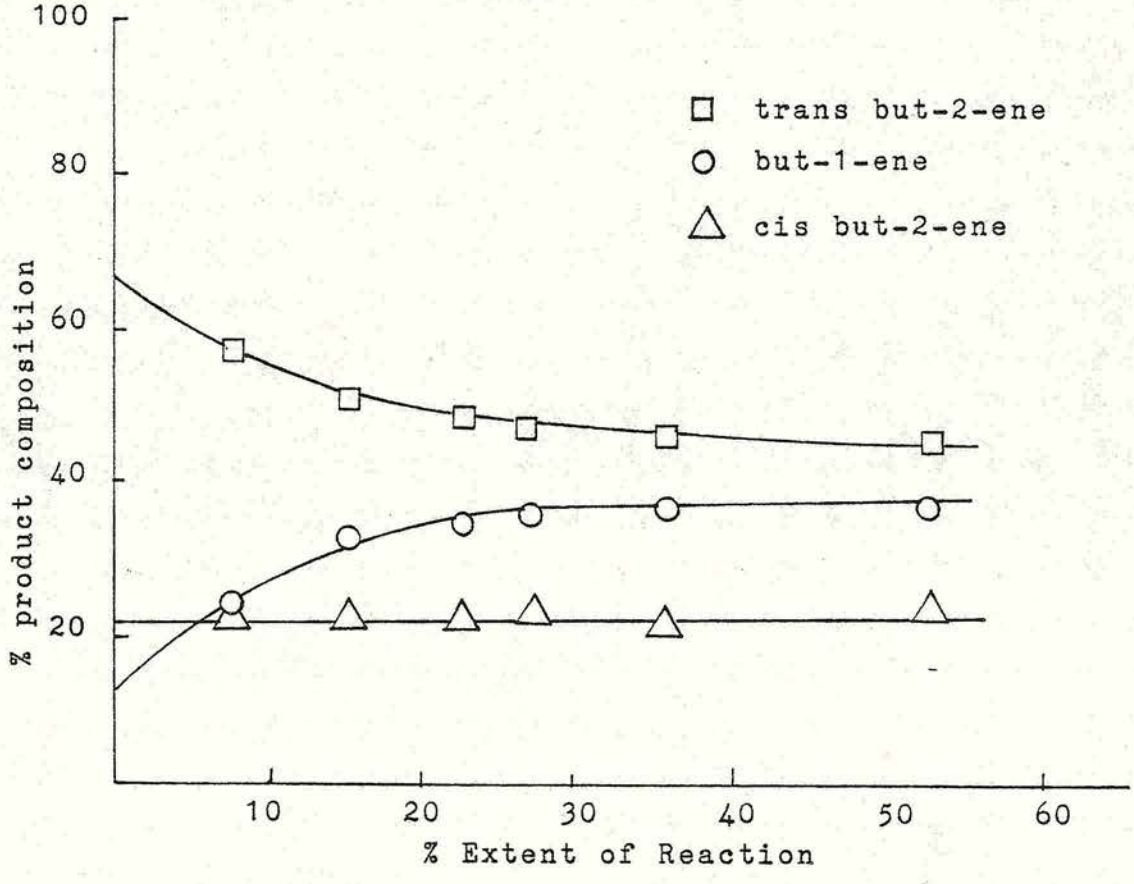

Figure 5.14. Variation in Product Composition with Extent of MCP Conversion at 394 K

energy was calculated to be 108 kJ mol^{-1}.

Reaction Temperature/K	Rate constant/10^{18} molecules $s^{-1}g^{-1}$
368	1.54
378	3.18
380	4.18
393	12.52
394	15.57
408	44.92

Table 5.11. Rate constants for MCP Isomerisation over H-ZSM-23

A study of the effect of flow rate on the isomerisation of MCP indicated a slight decrease in the rate with increasing flow rate. The results are listed in Table 5.12.

Reaction Temperature/K	Flow Rate/10^{-2} dm^3 s^{-1}	Rate Constant/10^{18} molecules $s^{-1}g^{-1}$
380	0.75	4.56
380	1.20	4.17
380	1.58	4.03

Table 5.12 Effect of Flow Rate on the Rate Constant for MCP Isomerisation over H-ZSM-23

Product Selectivity

The only products observed from the isomerisation of MCP over H-ZSM-23 were the n-butenes. The initial product distribution estimated by extrapolation to zero conversion and the product compositions at 10% and 30% are given in Tables 5.13 and 5.14 respectively.

The initial product distribution is in the order:

trans but-2-ene > cis but-2-ene > but-1-ene.

The estimated initial product compositions, given in Table 5.13 are significantly different from the equilibrium product ratios, indicating kinetic control. The product ratios at 10% and 30% conversion of MCP (Table 5.14) were found to be rather different to the initial product composition. A typical plot of the variation in product composition with percent conversion of MCP is illustrated in Figure 5.14. The product distribution after 30% conversion is

trans but-2-ene > but-1-ene > cis but-2-ene.

With increasing conversion of MCP the percent concentration of but-1-ene appears to increase while the trans but-2-ene percent concentration decreases. The percent concentration of cis but-2-ene remains approximately constant throughout the course of the reaction. Such data are compatible with a secondary isomerisation occurring between the trans but-2-ene and but-1-ene.

Reaction of But-1-ene After MCP Isomerisation

Reactions were carried out in which the

Reaction Temp./K	Initial Product Composition/%			Equilibrium Product Composition/%		
	B1	TB2	CB2	B1	TB2	CB2
368	7.5	83.7	8.8	6.3	66.7	27.0
380	10.6	70.0	19.4	7.0	65.3	27.7
393	12.7	66.8	20.5	7.7	63.9	28.4
394	12.4	66.1	21.5	7.7	63.9	28.4
408	12.0	68.0	20.0	8.5	62.4	29.1

Table 5.13. Product Composition from MCP Isomerisation over H-ZSM-23

Reaction Temp./K	Product Composition at 10% Conversion/%			Product Composition at 30% Conversion/%		
	B1	TB2	CB2	B1	TB2	CB2
368	27.5	53.9	18.6	34.8	44.2	21.0
380	25.1	54.0	20.9	36.0	43.0	21.0
393	20.8	58.8	20.4	30.9	48.7	20.4
394	18.3	60.0	21.7	27.4	51.2	21.4
408	15.0	64.9	20.1	20.4	59.4	20.2

Table 5.14. Product Composition at 10% and 30% Conversion of MCP

isomerisation of but-1-ene to but-2-ene was monitored after complete conversion of MCP. However, little, if any, reaction of the but-1-ene was found to occur. Such observations are in marked contrast to similar experimental studies over the zeolites omega and erionite[106] where the isomerisation of but-1-ene was found to have rate constants identical to those observed when but-1-ene was the initial reactant.

Reactions were carried out after 80% conversion of MCP in which the catalyst was evacuated for 30 minutes at reaction temperature and a dose of but-1-ene then admitted. The subsequent rate constant was found to be lower than that obtained for but-1-ene over a fresh sample of catalyst. However, the induction period was found to be reduced to about 7 minutes and no "tailing off" was observed. The cis/trans but-2-ene product ratio increased slightly at the start of this reaction and remained constant throughout the course of the reaction.

Reactions were also carried out in which the sample was evacuated at 723 K for 15 hours after 80% MCP conversion. The subsequent isomerisation of but-1-ene was monitored. In this case the activity of the catalyst was found to be restored.

Discussion

The only products observed from the isomerisation of MCP over H-ZSM-23 were the three n-butenes. A proton addition mechanism will account for all the observed products[104]. If the MCP molecule is considered as

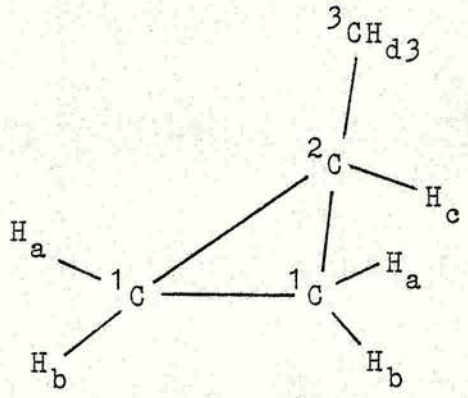

proton addition to ^{1}C would always result in the formation of the n-butenes through ^{1}C-^{2}C cleavage. Proton addition to ^{2}C is very much less favoured as it would involve the formation of an unstable primary carbonium ion. Since neither isobutene or cyclobutane was observed a hydride abstraction mechanism was not operating. A proton addition mechanism involving the secondary butyl carbonium ion has been proposed for the interconversion of the n-butenes over H-ZSM-23.

Studies of MCP isomerisation carried out over silica-alumina[104] and zeolite omega[106,162] have postulated the non-classical cyclopropyl carbonium ion as the reaction intermediate. A possible mechanism for the involvement of the non-classical ion is

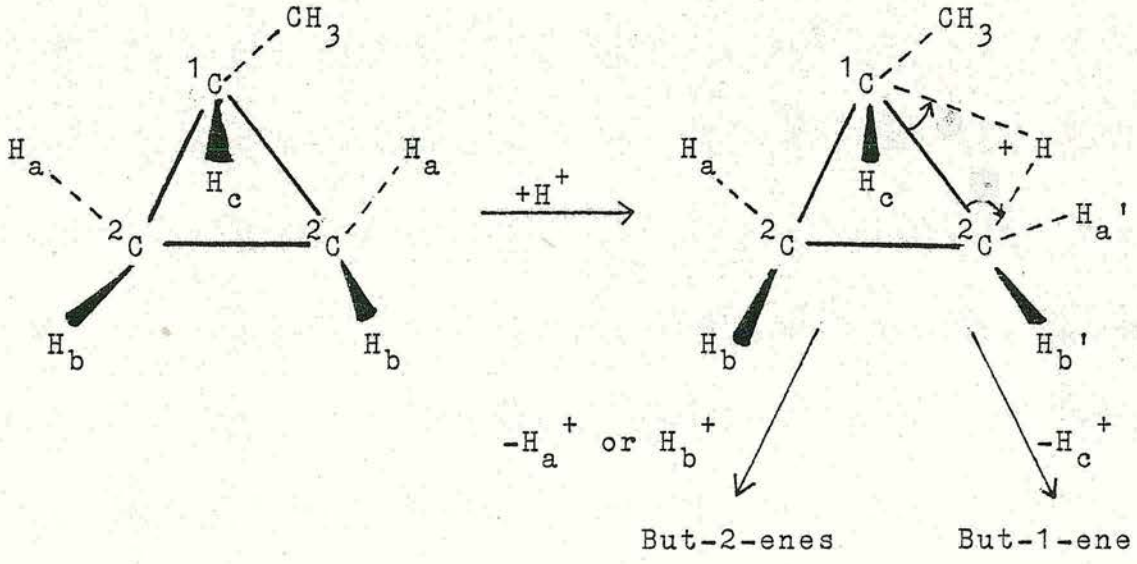

Cleavage of the C_1-C_2 bond in the non-classical ion can occur in two ways i.e. (i) resulting in the formation of a ^{1}C-H bond, the cleavage of a ^{1}C-H_c bond and the production of but-1-ene or (ii) resulting in the formation of a ^{2}C-H bond, the cleavage of either ^{2}C-H_a or ^{2}C-H_b and the production of cis and trans but-2-ene. Adsorption of the non-classical ion in a plane parallel to the cyclopropane ring would favour the production of trans but-2-ene and but-1-ene whose formation is dependent upon the abstraction of a proton (H_b or H_c) orientated towards the surface. The formation of cis but-2-ene which is dependent on the loss of H_a is more difficult. The observed product distributions resulting from the above mechanism were

trans but-2-ene > but-1-ene ⩾ cis but-2-ene[104].

A change in the product selectivity was observed during the isomerisation of MCP over H-ZSM-23. The initial product distribution of

trans but-2-ene > cis but-2-ene > but-1-ene

was similar to that observed during butene isomerisation while at 10% conversion of MCP the product distribution was found to be

trans but-2-ene > but-1-ene > cis but-2-ene

which is consistent with a mechanism involving the non-classical carbonium ion. This apparent change in selectivity could be a result of a change in the mechanism possibly associated with a change in the seat of activity. Alternatively, the apparent change in the but-1-ene and trans but-2-ene concentrations with extent of reaction could be the result of interconversion between the two isomers, the formation of cis but-2-ene being energetically unfavourable. It is unlikely that the observed product compositions are a result of diffusion control as the percent composition of cis but-2-ene would also be affected.

On both silica-alumina[104] and zeolite omega[106] the isomerisation of but-1-ene was found to occur if experiments were carried out for an extended period. This secondary isomerisation of but-1-ene was not observed over H-ZSM-23 suggesting that the isomerisation of MCP must occur on different sites from that of n-butene otherwise some poisoning of the MCP reaction would occur after some butene had been formed. The lack of secondary isomerisation suggests that poisoning of the sites for n-butene isomerisation has occurred.

5.1.4. Summary

The isomerisation of the n-butenes over H-ZSM-23 occurs via a carbonium ion type mechanism. The reduction of the temperature independent cis/trans but-2-ene product ratio (from but-1-ene isomerisation) from unity is due to diffusion effects. In common with studies over silica-alumina and other zeolites the secondary butyl carbonium ion has been postulated as an intermediate.

Evidence was found for the formation of butene polymer immediately upon exposure of H-ZSM-23 to n-butene. The polymeric butene formed reduced the surface area available to n-butane indicating that pore blocking had occurred. Evacuation at reaction temperature was insufficient to remove the butene polymer.

The products resulting from the isomerisation of methylcyclopropane were also indicative of a carbonium ion type mechanism. A change in product selectivty during the course of the reaction may be associated with a change in the mechanism or alternatively the result of an interconversion between trans but-2-ene and but-1-ene.

5.2. Reactions over H-EU-1

5.2.1. But-1-ene Isomerisation

The temperature ranges over which similar rates of but-1-ene isomerisation were observed differed for the two samples of H-EU-1, 331-387 K for H-EU-1(A) and 353-402 K for H-EU-1(B). Typical reaction profiles and first order plots are illustrated in Figures 5.15-18. All first order plots over H-EU-1 exhibited an initial acceleratory period of c.a. 35 minutes followed by a steady first order rate. H-EU-1(A) exhibited first order kinetics until 85% conversion of but-1-ene. H-EU-1(B) was found in most cases to exhibit a "tailing off" as observed during but-1-ene isomerisation over H-ZSM-23. The respective Arrhenius plots are illustrated in Figure 5.19. The rate constants obtained from the steady rate are tabulated in Tables 5.15 and 5.16 for H-EU-1(A) and H-EU-1(B) respectively. The apparent activation energies were calculated to be 46 kJ mol^{-1} and 67 kJ mol^{-1} for H-EU-1(A) and H-EU-1(B) respectively.

Figure 5.15. Reaction Profile for But-1-ene Isomerisation over H-EU-1(A) at 364 K

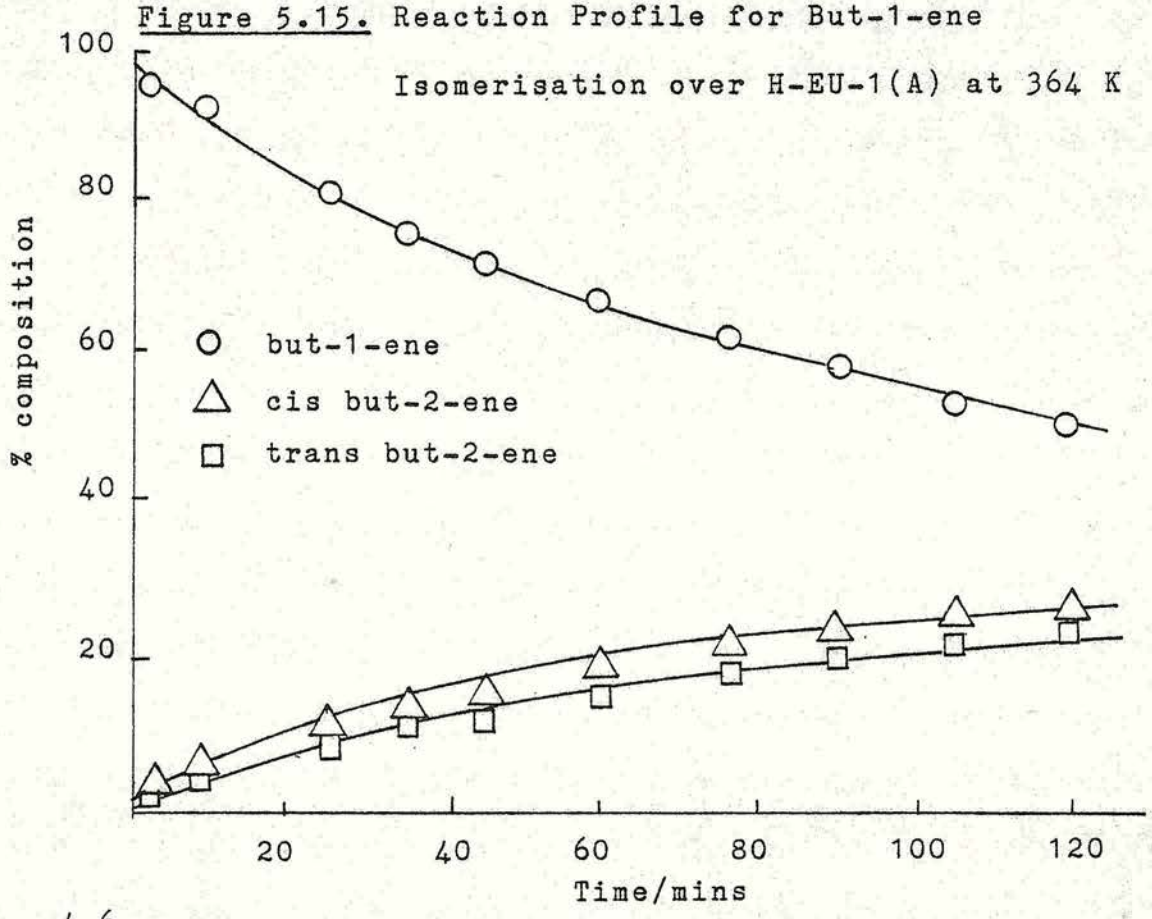

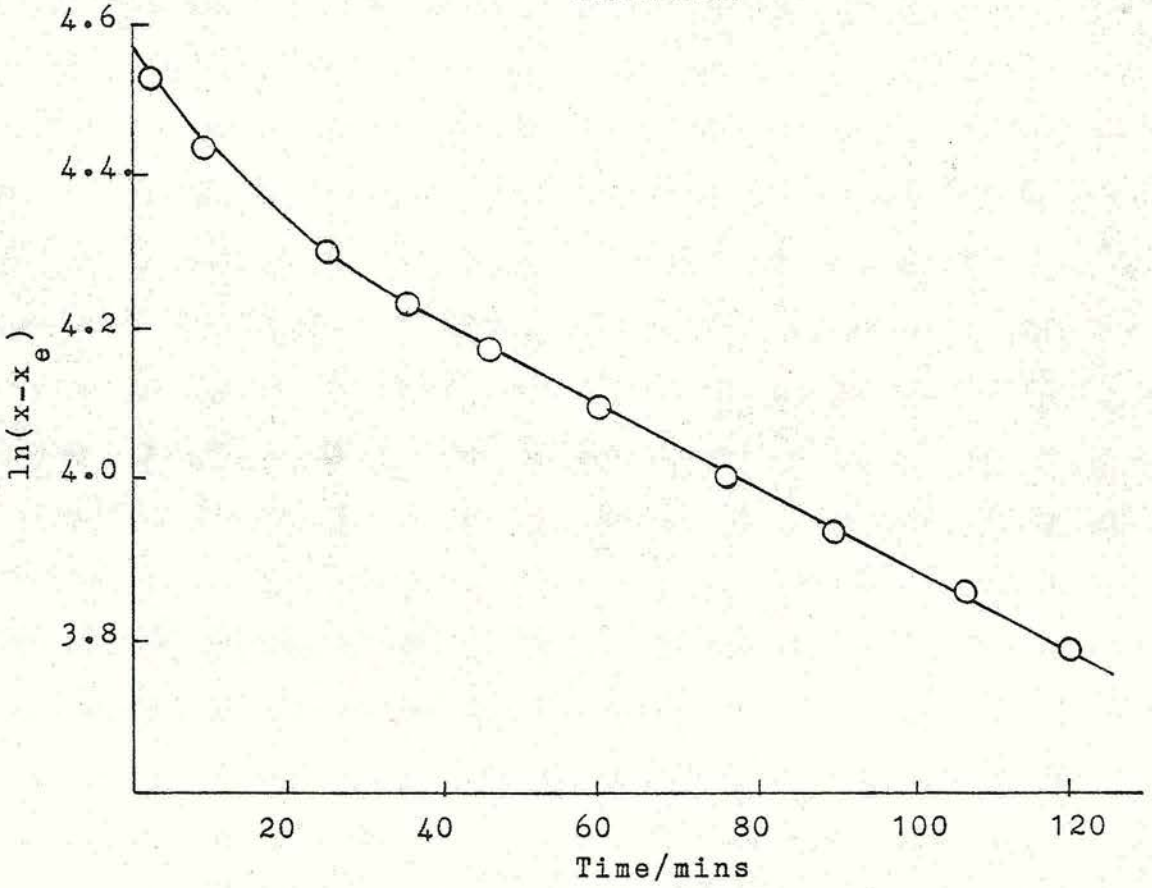

Figure 5.16. Derived First Order Plot

Figure 5.17. Reaction Profile for But-1-ene Isomerisation over H-EU-1(B) at 392 K

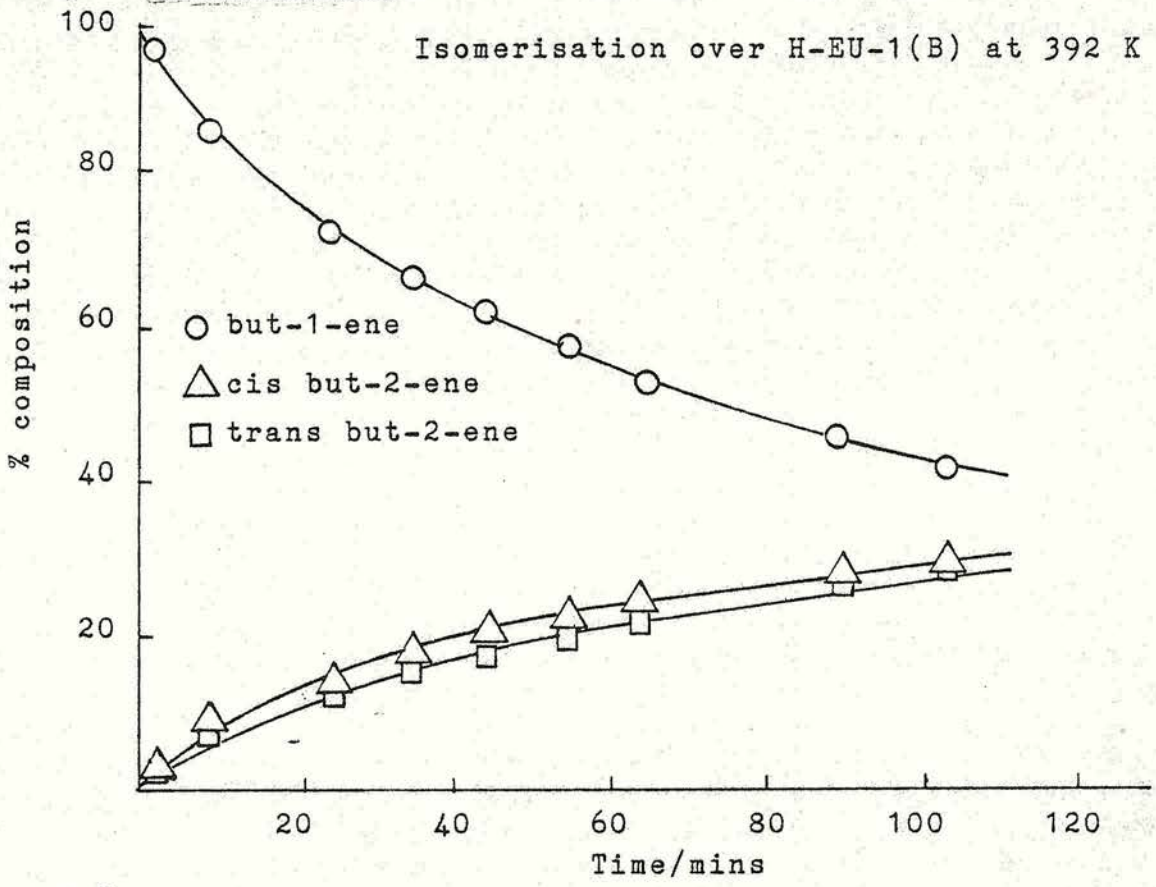

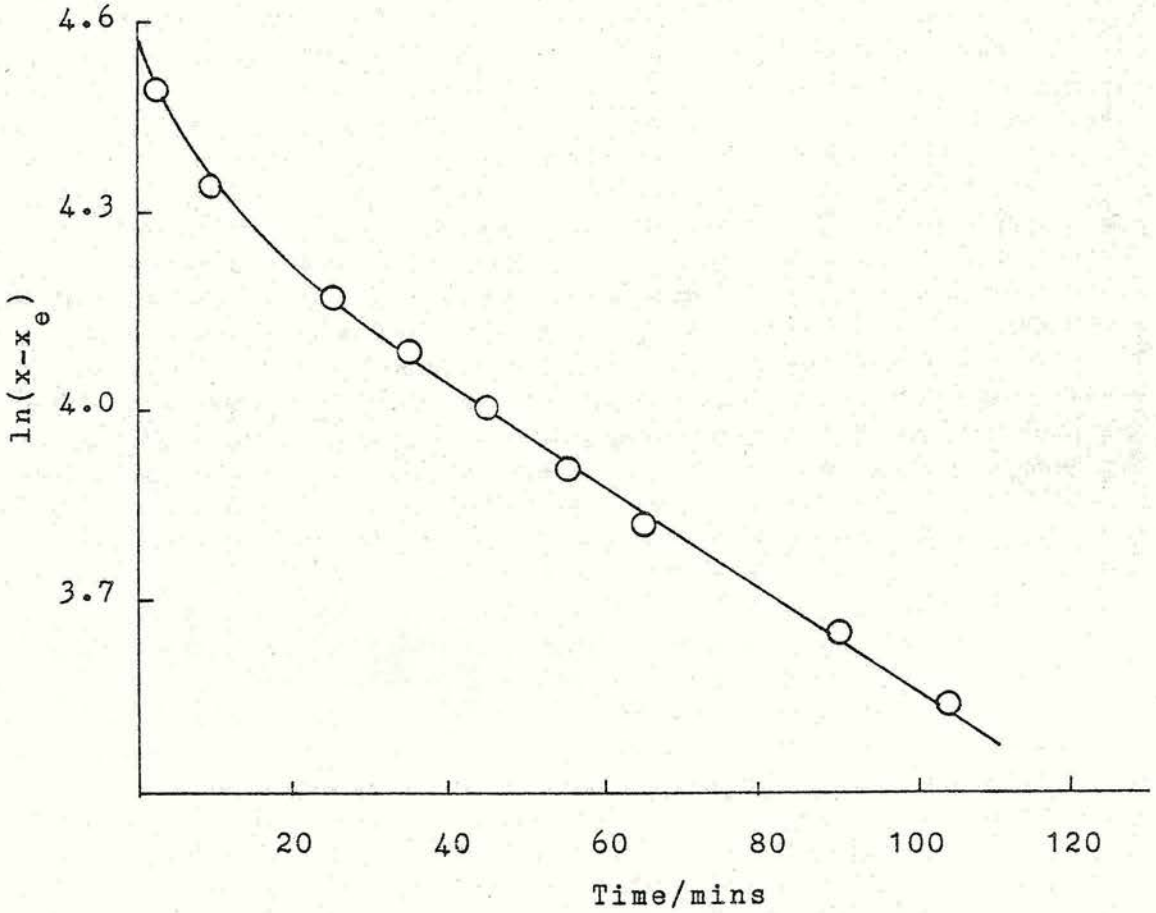

Figure 5.18. Derived First Order Plot

Figure 5.19. Arrhenius Plots for the Isomerisation of But-1-ene over H-EU-1

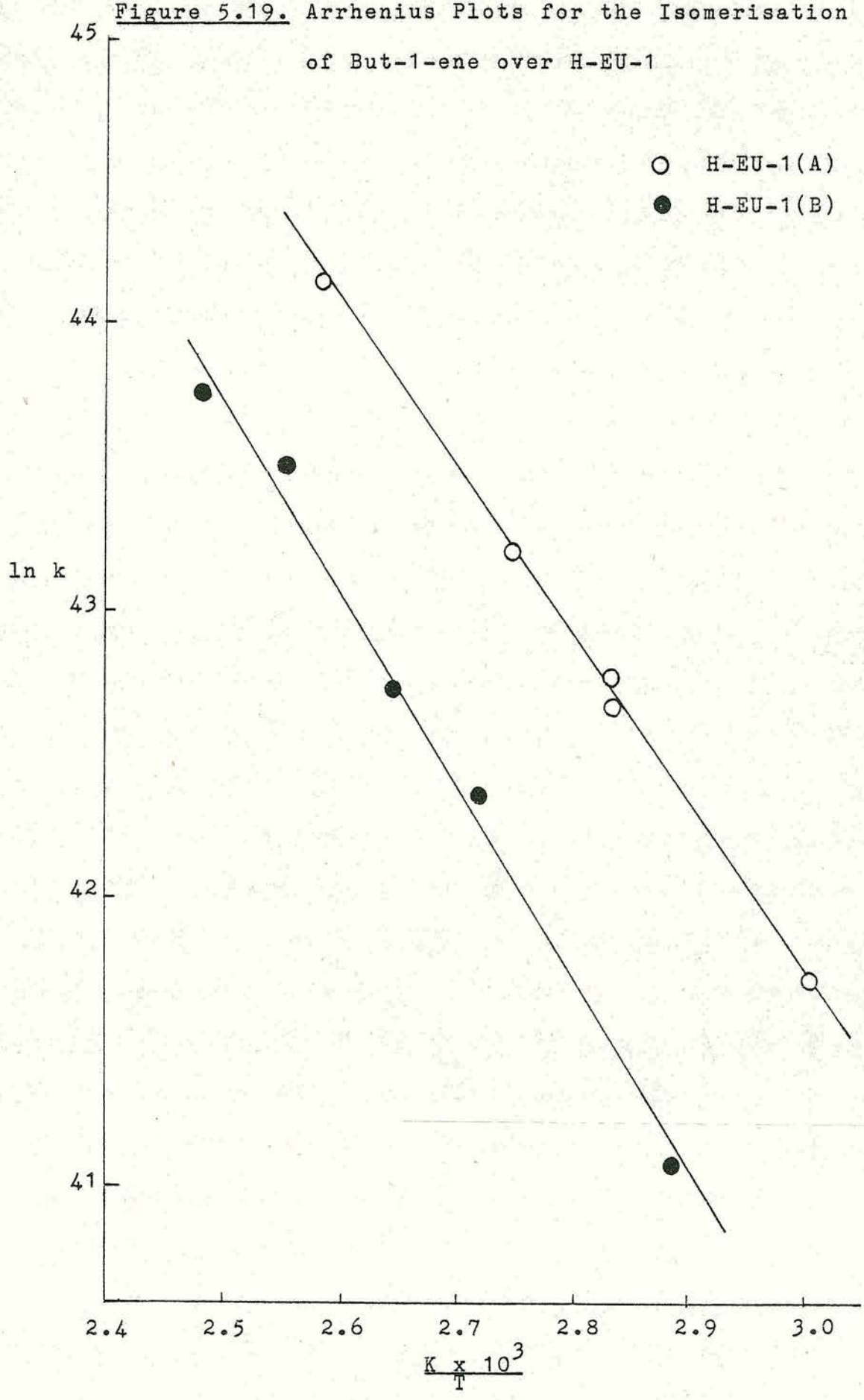

Reaction Temperature/K	Rate Constant/10^{18} molecules $s^{-1}g^{-1}$	Cis/Trans Product Ratio	
		Initial	Equilibrium
331	1.33	1.08	0.35
353	3.46	1.10	0.38
353	3.83	0.98	0.38
364	5.67	1.16	0.40
387	14.93	0.99	0.43

Table 5.15. First Order Rate Constants for But-1-ene Isomerisation over H-EU-1(A)

Reaction Temperature/K	Rate Constant/10^{18} molecules $s^{-1}g^{-1}$	Cis/Trans Product Ratio	
		Initial	Equilibrium
353	0.69	0.50	0.38
353	0.69	0.50	0.38
368	2.53	1.00	0.40
379	3.64	1.04	0.42
392	8.13	1.04	0.44
402	10.16	0.93	0.46

Table 5.16. First Order Rate Constants for But-1-ene Isomerisation over H-EU-1(B)

As in the case of H-ZSM-23 a study of catalyst activity for a second but-1-ene isomerisation (Run 2) was undertaken. The samples were evacuated at the reaction temperature for 30 minutes or at 723 K for 16 hours before a second dose of but-1-ene was admitted. The rate constants for the Run 2 isomerisations are listed in Table 5.17 together with the ratio of the first order

Catalyst	Evacuation Temperature/K	Evacuation Time/hours	Reaction Temperature/K	Rate Constant/10^{18} molecules s^{-1} g^{-1}	k_2/k_1	Initial Cis/Trans Product Ratio
H-EU-1(A)	387	0.50	387	5.45	0.36	1.10
H-EU-1(a)	723	16	387	13.31	0.89	1.08
H-EU-1(B)	402	0.50	402	3.93	0.39	1.06
H-EU-1(B)	723	16	392	6.56	0.81	0.99

Table 5.17. First Order Rate Constants (k_2) for Run 2 But-1-ene Isomerisation over H-EU-1.

rate constants (k_2/k_1).

The results in Table 5.17 illustrate the deactivation of H-EU-1 by the presence of but-1-ene molecules. The Run 2 isomerisation of but-1-ene after 30 minutes evacuation exhibited a rate constant which was considerably reduced with respect to the rate constant obtained during Run 1 while evacuation at 723 K was not sufficient to completely restore the activity of H-EU-1 as in the case of H-ZSM-23. Consideration of the first order plots obtained after 30 minutes evacuation indicated that H-EU-1(A) had an initial deceleratory period lasting for c.a. 25 minutes while H-EU-1(B) showed no induction period. The first order plots observed after evacuation at 723 K for 16 hours were similar to those obtianed during the Run 1 isomerisation. However, the induction period observed for H-EU-1(B) was reduced to c.a. 7 minutes.

The effect of flow rate on but-1-ene isomerisation over both samples of H-EU-1 was measured and the results are given in Table 5.18. For both samples varying the flow rate appeared to have no apparent effect on the observed rate constant.

Catalyst	Flow Rate/10^{-2} dm^3 s^{-1}	Reaction Temp./K	Rate Constant/10^{18} molecules $s^{-1}g^{-1}$
H-EU-1(A)	0.75	353	3.99
	1.20	353	3.83
	1.67	353	3.81
H-EU-1(B)	0.75	367	2.05
	1.20	367	2.53
	1.67	367	2.28

Table 5.18. Effect of Flow Rate on the First Order Rate Constant for But-1-ene Isomerisation over H-EU-1

The outgassing of H-EU-1(A) under vacuum at 723 K for 16 hours was accompanied by a slight colour change from white to cream/light brown possibly due to the residual carbon present in the sample (Section 4.1.1) Removal of the residual carbon was achieved by calcination of a sample of H-EU-1(A) for 16 hours at 823 K before the usual pretreatment for but-1-ene isomerisation. The first order plot obtained was similar to that observed from an uncalcined sample with an induction period of c.a. 35 minutes. However, the rate constant was only 50% of the value for the uncalcined sample.

Product Selectivity

The only products resulting from but-1-ene isomerisation over both samples of H-EU-1 were cis and trans but-2-ene. The initial cis/trans but-2-ene product ratios at zero percent but-1-ene conversion and the equilibrium values are listed in Tables 5.15 and 5.16 for H-EU-1(A) and H-EU-1(B) respectively. The product ratio was found to vary with extent of reaction and temperature as illustrated in Figure 5.20 (for H-EU-1(A)). The initial increase followed by a decrease in the product ratio made the extrapolation to zero percent difficult particularly at the higher temperatures. The increase in the product ratio coincides with the induction period while the decrease in product ratio is associated with the period of first order activity. This change in the product ratio is associated with a change in the product selectivty during the reaction. In order to obtain the initial product ratio associated with the period of first order activity the relevant portion of the product ratio graph was extrapolated to zero percent but-1-ene conversion. The results are given in Table 5.19.

Figure 5.20. Variation in Product Ratio for But-1-ene Isomerisation over H-EU-1(A)

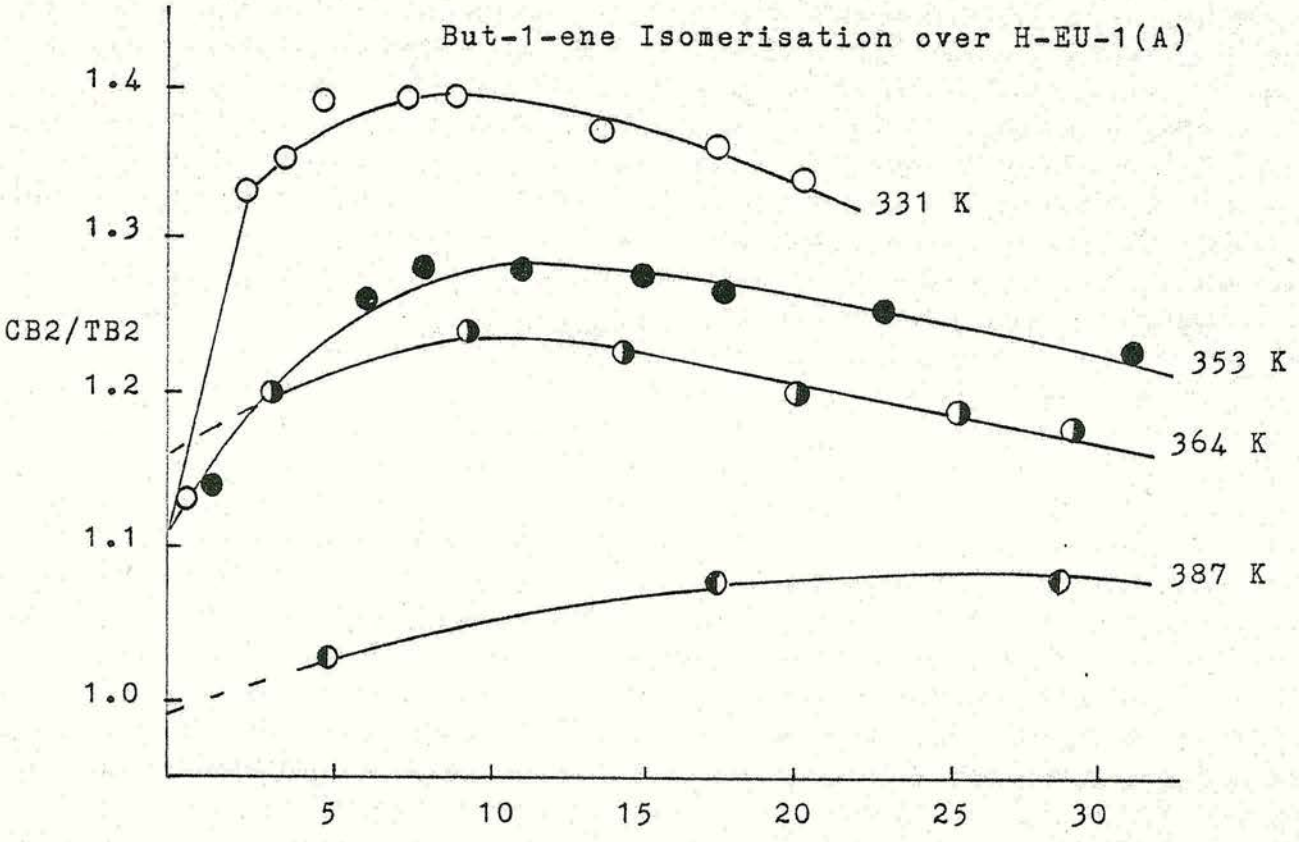

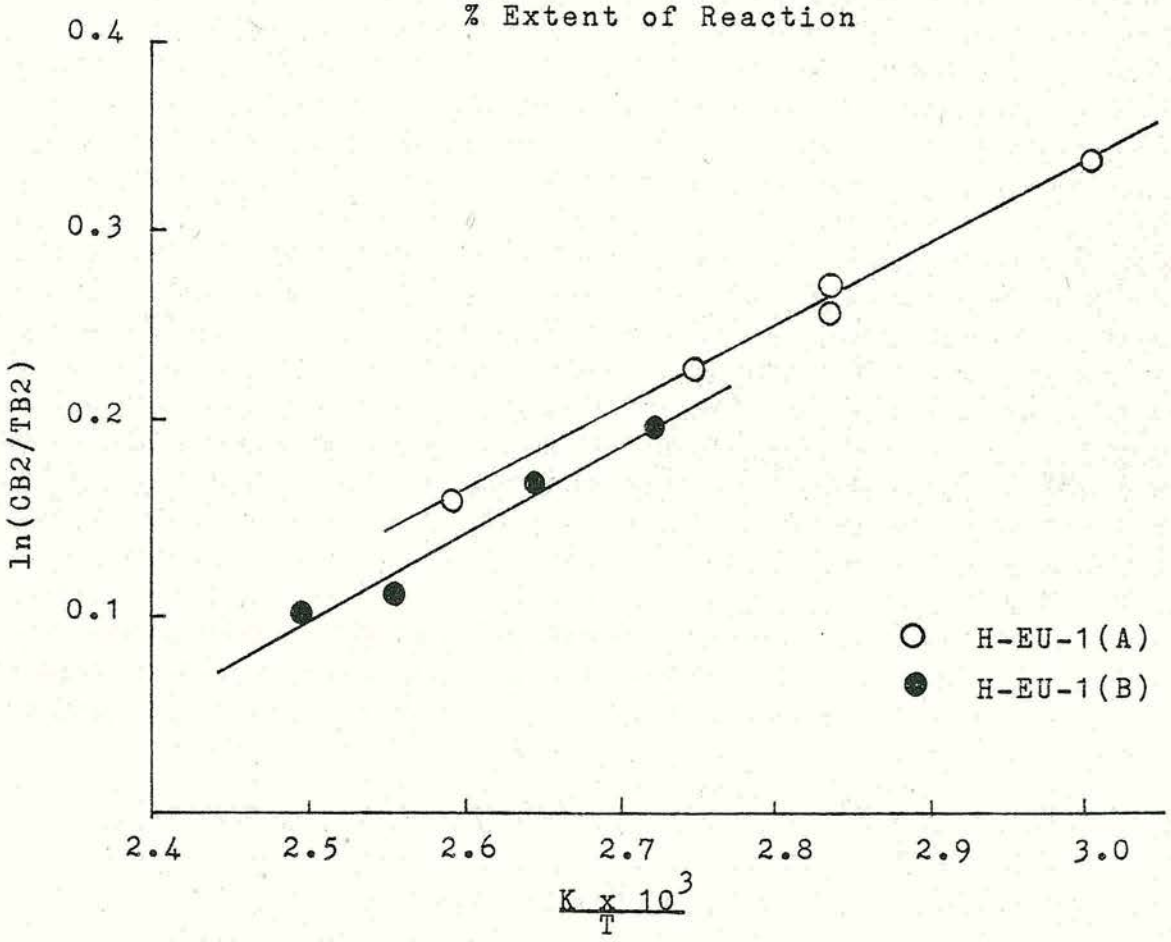

Figure 5.21. Arrhenius Plot of Variation in CB2/TB2 Product Ratio over H-EU-1

Catalyst	Reaction Temperature/K	Initial Cis/Trans Product Ratio
H-EU-1(A)	331	1.41
	353	1.30
	353	1.31
	364	1.27
	387	1.18
H-EU-1(B)	353	-
	353	-
	368	1.22
	379	1.19
	392	1.12
	402	1.11

Table 5.19. Initial Cis/Trans But-2-ene Product Ratio Associated with the Period of First Order Activity for H-EU-1

The initial product distributions resulting from but-1-ene isomerisation is indicative of the reaction mechanism. The cis/trans but-2-ene product ratio is higher than the thermodynamic equilibrium value i.e. the reaction is kinetically controlled. The initial cis/trans but-2-ene ratios given in Table 5.19 are dependent on reaction temperature, decreasing with increasing reaction temperature. This variation with temperature could be explained in terms of a difference in energy between the transition states leading to the products. The temperature dependence of the selectivity

is obtained from a plot of ln (cis/trans but-2-ene product ratio) vs. $1/T$[79,81] as illustrated in Figure 5.21. The activation energy differences for cis and trans but-2-ene formation were calculated to be c.a. 3 and c.a. 4 kJ mol^{-1} for H-EU-1(A) and H-EU-1(B) respectively.

The Run 2 reactions gave similar product ratio graphs to the above with a variation with extent of reaction No apparent difference was found in the initial product ratios obtained.

5.2.2. But-2-ene Isomerisation

Reactions with cis but-2-ene and trans but-2-ene were carried out on H-EU-1(A). A typical reaction profile for trans but-2-ene is illustrated in Figure 5.22 together with the derived first order plot (Figure 5.23). This plot, displaying an initial fast rate followed by a slower steady rate was similar to that observed for but-1-ene isomerisation and was observed for all reactions of cis and trans but-2-ene. The length of the induction period was however, found to vary. The induction periods for cis and trans but-2-ene isomerisation were c.a. 15 minutes and c.a. 7 minutes respectively. For the reactions of the n-butenes the ratio of the initial and steady first order rates were in the ratios of approximately 2.0:1 for but-1-ene and trans but-2-ene and c.a. 2.5:1 for cis but-2-ene. The first order rate constants are given in Tables 5.20 and 5.21. The apparent activation energies were calculated to be

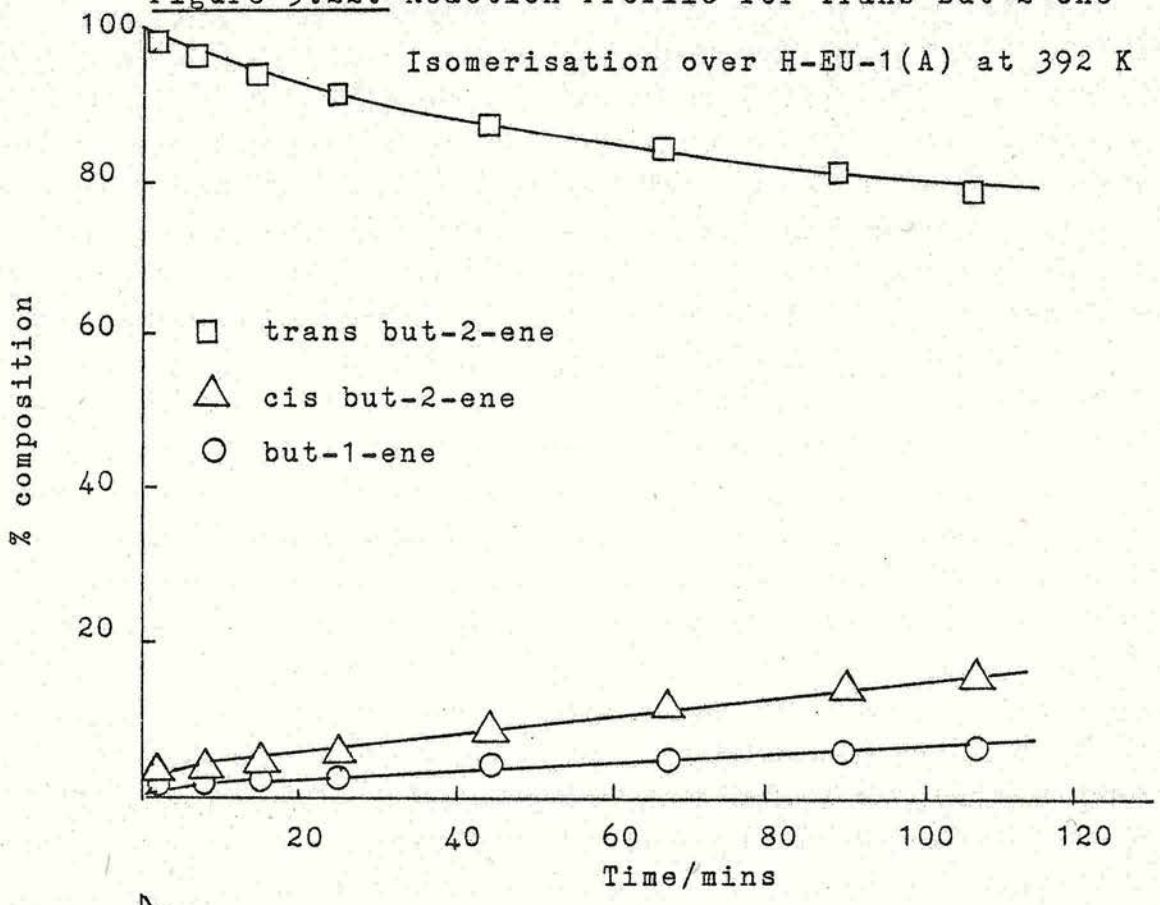

Figure 5.22. Reaction Profile for Trans But-2-ene Isomerisation over H-EU-1(A) at 392 K

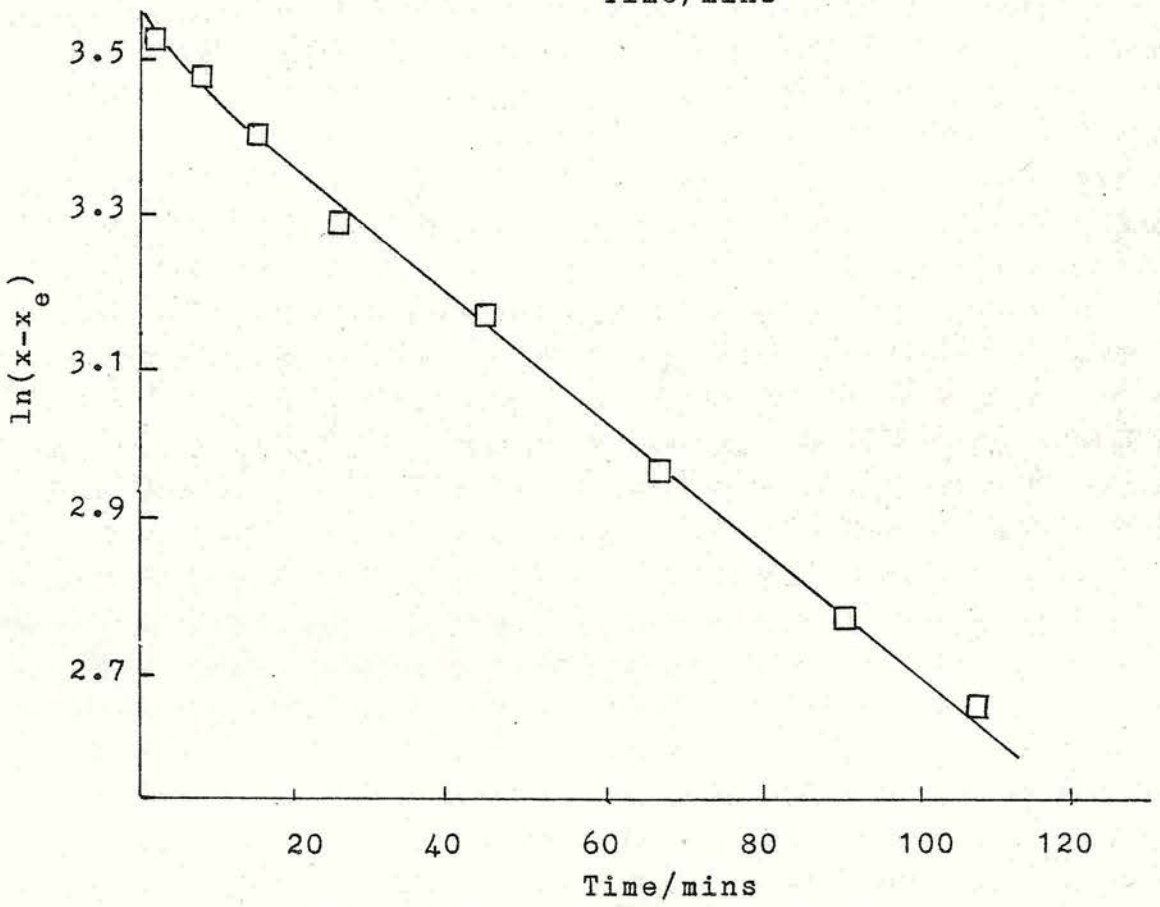

Figure 5.23. Derived First Order Plot

75 kJ mol^{-1} for cis but-2-ene and 70 kJ mol^{-1} for trans but-2-ene isomerisation. The Arrhenius plots for cis and trans but-2-ene are illustrated in Figure 5.24.

Reaction Temperature/K	Rate Constant/10^{18} molecules $s^{-1}g^{-1}$	TB2/B1 Product Ratio	
		Initial	Equilibrium
361	1.40	0.90	11.31
365	1.91	0.92	10.85
387	7.93	1.04	8.79
395	11.80	1.07	8.19

Table 5.20 Rate Constants for the Isomerisation of Cis But-2-ene over H-EU-1(A)

Reaction Temperature/K	Rate Constant/10^{18} molecules $s^{-1}g^{-1}$	CB2/B1 Product Ratio	
		Initial	Equilibrium
380	4.66	2.78	3.97
386	5.60	2.01	3.84
392	8.88	3.15	3.72
411	23.56	1.47	3.37

Table 5.21. Rate Constants for the Isomerisation of Trans But-2-ene over H-EU-1(A)

Varying the flow rate was found to have no effect on the rate of cis and trans but-2-ene isomerisation as illustrated in Table 5.22 and is in marked contrast to the observations over H-ZSM-23.

Figure 5.24. Arrhenius Plots for the Isomerisation of But-2-ene

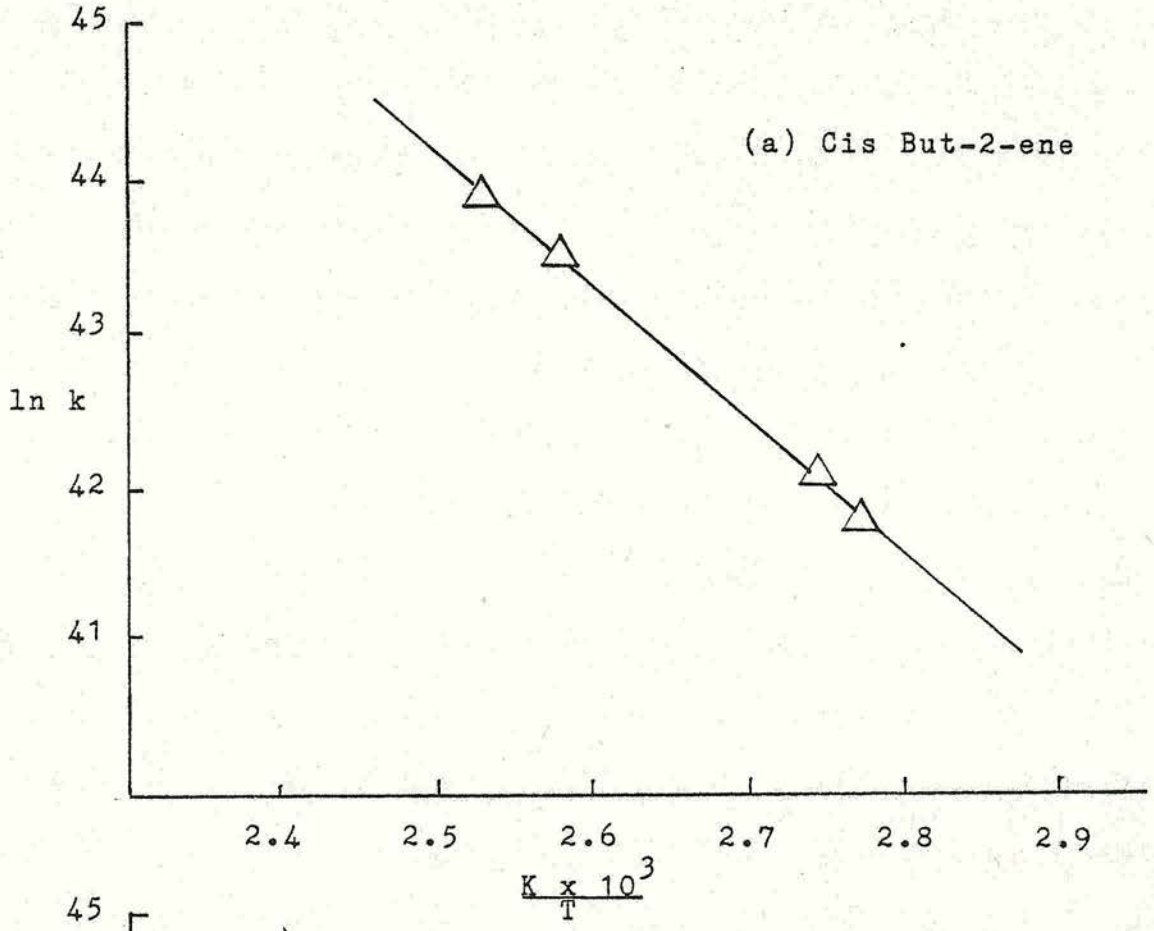

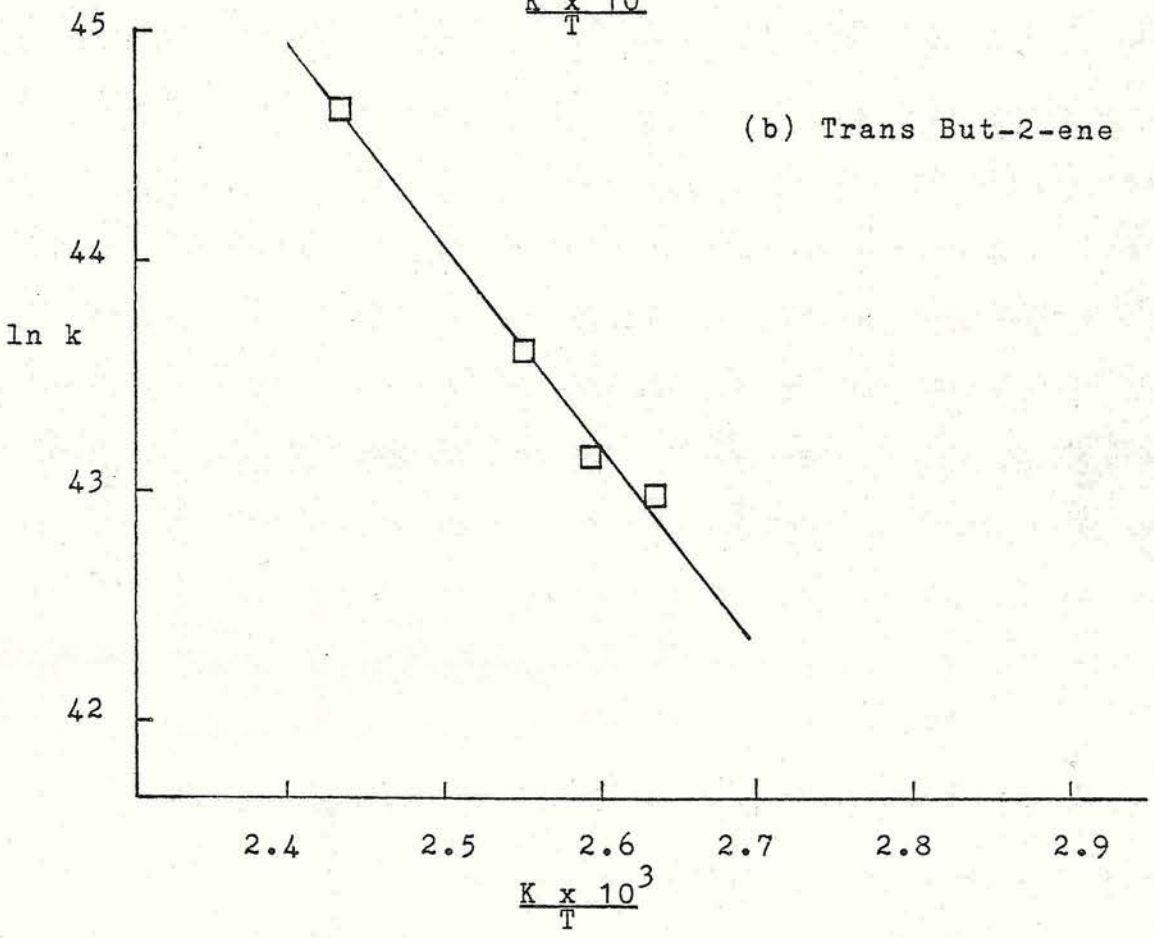

Reactant	Flow Rate /10^{-2} dm^3 s^{-1}	Rate Constant/10^{18} molecules $s^{-1}g^{-1}$
cis but-2-ene	0.75	1.68
	1.20	1.91
	1.58	1.71
trans but-2-ene	0.75	7.76
	1.20	5.60
	1.58	6.71

Table 5.22 Effect of Flow Rate on Rate Constants for the Isomerisation of Cis But-2-ene at 365 K and Trans But-2-ene at 386 K

Product Selectivity

The isomerisation of cis and trans but-2-ene over H-EU-1 resulted in the formation of but-1-ene and the other but-2-ene isomer as products. The product ratio from either reaction was found to vary throughout the course of the reaction as illustrated in Figure 5.25 and 5.26. A considerable alteration in the product ratio during the initial 5% of reaction for trans but-2-ene made accurate determination of the initial product ratio difficult. Initial product ratios have been estimated and are given in Table 5.21. The initial product ratios observed for cis but-2-ene (Table 5.20) suggest that double bond migration is favoured relative to cis-trans isomerisation. In addition to this, the initial product ratios from both cis and trans but-2-ene isomerisation appear to be temperature dependent. Calculation of the

Figure 5.25. Variation in TB2/B1 Product Ratio with Extent of Cis But-2-ene Conversion over H-EU-1(A) at 395 K

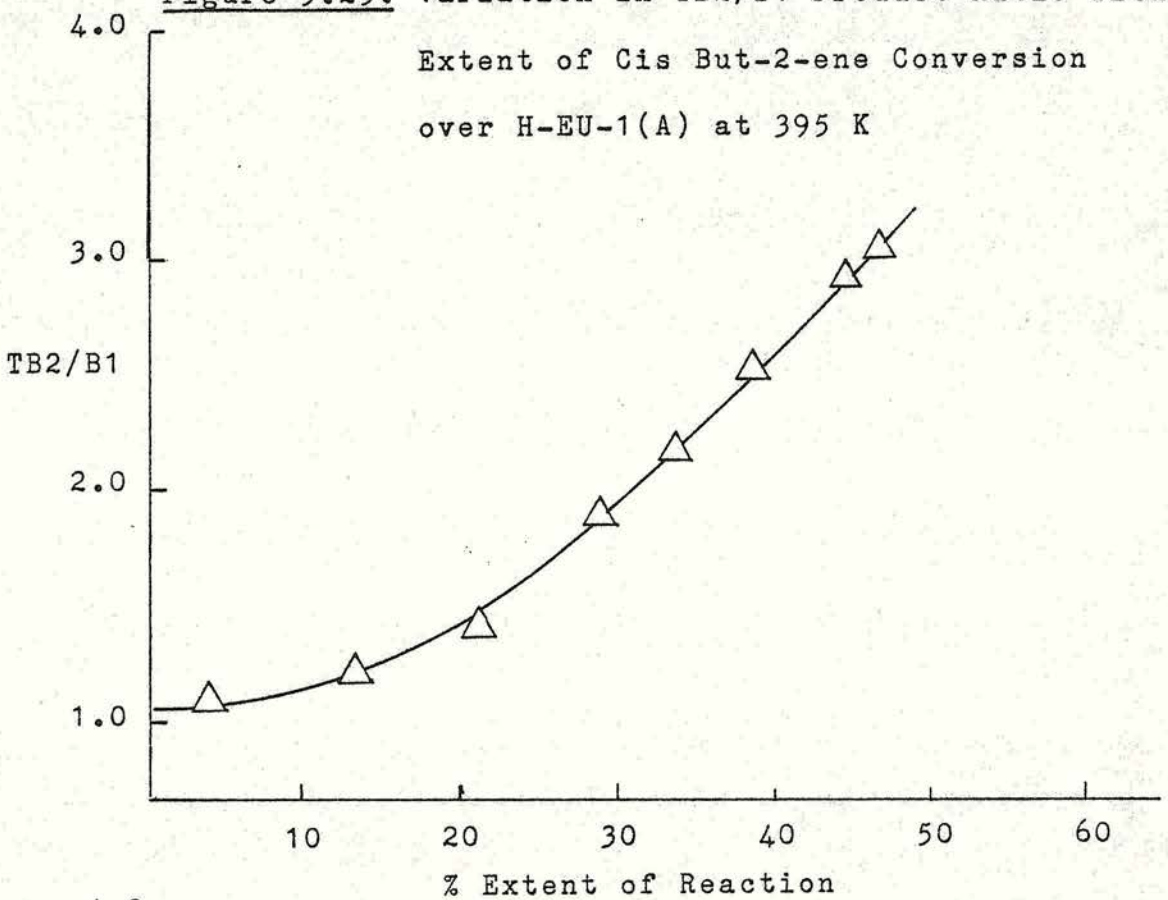

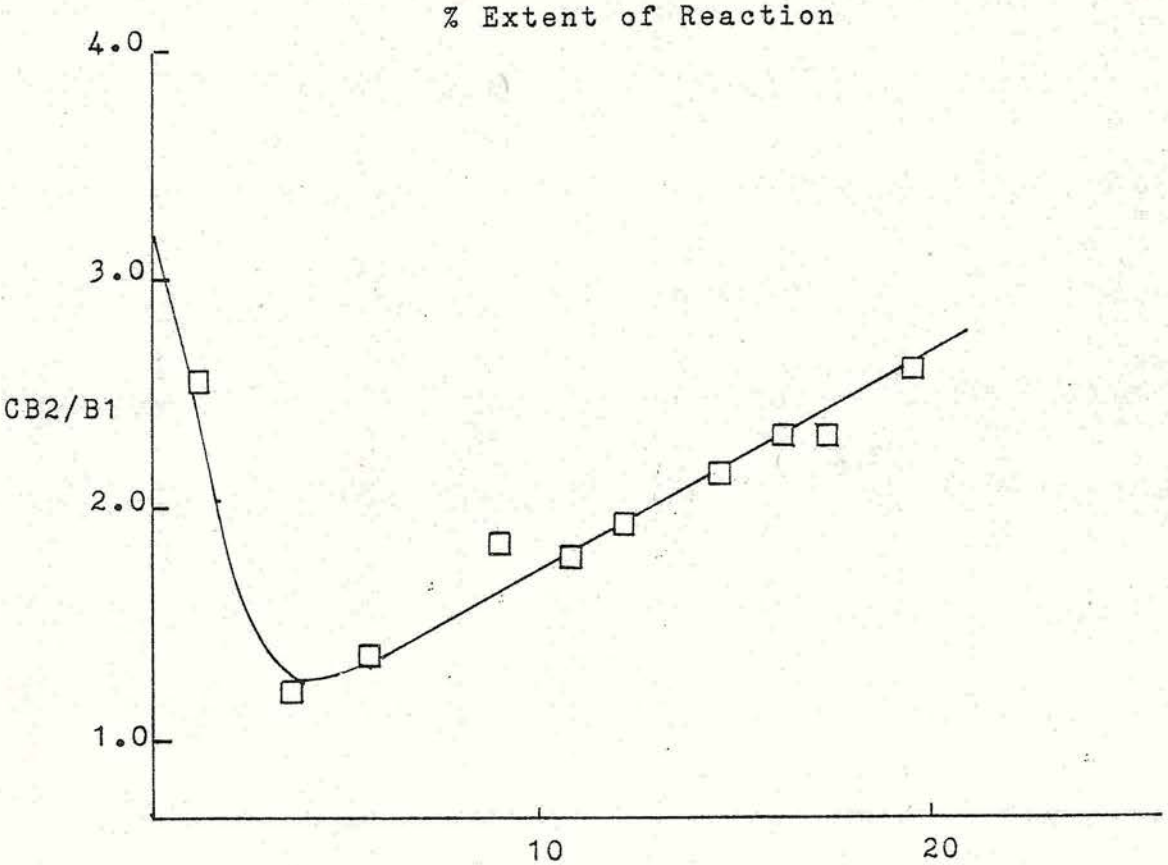

Figure 5.26. Variation in CB2/B1 Product Ratio with Extent of Trans But-2-ene Conversion over H-EU-1(A) at 392 K

differences in activation energies from the temperature dependence of the product ratios (Figure 5.28 and 5.29) gives values of c.a. 10 kJ mol^{-1} for trans but-2-ene isomerisation and c.a. 6 kJ mol^{-1} for cis but-2-ene isomerisation. Combination of these results gives a difference in the activation energies of cis and trans but-2-ene of 4 kJ mol^{-1} which is similar to the value calculated from the temperature dependence of the cis/trans but-2-ene product ratio (3 kJ mol^{-1}).

Discussion

As previously shown the initial product distributions resulting from n-butene isomerisation can be a guide to the operative reaction mechanism. Throughout the temperature range studied

$$\frac{\text{trans but-2-ene}}{\text{but-1-ene}} \times \frac{\text{but-1-ene}}{\text{cis but-2-ene}} \times \frac{\text{cis but-2-ene}}{\text{trans but-2-ene}} = 0.8$$

for H-EU-1(A). It is a necessary requirement of the triangular reaction scheme that the above product should be unity[71]. In view of the inherent errors involved in determining the product ratios the value of 0.8 is believed to be not incompatible with such a reaction scheme.

The acid catalysed isomerisation of butene is considered to proceed via proton addition with first order kinetics[35]. A common intermediate (the secondary butyl carbonium ion) provides a direct pathway between

Figure 5.27. Arrhenius Plot of Variation in CB2/B1 over H-EU-1(A)

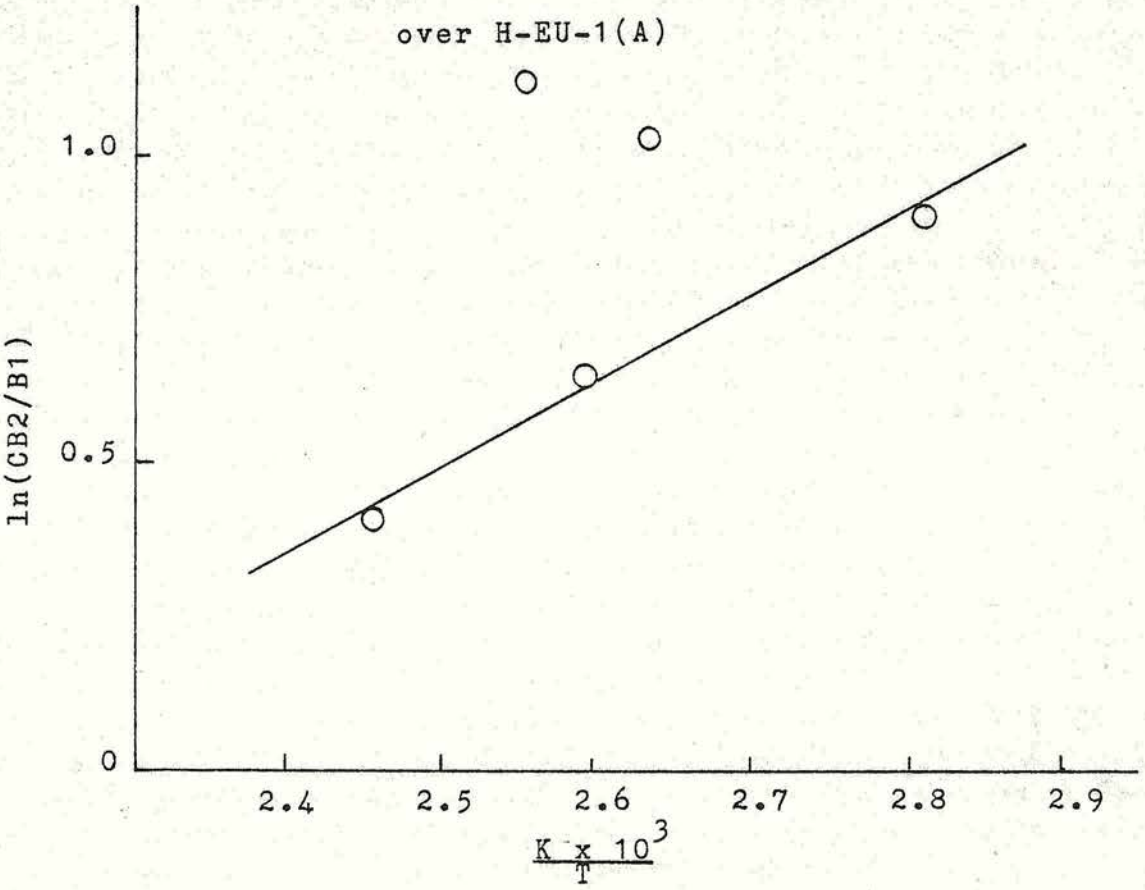

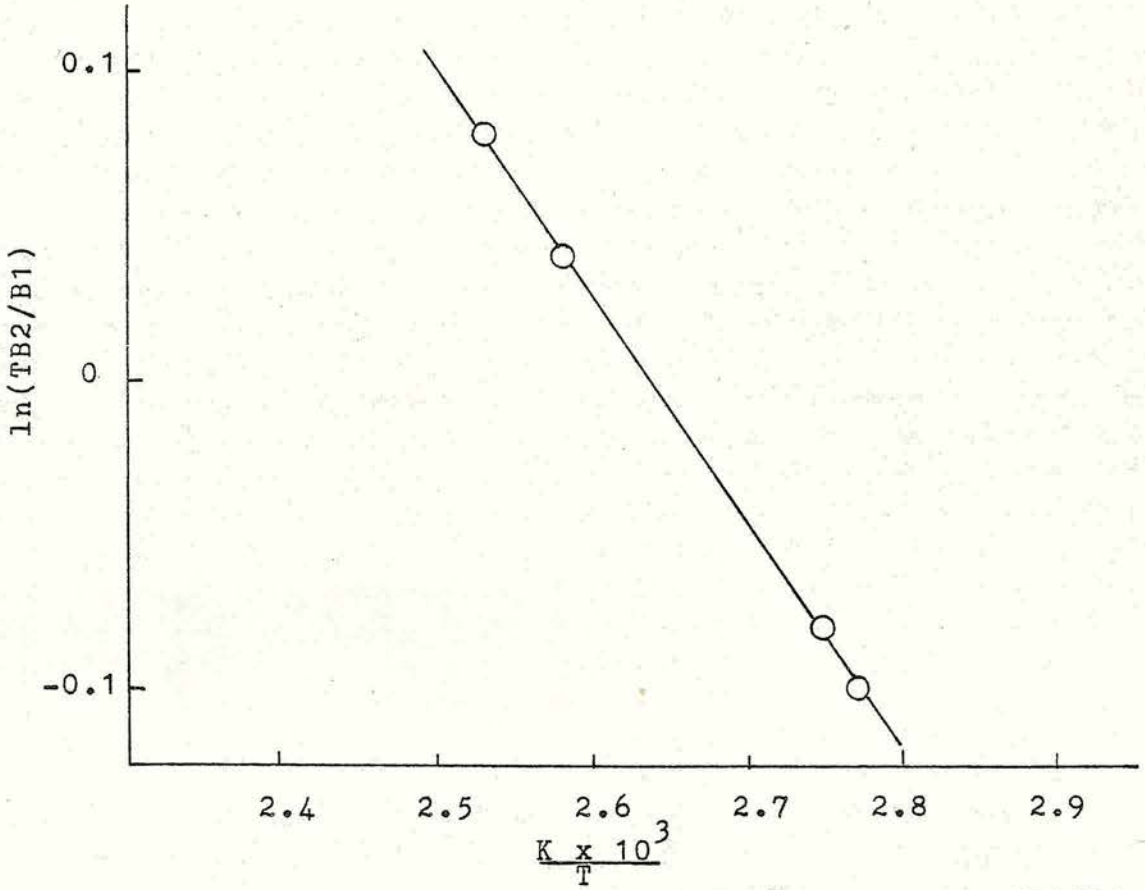

Figure 5.28. Arrhenius Plot of Variation in TB2/B1 over H-EU-1(A)

all three isomers. The isomerisation proceeding through this intermediate can be represented as:

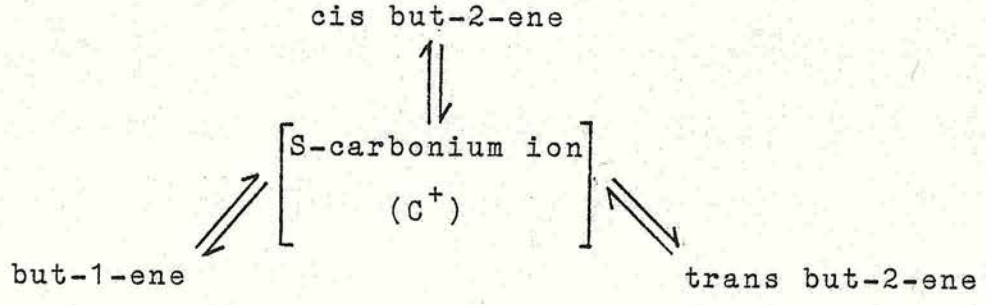

Cis/trans but-2-ene ratios which are close to unity are considered to be indicative of the above carbonium ion mechanism[35,85]. The cis/trans but-2-ene product ratios reported here for H-EU-1 are close to unity. The data of Table 5.19 indicate that the reaction is kinetically controlled since the initial product distribution differs from the thermodynamic equilibrium values (the cis/trans but-2-ene product ratio is 0.41 at 373 K). However, a product ratio of unity is not sufficient evidence alone for the carbonium ion mechanism. It is a prerequisite of this mechanism that the product ratio is temperature independent[35]. This was not the case over H-EU-1. Temperature dependent cis/trans but-2-ene product ratios have been reported by other workers[87,93,106] and are sometimes found for acid catalysed reactions. The activation energy calculated from the temperature dependency of the cis/trans but-2-ene product ratio was c.a. 3 kJ mol^{-1} for H-EU-1(A). This value is similar to that obtained by Tsuchiya et al[93] for but-1-ene isomerisation over H-ZSM-5. Further evidence for a

carbonium ion mechanism is a comparison of the rates of isomerisation. Over most acidic catalysts the observed rates of isomerisation are in the order but-1-ene > cis but-2-ene > trans but-2-ene[163]. This is also the case with H-EU-1(A) and it can be concluded that the isomerisation of butene over H-EU-1 most probably occurs via the secondary butyl carbonium ion.

The cis but-2-ene/but-1-ene product ratios obtained from the isomerisation of trans but-2-ene were found to be slightly lower than the corresponding thermodynamic equilibrium values (Table 5.21) while the trans but-2-ene/but-1-ene ratios obtained from the isomerisation of cis but-2-ene differed considerably from the thermodynamic equilibrium values and were similar to the values obtained using H-ZSM-23 i.e. double bond migration favoured relative to cis-trans isomerisation. Calculation of the differences in activation energies from the temperature dependence of the product ratios gave the following values

$$E_{\text{but-1-ene}} - E_{\text{cis but-2-ene}} = 10 \text{ kJ mol}^{-1}$$

$$E_{\text{but-1-ene}} - E_{\text{trans but-2-ene}} = 6 \text{ kJmol}^{-1}$$

These values are slightly higher than those obtained over other acid catalysts[81]. Hightower and Hall [79] proposed that the selectivities for product formation over silica-alumina depended principally on the differences in barrier heights between the carbonium ion and the products. Tsuchiya et al[93] explained similar high values obtained over H-ZSM-5 by the suppresion of cis-trans isomerisation in the narrow space of the channels in

H-ZSM-5 and suggested that the suppression was due to transition-state selectivity.

As in the case of H-ZSM-23 evidence was found for the formation of butene polymer. Extrapolation of the product composition curves to zero contact time indicated a conversion of c.a. 1%. The Run 2 reactions carried out after 30 minutes evacuation at reaction temperature did not show this initial conversion suggesting that the polymer had not been removed by evacuation at reaction temperature. The presence of but-1-ene molecules was found to deactivate H-EU-1(A) more than H-EU-1(B) (Table 5.17). This is in agreement with the results presented in Section 4.1.3 where the n-butane surface area after but-1-ene exposure was reduced by 29% for H-EU-1(A) compared to 14% for H-EU-1(B).

During the course of but-1-ene isomerisation a change in the cis/trans but-2-ene product ratio associated with a change in product selectivity was observed. The initial formation of butene polymer may cause some pore blockage and thus alter the rates of diffusion of the product molecules. The results presented in Section 4.2.2 indicate that cis but-2-ene has the lowest rate of diffusion. If the diffusion of cis but-2-ene was restricted then there is the possibility of further reaction to but-1-ene and trans but-2-ene (which have faster rates of diffusion) resulting in a distortion of the observed cis/trans but-2-ene product ratio.

Comparison of the rates of but-1-ene isomerisation

presented in Tables 5.15 and 5.16 for H-EU-1(A) and H-EU-1(B) respectively, show H-EU-1(A) to be the more active catalyst. It has been previously shown (Chapter 4), that H-EU-1(A) has a smaller crystal size (and thus a correspondingly shorter diffusion path) and a faster rate of diffusion of but-1-ene than H-EU-1(B). Thus but-1-ene will reach the active centres and react faster in H-EU-1(A) than H-EU-1(B).

Starting with trans but-2-ene, the ratio of cis but-2-ene to but-1-ene increases with increasing acidity of the catalyst. Kinetic studies[85] suggest that the energy barrier height between the secondary carbonium ion and but-1-ene varies directly with catalyst acidity. A similar conclusion was reached by Misono and Yoneda[81] using aluminium and magnesium sulphates. The secondary carbonium ion is stabilised with the stronger acid catalyst and conversion to cis but-2-ene rather than to but-1-ene becomes more favourable. Comparison of the trans but-2-ene isomerisation results for H-EU-1(A) (Table 5.21) and H-ZSM-23 (Table 5.6) suggest that H-ZSM-23 is more acidic than H-EU-1.

5.2.3. Methylcyclopropane Isomerisation

The isomerisation of MCP was investigated over H-EU-1(A). A typical reaction profile is illustrated in Figure 5.29. MCP isomerisation followed first order kinetics as illustrated by Figure 5.30. Induction periods of c.a. 10 minutes were observed for reactions carried out at 357 K and 375 K while reactions at higher

Figure 5.29. Reaction Profile for MCP Isomerisation over H-EU-1(A) at 386 K

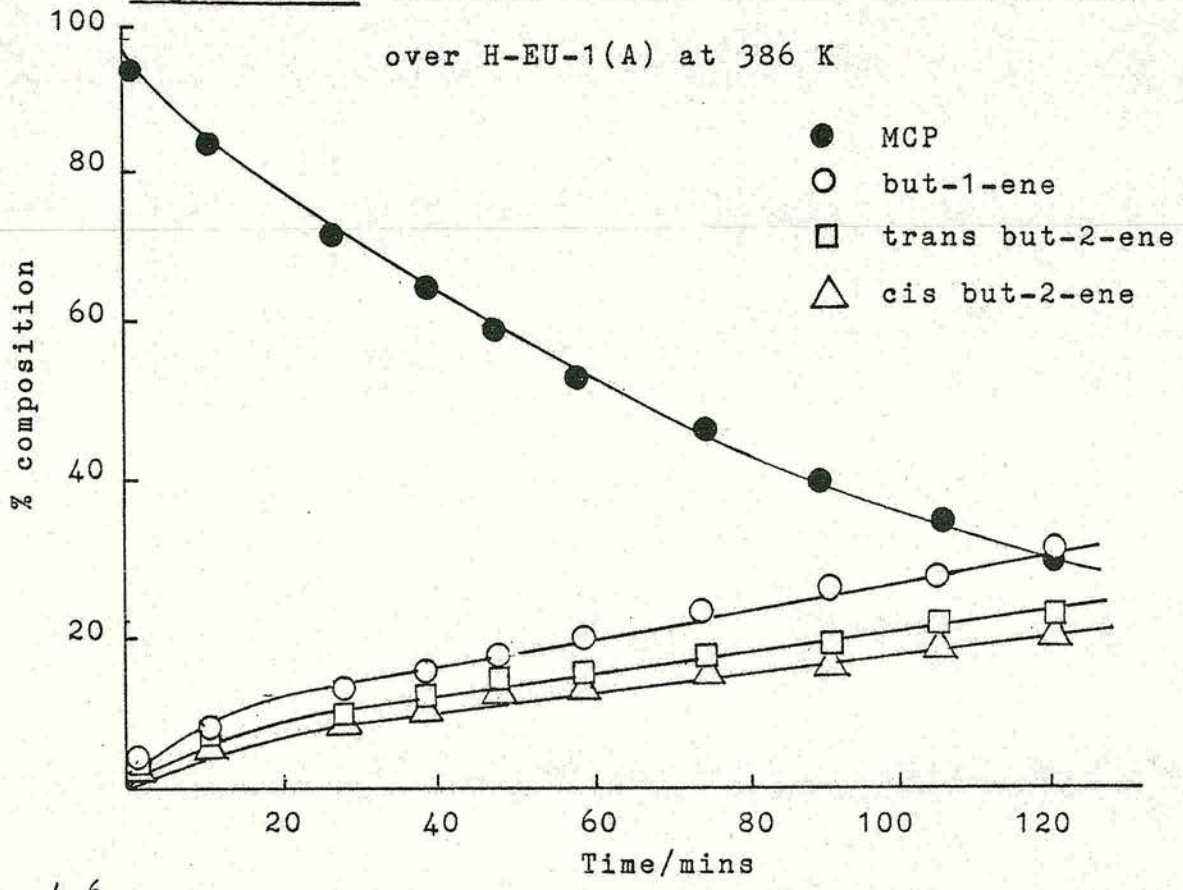

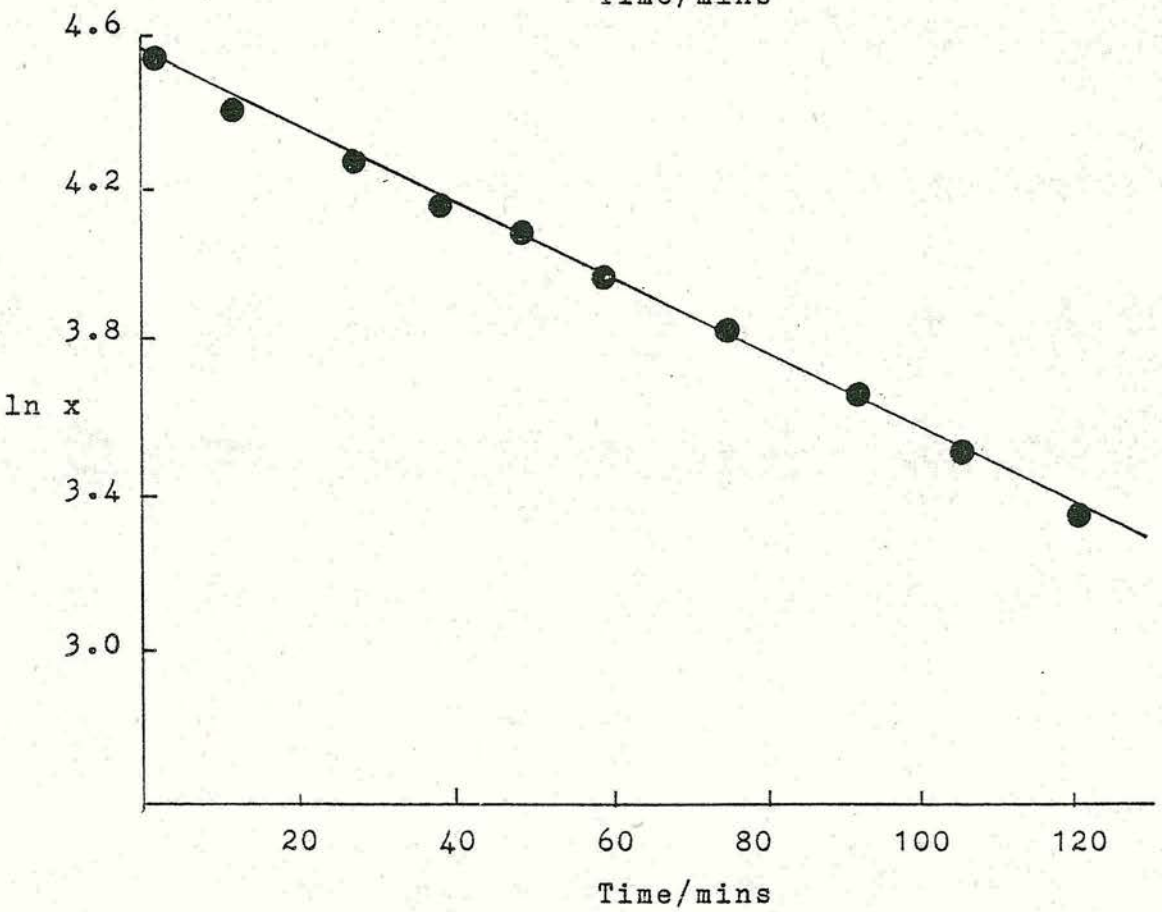

Figure 5.30. Derived First Order Plots

temperatures exhibited first order kinetics from the begining of the reaction. Table 5.23 lists the observed first order rate constants. The Arrhenius plot is illustrated in Figure 5.31. The apparent activation energy was calculated to be 85 kJ mol^{-1}.

Reaction Temperature/K	Rate Constant/10^{18} molecules $s^{-1}g^{-1}$
357	1.47
375	5.59
386	11.39
388	15.74

Table 5.23. Rate Constants for MCP Isomerisation over H-EU-1(A)

Varying the flow rate has been shown previously to have no effect on the isomerisation of the n-butenes over H-EU-1(A). As Table 5.24 shows this was also the case in MCP isomerisation.

Figure 5.31. Arrhenius Plot for the Isomerisation of MCP over H-EU-1(A)

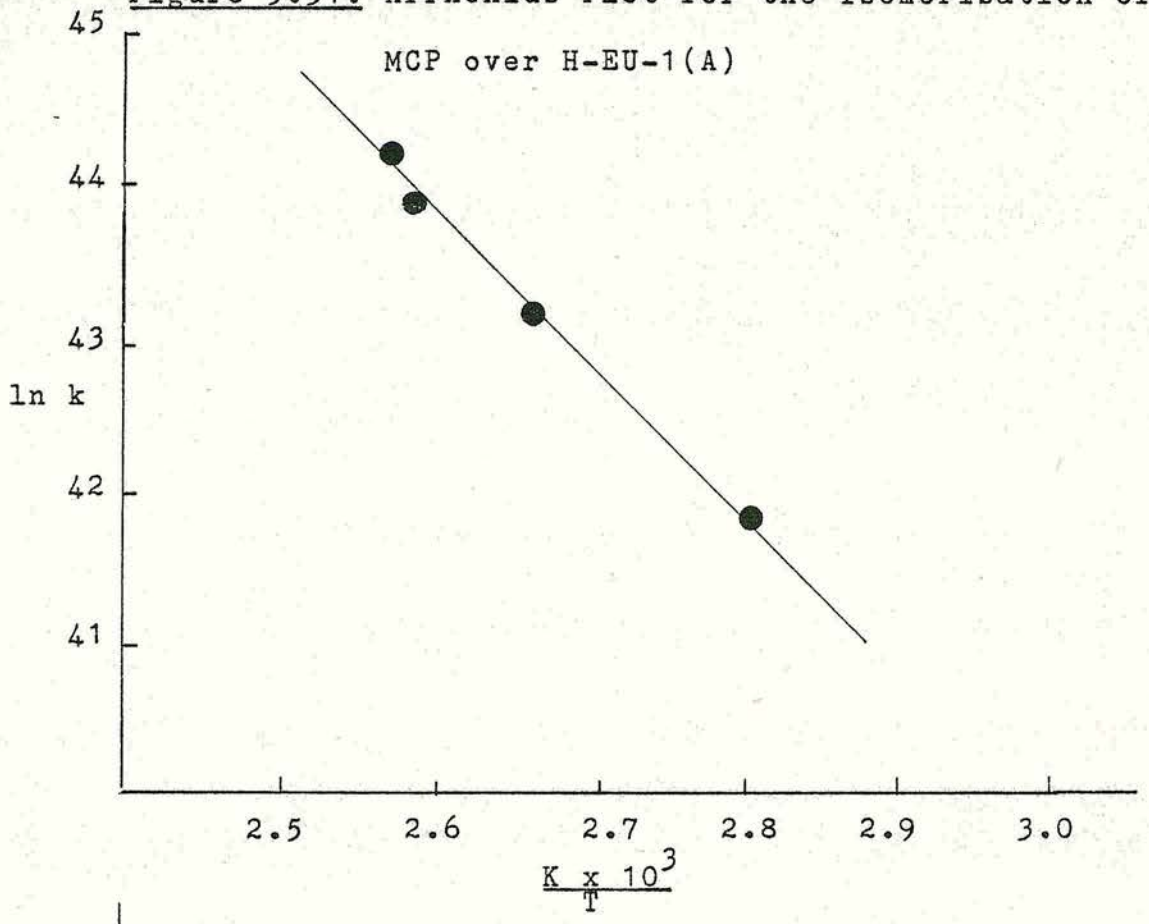

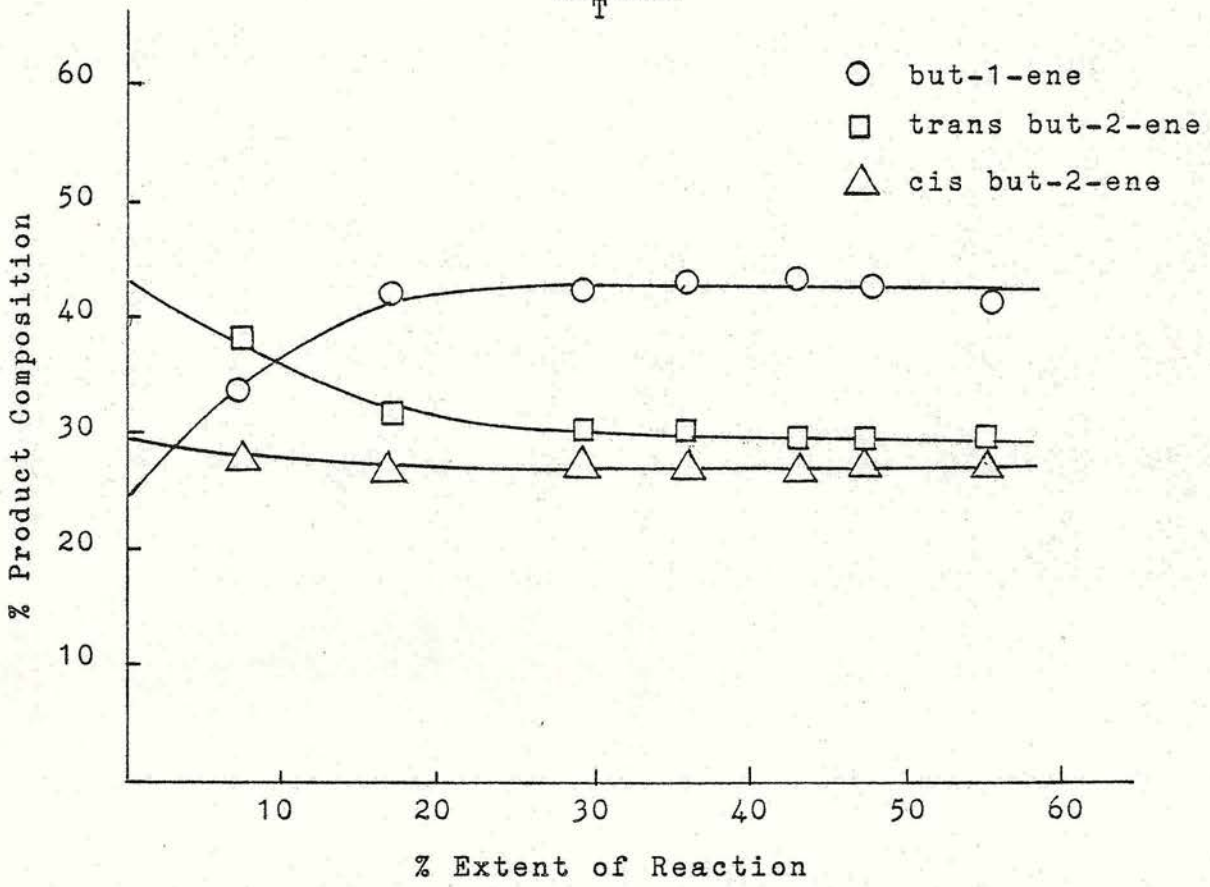

Figure 5.32. Variation in Product Composition with Extent of MCP conversion over H-EU-1(A) at 386 K

Reaction Temperature/K	Flow Rate/10^{-2} $dm^3\ s^{-1}$	Rate Constant/10^{18} molecules $s^{-1}g^{-1}$
357	0.75	1.80
357	1.20	1.47
357	1.50	1.58

Table 5.24. Effect of Flow Rate on the Rate Constant for MCP Isomerisation over H-EU-1(A)

Product Selectivity

The n-butenes were the only products observed during MCP isomerisation over H-EU-1(A). The initial product compositions estimated by extrapolation to zero percent conversion of MCP are listed in Table 5.25. together with the equilibrium values. The initial product distributions are very different from the equilibrium values indicating kinetic control. The product distributions were found to vary considerably throughout the course of the reaction as illustrated by Figure 5.32. Table 5.26 gives the product compositions at 10% and 30% MCP conversion.

The variation of the initial product ratios can be plotted according to the Arrhenius equation to determine the activation energy differences between paths leading to each of the three n-butene products. The values derived were in good cyclic agreement; the sum of ΔE values between cis but-2-ene and but-1-ene and between cis and trans but-2-ene ($5 + 22 = 27$ kJ mol^{-1}) was nearly the same as the ΔE value between trans but-1-ene and

Reaction Temp./K	Initial Product Composition/%			Equilibrium Product Composition/%		
	B1	TB2	CB2	B1	TB2	CB2
357	18.5	58.5	23.0	5.8	67.9	26.3
375	34.0	46.0	20.0	6.7	65.9	27.4
386	25.6	44.6	29.8	7.3	64.7	28.0
388	28.7	41.6	29.7	7.4	64.5	28.1

Table 5.25. Product Composition from MCP Isomerisation over H-EU-1(A)

Reaction Temp./K	Product Composition at 10% Conversion/%			Product Composition at 30% Conversion		
	B1	TB2	CB2	B1	TB2	CB2
357	41.4	29.5	29.1	-	-	-
375	40.8	34.4	24.8	43.4	29.4	27.2
386	37.6	35.2	27.2	43.3	30.3	26.4
388	36.5	34.4	29.1	42.8	29.8	27.4

Table 5.26. Product Composition at 10% and 30% Conversion of MCP

but-1-ene ($\sim$27 kJ mol^{-1}).

Reaction of But-1-ene After MCP Isomerisation

No secondary isomerisation of but-1-ene occurred after complete conversion of MCP. However, when a dose of but-1-ene was admitted to the catalyst following 80% MCP conversion and evacuation for 30 minutes at reaction temperature first order kinetics were observed. The induction period was reduced to c.a. 7 minutes. Comparison of the rate constants with those obtained over a fresh catalyst showed a reduction in activity.

Evacution for 16 hours at 723 K following MCP conversion did not completely restore the but-1-ene activity.

Discussion

The absence of isobutene and cyclobutane from the observed products over H-EU-1 is indicative of a proton addition mechanism. The formation of isobutene would require an unstable primary carbonium ion as intermediate whereas the observed products can be explained on the basis of a secondary carbonium ion intermediate. A proton addition mechanism involving the secondary butyl carbonium ion has been proposed for n-butene isomerisation over H-EU-1.

The observed variation of the product ratios with temperature indicates some contribution of transition state selectivity levels to the observed selectivity.

The initial product distributions over H-EU-1(A)

and H-ZSM-23 are similar: with product distributions in the order trans but-2-ene > cis but-2-ene > but-1-ene. The non-classical cyclopropyl carbonium ion postulated as intermediate in MCP ismerisation over silica-alumina[104] and zeolite omega[106,162] requires an initial product distribution in the order trans but-2-ene > but-1-ene ≥ cis but-2-ene. The product distribution at 10% conversion of MCP was found to be but-1-ene > trans but-2-ene > cis but-2-ene and may reflect a change in the mechanism possibly associated with a change in the seat of activity. However, the concentration of trans but-2-ene appears to decrease as the concentration of but-1-ene increases and could possibly be the result of an interconversion between the two isomers. The concentration of cis but-2-ene remains approximately constant throughout the course of the reaction.

The lack of secondary reaction of the n-butenes suggests that the sites responsible for the isomerisation of the n-butenes have been poisoned by the isomerisation reaction of MCP.

5.2.4. Summary

The isomerisation of the n-butenes over H-EU-1 occurs via a carbonium ion type mechanism with the secondary butyl carbonium ion as intermediate. Temperature dependent product ratios were obtained in all cases and these may indicate differences in the barrier heights between the carbonium ion and the products[79] or the suppression of cis-trans isomerisation in the zeolite channels due to transition state selectivity[93].

As in the case of H-ZSM-23 evidence was found for the formation of butene polymer on exposure of H-EU-1 to n-butene.

The absence of isobutene and cyclobutane from the observed products of MCP isomerisation is indicative of a proton addition mechanism. The initial product distribution was similar to that expected on the basis of a secondary butyl carbonium ion intermediate. However, a change in the product distribution with percent conversion of MCP may be associated with a change in the mechanism, possibly associated with a change in the seat of activity. The lack of secondary reaction of the n-butenes suggests that MCP isomerisation has poisoned the sites responsible for the isomerisation of the n-butenes.

CHAPTER 6

Results and Discussion:- Part III

Isomerisation and Hydrogenolysis Reactions over RuY Zeolites

6.1. Isomerisation of 3,3-Dimethylbut-1-ene

The aim of this section is to compare the activity of the ruthenium loaded zeolites RuNaY20, RuNaLaY20 and RuLaY20 as catalysts for the isomerisation of 3,3-dimethylbut-1-ene. The catalysts were pretreated as described in Chapter 3.

6.1.1. RuNaY20

The isomerisation of 3,3-dimethylbut-1-ene (I) over RuNaY20 was studied in the temperature range 272-303 K following pretreatment. A typical reaction plot is illustrated in Figure 6.1.

In addition to the isomerisation products 2,3-dimethylbut-1-ene (II) and 2,3-dimethylbut-2-ene (III), traces of but-1-ene and significant quantities of 2,2-dimethylbutane were formed. No 2,3-dimethylbutane was observed. As Figure 6.1 illustrates there was an initial fast rate of formation of 2,2-dimethylbutane (c.a. 10% at 30 minutes) and then a much slower rate. Experiments in which the initial dose of I was evacuated and a fresh dose admitted gave no hydrogenation product. It was concluded that the formation of 2,2-dimethylbutane was due to the hydrogenation of I by residual hydrogen from the reduction stage of the pretreatment. Calculations indicated that the hydrogen involved in the hydrogenation was less than 1% of that used in the reduction.

At all temperatures studied first order plots were obtained for the disappearance of I in which an initial

Figure 6.1. Reaction Profile for 3,3-dimethylbut-1-ene Isomerisation over RuNaY20 at 385 K

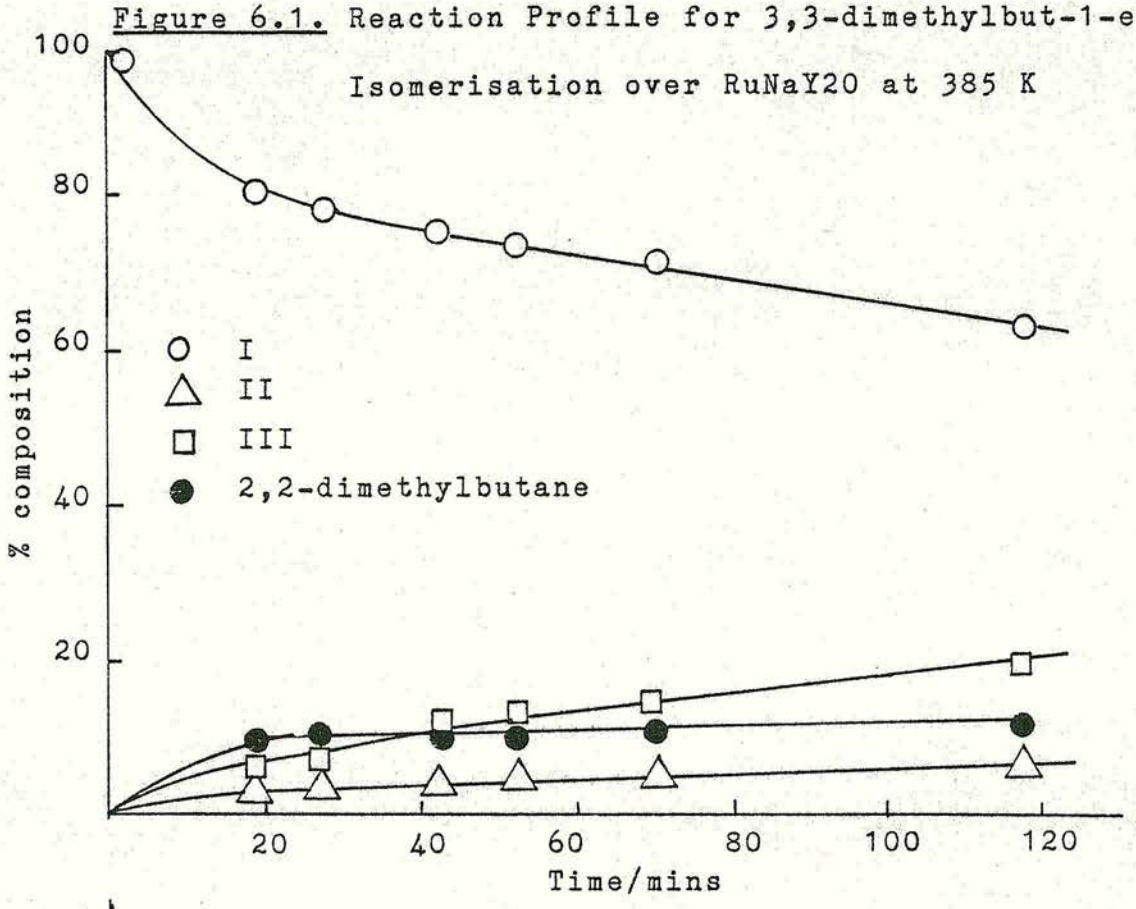

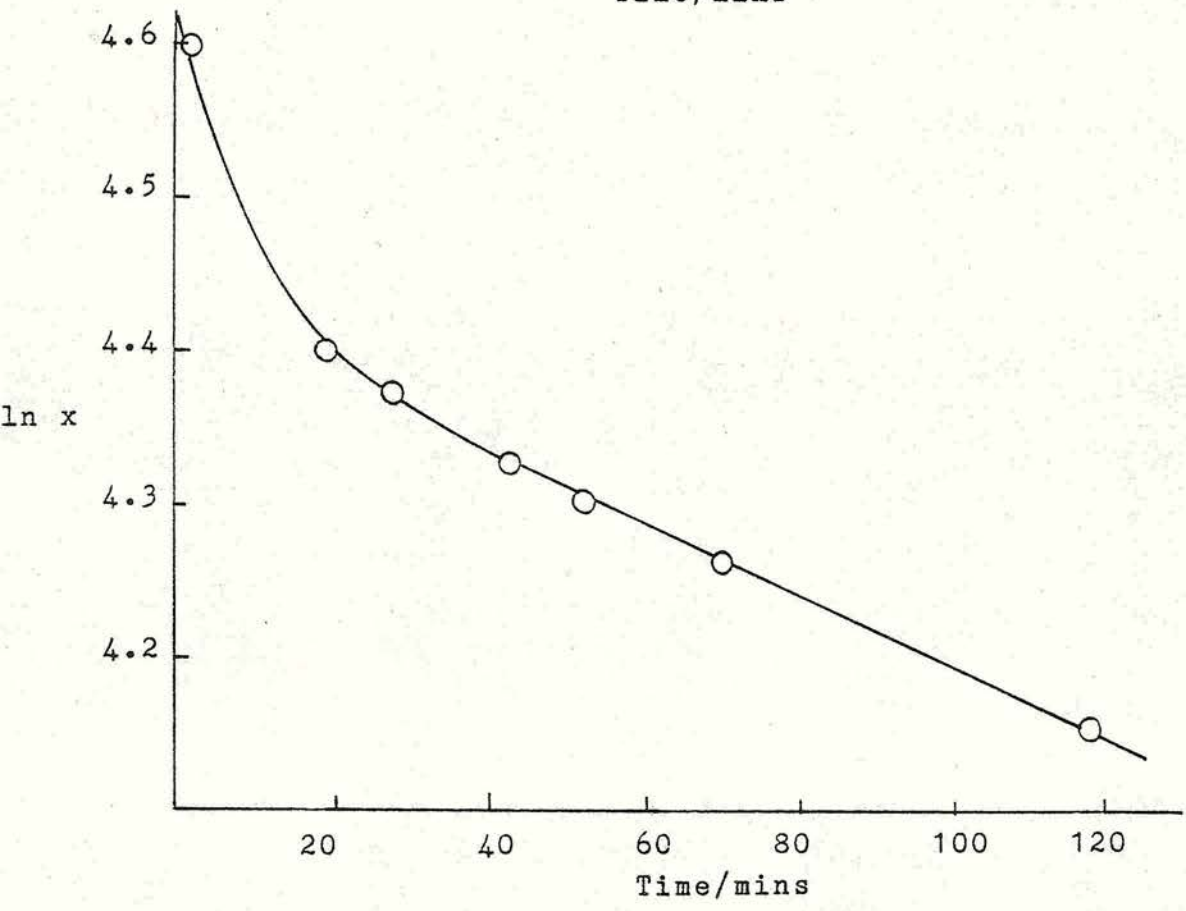

Figure 6.2. Derived First Order Plot

fast rate and a slower steady rate were apparent as illustrated in Figure 6.2. The first order rate constant was derived from the linear portion of the plot. Calculation of the rate constant for hydrogenation (k_h) during this period enabled the rate constant for isomerisation (k_i) to be found. The results for the isomerisation and hydrogenation of I are presented as Arrhenius plots in Figure 6.3. Table 6.1 lists the rate constants and derived Arrhenius parameters.

Temp. /K	Isomerisation			Hydrogenation		
	k_i* /10^{16}	Ea kJ mol^{-1}	ln A	k_h* /10^{16}	Ea kJ mol^{-1}	ln A
272	0.74	73	68.77	0.11	63	62.71
279	1.49			0.22		
285	3.64			0.34		
295	7.12			1.07		
303	21.74			0.81		

Table 6.1. Rate Constants and Arrhenius Parameters for Isomerisation and Hydrogenation of I

* Rate constant units: molecules s^{-1} g^{-1}

Following the initial reaction the catalyst samples were evacuated and slowly heated to 573 K over a period of 90 minutes. After outgassing overnight repeat reactions (Run 2) were performed on the reactivated catalyst at the same temperature as the initial reaction (Run 1). After the reactivation process the catalyst

Figure 6.3. Arrhenius Plot for 3,3-dimethylbut-1-ene Isomerisation and Hydrogenation over RuNaY20

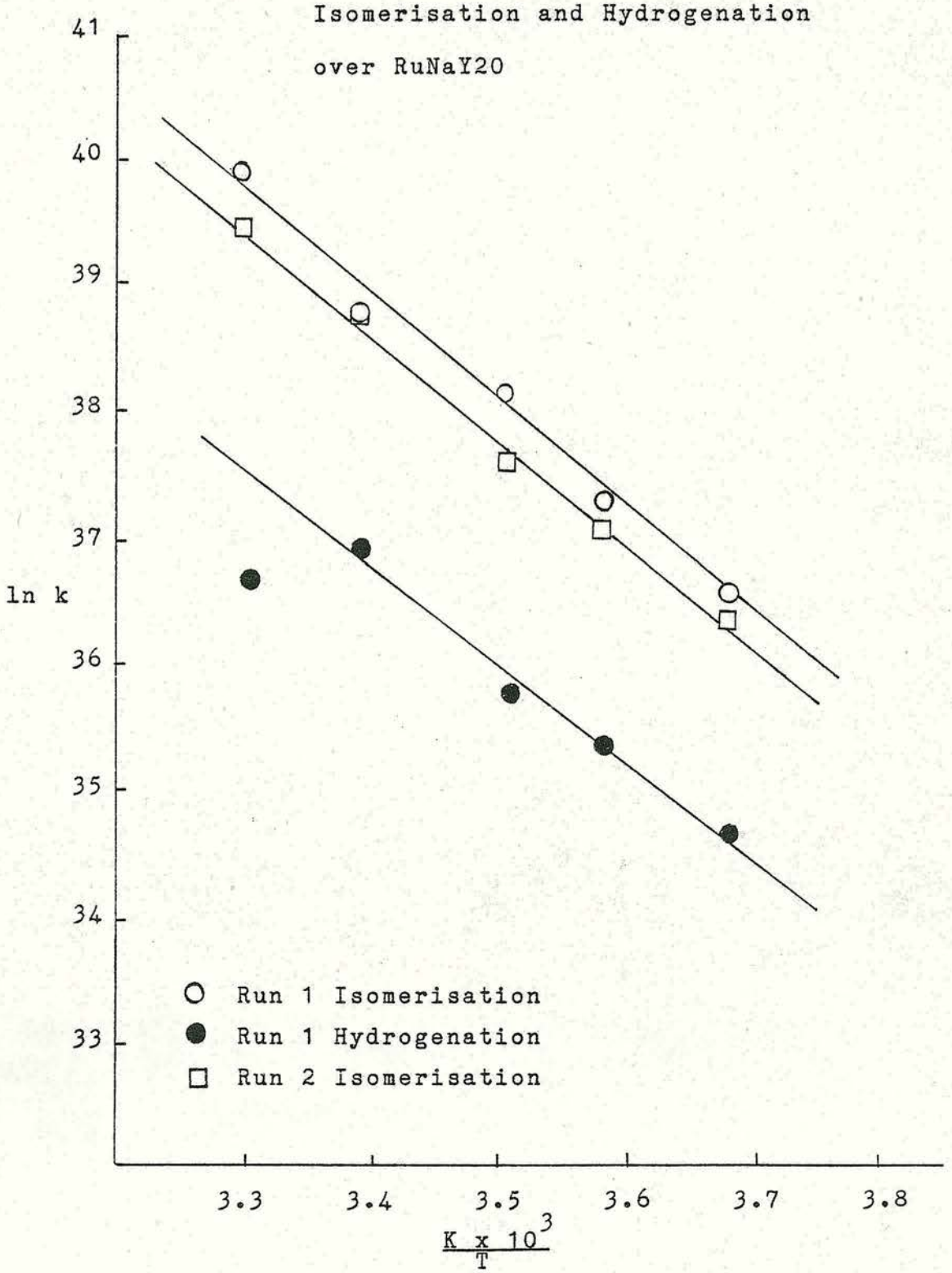

samples were found to have darkened in colour - possibly due to carbon laydown on the catalyst surface.

A typical reaction profile for the reactivated catalyst is shown in Figure 6.4. Traces of but-1-ene were formed at all temperatures studied. The absence of 2,2-dimethylbutane in the reaction products confirmed that its formation was due to the hydrogenation of I by residual hydrogen from the reduction stage of the initial pretreatment.

At all temperatures studied in the repeat reactions first order plots were obtained for the disappearance of I. At the lower temperatures of 272 K and 279 K there was an initial slow rate over the first 10-20 minutes before a faster steady rate was achieved. At temperatures of 285 K and above an initial fast rate (lasting 10-20 minutes) followed by a slower steady rate were observed. The first order rate constants (k_2) were derived from the linear portions of the graphs. The results for the isomerisation of I are presented as an Arrhenius plot in Figure 6.3. Table 6.2 lists the derived first order rate constants and the Arrhenius parameters. The apparent activation energy for the Run 2 reaction was similar to that observed for the initial reaction.

Table 6.2 demonstrates that for each catalyst sample studied the first order rate constant for the repeat reaction (k_2) was reduced with respect to the first order rate constant for the initial reaction (k_i). The ratio k_2/k_i is less than unity for each temperature

Figure 6.4. Run 2 Isomerisation of 3,3-dimethylbut-1-ene over RuNaY20 at 385 K

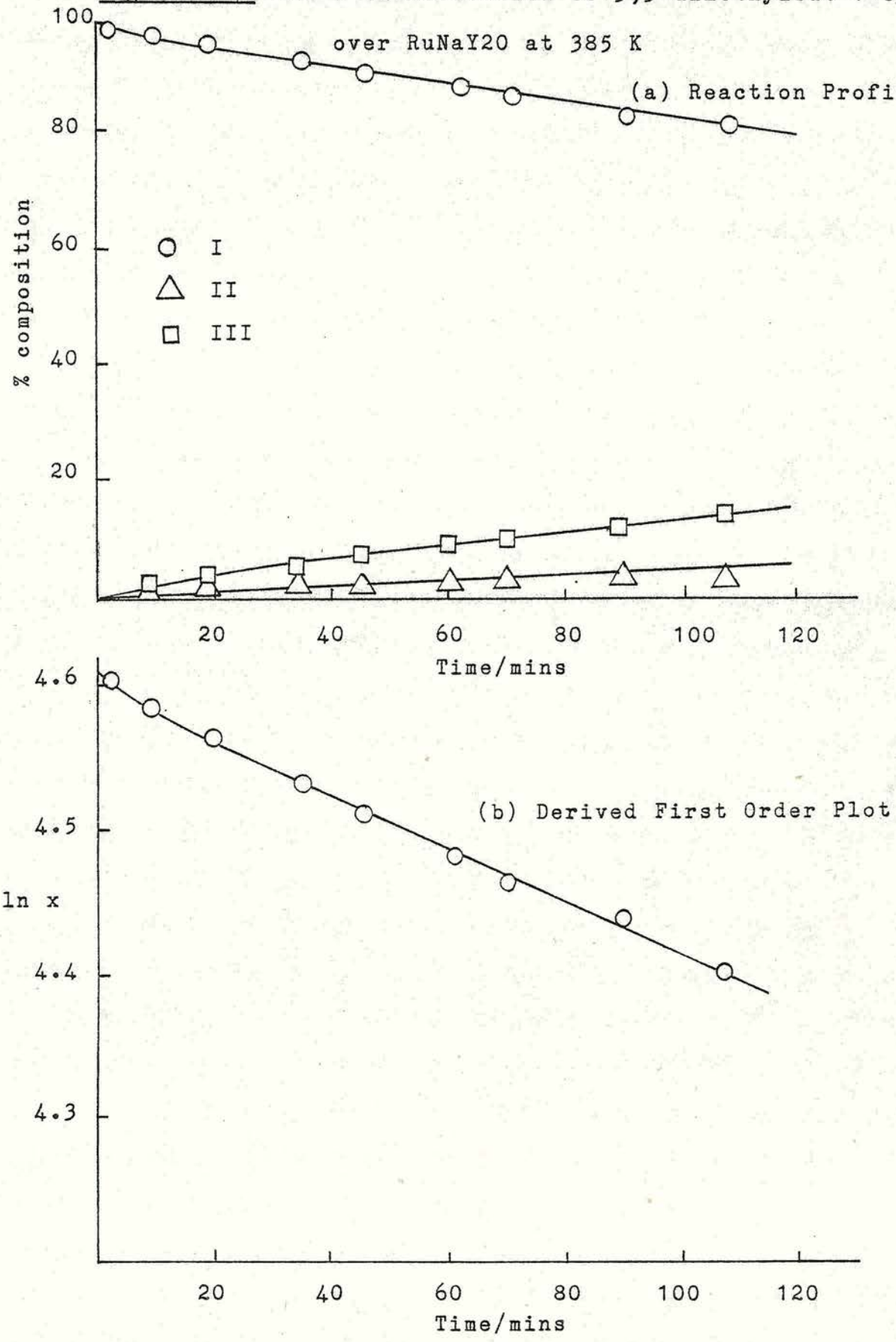

studied and demonstrates that the catalyst was deactivated after the initial reaction.

Temp. /K	$k_2/10^{16}$ molecules s^{-1} g^{-1}	Ea kJ mol^{-1}	ln A	k_2/k_i
272	0.62	69	67.10	0.84
279	1.23			0.85
285	2.06			0.56
295	7.08			0.99
303	13.79			0.63

Table 6.2. Rate Constants and Arrhenius Parameters for Run 2 Isomerisation of I over RuNaY20

Several repeat reactions were carried out on one catalyst sample and it was found that with each repeat reaction the rate constant was further reduced and the catalyst colour became progressively black due probably to carbon laydown on the catalyst surface.

Mass balance calculations during the course of the reaction indicated that carbon was lost to the surface of the catalyst during the course of the reaction. Table 6.3 lists the percent sample loss, from the gas phase, for the reactions studied. The expected sample loss due to sampling was c.a. 1% per sample. In all cases, as indicated by Table 6.3, there appears to be significant carbon loss to the catalyst surface: the amount increasing with increasing reaction temperature.

Temperature/K	Percent per sample	
	Run 1	Run 2
272	2.8	2.8
279	2.9	2.6
285	4.3	3.6
295	3.5	3.4
303	5.8	5.3

Table 6.3. Percent Sample Loss During Run 1 and Run 2

Product Selectivity

The isomerisation of I over RuNaY20 gave both 2,3-dimethylbut-1-ene (II) and 2,3-dimethylbut-2-ene (III) as products with III predominating. The product ratio III/II was found to vary throughout the course of the reaction as illustrated in Figure 6.5 for the reactions at 279 and 303 K. The product ratio was found to initially increase and then decrease. The decrease in the product ratio did not coincide with the period of linear first order activity. The first order rate constants were found to be reproducible but significant variations were observed in the product ratios.

A comparison of the experimental product ratio (a value taken from the start of the linear portion of the first order plot) with the thermodynamic equilibrium value extrapolated from the data of Kilpatrick et al[117], at all temperatures studied, is given in Table 6.4. In all cases the experimental value was lower than the thermodynamic equilibrium value possibly suggesting a

Figure 6.5. Variation in III/II Product Ratio with Extent of Isomerisation of I over RuNaY20

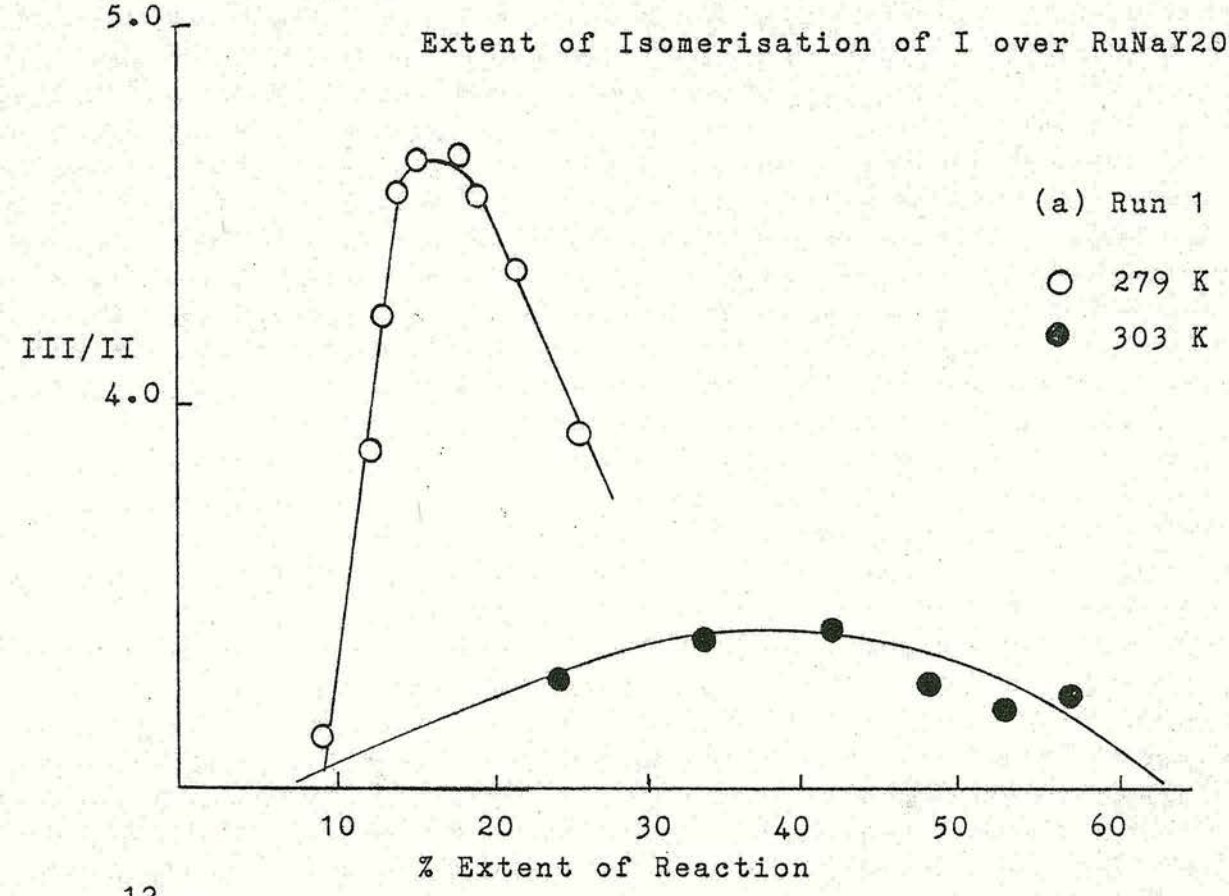

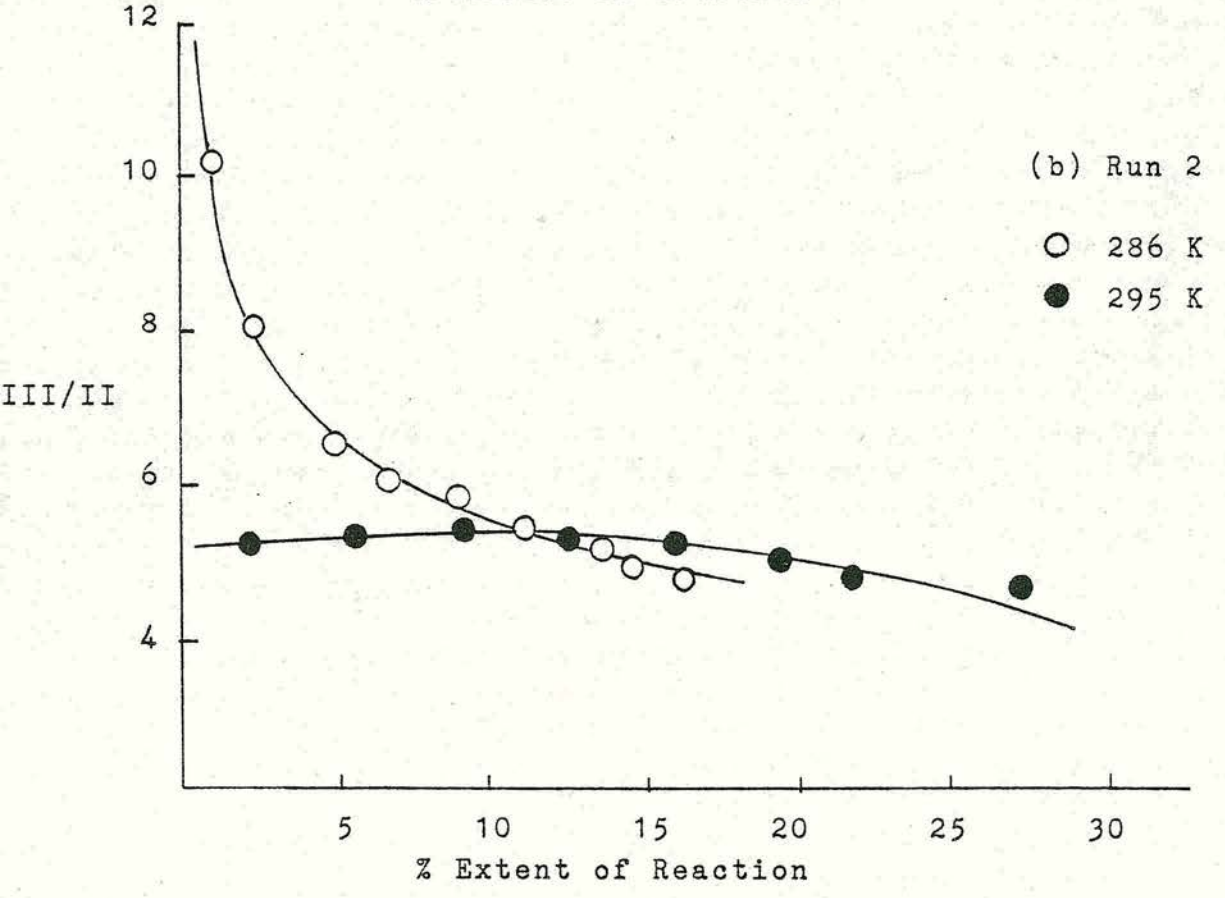

slight preference for the II isomer. No trend in the product ratio with increasing reaction temperature was apparent.

Temperature K	Experimental Product Ratio III/II		Thermodynamic Product Ratio [117]
	Run 1	Run 2	
272	2.72	Only III	5.88
279	4.24	only III	5.50
285	3.65	6.61	5.19
295	4.44	5.26	4.73
303	3.27	4.52	4.46

Table 6.4. Comparison of Experimental Product Ratios for Run 1 and Run 2 with the Thermodynamic Equilibrium Ratio[117]

The product ratio graphs for the Run 2 reactions differ from those of the Run 1 reactions. For the Run 2 reactions at 285 K and 295 K (as illustrated in Figure 6.5) the product ratio graphs decrease substantially from the start of the reaction while the product ratio graphs for the reactions at higher temperatures decrease very slightly throughout the course of the reaction. The estimated product ratios (taken from the start of the linear portion of the first order plot) given in Table 6.4, appear to decrease with increasing reaction temperature and at the higher reaction temperatures are

similar to the thermodynamic equilibrium values.

Effect of Ammonia on the Catalytic Activity of RuNaY20

The method employed for the adsorption of ammonia on RuNaY20 was as follows:- after the initial pretreatment the sample was cooled to liquid nitrogen temperature. The catalyst sample was exposed to a small pressure of ammonia for five minutes. After warming to the reaction temperature of 285 K the sample was evacuated for five minutes. Knowledge of the pressure of ammonia adsorbed enabled the maximum number of ammonia molecules to be established. The isomerisation of I was subsequently monitored.

The effect of ammonia on the rate of isomerisation and hydrogenation of I over RuNaY20 is shown in Table 6.5 and Figure 6.6 and indicates that the presence of ammonia reduced the rate constants for both isomerisation and hydrogenation. Extrapolation of the profile for hydrogenation suggests that a maximum of c.a. 1.5×10^{20} molecules of ammonia per gram of zeolite would poison the hydrogenation of I over RuNaY20.

The III/II product ratios on the poisoned catalyst were found to vary with extent of reaction - increasing slightly and then decreasing throughout the remaining reaction. The product ratios quoted in Table 6.5 are taken from the start of the linear portion of the first order plot.

Run 2 reactions indicated that part of the activity of RuNaY20 was lost by adsorption of ammonia. The

Maximum Number of Adsorbed NH_3 $/10^{20}$ gram^{-1}	k_h* $/10^{15}$	k_i* $/10^{16}$	III/II	k_2* $/10^{16}$
0	3.45	3.64	3.65	2.06
0.11	0.50	1.68	4.37	1.74
0.34	0.09	2.22	3.89	1.71
0.90	0.31	1.73	4.92	1.79
1.47	0.02	2.17	5.00	1.72

Table 6.5. The Effect of Adsorbed Ammonia on the Isomerisation and Hydrogenation of I

* Rate constant units: molecules s^{-1} g^{-1}

Maximum Number of Adsorbed H_2O $/10^{20}$ gram^{-1}	k_h* $/10^{15}$	k_i* $/10^{16}$	III/II	k_2* $/10^{16}$
0	3.45	3.64	3.65	2.06
0.35	0.42	2.67	3.71	1.61
2.20	0.89	2.74	2.82	-
4.13	0.19	1.76	2.98	2.02

Table 6.6. The Effect of Adsorbed Water on the Isomerisation and Hyrogenation of I

* Rate constant units: molecules s^{-1} g^{-1}

Figure 6.6. Effect of Adsorbed NH_3 on the Isomerisation of 3,3-Dimethylbut-1-ene over RuNaY20

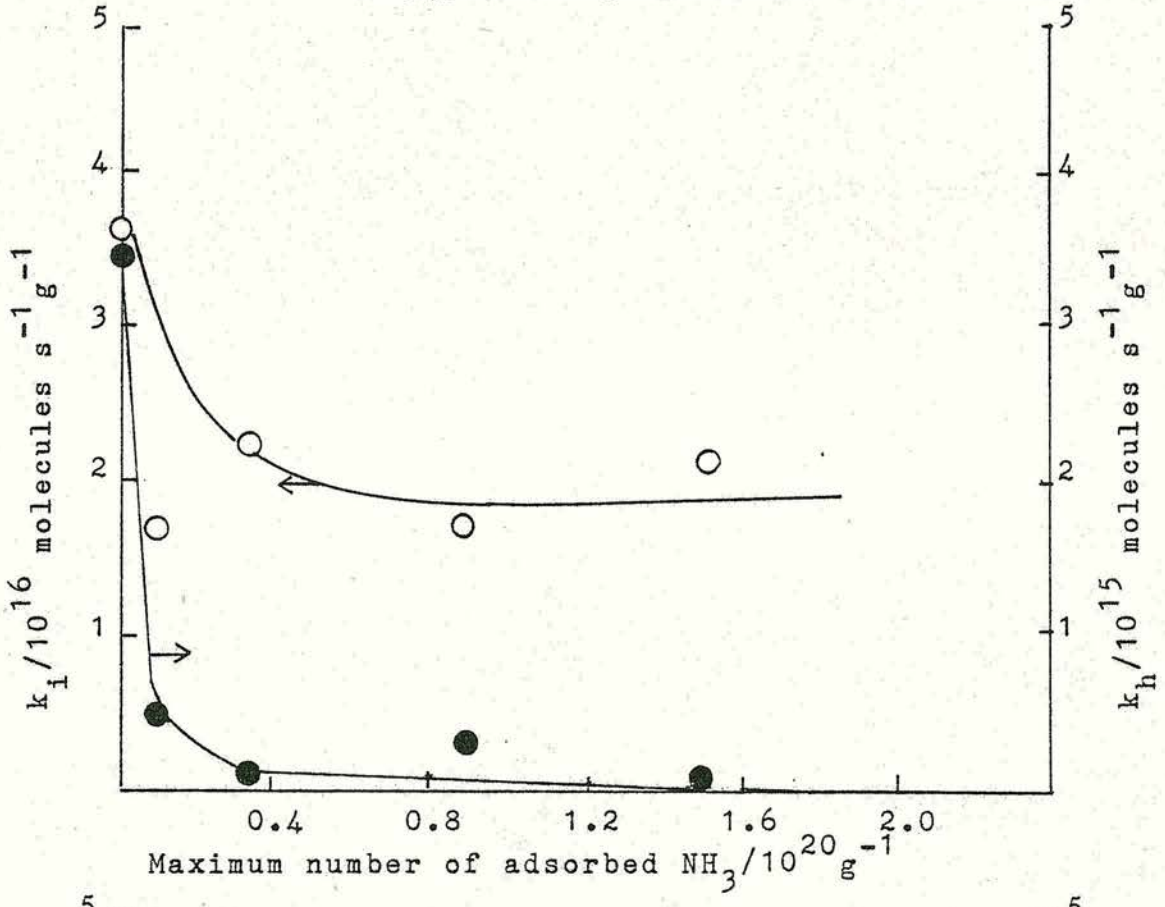

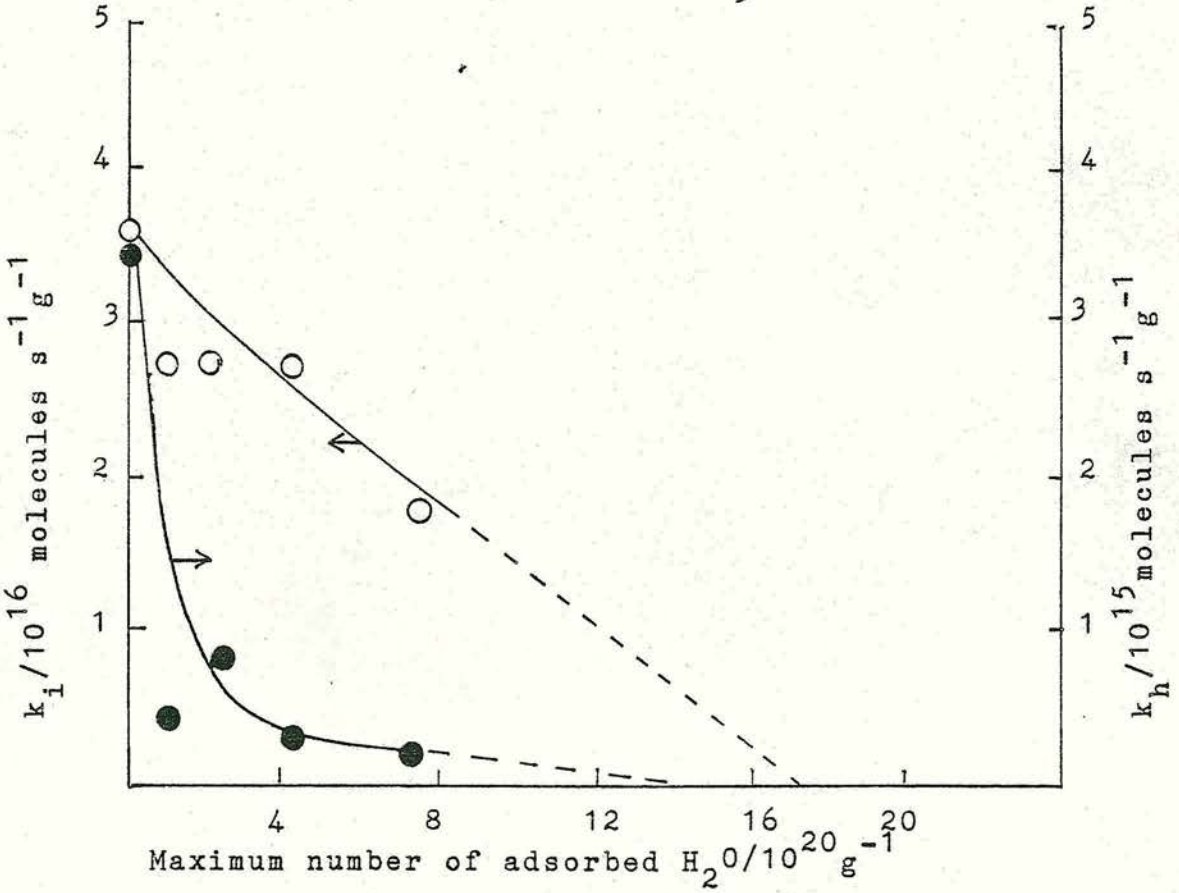

Figure 6.7. Effect of Adsorbed H_2O on the Isomerisation of 3,3-Dimethylbut-1-ene over RuNaY20

results given in Table 6.5 indicate that the Run 2 reactions carried out after ammonia poisoning and subsequent evacuation at 573 K gave similar first order rate constants which were all lower than that obtained with no prior contact with ammonia.

Effect of Water on the Catalytic Activity of RuNaY20

The experimental method of water adsorption was the same as the method described previously for the adsorption of ammonia. The adsorption and reaction temperatures were 77 K and 285 K respectively. The effects of water on the observed rate constants for isomerisation and hydrogenation are given in Table 6.6.

The activity profile given in Figure 6.7 suggests that the sites on which water was adsorbed were also responsible for the hydrogenation and isomerisation of I. Extrapolation of the profiles suggests that c.a. 14×10^{20} and c.a. 17×10^{20} molecules of water per gram of zeolite would totally poison RuNaY20 for the hydrogenation and isomerisation of I respectively.

The product ratio III/II was found to vary in the same manner as that obtained without prior adsorption of water. The product ratio given in Table 6.6 was obtained at the start of the period of linear first order activity.

Run 2 results obtained after overnight evacuation at 573 K and listed in Table 6.6 suggest that the prior adsorption of water resulted in some loss of activity.

Discussion

A pronounced enhancement in catalytic activity for the isomerisation of 3,3-dimethylbut-1-ene (I) was found to occur upon incorporation of ruthenium into the NaY lattice. Isomerisation of I occurs at high temperature (e.g. 474 K) over NaY zeolite[147] while on RuNaY20 isomerisation occurs at 272 K.

The skeletal isomerisation of I to 2,3-dimethylbut-1-ene (II) and 2,3-dimethylbut-2-ene (III) has been shown to proceed via a carbonium ion mechanism[77,94] according to the scheme illustrated in Figure 2.5. The initial formation of a secondary carbonium ion is followed by rearrangement to the more stable tertiary ion. The subsequent loss of H^+ from this species results in the formation of II and III. On catalysts such as magnesium oxide which do not readily form carbonium ions the isomerisation of I is likely to occur only with great difficulty[97]. The results presented in the previous sections indicate that the isomerisation of I over RuNaY20 proceeds via a carbonium ion mechanism.

Haag and Pines[77,94] observed the formation of methylpentenes and n-hexenes in their study of the isomerisation of I over alumina, however, a temperature of 623 K was employed. Evidence for the formation of methylpentenes at temperatures greater than 348 K was also found by Hoser and Krzyzanowski[91] in a study of cobalt exchanged zeolite X. In the present work the isomerisation of I was limited to the products II and

III. The formation of methylpentenes and n-hexenes may require a higher reaction temperature or more strongly acid sites.

In addition to the isomerisation products 2,2-dimethylbutane was also formed. The formation of 2,2-dimethylbutane can be attributed to the presence of chemisorbed hydrogen from the reduction stage of the pretreatment. The temperature programmed reduction results discussed in Chapter 4 show ruthenium to have two distinct types of hydrogen chemisorption: a strong activated chemisorption and a weak non-activated chemisorption. This strongly chemisorbed hydrogen is possibly dissolved in the subsurface layers of the ruthenium crystallites and requires high temperatures for removal. The isomerisation results suggest that all the strongly chemisorbed hydrogen is removed during the Run 1 reaction as subsequent reactions produced no 2,2-dimethylbutane.

A feature of the isomerisation of I over RuNaY20 was the manner in which the product ratio III/II varied during the course of the reaction. Previous studies on CoX[91] and CuX[98,99] found the product ratio to remain effectively constant during the course of the reaction. The resulting product ratio obtained over RuNaY20 was lower than the thermodynamic equilibrium value[117] suggesting a slight preference for the II isomer.

Rollman and Walsh[148] have shown that coking tendency is a function of zeolite pore structure with coke yield increasing with increasing pore size. Rate of

sample loss calculations indicate that during the isomerisation of I over RuNaY20 carbon is lost to the surface of the catalyst and that the rate of loss increases with increasing reaction temperature. It is possible that the loss of carbon to the catalyst surface causes a change in the product selectivity resulting in the observed variation in product ratio.

Ammonia is a hard base which is small in size. Adsorption of ammonia leads to a variety of chemically distinct species which can be identified by infra-red spectroscopy[36]. Adsorption on Bronsted acid sites gives rise to ammonium ions with a characteristic infra-red absorption frequency of 1475 cm^{-1}. Adsorption of ammonia on Lewis acid sites, i.e. tricoordinated aluminium ions, occurs via a coordinate bond giving an absorption frequency of 1630 cm^{-1}. In addition, complex formation with the exchangeable cations can occur resulting in an absorption frequency which varies with cation.

The results of ammonia adsorption on RuNaY20 indicate that both the isomerisation and hydrogenation of I are poisoned. It is not, however, possible from the available data to identify the sites responsible for ammonia adsorption.

The addition of small amounts of water has been shown to enhance the activity of zeolites for carbonium ion type reactions[149]. The increased activity has been ascribed to the interaction of water with the cation to produce species such as $M^{n+}OH_2$ or $M^{n+}OH$ which can act as protonic centres.

Cross et al[89] found that the addition of small amounts of water in the isomerisation of but-1-ene over nickel exchanged X zeolite caused a poisoning effect and concluded that the reaction did not occur via a carbonium ion mechanism.

The effect of adsorbed water on the isomerisation of I over copper exchanged X zeolite was to lower the rate[98]. This observed poisoning effect was explained by the authors in terms of the preferential formation of a copper aquo complex.

The adsorption of small amounts of water on RuNaY20 resulted in the poisoning of both the isomerisation and hydrogenation of I. Consideration of the maximum number of adsorbed molecules necessary for total poisoning of the hydrogenation reaction gives values of c.a. 1.5×10^{20} and c.a. 14×10^{20} molecules for adsorbed ammonia and water respectively. This suggests that different sites were involved in the poisoning reactions.

6.1.2. RuNaLaY20 and RuLaY20

The isomerisation of I over RuNaLaY20 and RuLaY20 was studied in the temperature ranges 250-312 K and 250-285 K respectively. A typical reaction plot showing the preferential formation of II is illustrated in Figure 6.8 for RuNaLaY20.

2,2-dimethylbutane (<5%) was formed at all temperatures studied over both zeolites. Traces of but-1-ene were formed at all temperatures studied over RuNaLaY20 and at temperatures greater thean 272 K over

Figure 6.8. Reaction Profile for 3,3-Dimethylbut-1-ene Isomerisation over RuNaLaY20 at 312 K

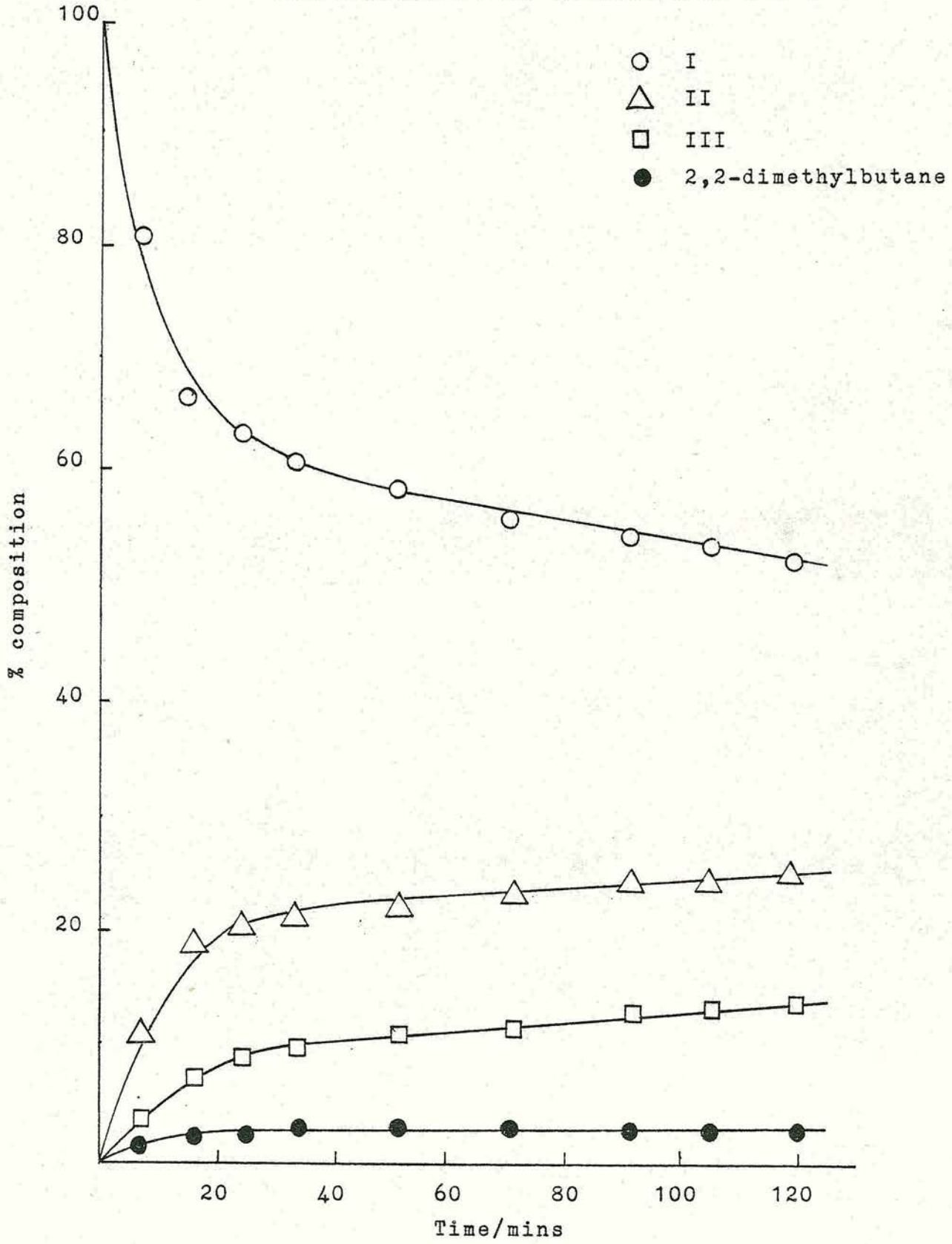

RuLaY20. In addition to the aforementioned products traces of two additional products were formed over both zeolites. With increasing temperatures the percent of all products formed increased with the exception of 2,2-dimethylbutane. Repeat reactions on the same catalyst sample showed an absence of 2,2-dimethylbutane suggesting as in the case of RuNaY20 that it was formed by the hydrogenation of I by residual hydrogen from the reduction stage of the pretreatment procedure. Calculations indicated that the hydrogen involved in the hydrogenation was less than 0.5% of that used in the reduction stage.

Figure 6.8 indicates an initial fast rate of formation followed by a much slower rate of formation for all products over RuNaLaY20. Similar profiles were obtained for RuLaY20. Ballivet et al[83] have reported the deactivation of silica-alumina in the presence of cis but-2-ene and have assigned the initial rapid deactivation (slope c_1) to the presence of Lewis acidity (exposed aluminium ions) and the slower deactivation slope (slope c_2) to Bronsted acidity. The data for the isomerisation of I over RuNaLaY20 and RuLaY20 have been treated in a similar manner to give c_1 and c_2 values for each catalytic reaction.

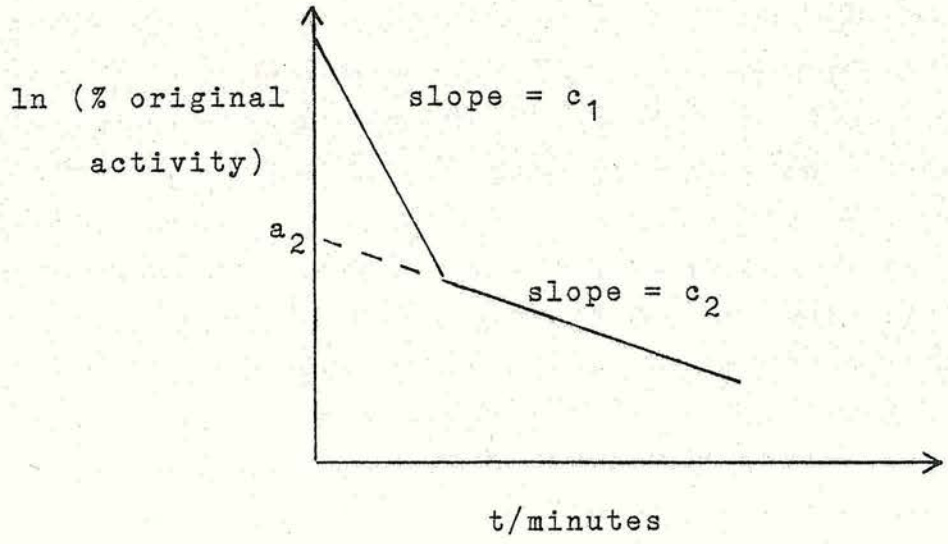

The c_1 and c_2 values obtained together with the extrapolated a_2 are given in Table 6.7 The value of the exponential (a_2) gives the limiting value for the factor causing deactivation characterised by the slope c_2 for a non-deactivated catalyst. The percent original activity was taken as the percent of I remaining at time t. Typical logarithmic plots are illustrated in Figure 6.9 for both zeolites.

The data from Table 6.7 can be used to construct an Arrhenius plot for each catalyst as shown in Figures 6.10 and 6.11 for RuNaLaY20 and RuLaY20 respectively. The values of the apparent activation energies for the isomerisation of I were calculated from the slopes of Figures 6.10 and 6.11 according to the Arrhenius equation (Equation 3.3) and are given in Table 6.8.

At the end of the first isomerisation reaction each catalyst was evacuated and slowly heated to 573 K over a period of 90 minutes. After overnight evacuation I was readmitted to the reaction vessel containing the catalyst at the original reaction temperature. The subsequent

Catalyst	Temperature /K	c_1* /10^{17}	c_2* /10^{16}	a_2 %
RuNaLaY20	250	1.63	0.19	92.04
	273	2.47	0.96	84.06
	274	2.41	0.90	82.98
	287	3.48	1.47	79.04
	312	3.60	2.89	65.59
RuLaY20	250	1.63	0.38	92.15
	272	3.28	0.91	83.20
	272	2.74	1.19	80.65
	284	4.04	1.53	77.56
	285	6.64	1.59	74.96

Table 6.7. c_1, c_2 and Exponential (a_2) Values for RuNaLaY20 and RuLaY20

* Rate constant units: molecules s^{-1} g^{-1}

Catalyst	c_1		c_2	
	Ea kJ mol^{-1}	ln A	Ea kJ mol^{-1}	ln A
RuNaLaY20	9	43.92	28	48.83
RuLaY20	14	45.87	27	48.32

Table 6.8. Apparent Activation Energies (Ea) for the Isomerisation of I over RuNaLaY20 and RuLaY20

Figure 6.9. First Order Plots for the Isomerisation of 3,3-Dimethylbut-1-ene over RuNaLaY20 and RuLaY20

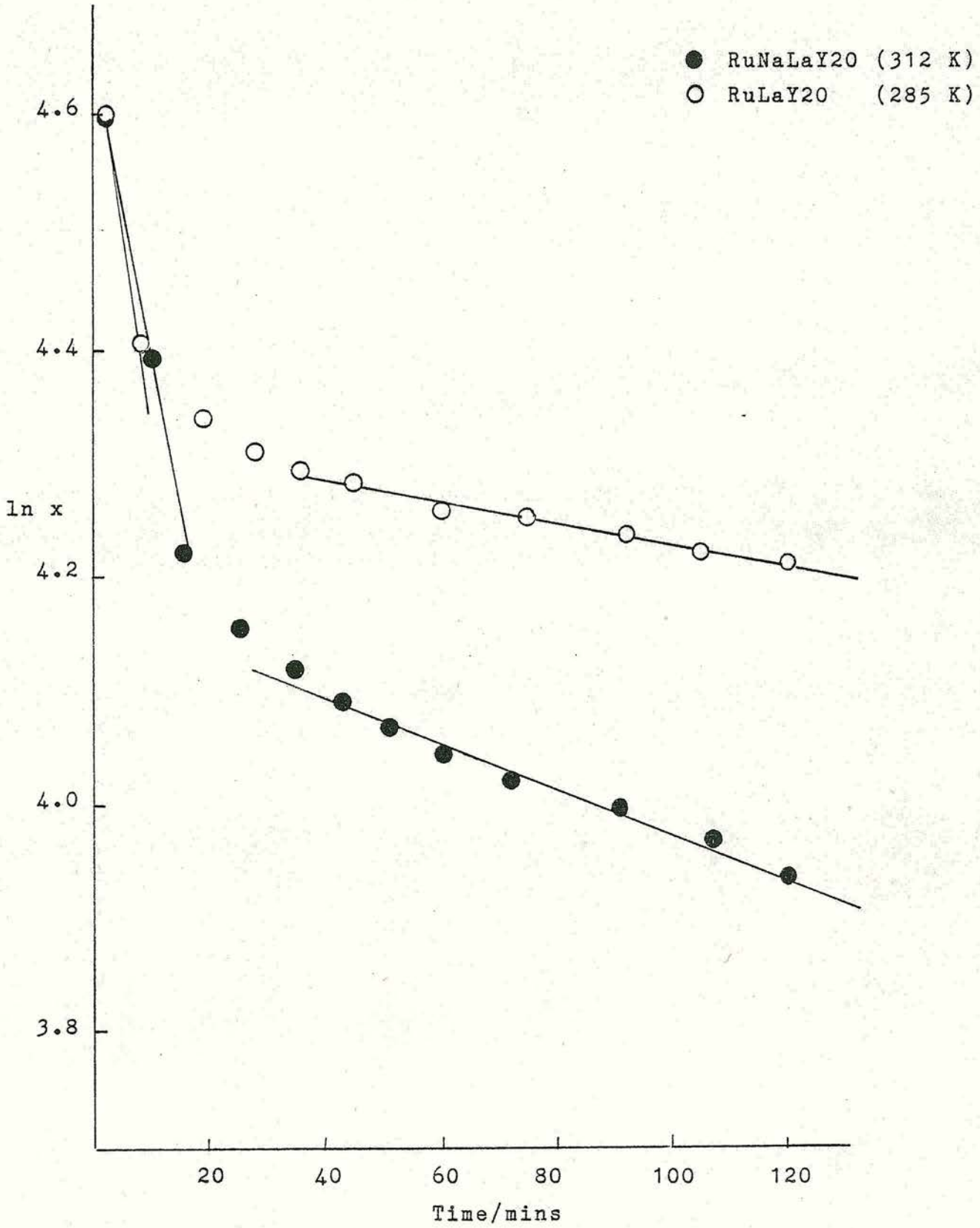

Figure 6.10. Arrhenius Plot for the Isomerisation of 3,3-Dimethylbut-1-ene over RuNaLaY20

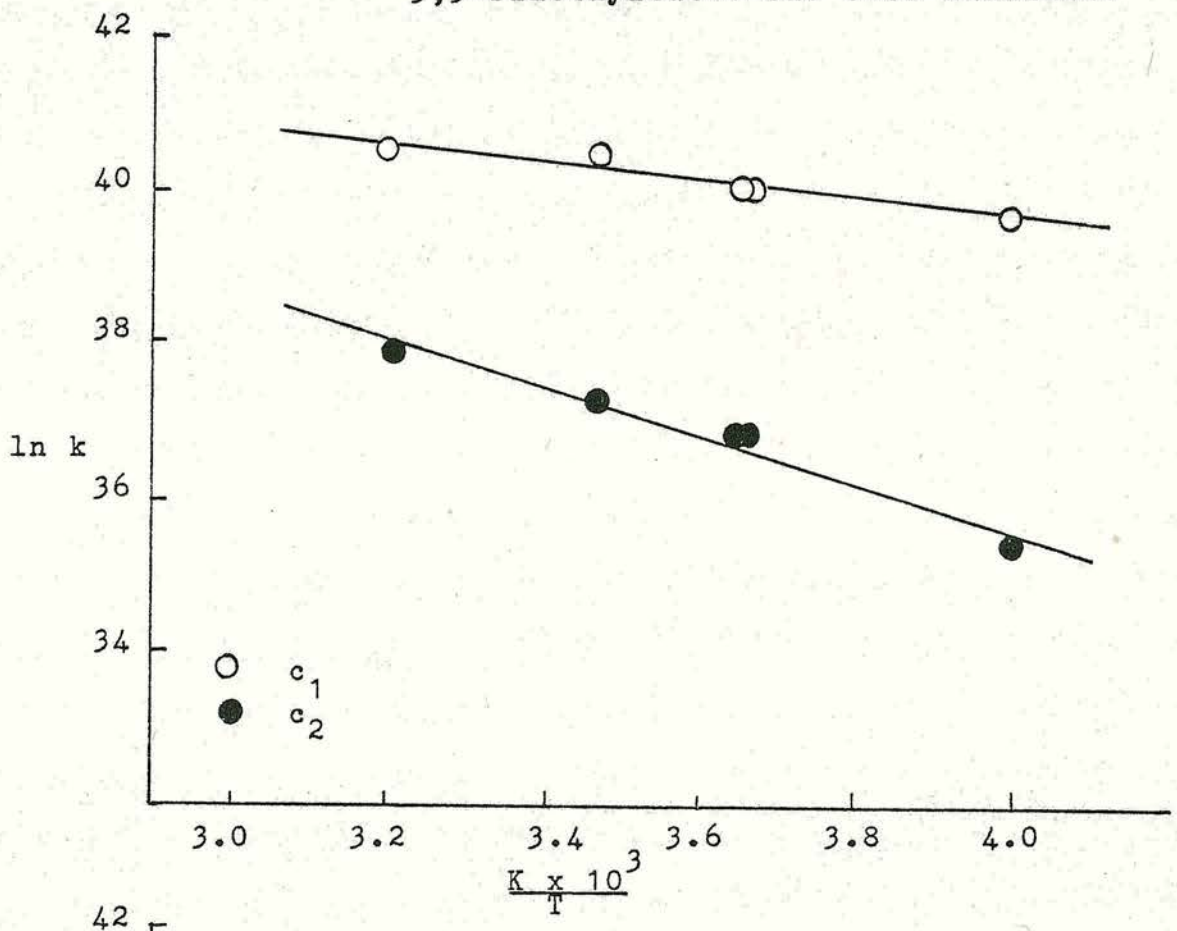

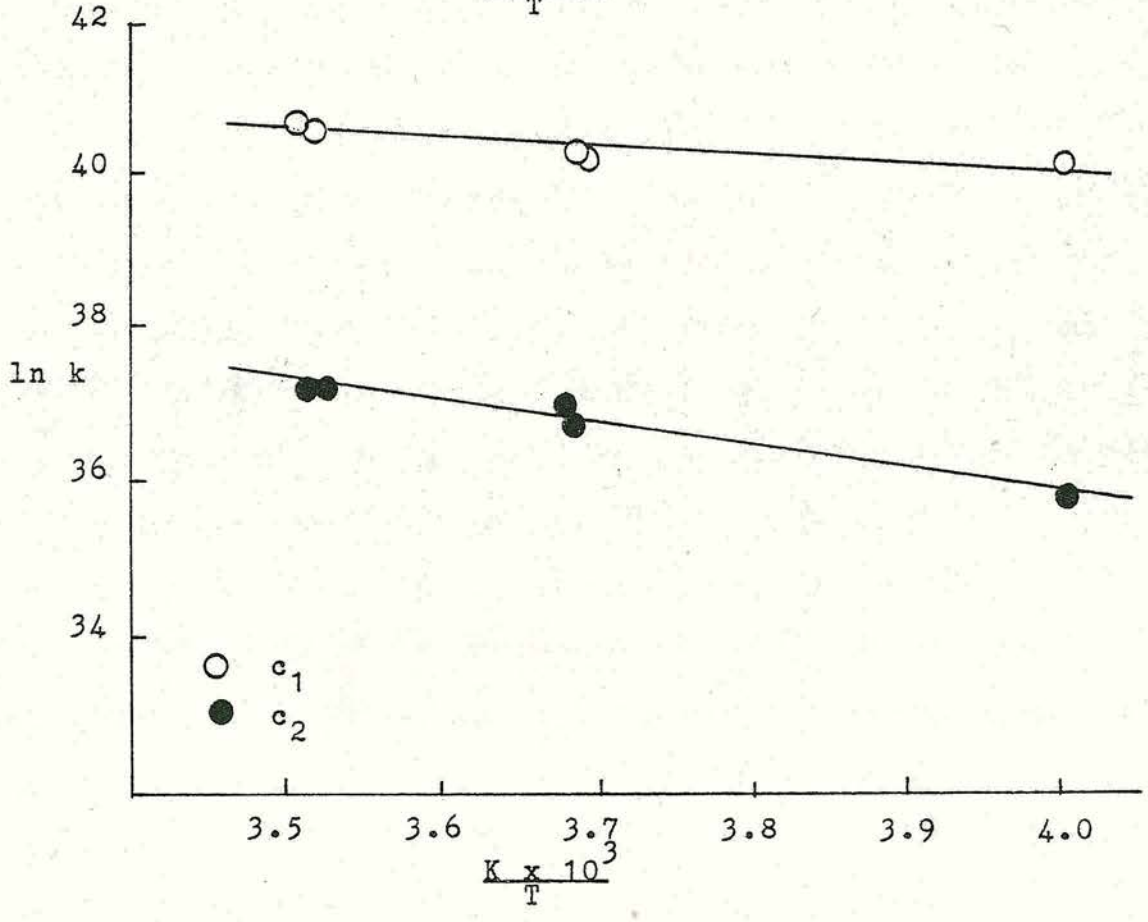

Figure 6.11. Arrhenius plot for the Isomerisation of 3,3-Dimethylbut-1-ene over RuLaY20

data recorded for this second reaction were treated in the same manner as those for Run 1. Table 6.9 demonstrates that the rate constants (c_1^2 and c_2^2) established for Run 2 were reduced with respect to the rate constants for Run 1. The ratio of the rate constants (c^2/c) is also shown (in Table 6.9) for each reaction temperature studied.

Table 6.9 demonstates that both catalysts were significantly deactivated after the reactivation process. During the reactivation process both catalyst samples were found to darken in colour possibly due to carbon laydown on the catalyst surface. 2,2-Dimethylbutane was not formed during the Run 2 reaction. Logarithmic plots similar to those obtained during Run 1 reactions were obtained during Run 2 for both catalysts. The Arrhenius plots for the Run 2 isomerisation of I gave apparent activation energy values (Table 6.10) that do not differ markedly from those given in Table 6.8 for the Run 1 conversion.

Mass balance calculations during the course of the isomerisation of I over RuNaLaY20 and RuLaY20 indicated that carbon was lost to the surface of the catalyst during the course of the reaction. Figure 6.12 indicates that at the beginning of the reaction (the period corresponding to c_1) more carbon was lost than would be expected due to sampling whereas during the period corresponding to c_2 the sampling loss was slightly greater than 1% per sample (the expected loss due to sampling) indicating that there was still some slight

Catalyst	Temp /K	c_1^2 /10^{17}*	c_1^2/c_1	c_2^2 /10^{16}*	c_2^2/c_2
RuNaLaY20	250	1.32	0.81	0.19	0.98
	273	1.78	0.72	0.87	0.91
	274	1.96	0.81	0.95	1.05
	312	4.73	1.31	2.63	0.91
RuLaY20	250	1.35	0.83	0.27	0.71
	272	2.07	0.63	0.90	0.99
	272	2.59	0.95	0.40	0.34
	284	2.71	0.68	1.00	0.65
	285	2.77	0.42	1.32	0.83

Table 6.9. Rate Constants for the Isomerisation of I over RuNaLaY20 and RuLaY20 (Run 2)

* Rate constant units: molecules s^{-1} g^{-1}

Catalyst	c_1		c_2	
	Ea kJ mol^{-1}	ln A	Ea kJ mol^{-1}	ln A
RuNaLaY20	14	45.87	27	48.32
RuLaY20	12	45.31	25	47.49

Table 6.10. Activation Energy Values (Ea) for the Isomerisation of I over RuNaLaY20 and RuLaY20 (Run 2)

Figure 6.12. Sample Loss Plot for the Isomerisation of 3,3-Dimethylbut-1-ene over RUNaLaY20 at 312 K

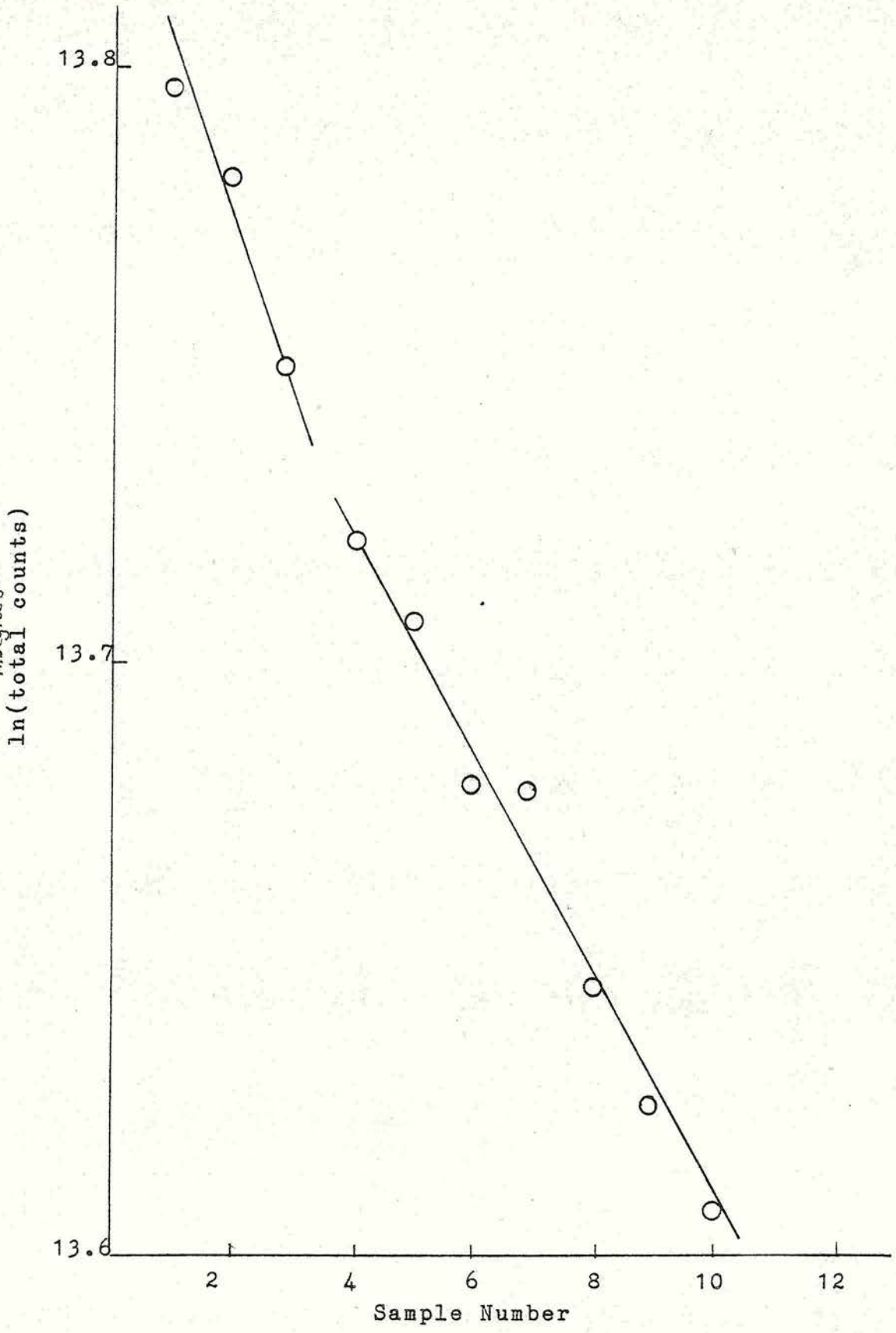

loss of carbon. Table 6.11 illustrates the percent sample loss initially (corresponding to c_1) and finally (corresponding to c_2).

Catalyst	Temperature/K	Percent per Sample	
		Initial	Final
RuNaLaY20	250	7.9	1.9
	273	5.2	1.7
	274	15.8	1.0
	287	15.1	1.0
	312	2.4	1.9
RuLaY20	250	5.0	1.2
	272	8.8	1.6
	272	5.3	1.5
	284	7.2	1.3
	285	8.5	1.8

Table 6.11. Percent Sample Loss During Run 1 Isomerisation of I over RuNaLaY20 and RuLaY20

The data in the above table show no apparent trend with reaction temperature. Similar data were obtained for the Run 2 reactions.

Product Selectivity

The isomerisation of I over RuNaLaY20 and RuLaY20 gave both 2,3-dimethylbut-1-ene (II) and 2,3-dimethylbut-2-ene (III) as products with II as the major product. All previous studies[77,94,96-100] on the

isomerisation of I have found III to be the major product.

The product ratio III/II was found to increase during the course of the reaction and was always less than unity. Comparison of the experimental product ratios with thermodynamic equilibrium values extrapolated from the data of Kilpatrick et al[117] show them to be markedly different. Initial samples from the reactions over RuLaY20 indicated the only isomerisation product to be II.

The major product formed during the Run 2 reaction was also found to be II. Similar increasing product ratio values were observed during the course of the reaction.

Effect of Acetone on the Catalytic Activity of RuNaLaY20 and RuLaY20

After the initial pretreatment the catalyst sample was cooled to liquid nitrogen temperature and exposed to a small pressure of acetone for 5 minutes. The sample was warmed to the reaction temperature of 285 K and evacuated for 5 minutes. The maximum number of acetone molecules adsorbed by the sample was established by pressure measurements. The isomerisation of I was subsequently monitored.

The data given in Table 6.12 indicate that the adsorption of acetone reduced the values of c_1 and c_2 over both RuNaLaY20 and RuLaY20.

Catalyst	Maximum Number of Adsorbed Acetone $/10^{20}$ gram^{-1}	c_1 $/10^{17}$*	c_2 $/10^{16}$*
RuNaLaY20	0	3.04	1.30
	1.50	2.26	0.58
	2.93	2.79	0.53
	4.55	1.37	0.60
	7.76	0.39	0.44
RuLaY20	0	6.64	1.59
	1.50	2.73	0.65
	2.47	2.85	0.53
	4.21	1.64	0.77
	7.98	0.18	0.53

Table 6.12. The Effect of Adsorbed Acetone on the Rate Constants c_1 and c_2 over RuNaLaY20 and RuLaY20

* Rate constant units: molecules s^{-1} g^{-1}

The activity profiles for RuNaLaY20 and RuLaY20 given in Figure 6.13 suggest that the active sites responsible for the isomerisation of I were also involved in the adsorption of acetone. The extrapolation of the c_1 profiles (see dotted line Figure 6.13) suggests that c.a. 8.6×10^{20} and c.a. 8.3×10^{20} molecules of acetone per gram of catalyst would completely poison c_1 for RuNaLaY20 and RuLaY20 respectively. The observed c_2 rate constants given in Table 6.12 indicate that the presence of acetone reduced the rates of isomerisation of I over

Figure 6.13. Effect of Adsorbed Acetone on the Isomerisation of 3,3-Dimethylbut-1-ene over RuNaLaY20 and RuLaY20

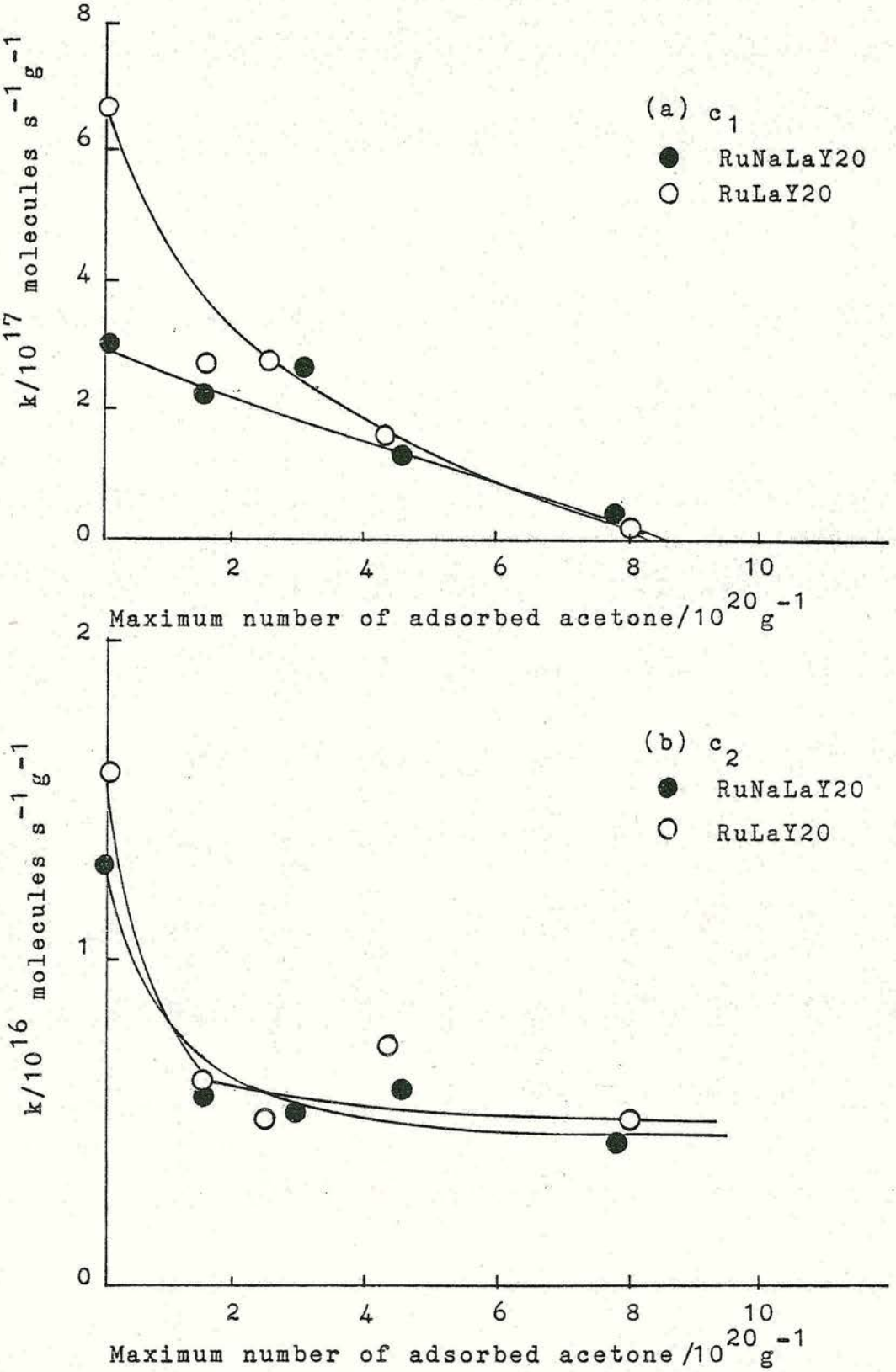

both catalysts to an approximately constant value. However, it is possible that acetone molecules did not adsorb on all the active sites present in both zeolites.

The major product observed in the isomerisation of I over the acetone poisoned samples was II. The product ratio III/II increased during the course of the reaction and all values observed were less than unity. 2,2-Dimethylbutane ($\leqslant$1%) was formed in all reactions studied. Mass balance calculations indicated that acetone poisoning did not prevent a loss of carbon to the catalyst surface during the period corresponding to c_1.

Run 2 reactions on the previously poisoned catalyst indicated that the activity of c_1 could be restored to the expected Run 2 activity (within experimental error) while the c_2 rate constants were reduced with respect to the expected c_2 values for Run 2.

Discussion

The isomerisation of I is a reaction which proceeds readily on a catalyst surface which can promote the formation of carbonium ions from the alkene. On catalysts such as magnesium oxide[97], which does not readily form carbonium ions the reaction is much more difficult. The isomerisation of I over RuNaLaY20 and RuLaY20 occurs at similar temperatures to the reaction over RuNaY20 which has already been shown to promote the formation of carbonium ions (Section 6.1.1). The data presented in this work demonstrate the ability of both RuNaLaY20 and RuLaY20 to display acidic-type catalytic

behaviour.

The results obtained over RuNaLaY20 and RuLaY20 differ from other observed results over zeolites[97-100] in that there was the apparent preferential formation of II rather than III. No methylpentenes were formed suggesting the sites were not strongly acidic.

The isomerisation of I over RuLaNaY20 and RuLaY20 is associated with a loss in activity at the beginning of each catalytic run. Similar deactivation phenomena have been observed over silica-alumina[83] (for cis-but-2-ene isomerisation) and hydrogen or dehydroxylated Y zeolite[87] (for n-butene isomerisation). These phenomena were attributed to the formation of a polymeric species on the catalyst surface. This active residue was formed on the surface of the catalyst during the first few minutes with which the reactant was contacted with the catalyst. At the same time the activity was decreased by a poisoning effect. The mass balance calculations discussed previously for RuNaLaY20 and RuLaY20 suggest a loss of carbon to the catalyst surface and it is possible that in the isomerisation of I over both zeolites there is the formation of a polymeric species which causes a poisoning effect during the first few minutes of reaction.

Alternatively, it may be that the loss of carbon to the catalyst surface may be the result of a preferential adsorption of one of the products. During the first few minutes of reaction 2,2-dimethylbutane is formed. The amount of 2,2-dimethylbutane present hardly increases during the course of the reaction. However,

2,2-dimethylbutane is not formed during the Run 2 reactions which also show the same loss of carbon to the catalyst surface. Thus, it seems unlikely that the adsorption of 2,2-dimethylbutane on the catalyst surface is responsible for the deactivation phenomenon. As in the case of RuNaY20 the formation of 2,2-dimethylbutane can be attributed to the presence of stongly chemisorbed hydrogen from the reduction stage of the pretreatment. The preferential adsorption of III on the catalyst surface could account for the loss of carbon and also account for the observed III/II product ratios differing from the thermodynamic equilibrium values of Kilpatrick et al[117]. Unfortunately due to the highly air sensitive nature of the ruthenium loaded zeolites and the pretreatment procedure involved, it was not possible to ascertain whether the carbon loss was due to the formation of a polymeric species or the preferential adsorption of III on the zeolite surface.

The skeletal isomerisation of I has been shown to proceed via carbonium ion intermediates over zeolites[97-100] according to the reaction scheme illustrated in Figure 2.5. II and III are formed as products. If this mechanism was operating over both RuNaLaY20 and RuLaY20 then it is possible that the energy barrier from the carbonium ion intermediate to the III isomer is higher than that to the II isomer leading to the preferential formation of II. If this was the case then a temperature dependent product ratio would be expected, but these were not observed.

Irvine et al[96] have postulated a carbonium ion mechanism which is Lewis acid induced giving II as the only product (Figure 6.14) The postulated mechanism involves adsorption of the alkene onto a Lewis acid site followed by two rearrangements and the release of the product II.

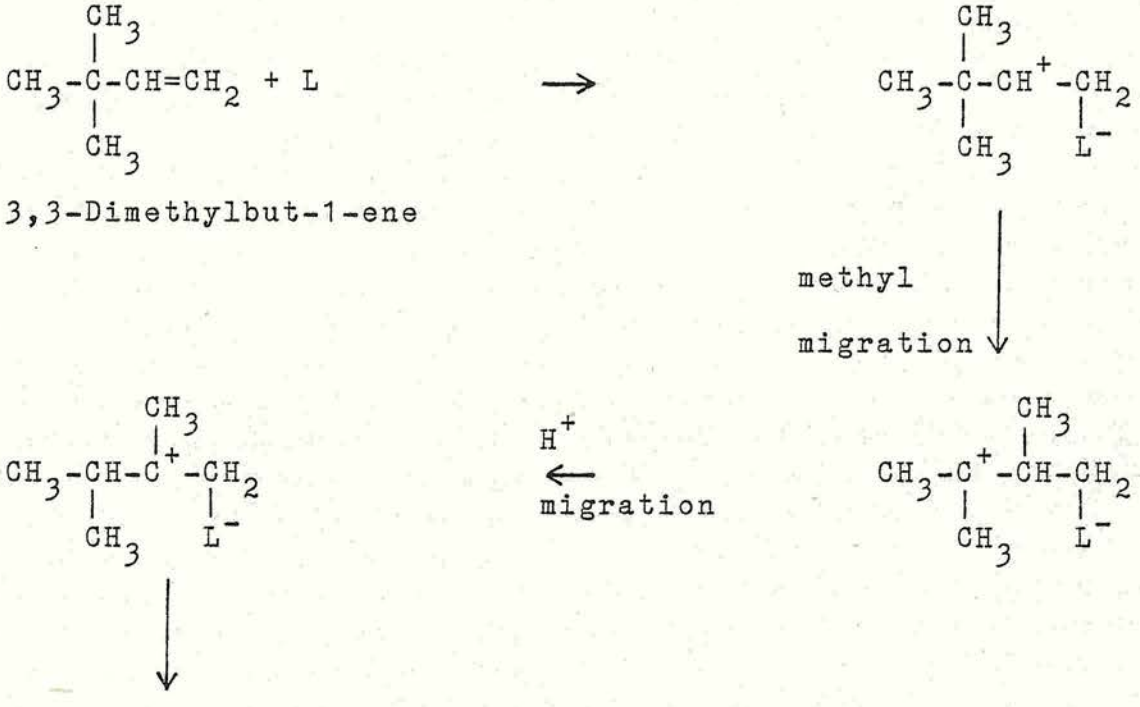

Figure 6.14. Lewis Acid Induced Carbonium Ion Mechanism[96]

Conversion of II to III would account for the formation of III. Experiments starting with II over RuNaLaY20 and RuLaY20 showed the reaction to be more facile than that of I with the reaction proceeding rapidly at 237 K. The major feature of the reaction was the conversion of II to III with no I being formed. The interconversion of II⇌III can be explained by a mechanism

involving radicals or carbanions[35]. Consideration of the observed product ratio III/II increasing to near unity during the course of the reaction over both RuNaLaY20 and RuLaY20 suggests that the amount of III is increasing relative to II and is possible evidence for the interconversion of II to III. The slower than expected rate of interconversion may be due to the adsorption of carbon polymer on the sites active for the interconversion.

Further support for a Lewis acid mechanism is obtained from the poisoning results. Ballivet et al[83] postulated that the activity characterised by c_1 was associated with Lewis acid sites while c_2 was characterised by Bronsted sites. Acetone is a soft base which is known to react with Lewis acid sites[150]. The results presented earlier indicate that an increase in the amount of acetone adsorbed leads to a decrease in the value obtained for c_1 while the value obtained for c_2 decreased reaching a constant value. This is evidence that c_1 is associated with Lewis acid sites but does not account for the slight poisoning of c_2.

The association of c_1 with Lewis acid sites leads to the conclusion that the isomerisation of I over both RuNaLaY20 and RuLaY20 is via a Lewis acid induced carbonium ion mechanism in which II is formed as the only isomerisation product. III is formed by interconversion of II, a facile reaction on both catalysts. The deactivation of the catalysts is due probably to the formation of a polymeric residue which also poisons the

sites responsible for the interconversion of II to III.

The differences between the reactions on RuNaY20 and RuNaLaY20 and RuLaY20 must be due to the presence of La^{3+} in the latter. Naccache and Ben Taarit[151] have reported that in order to have highly dispersed metal zeolites the location of the cations before reduction plays an important role. The mobility and the reducibility of cations in the sodalite cages or hexagonal prisms is low and these sites should be avoided when a highly dispersed metal catalyst is required. Na^{+} should be exchanged with unreducible cations such as La^{3+} which show a strong preference for S_1 and $S_{1'}$ sites then introduction of the active component (in this case ruthenium) which will then remain in the supercages. Both RuNaLaY20 and RuLaY20 were prepared in this manner.

6.1.3. Summary

The isomerisation of I was found to occur readily over the ruthenium containing zeolites RuNaY20, RuNaLaY20 and RuLaY20. Carbonium ion mechanisms were responsible for the isomerisation in each case.

The isomerisation of I over RuNaY20 occurred via the mechanism postulated by Haag and Pines[77] with II and III as the only isomerisation products. A Lewis acid induced mechanism[96] with II as the only isomerisation product is thought to be responsible for the isomerisation of I over both RuNaLaY20 and RuLaY20, with the formation of III occuring by the interconversion of II. The formation of a polymeric residue is postulated over RuNaLaY20 and RuLaY20.

2,2-Dimethylbutane was formed over all three ruthenium containing zeolites. The formation was due to the hydrogenation of I by hydrogen dissolved in the subsurface layers of the ruthenium crystallites.

6.2. Hydrogenolysis

Hydrogenolysis reactions involve the rupture of carbon-carbon bonds and the formation of carbon-hydrogen bonds. The nature of the hydrogenolysis process as revealed by the distribution of reaction products is dependent upon the metal and the support. In addition, the structure of the hydrocarbon can explain the hydrogenolysis patterns by the assumption of various possible intermediates for hydrogenolysis such as 1,2-, 1,3-, 1,4- and 1,5-diadsorbed species. Compounds containing quaternary carbon atoms have the advantage that some mechanisms can be excluded because certain types of adsorption e.g. 1,2- and 1,3-diadsorbed species are sterically hindered or impossible.

The hydrogenolysis reactions of n-butane, 2,2-dimethylpropane and cyclopentane were studied over the ruthenium loaded zeolite RuNaY20 using the procedure detailed in Chapter 3. Reactions with RuNaLaY20 were carried out for comparison.

6.2.1. n-Butane Hydrogenolysis

The hydrogenolysis of n-butane over RuNaY20 was studied in the temperature range 319-354 K following pretreatment as detailed in Section 3.3.3. Hydrogenolysis to species of a lower carbon number was accompanied at higher reaction temperatures by isomerisation of the reactant to 2-methylpropane.

The results were calculated as percent C_4 using the procedure described in Section 3.3.4. A typical reaction

plot showing the pattern of product appearance with time is illustrated in Figure 6.15 for RuNaY20. Rates of product appearance were calculated by taking the tangent to the curve and are listed in Table 6.13 (expressed as molecules s^{-1} g^{-1}) for RuNaY20 and RuNaLaY20. The rates of product appearance increase with temperature.

Temperature /K	Rate of Product Appearance /10^{15} molecules s^{-1} g^{-1}				
	CH_4	C_2H_6	C_3H_8	i-C_4H_{10}	n-C_4H_{10}
319	0.15	0.84	0.20	0	-1.42
329	0.40	2.42	0.67	0	-3.54
344	1.38	12.20	3.04	0.06	-17.82
354	3.58	38.32	9.50	0.27	-53.74
331*	0.82	5.33	1.07	0.08	-7.54

Table 6.13. Initial Rate of Product Appearance for n-Butane Hydrogenolysis over RuNaY20 and RuNaLaY20

* Results for RuNaLaY20

Table 6.14 lists the values of the activation energies calculated from plots of ln k versus 1/T (Figure 6.16) for the different species using the data given in Table 6.13 for RuNaY20. The activation energy for n-butane hydrogenolysis was found to 98 kJ mol^{-1}.

Figure 6.15. Reaction Profile for n-Butane Hydrogenolysis over RuNaY20 at 354 K

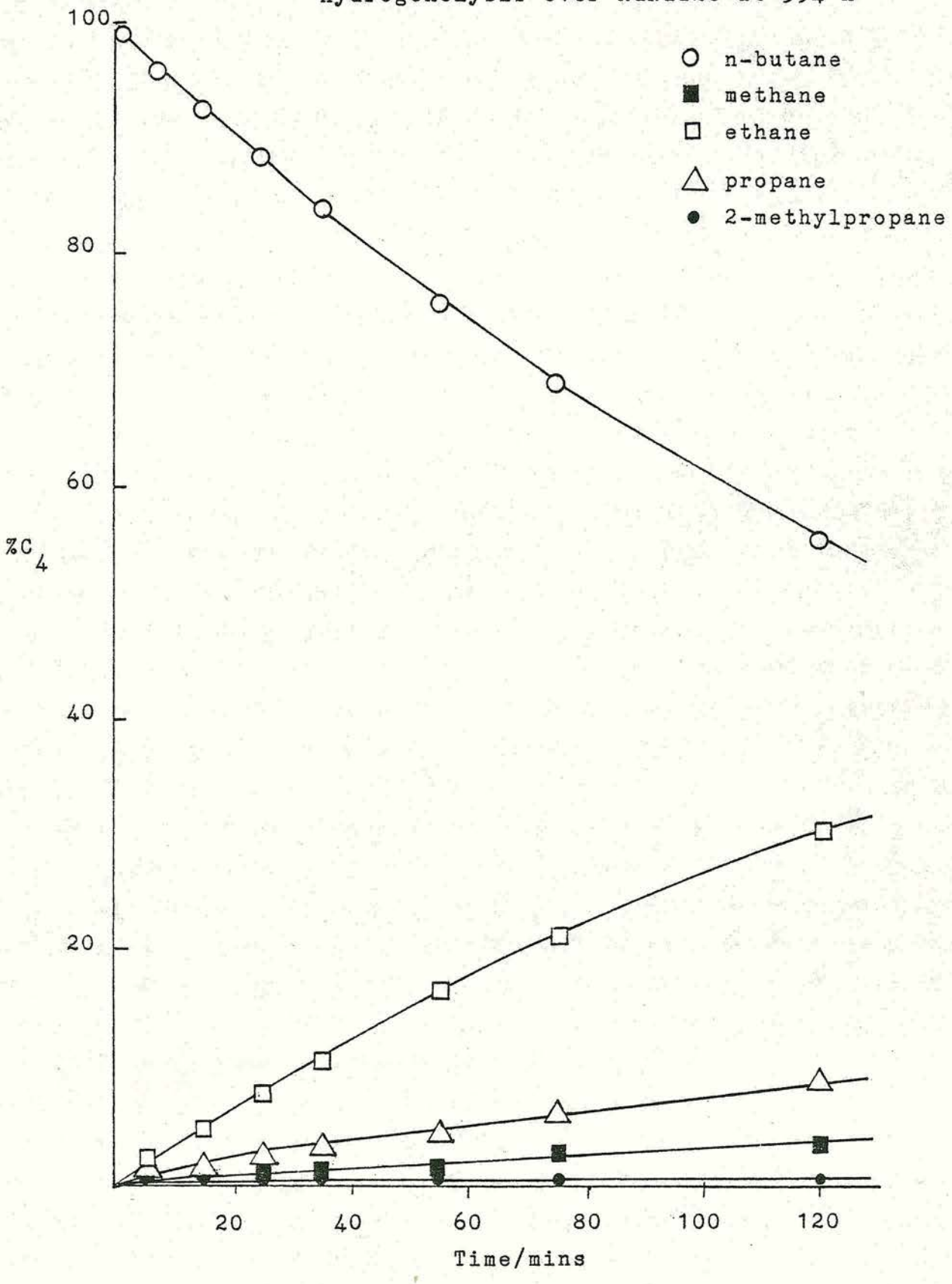

Figure 6.16. Arrhenius Plots for n-Butane Hydrogenolysis over RuNaY20

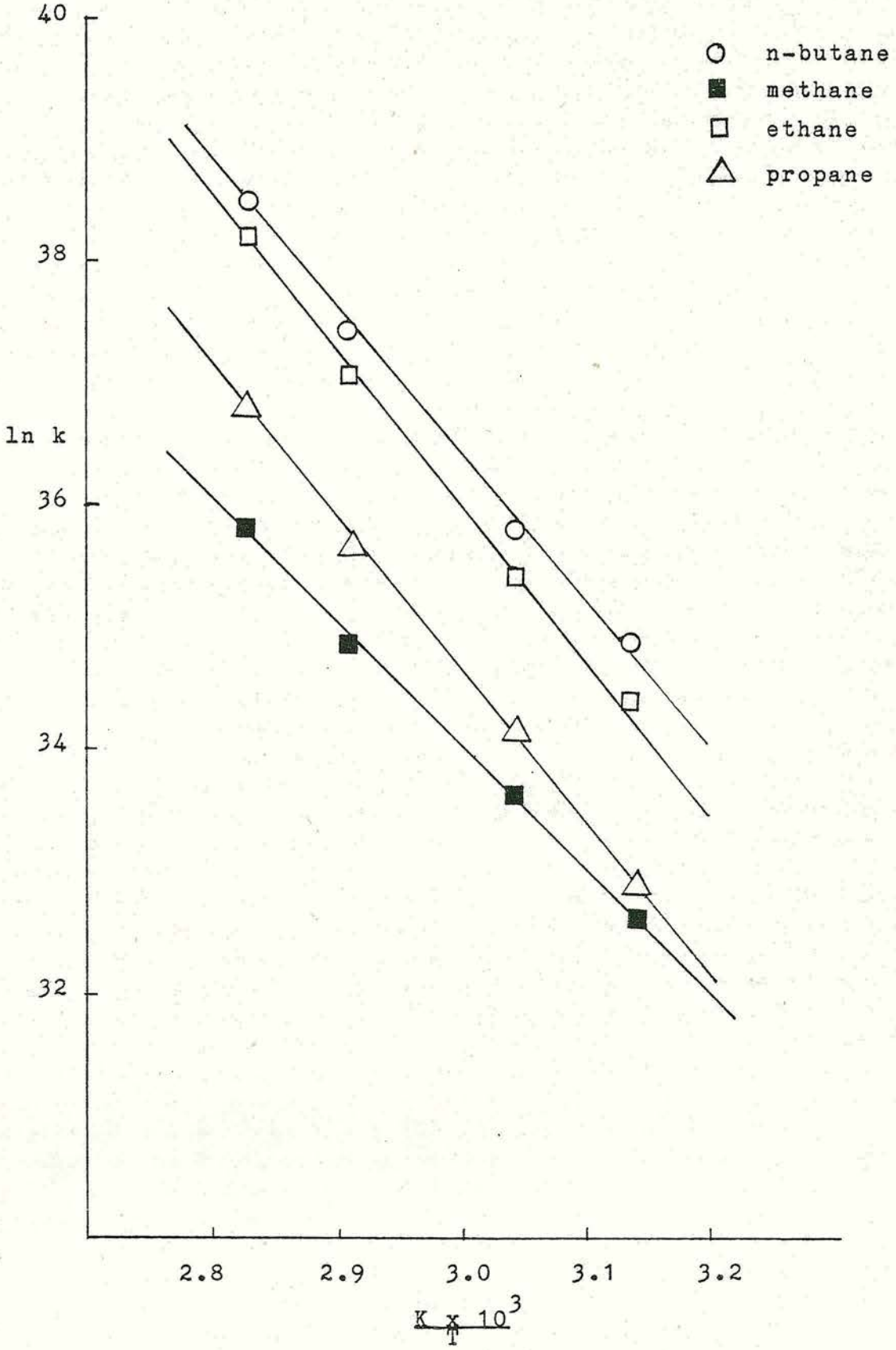

Product	Activation Energy kJ mol^{-1}	Type of Bond Cleavage
methane	84±5	terminal
ethane	102±6	central
propane	102±5	terminal
n-butane	98±9	

Table 6.14. Activation Energies for the Products of n-Butane Hydrogenolysis

The activation energies for methane and propane (Table 6.14) are not similar indicating that methane was not only formed by the cracking of n-butane to methane and propane i.e terminal bond cleavage. The activation energy values obtained for ethane and propane were similar indicating that they are only formed by the cracking of n-butane i.e. central bond cleavage. Comparison of the values for methane and ethane and propane shows them to be slightly different indicating that there was not an equal statistical probability of bond cleavage at C_1-C_4 bonds in n-butane. The lower value for methane may indicate a preference for multiple bond cleavage.

The selectivites of the reactions were measured as moles of each product formed for each mole of reactant used and in each case it was possible to extrapolate back to zero conversion. The plots obtained were good straight lines over the temperature range studied. The initial product distributions were obtained from the

gradients of these plots and are listed in Table 6.15 for RuNaY20 and RuNaLaY20. The values quoted are thus initial values uncomplicated by any contributions from sequential reactions of the products first formed. Curved plots would be obtained if one product was being increased at the expense of another.

Temperature /K	Initial Product Distribution moles product formed/moles reactant used				
	CH_4	C_2H_6	C_3H_8	i-C_4H_{10}	Multiple Cleavage
319	0.31	1.52	0.22	0	0.09
329	0.27	1.49	0.25	0	0.02
344	0.30	1.47	0.25	0	0.05
354	0.33	1.39	0.28	0.01	0.05
331*	0.22	1.63	0.17	0.01	0.05

Table 6.15. Initial Product Distributions from n-Butane Hydrogenolysis over RuNaY20 and RuNaLaY20

* Results for RuNaLaY20

The initial product distributions for n-butane hydrogenolysis over both RuNaY20 and RuNaLaY20 (Table 6.15) show marked preference for central bond cleavage as opposed to terminal bond cleavage. The results also indicate that with increasing reaction temperature over RuNaY20 terminal bond cleavage increases at the expense of central bond cleavage. A small degree of multiple bond cleavage is also evident at all

temperatues studied as shown by the slight excess of methane over propane.

Methane formation has been found to predominate in n-butane hydrogenolysis on ruthenium black and ruthenium supported on silica[111]. In the case of n-butane hydrogenolysis over $RuFe/SiO_2$[111], similar amounts of methane and ethane were formed and this was attributed to carbon-carbon bond rupture in the middle position of the n-butane molecule due to increased metal dispersion as iron oxide hinders the agglomeration of ruthenium particles.

n-Butane hydrogenolysis over Ru, Rh and Ir blacks has been investigated by Sarkany et al[112]. Initial multiple bond rupture indicated that multiple/strong carbon-metal bonds were formed. The stronger interaction leads to a longer residence time on the surface, resulting in hinderance to product desorption. When product desorption is slow an initial multiple bond rupture can take place easily. It was concluded that on the Ru, Rh and Ir catalysts the rate limiting step of hydrogenolysis was product desorption. With increasing reaction temperature the product distribution was found to shift in the direction of the dominant formation of methane.

Calculation of carbon mass balance during the hydrogenolysis of n-butane suggest that there was a slight loss of carbon to the catalyst surface as indicated by the results presented in Table 6.16. The expected percent loss due to sampling was c.a. 1%.

Temperature /K	Percent Sample Loss
319	2.0
329	2.5
344	1.5
354	2.4

Table 6.16. Percent Sample Loss During n-Butane Hydrogenolysis over RuNaY20

6.2.2. 2,2-Dimethylpropane Hydrogenolysis

The hydrogenolysis of 2,2-dimethylpropane was studied in the temperature range 356-393 K over RuNaY20 following pretreatment as described in Section 3.3.3. Only hydrogenolysis products were observed i.e. methane, ethane, propane and 2-methylpropane. No isomerisation products (2-methylbutane and n-butane) were observed. A typical reaction profile is illustrated in Figure 6.17 for RuNaY20. Initial rates were calculated by taking the tangent to the curve and are listed in Table 6.17 for RuNaY20 and RuNaLaY20. Traces of n-butane impurity in the 2,2-dimethylpropane made the determination of the initial rate of formation of ethane more difficult but values have been estimated and are included in Table 6.17.

Figure 6.17. Reaction Profile for 2,2-dimethylpropane Hydrogenolysis over RuNaY20 at 393 K

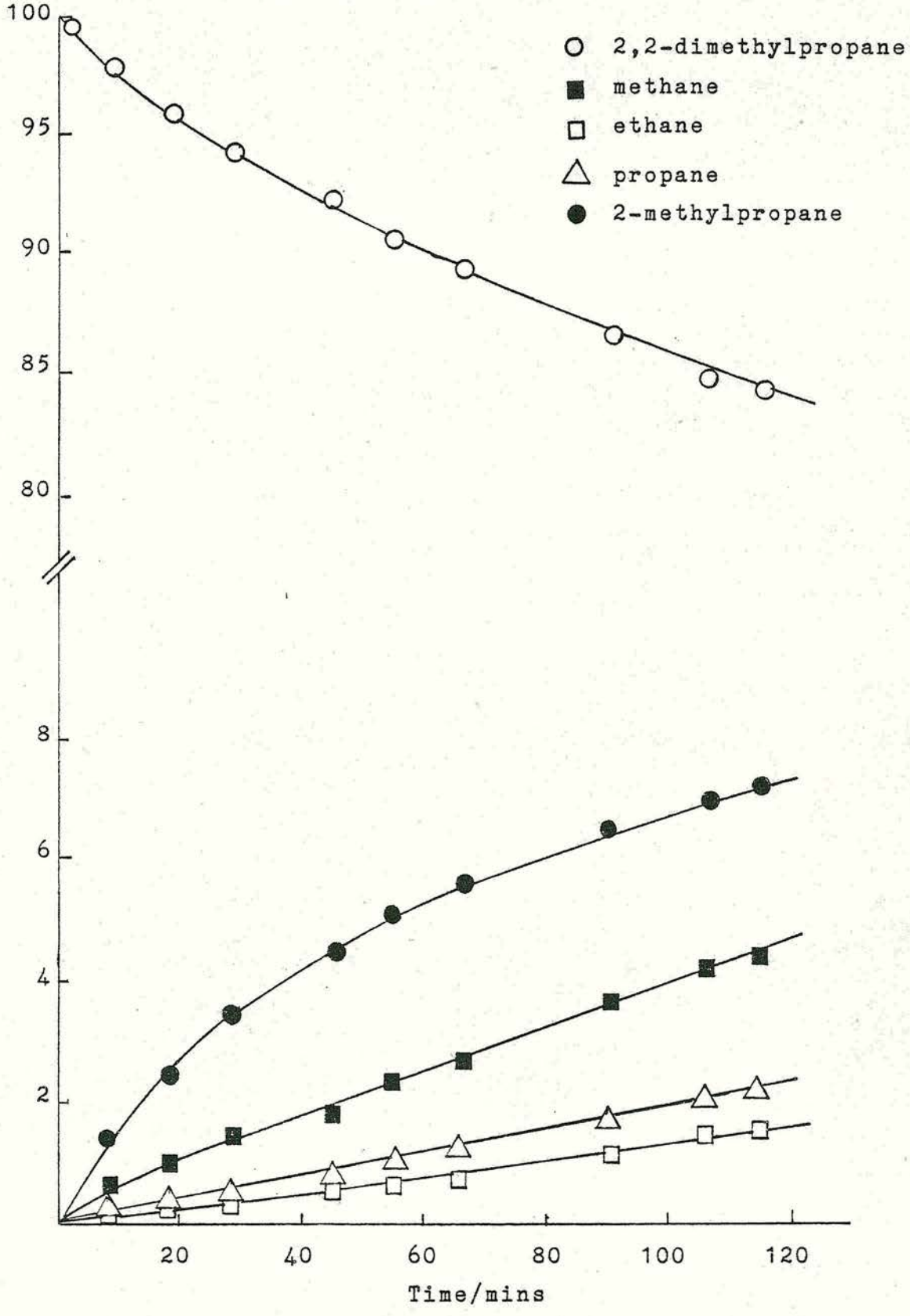

Temperature /K	Rate of Product Appearance /10^{15} molecules s^{-1} g^{-1}				
	CH_4	C_2H_6	C_3H_8	i-C_4H_{10}	neo-C_5H_{12}
356	0.68	0.10	0.05	0.82	-1.64
357	0.50	0.11	0.08	1.31	-1.97
372	2.36	0.35	0.57	5.46	-8.97
393	6.52	1.39	3.47	25.90	-37.10
368*	1.29	0.16	0.13	3.78	-5.40

Table 6.17. Initial Rates of Product Appearance over RuNaY20 and RuNaLaY20

* Results for RuNaLaY20

The data from Table 6.17 have been plotted as Arrhenius plots in Figure 6.18. and the corresponding apparent activation energies (calculated from the slopes) are listed in Table 6.18 The apparent activation energy for 2,2-dimethylpropane hydrogenolysis (97 kJ mol^{-1}) compares favourably with the value obtained for n-butane hydrogenolysis (98 kJ mol^{-1}) and suggests a common mode of adsorption. The activation energies for methane and 2-methylpropane formation are significantly different indicating that the cracking of 2,2-dimethylpropane to methane and 2-methylpropane was not the only mode of methane formation.

Figure 6.18. Arrhenius Plots for 2,2-dimethylpropane Hydrogenolysis over RuNaY20

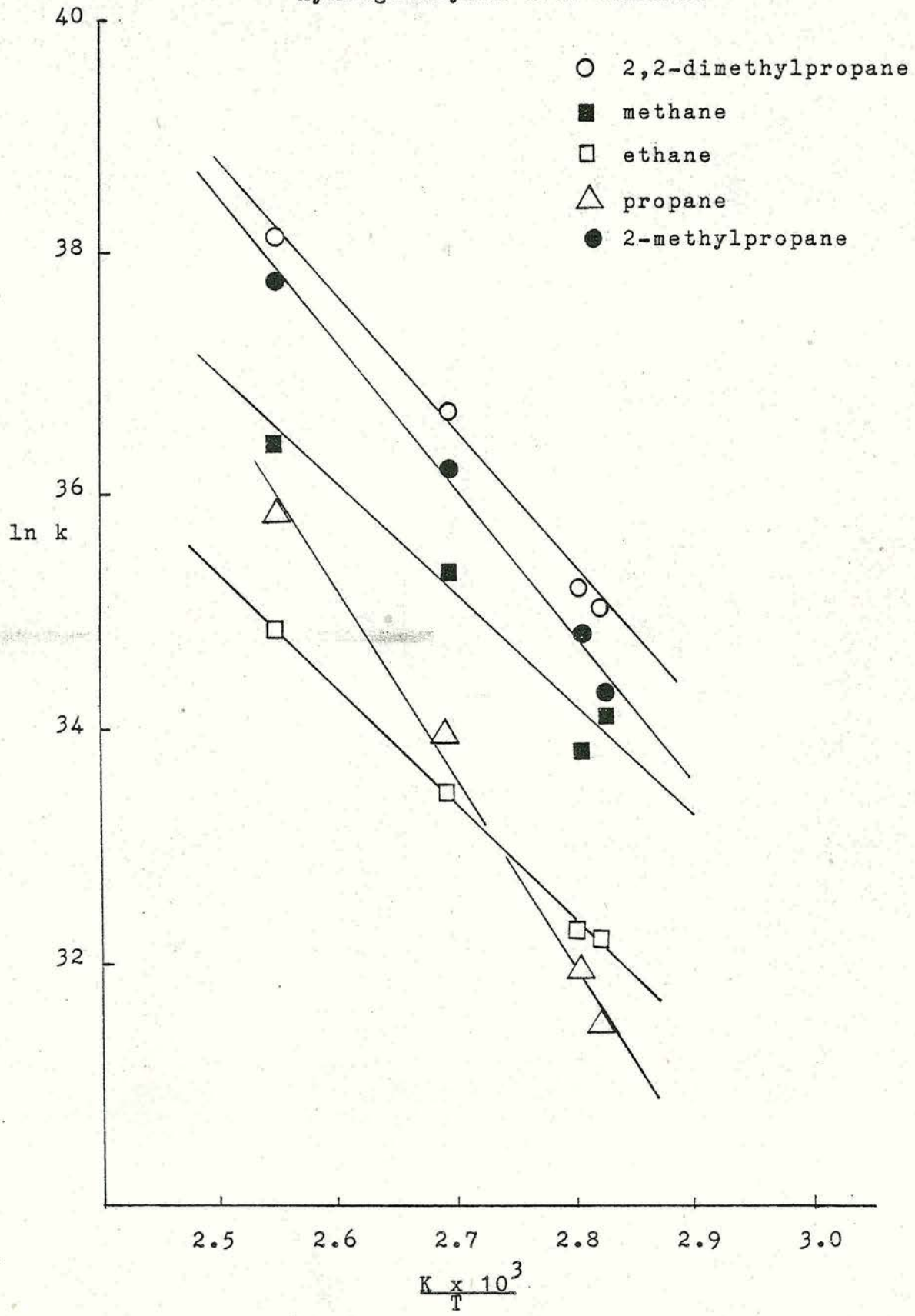

Product	Activation Energy kJ mol^{-1}
methane	69±12
ethane	82±4
propane	128±19
2-methylpropane	103±14
2,2-dimethylpropane	97±11

Table 6.18. Activation Energies for the Products of 2,2-Dimethylpropane Hydrogenolysis

The initial product distributions were determined form plots of moles of product formed per mole of reactant used and are given in Table 6.19 for RuNaY20 and RuNaLaY20. At the higher reaction temperatures of 372 K and 393 K for RuNaY20 the plots were slightly curved showing sequential reactions of the initial products. The plot for 2-methylpropane began to curve downwards indicating that it was undergoing further reaction while the plots for ethane and propane began to curve upwards indicating formation from a source other than 2,2-dimethylpropane.

Temperature /K	Initial Product Distribution (moles product formed/mole reactant used)				
	CH_4	C_2H_6	C_3H_8	i-C_4H_{10}	Methane Balance
356	1.15	0.10	0.04	0.82	1.20
357	1.17	0.10	0.05	0.855	1.24
372	1.30	0.09	0.08	0.84	1.26
393	1.31	0.12	0.08	0.81	1.45
368*	1.13	0.06	0.07	0.89	1.21

Table 6.19. Initial Product Distribution from 2,2-Dimethylpropane Hydrogenolysis over RuNaY20 and RuNaLaY20

* Results for RuNaLaY20

From the data presented in Table 6.19 it can be seen that the main reaction ocurring over both RuNaY20 and RuNaLaY20 was single bond cleavage to give methane and 2-methylpropane but some multiple bond cleavage occurred as evident by the excess of methane over 2-methylpropane. Small amounts of ethane and propane were found.

Hydrogenolysis of 2,2-dimethylpropane cannot occur via a 1,2-diadsorbed species but must occur via a 1,3-diadsorbed species with the main reaction being the cleavage of one carbon-carbon bond to give as products a molecule of methane and a molecule of 2-methylpropane.

Anderson and Avery[152] have concluded that the hydrogenolysis of higher molecular weight hydrocarbons

involves a 1,3-diadsorbed intermediate. This is based on their observation that 2,2-dimethylpropane which can form a 1,3-diadsorbed species but not a 1,2-diadsorbed species exhibits about the same reactivity as that found for n-butane, 2-methylpropane and 2-methylbutane but much higher than that found for ethane.

The origin of ethane and propane as reaction products may occur by successive demethylation of the adsorbed species. If this process is in operation it follows that the amount of methane formed would be given by:[108]

$$C_1 = C_4 + 2C_3 + 3C_2$$

for the hydrogenolysis of 2,2-dimethylpropane. C_1, C_2 etc. represent the moles of alkanes of various carbon number in the product. According to this expression one mole of methane is formed per mole of C_4, two moles are formed per mole of C_3 etc. Values for methane balance have been calculated for each temperature studied and are listed in Table 6.19. Comparison of the methane balance values with the amounts of methane observed over both RuNaY20 and RuNaLaY20 indicates that the amounts of methane observed are lower than would be expected if the hydrogenolysis occured by successive demethylation steps. This is in agreement with the literature[108] where the successive demethylation scheme of hydrogenolysis has been shown to be operative for iron, cobalt and nickel catalysts but not for the platinum metals.

Another possible source of ethane and propane would be the isomerisation of 2,2-dimethylpropane to other C_5

molecules. If the isomerised C_5 species on the catalyst surface suffers carbon-carbon bond cleavage before it can desorb as an isomerised C_5 molecule then equal amounts of ethane and propane would be produced. However, no isomerised C_5 molecules were observed. It is possible that any isomerised C_5 molecules were destroyed by hydrogenolysis very rapidly but it must be noted that even traces of isomerised C_5 molecules could have been detected readily.

Among all the metals of Group VIII plus Cu and Au, only Ir, Pt and Au have been found to isomerise 2,2-dimethylpropane to 2-methylbutane[113]. It has been speculated by the authors that the ability of these metals to isomerise 2,2-dimethylpropane to 2-methylbutane is related to their high electronegativity and to a readily shifted surface valency as a result of promotion of d electrons to empty s levels. The rates of hydrogenolysis of 2,2-dimethylpropane were also measured on supported metal catalysts containg Ru, Rh, Pd, Os, Ir and Au[113]. Ruthenium was found to be the most active metal investigated and gold the least active.

Foger and Anderson[153] have studied the hydrogenolysis of 2,2-dimethylpropane over NaY, LaY and PtY zeolite catalysts. The reactions over NaY and LaY were extremely slow when compared to PtY catalysts. Over NaY the reaction required a temperature of 623 K in order to reach the same rate as was achieved at 473 K over PtY. The authors concluded that because of the nature of the reactant molecule and the relatively low catalytic

activity of NaY for the hydrogenolysis of 2,2-dimethylpropane the reaction was entirely confined to the platinum metal and the zeolite support did not effect the results obtained.

From the results of Foger and Anderson[153] it can thus be concluded that the hydrogenolysis of 2,2-dimethylpropane over RuNaY20 and RuNaLaY20 is entirely confined to the metal ruthenium (the La^{3+} being located in the sodalite cages or hexagonal prisms[151] and inacessible to 2,2-dimethylpropane) with the zeolite support playing no role. The hydrogenolysis reaction occurs via a 1,3-diadsorbed species with bond cleavage giving methane and 2-methylpropane as products. The formation of ethane and propane as products is probably due to the isomerisation, on the catalyst surface, of 2,2-dimethylpropane to other C_5 species which undergo rapid hydrogenolysis.

It has previously been shown (Section 6.2.1) that carbon is lost to the surface of the catalyst during the hydrogenolysis of n-butane over RuNaY20. Similar mass balance calculation indicate that this is also the case for the hydrogenolysis of 2,2-dimethylpropane.

6.2.3. Cyclopentane Hydrogenolysis

Following pretreatment (as decribed in Chapter 3) the hydrogenolysis of cyclopentane was studied in the temperature range 403-445 K over RuNaY20. A reaction with RuNaLaY20 was studied for comparison. The main reaction observed was "ring-opening" to n-pentane.

Hydrogenolysis to smaller alkanes was also observed.

Initial rates of formation (expressed as $\%C_5$ $minutes^{-1}$ $gram^{-1}$) have been estimated from the tangents to the curve and are listed in Table 6.20 for both RuNaY20 and RuNaLaY20.

If the only reaction occurring was "ring-opening" to n-pentane then the rate of disappearance of cyclopentane should be equal to the rate of appearance of n-pentane. From Table 6.20 it can be seen that this is not the case and hydrogenolysis must be accompanying the "ring-opening" reaction. Rates for hydrogenolysis have been calculated and are presented in Table 6.21.

Temperature /K	Initial Rates/% C_5 min^{-1} g^{-1}		$\frac{100\ r_2}{r_1}$
	Ring-opening r_1	Hydrogenolysis r_2	
403	1.55	0.63	40.6
406	1.61	0.55	34.2
415	2.22	0.68	30.6
445	4.87	3.15	64.7
406*	3.00	1.50	50.0

Table 6.21. Initial Rates of Ring-opening and Hydrogenolysis over RuNaY20 and RuLaY20

* Results for RuNaLaY20

The above table indicates that both the rate of "ring-opening" and hydrogenolysis increase with temperature. Arrhenius plots for the hydrogenolysis of

Temperature/K	Initial Rate/%C_5 min.g^{-1}.							
	CH_4	C_2H_6	C_3H_8	C_4H_{10}	i-C_4H_{10}	i-C_5H_{10}	n-C_5H_{12}	c-C_5H_{12}
403	0.22	0.09	0.09	0.17	-	-	1.55	-2.18
406	0.19	0.08	0.08	0.14	-	-	1.61	-2.16
415	0.20	0.09	0.10	0.20	-	-	2.22	-2.90
445	0.84	0.42	0.42	0.86	0.10	0.50	4.87	-8.02
406*	0.50	0.19	0.25	0.42	-	-	3.00	-4.50

Table 6.20. Initial Rates of Product Appearance for Cyclopentane Hydrogenolysis over RuNaY20 and RuNaLaY20.

*Results for RuNaLaY20.

cyclopentane and the formation of n-pentane are illustrated in Figure 6.19 for RuNaY20. Calculation of the apparent activation energies for RuNaY20 gives values of 62 kJ mol^{-1} for the hydrogenolysis of cyclopentane and 41 kJ mol^{-1} for the formation of n-pentane i.e. "ring-opening".

Comparison of the apparent activation energy obtained for cyclopentane hydrogenolysis over RuNaY20 with the values obtained for the hydrogenolysis of n-butane and 2,2-dimethylpropane (Sections 6.2.1 and 6.2.2) indicates significant differences in the patterns of activity and suggests that bond breaking must occur by different mechanisms, possibly through 1,2-diadsorbed intermediates with cyclopentane and through 1,3-diadsorbed species with n-butane and 2,2-dimethylpropane.

Consideration of the initial product distribution (Table 6.22) indicates that there is formation of smaller alkanes as well as n-pentane formation by the bond breaking "ring-opening" reaction. Calculation of the initial product distribution for methane was complicated by a transient initial burst of methane but values have been estimated and are included in Table 6.22. The burst of methane can possibly be explained on the basis of a small concentration of highly active sites for deep hydrogenolysis being quickly poisoned probably by coking. Alternatively, some of this methane could have been formed by flash pyrolysis. However, the amount of methane initially formed remained approximately similar

Figure 6.19. Arrhenius Plots for the Hydrogenolysis and Ring-opening of Cyclopentane

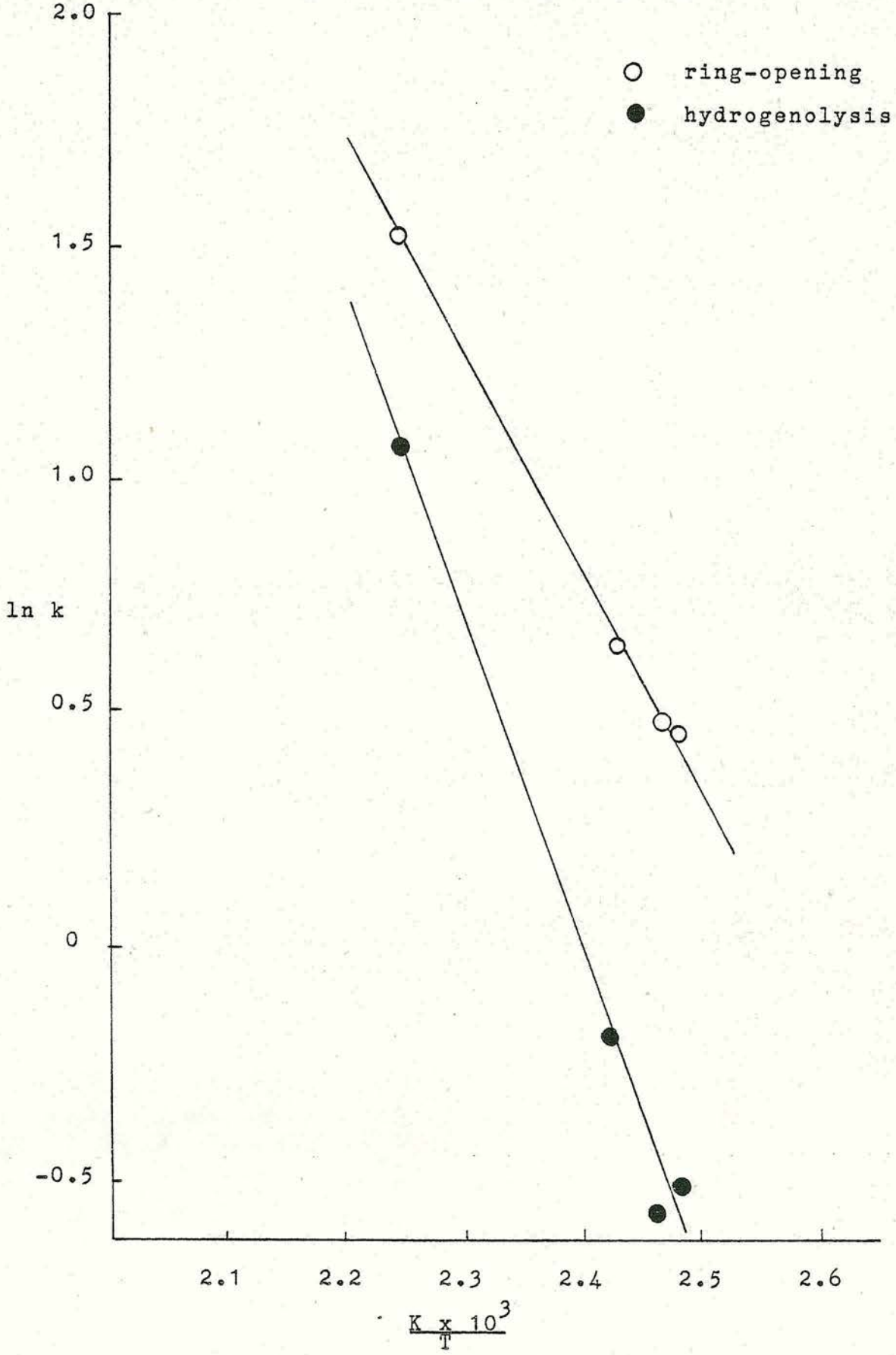

Temperature/K	Initial Product Distribution (moles product formed/moles reactant used)						
	CH_4	C_2H_6	C_3H_8	C_4H_{10}	$i\text{-}C_4H_{10}$	$i\text{-}C_5H_{10}$	$n\text{-}C_5H_{10}$
403	0.31	0.08	0.06	0.10	-	-	0.77
406	0.26	0.05	0.05	0.09	-	-	0.80
415	0.23	0.07	0.04	0.09	-	-	0.81
445	0.60	0.10	0.08	0.16	0.01	0.06	0.60
406*	0.45	0.09	0.08	0.12	-	-	0.70

Table 6.22. Initial Product Distribution over RuNaY20 and RuNaLaY20.

*Results for RuNaLaY20.

regardless of reaction temperature thus favouring the former explanation.

The initial product distribution indicates that the amount of n-pentane formed increases with temperature. The reaction at 445 K is complicated by hydrogenolysis of the n-pentane. The amounts of methane and butane formed increase as the amount of n-pentane decreases indicating a preference for primary bond cleavage of n-pentane (giving methane and butane) as opposed to secondary bond cleavage (giving ethane and propane). The data also indicate that some multiple bond cleavage occured.

In addition to the products listed in Table 6.22 traces of 2-methylbutane and 2-methylpropane were formed during the course of all reactions studied. Only the reaction at 445 K gave 2-methylbutane and 2-methylpropane as initial products. At a reaction temperature of 445 K the product distribution plot indicated that sequential reactions of the initial products was occurring with the amounts of methane, ethane, propane and butane increasing at the expense of 2-methylbutane and n-pentane.

Ghoneim[114] found the only products in cyclopentane hydrogenolysis over ruthenium supported on silica to be methane and ethane. The low percent conversion of cyclopentane was attributed to a strong adsorption of cyclopentane on the catalyst surface which possibly inhibited hydrogen adsorption causing a decrease in the rate of hydrogenolysis.

The hydrogenolysis of cyclopentane over RuNaY20 and

RuNaLaY20 occurs via a 1,2-diadsorbed species with the main reaction being "ring-opening" to give n-pentane. The n-pentane formed undergoes hydrogenolysis to give methane and n-butane as the major products.

Mass balance calculations during the course of the reactions on RuNaY20 indicated that in all cases carbon was lost to the surface of the catalyst. Table 6.23 indicates that the amount of carbon lost to the surface appears to increase with increasing reaction temperature. The expected loss due to sampling was 1%.

Temperature/K	Percent Sample Loss
403	2.7
406	1.5
415	2.9
445	6.3

Table 6.23. Percent Sample Loss During Cyclopentane Hydrogenolysis over RuNaY20

With increasing reaction temperature the amount of n-pentane formed increases and this coincides with an increase in the amount of carbon lost to the surface. Reactions starting with n-pentane over RuNaY20 indicated a large loss of carbon to the catalyst surface due to the adsorption of n-pentane on the catalyst surface. It can therefore be concluded that the carbon loss from cyclopentane hydrogenolysis was due to the adsorption of n-pentane, formed by "ring-opening", on the catalyst

surface.

6.2.4. Summary

The hydrogenolysis of n-butane, cyclopentane and 2,2-dimethylpropane occurred readily over RuNaY20 and RuNaLaY20. Comparison of the apparent activation energies suggested that the hydrogenolysis of n-butane and 2,2-dimethylpropane (98 and 97 kJ mol^{-1} respectively) occurred by a common mode of adsorption, a 1,3-diadsorbed species, while the apparent activation energy for the reaction of cyclopentane was lower (62 kJ mol^{-1}) suggesting a 1,2-diadsorbed species. Further evidence for these modes of adsorption was obtained from the initial product distributions.

REFERENCES

1. Cronstedt A.F., Akad. Handl. Stockholm, 17, 120 (1756).
2. Breck D.W., "Zeolite Molecular Sieves" John Wiley and Sons, (1973) Chapter 3.
3. Reference 2, Chapter 4.
4. Whyte T.E. and Dalla Betta R.A., Catal. Rev. Sci. Eng., 24 (4), 567 (1982).
5. Barrer R.M., J. Chem. Soc., 971 (1961).
6. Young L.B., U.S. Patent 4,100,217 (1978).
7. Casci J.L., Whittam T.V. and Lowe B.M., European Patent Application 0042226 (1981).
8. Flanigen E.M., Bennett R.M., Grose R.W., Cohen J.P., Patton R.L., Kirchner R.M. and and Smith J.V., Nature, 271, 512 (1978).
9. Loewenstein W., Amer. Mineral., 39, 92 (1942).
10. Reference 2, Chapter 1.
11. Meier W.M. and Olsen D.H., "Atlas of Zeolite Structure Types" (Special Publication By International Zeolite Association) Polycrystal Book Service, Pittsburgh USA (1978).
12. Reference 2, Chapter2.
13. Kokotailo G.T., Lawton S.L. Olsen D.H. and Meier W.M., Nature, 272, 437 (1978).
14. Olsen D.H., Kokotailo G.T., Lawton S.L. and Meier W.M., J. Phys. Chem., 85, 2238 (1981).
15. Barrer R.M., J. Chem. Soc., 2342 (1950).

16. Sherry H.S., J. Phys. Chem., 72, 4086 (1968).

17. Chen N.Y., J. Phys. Chem., 80, 60 (1976).

18. Reference 2, Chapter 7.

19. Uytterhoeven J.B., Acta Physica et Chemica, (Hungary), 24, 53 (1978).

20. Townsend R.P., Chemistry and Industry, 246 (1984).

21. Breck D.W., "Properties and Applications of Zeolites" (Ed. Townsend R.P.) Chem. Soc., Special Publication, 33, 391 (1980).

22. Derouane E.G., "Intercalation Chemistry", (Ed. Whittingham M.S. and Jacobson A.J.), Academic Press, New York, 101 (1982).

23. Barrer R.M., NATO ASI, (Portugal), (1983).

24. Reference 2, Chapter 8.

25. Dwyer J., Chemistry and Industry, 258 (1984).

26. Quig A. and Rees L.V.C., J. Chem. Soc. Farad. 1, 72, 771 (1976).

27. Barrer R.M., "Molecular Sieve Zeolites", (Ed. Flanigen E.M. and Sand L.B.), ACS, Monograph 102, 171 (1971).

28. Gorring R.L., J. Catal., 31, 13 (1973).

29. Satterfield C.N. and Katzer J.R., "Molecular Sieve Zeolites", (Ed. Flanigen E.M. and Sand L.B.), ACS, Monograph 102, 193 (1971).

30. Barrer R.M. and Clarke D.J., J. Chem. Soc. Farad. I, 70 , 535 (1974).

31. Venuto P.B., Chem. Tech., 215 (1971).

32. Minachev Kh.M. and Isakov Ya.I., "Zeolite Chemistry and Catalysis", (Ed. Meier W.M. and Uytterhoeven

J.B.), ACS, Mongraph 121, 451 (1973).

33. Isakov Ya.I. and Minachev Kh.M., Russ. Chem Reviews, 51, 1188 (1982).

34. Vaughan D.E.W., "Properties and Applications of Zeolites", (Ed. Townsend R.P.), Chem. Soc. Special Publication, 33, 294 (1980).

35. Jacobs P.A., "Carboniogenic Activity of Zeolites", Elsvier, Amsterdam (1977).

36. Ward J., "Zeolite Chemistry and Catalysis", (Ed. Rabo J.A.), ACS, Mongraph 171, 118 (1976).

37. Barthomeuf D., "Catalysis by Zeolites", Studies in Surface Science and Catalysis, 5, Elsevier, Amsterdam, 55 (1980).

38. Ward J., J. Catal., 9, (1967).

39. Ward J., J. Colloid and Interface Sci., 28, 269 (1968).

40. Jacobs P.A. and Heylen C.F., J. Catal., 34, 267 (1974).

41. Haag W.O., Lago R.M. and Weisz P.B., Nature, 309, 589 (1984).

42. Weisz F.B. and Frilette V.J., J. Phys. Chem., 64, 382 (1960).

43. Csicsery S.M., "Zeolite Chemistry and Catalysis" (Ed. Rabo J.A.), ACS, Monograph 171, 680 (1976).

44. Weisz P.B., Pure and Appl. Chem., 52, 2091 (1980).

45. Tempere J.F. and Imelik B., Bull. Soc. Chim. Fr., 4227 (1970).

46. Cormerais F.X., Perot G. and Guisnet M., Zeolites, 1, 141 (1981).

47. Chen N.Y., Kaeding W.W. and Dwyer F.G., J. Amer. Chem. Soc., 101, 6783 (1979).

48. Kaeding W.W., Chu C., Young L.B., Weinstein B. and Butter S.A., J. Catal., 67, 159 (1981).

49. Young L.B., Butter S.A. and Kaeding W.W., J. Catal., 76, 418 (1982)

50. Hilaireau P., Bearez C., Chevalier F., Perot G. and Guisnet M., Zeolites, 2, 69 (1982).

51. Haag W.O., Lago R.M. and Weisz P.B., "Selectivity in Heterogenous Catalysis", Faraday General Discussion, 72, 317 (1982).

52. Rollman L.D. and Walsh D.E., J. Catal., 56, 139 (1979).

53. Derouane E.G. and Gabelica Z., J. Catal., 65, 486 (1980).

54. Mirodatos C. and Barthomeuf D., J. Catal., 93, 246 (1985).

55. Verdonck J.J., Jacobs P.A., Genet M. and Poncelet G., J. Chem. Soc. Farad. I, 76, 403 (1980).

56. Pearce J.R., Mortier W.J. and Uytterhoeven J.B., J. Chem. Soc. Farad. I, 75, 1395, (1979).

57. Lunsford J.H., "Metal Microstructure in Zeolites", Studies in Surface Science and Catalysis, 12, Elsevier, Amsterdam, 1 (1982).

58. Chen Y.W., Wang H.T. and Goodwin J.G., J. Catal., 83, 415 (1983).

59. Audier M., Klinowski J and Benfield R.E., J. Chem. Soc. Chem. Comm., 626 (1984).

60. Gallezot P., Alarcon-Diaz A., Dalman J.A., Renouprez A.J. and Imelik B., J. Catal., 39, 334 (1975).

61. Elliott D.J. and Lunsford J.H., J. Catal., 57, 11 (1979).

62. Dufaux M., Gelin P and Naccache C., "Catalysis by Zeolites", Studies in Surface Science and Catalysis, 5, Elsevier, Amsterdam, 261 (1980).

63. Pederson L.A. and Lunsford J.H., J. Catal., 61, 39 (1980).

64. Jaeger N.I., Ryder P. and Schulz-Ekloff G., "Structure and Reactivity of Modified Zeolites", Studies in Surface Science and Catalysis, 18, Elsevier, Amsterdam (1984).

65. Candy J.P., Fouilloux P and Renouprez A.J., J. Chem. Soc. Farad. I, 76, 616 (1980).

66. de Menorval L.C., Fraissard J.P. and Ito T., J. Chem. Soc. Farad. Trans. I, 78, 403 (1982).

67. Fraissard J., Ito T., de Menorval L.C. and Springuel-Huet M.A., "Metal Microstructures in Zeolites", Studies in Surface Science and Catalysis, 12, Elsevier, Amsterdam, 179 (1982).

68. Gentry S,J., Hurst N.W. and Jones A., J. Chem. Soc. Farad. Trans. I, 75, 1688 (1977).

69. Coughlan B., Narayanan S., M^{c}Cann W.A. and Carroll W.M., J. Catal., 49, 97 (1977).

70. Bond G.C. and Wells P.B., Advances in Catalysis, 15, 91 (1964).

71. Haag W.O. and Pines H., J. Amer. Chem. Soc., 82,

387 (1960).

72. Hattori H., Maruyama K. and Tanabe K., J. Catal., 44, 50 (1976).

73. Baird M.J. and Lunsford J.H., J. Catal., 26, 440 (1972).

74. Chang C.C., Conner W.C. and Kokes R.J., J. Phys. Chem., 77, 1957 (1973).

75. Rosynek M.P., Fox J.S. and Jenson J.L., J. Catal., 71, 64 (1981).

76. Turkevich J. and Smith R.K., J. Chem. Phys., 16, 446 (1948).

77. Haag W.O. and Pines H., J. Amer. Chem. Soc., 82, 2488 (1960).

78. Foster N.F. and Cvetanovic R.J., J. Amer. Chem. Soc., 82, 4274 (1960).

79. Hightower J.W. and Hall W.K., J. Phys. Chem., 71, 1014 (1967).

80. Misono M., Saito Y. and Yoneda Y., J. Catal., 9, 135 (1967).

81. Misono M. and Yoneda Y., J. Phys. Chem., 76, 44 (1972).

82. Hightower J.W. and Hall W.K., J. Amer. Chem. Soc., 89, 778 (1967).

83. Ballivet D., Barthomeuf D. and Trambouze Y., J. Catal., 26, 34 (1972).

84. Detrekoy E.J., Jacobs P.A., Kallo D. and Uytterhoeven J.B., J. Catal., 32, 442 (1974).

85. Lombardo E.A., Sill G.A. and Hall W.K., J. Catal., 22, 54 (1971).

86. Weeks T.J., Angell C.L., Ladd I.R. and Bolton A.P., J. Catal., 33, 256 (1974).

87. Jacobs P.A., Declerck L.J., Vandamme L.J. and Uytterhoeven J.B., J. Chem. Soc. Farad. Trans. I, 71, 1545 (1975).

88. Dakta J., J. Chem. Soc. Farad. I, 76, 2437 (1980).

89. Cross N.E., Kemball C. and Leach H.F., J. Chem. Soc. (A), 3315 (1971).

90. Cross N.E., Kemball C. and Leach H.F., "Molecular Sieve Zeolites", (Ed. Flanigen E.M. and Sand L.B.), ACS, Monograph 102, 389 (1971).

91. Hoser H. and Krzyzanowski S., J. Catal., 38, 366 (1975).

92. Dirringer M.C. and Fajula F., Zeolites, 3, 163 (1983).

93. Tsuchiya S., Ito S., Namba S. and Yashima T., Zeolites, 3, 193 (1983).

94. Pines H. and Haag W.O., J. Amer. Chem. Soc., 82, 2471 (1960).

95. Whitmore F.C., Chem. Eng. News, 26, 668 (1947).

96. Irvine E.A., John C.S., Kemball C., Pearman A.J., Day M.A., and Sampson R.J., J. Catal., 61, 326 (1980).

97. Kemball C., Leach H.F., Skundric B. and Taylor K.C., J. Catal., 27, 416 (1972).

98. Kemball C., Leach H.F. and Moller B.W., J. Chem. Soc. Farad. I, 69, 624 (1973).

99. Scurrell M.S., Moller B.W. and Kemball C., J. Chem. Soc. Farad. Trans. I, 72, 2512 (1976).

100. John C.S. and Leach H.F., J. Chem. Soc. Farad Trans. I, 73, 1595 (1977).

101. Larson J.G., Gerbich H.R. and Hall W.K., J. Amer. Chem. Soc., 87, 1880 (1965).

102. Bartley B.H., Habgood H.W. and George Z.M., J. Phys. Chem., 72, 1689 (1968).

103. Nguyen T.T., Cooney R.P. and Curthoys G., J. Catal., 44, 81 (1976).

104. Hightower J.W. and Hall W.K., J. Amer. Chem. Soc., 90, 851 (1968).

105. Gerberich H.R., Hightower J.W. and Hall W.K., J. Catal., 8, 391.(1967).

106. Marsden C., Ph.D. Thesis, University of Edinburgh (1978).

107. Sinfelt J.H., Catalysis Reviews, 3, 175 (1970).

108. Sinfelt J.H., Advances in Catalysis, 23, 91 (1973).

109. Kikuchi E., Tsurmi M and Morita Y., J. Catal., 22, 226 (1971).

110. Galvagno S., Schwank J., Gubitosa G. and Tauszik G.R., J. Chem. Soc. Farad. Trans. I, 78, 2509 (1982).

111. Guczi L., Matusek K., Sarkany A. and Tetenyi P., Bull. Soc. Chem. Belg., 88, 497 (1979).

112. Sarkany A., Matusek K. and Tetenyi P., J. Chem. Soc. Farad. Trans. I, 73, 1699 (1977).

113. Boudart M. and Ptak L.D., J. Catal., 16, 90 (1970).

114. Ghoneim F.B., Egypt. J. Chem., 16, 497 (1973).

115. Sauvion G.N., Djemel S., Tempere J.F., Guilleux M.F. and Delafosse D., "Catalysis by

Zeolites", Studies in Surface Science and Catalysis, 5, Elsevier, Amsterdam, 245 (1980).

116. Jacobs P.A., Private Communication.

117. Kilpatrick J.E., Prosen E.J., Pitzer K.S. and Rossini F.D., J. Res. Nat. Bur. Stand., 36, 559 (1946).

118. Ultra Microweight Determination in Controlled Environments, (Ed. Wolsky and Zdanuk), Wiley Interscience (1969).

119. Day R.E., Parfitt G.D. and Peacock J., Proc. Vac. Microbalance Tech., 2, 61 (1973).

120. Hurst N.W., Jones A. and M^{c}Nicol B.D., Catal. Rev. Sci. Eng., 24 (2), 233 (1982).

121. Casci J.L., Whittam T.V. and Lowe B.M., "Proc. Sixth Int. Zeolite Conference", (Ed. Olsen D. and Bisio A.), Butterworths, London, 894 (1984).

122. Casci J.L., Ph.D. Thesis, University of Edinburgh (1982).

123. Olsen D.H., Haag W.O. and Lago R.M., J. Catal., 61, 390 (1980).

124. Kokotailo G.T., Chu P. and Lawton S.L., Nature, 275, 119 (1978).

125. M^{c}Clellan H.L. and Harnsberger H.F., J. Colloid Interface Sci., 23, 577 (1967).

126. Mobil Oil Corportion, U.K. Patent 1,491,398 (1976).

127. Casci J.L., Private Communication.

128. Dessau R.M., U.S. Patent 4,423,280 (1983).

129. Kibby C.L., Perrolta A.J. and Massoth F.E., J. Catal., 35, 256 (1974).

130. Chang C.D., Catal. Rev. Sci. Eng., 25, 1 (1983).

131. Harrison I.D., Private Communication.

132. Eberly P.E., "Zeolite Chemistry and Catalysis", (Ed. Rabo J.A.), ACS, Monograph 171, 392 (1976).

133. Harrison I.D., Leach H.F. and Whan D., "Proc. Sixth Int. Zeolite Conference", (Ed. Olsen D. and Bisio A.), Butterworths, London, 479 (1984).

134. Jacobs P.A., Nijs H.H., Verdonck J.J. and Uytterhoeven J.B., Prepr. Div. Petrol. Chem. A.C.S., 23, 469 (1978).

135. Jacobs P.A., Chantillon R., De Laet P., Verdonck J.J. and Tielen M., A.C.S. Symp. Ser., 128, 439 (1983).

136. Verdonck J.J., Schoonheydt R.A. and Jacobs P.A., J. Phys. Chem., 85, 2393 (1981).

137. Goodwin J.G. and Naccache C., J. Catal., 64, 482 (1980).

138. Sawyer D.T. and Roberts J.L., Experimental Electrochemistry for Chemists, Wiley Interscience (1979).

139. Handbook of Chemistry and Physics, (Ed. Weast R.C.), 57th edition, CRC Press (1976-77).

140. Verdonck J.J., Jacobs P.A. and Uytterhoeven J.B., J. Chem. Soc. Chem. Comm., 181 (1979).

141. Goodwin J.G., J. Catal., 68, 227 (1981).

142. Koopman P.G.J., Kieboom A.P.G. and van Bekkum H., J. Catal., 69, 172 (1981).

143. Yang C.H. and Goodwin J.G., J Catal., 78, 182

(1982).

144. Wang H.T., Chen Y.W. and Goodwin J.G., Zeolites, 4, 56 (1984).

145. Gustafson B.L. and Lunsford J.H., J. Catal., 74, 393 (1982).

146. Pelrine B.P. and Chen N.Y., U.S. Patent 4,222,855 (1980).

147. Dabrowski A., unpublished results.

148. Rollman L.D. and Walsh D.E., Progress in Catalyst Deactivation, (Ed. Figueredo J.L.), NATO Advanced Study Institute Series E, Applied Sciences, 54, 81 (1981).

149. Benesi H.A., J. Catal., 8, 368 (1967).

150. Knozinger H., Advances in Catalysis, 25, 184 (1976).

151. Naccache C. and Ben Taarit Y., Acta Physica et Chemica, 24, 23 (1978).

152. Anderson J.R. and Avery N.R., J. Catal., 5, 446 (1966).

153. Foger K. and Anderson J.R., J. Catal., 54, 318 (1978).

154. Dimitrov CHR. and Leach H.F., J. Catal., 14, 336 (1969).

155. Irvine J.D.N., Ph.D. Thesis, University of Edinburgh (1981).

156. Catalyst Handbook, ICI Ltd. Agric. Division, Wolfe Scientific Books (1970).

157. Ruthven D., Derrah R.I., Loughlin K.F., Can. J. Chem., 51, 3514 (1973).

158. Datka J., Zeolites, 1(2), 113 (1981).

159. Weeks T.J. and Bolton A.P. J. Chem. Soc. Farad. I, 70,1676 (1974).

160. Weeks T.J. and Bolton A.P. "Molecular Sieves" (Ed. Uytterhoeven J.B.), Proc. Third Int. Conf. Mol. Sieves, 426 (1973).

161. Wright P.A., Thomas J.M., Millward G.R., Ramdas S. and Barrie S.A.I., J. Chem. Soc. Chem. Comm., 1117 (1985).

162. Leach H.F. and Marsden C., "Catalysis by Zeolites", Studies in Surface Science and Catalysis, 5, Elsevier, Amsterdam, 141 (1980).

163. Goldwasser J. and Hall W.K., J. Catal., 71, 53 (1981).

Courses Attended

Catalytic Group Seminars 1981/2, 1982/3, 1983/4.

Conference on Zeolites - Chislehurst, July 1984.

Lasers in Chemistry

Prof. R.J. Donovan and Dr. C. Fotakis

Modern Liquid Phase Separation Techniques

Prof. J. Knox

Physical Techniques for the Characterisation of Surfaces

Dr. H.F. Leach

Homogenous Catalysis

Dr. T.A. Stephenson

History of the Department of Chemistry, Edinburgh University

Dr. W. Doyle

Topics in Transition Metal Co-ordination Chemistry

Dr. M. Schroder